THE ROLE OF BONDING ON THE TENSILE CREEP BEHAVIOR OF PAPER

A Dissertation
Presented to
The Academic Faculty

By

Andrew Marc DeMaio

In Partial Fulfillment
Of the Requirements for the Degree
Doctor of Philosophy in the
School of Mechanical Engineering

Georgia Institute of Technology

August 2006

THE ROLE OF BONDING
ON THE TENSILE CREEP BEHAVIOR OF PAPER

Approved by:

Dr. Timothy Patterson, Advisor
School of Mechanical Engineering
Georgia Institute of Technology

Dr. Frederick Ahrens
School of Mechanical Engineering
Georgia Institute of Technology

Dr. David Orloff
School of Mechanical Engineering
Georgia Institute of Technology

Dr. Preet Singh
School of Material Science and Engineering
Georgia Institute of Technology

Dr. Douglas Coffin
School of Engineering and Applied Science
Miami University

Date Approved: June 7, 2006

Don't let schooling interfere with your education.
-Mark Twain

ACKNOWLEDGEMENTS

Although a doctorate is a personal achievement, there are many individuals that offer help, advisement and support along the way. Without such people, the task of completing doctoral research and writing a dissertation becomes much more daunting. I am proud to say that over the last five years, there were many individuals to whom I cannot express enough thanks for everything they have done for me. Many are people I already knew going into this endeavor, while others are new colleagues and friends that I have met along the way. The following are those individuals I felt deserved recognition and inclusion in my personal achievement.

First and foremost, I would like to thank my family and lifelong friends for all of their optimistic support. They have always believed that I could do anything I put my mind to. I would especially like to thank my mother, Chris DeMaio, my grandparents, Lorraine DeMaio and Anthony DeMaio, and my good friends, Bill Colpetzer and David Horn.

I would also like to thank my research advisor, Dr. Timothy Patterson, for all of his sound advice and support. He allowed me to work freely, giving me the opportunity to develop as a researcher, educator and individual. The remainder of my research committee, which includes: Dr. Douglas Coffin, Dr. Frederick Ahrens, Dr. David Orloff and Dr. Preet Singh have also been instrumental in my success, by offering their advisement and support.

In addition, I would like to thank all my fellow IPST/ Georgia Tech students (past and present) who have helped me and become good friends over the last five years.

Specifically, I would like to thank my officemates, Lauri Lehtonen, Brett Brotherson (who is also my roommate), Fran Jacobson, and Cameron Thomson. They have all played their part in keeping me sane with sound technical advice, necessary diversions and their senses of humor. I would also like to thank Rebecca Jones for keeping me thinking rationally as well as helping me with the editing process. Sara Garlington, a Georgia Tech undergrad (who recently graduated) helped tremendously with the accelerated creep portion of my thesis with needed laboratory assistance and experimentation for a semester. Another officemate, Rob Lowe deserves special recognition for working tirelessly on the microscope for many hours as well as offering his sound technical skill with the microscopy portion of my thesis.

I would also like to thank the IPST/ Georgia Tech staff for all of their help, with special mention to Kennisha Collins, Tuwanda Strowbridge and Major Hank White. These three individuals made conducting research at IPST much easier because of their technical skills, support in the laboratory and friendly conversation. Lastly, I would like to thank all of those in the graduate office at the Georgia Tech School of Mechanical Engineering. They, especially Glenda Johnson, made my transition from IPST to IPST at Georgia Tech much easier.

TABLE OF CONTENTS

LIST OF TABLES

LIST OF FIGURES

LIST OF EQUATIONS

NOMENCLATURE

A	=	empirical creep model material constant
A_1	=	rheological creep model viscous material constant for primary creep
A_2	=	rheological creep model viscous material constant for secondary creep
A_e	=	Eyring dashpot material constant
A_f	=	average fiber cross section
a_1	=	empirical creep model material constant
a_2	=	empirical creep model material constant
a_3	=	empirical creep model material constant
a_o	=	empirical creep model material constant
α	=	empirical creep model material constant
B	=	empirical creep model material constant
B_1	=	rheological creep model viscous material constant for primary creep
B_2	=	rheological creep model viscous material constant for secondary creep
B_e	=	Eyring dashpot material constant
b	=	empirical creep model material constant
b_o	=	empirical creep model material constant
b_s	=	specific bond strength
β	=	empirical creep model material constant
C	=	empirical creep model material constant
C_i	=	integration constant
c	=	empirical creep model material constant

D	=	empirical creep model material constant
ΔG_o	=	energy required to jump a potential barrier in an unstressed state
ΔG_1	=	energy required to jump a potential barrier in a stressed state in the direction of the applied stress
E	=	elastic modulus
E_1	=	rheological creep model elastic modulus constant for primary creep
E_e	=	rheological creep model elastic modulus constant
E_f	=	elastic modulus of a fully efficient loaded paper
E_i	=	elastic modulus of an inefficiently loaded paper
E_m	=	elastic modulus parameter for a Maxwell Model
E_v	=	elastic modulus parameter for a Voigt Model
e	=	standard error
ε	=	strain, creep strain
ε_1	=	rheological creep model primary creep strain
ε_2	=	rheological creep model secondary creep strain
ε_e	=	rheological creep model initial elastic strain
ε_o	=	initial strain
ε_p	=	plastic strain
η	=	viscosity
η_m	=	viscosity parameter for a Maxwell Model
η_v	=	viscosity parameter for a Voigt Model
F	=	empirical creep model material constant
g	=	acceleration due to gravity
γ	=	empirical creep model material constant

h	=	Planck's constant
IPST	=	Institute of Paper Science and Technology
J	=	creep compliance
k	=	Boltzmann constant
L	=	fiber length
LS	=	light scatter
Ml	=	middle lamella that separates wood cells
n	=	sample size, number of repetitions in measurement
n_b	=	frequency of molecular segments jumping a potential barrier in a stressed state in the direction opposite to the applied stress
n_f	=	frequency of molecular segments jumping a potential barrier in a stressed state in the direction of the applied stress
n_o	=	frequency of molecular segments jumping a potential barrier in an unstressed state
P	=	perimeter of fiber cross section
Pr	=	primary wall of a wood cell
φ	=	efficiency factor
Q	=	flow rate
R_o	=	reflectance of a single layer of paper against an ideal black background
R_∞	=	reflectance of multiple layers of the same paper where the addition of additional layers will not change the reflectance
RBA	=	relative bonded area
ρ	=	fiber density
S_1	=	outer layer of the secondary wall of a wood cell
S_2	=	middle layer of the secondary wall of a wood cell

S_3 = inner layer of the secondary wall of a wood cell

s = standard deviation

σ = stress

σ_d = dashpot stress

σ_k = rheological creep model activation stress constant

σ_o = initial applied stress

σ_r = reference stress constant

σ_s = spring stress

T = absolute temperature

T_s = tensile strength

t = time

t_1 = reference time constant

t_o = empirical creep model material constant

t_r = reference time constant

V = molecular segment volume in a polymeric material

v = empty space volume (void volume) in a polymeric material

W = warty layer inside the lumen of a wood cell

w = paper grammage

Z = zero-span tensile strength

SUMMARY

The role of bonding in the tensile creep behavior of paper was analyzed. This was accomplished by producing handsheets at a range of different bonding levels through manipulation of relative bonded area and specific bond strength. This was done by varying the level of wet pressing (to change relative bonded area) and using debonding and bonding agents (to change specific bond strength). Once manufactured, sheets underwent an extensive battery of physical testing and creep testing. Creep testing was conducted under constant humidity and cyclic humidity (accelerated creep) conditions. Microscopic analysis techniques were also employed to visually study bonded area loss from creep strain. Two mathematical models (one empirical and one rheological) were created to isolate, account for, and incorporate bonding into predicting tensile creep behavior in paper. Overall, the results from this thesis show that the role of bonding in tensile creep behavior (and accelerated creep behavior) is no different than its role in stress-strain behavior, which is a new finding. This means the bonding influence on tensile creep behavior is related to sheet efficiency and how effectively stress is distributed within the structure, bonded area loss is a strain-induced phenomenon and bonding is not the cause of accelerated creep behavior.

CHAPTER 1: INTRODUCTION

When a load is applied to paper and held constant, the paper will exhibit a time dependent deformation otherwise know as creep. Creep behavior in paper has been of great historical interest to researchers and the paper industry for many years. Over the past fifty years, considerable research has been conducted in an attempt to better understand and characterize this behavior. Unfortunately, no specific attention has been given to how bonding influences creep behavior in paper. This is surprising, because bonding is one of the most important components of paper structure; bonds are responsible for the distribution of load between the fibers in paper. Paper is a material that consists of a network structure of bonded fibers. This network is primarily random in nature even when processes that produce paper with an orientation are used. In order to effectively understand and characterize any deformation behavior in paper, an understanding of fiber deformation by itself is wholly inadequate. An understanding of the structural aspects of paper, specifically bonding, is also necessary.

Therefore, the overall objective of this thesis was to better discern the role bonding has in the creep behavior of paper. Because a fundamental knowledge of creep behavior in paper was lacking with regard to bonding influence, it was not possible, in a reasonable time frame, to fully explore the entire range of possible creep behaviors. As a result, this thesis was limited to developing a fundamental foundation from which more complete studies can be based. The research was limited to discerning the role of bonding in creep behavior under tensile conditions. Furthermore, all studies were conducted using the same raw materials, drying techniques and fiber orientations.

The following thesis contains a literature review which only topics relevant and related to satisfying the overall objective of this thesis are covered. Specific focus was given to tensile creep behavior in paper and fibers. Further review is given to polymeric materials, as fibers are composed of naturally occurring polymers. Bonding and other tensile deformation behaviors in paper were discussed when relevant. Reference to modeling and accelerated creep behavior under tension was also covered within the literature review.

The remainder of the thesis is comprised of a series of results chapters. These chapters present results that satisfy the objective of discerning the role of bonding in the tensile creep behavior of paper. From these results chapters, several unique findings and analyses are presented which are fundamentally significant and were previously unknown (or unclear) with regard to bonding and tensile creep behavior in paper. These are summarized below.

- A comprehensive analysis of paper produced under a range of bonding levels has shown how bonding influences tensile creep behavior. Specifically, it was proven that bonding influence on tensile creep behavior is related to sheet efficiency and how effectively stress is distributed within the sheet structure.
- Analysis of bonded area loss during creep straining has shown what influence it has on tensile creep behavior. That is, bonded area loss is a strain-induced phenomenon. Thus, bonded area is lost only as a result of straining and does not contribute toward strain.

- It has been shown that it is possible to isolate, account for, and incorporate bonding into a mathematical model based on the fundamental deformation mechanisms of the components of which the fibers are comprised.
- The role of bonding in accelerated creep was clarified and was used to justify or refute proposed accelerated creep mechanisms. Specifically, it was shown that bonding is not the cause of accelerated creep behavior. Bonding does not influence accelerated creep behavior any more than it influences constant humidity creep.
- Overall, it was found that the role of bonding in tensile creep behavior (and accelerated creep) is no different than its role in stress-strain behavior.

CHAPTER 2: LITERATURE REVIEW

2.1 Fiber Composition and Morphology

Paper is a complex structure composed of a network of bonded fibers. According to Kortschot [1], this paper structure can be analyzed or characterized on many hierarchal levels. Paper structure and behavior can be considered as a function of the fiber composition and morphology and the subsequent processing, orientation, distribution, and interaction of these fibers to form a network structure and create paper. When considering the deformation behavior of paper, all of these factors will have an influence. This section specifically addresses fiber composition and morphology. As fibers are the raw material used to manufacture paper, they will dictate its fundamental behavior.

The fibers used to manufacture paper are often derived from naturally occurring, renewable resources. Specifically, wood cells of softwood and hardwood trees are processed into fibers for papermaking. As a result of being a natural raw material, there will be a great deal of variability and heterogeneity associated with it. This variability and heterogeneity manifests itself across tree species, within tree species, wood cells within a tree, and the composition within a wood cell [2]. As a result, the properties of papermaking fibers will vary considerably and therefore have a corresponding influence on paper properties. That said, wood cells all have the same general composition and morphology. Wood cells are composed of natural polymers consisting of cellulose, hemicelluloses, and lignin [1-4].

Other than their molecular makeup, these polymeric constituents are defined by the composition of their molecular network. When reference is given to the molecular

network of the polymers within a wood cell, papermaking fiber, or other polymeric material, it refers to the arrangement of the molecules that compose the polymer (i.e. the molecular network arrangement is amorphous (disordered), crystalline or partially crystalline). Reference to these types of molecular networks are given throughout this thesis.

Cellulose is a polysaccharide of β-D Glucopyranose and is a linear chain molecule that is arranged in a partially crystalline molecular network within wood cells [1-3]. Crystallinity ranges between 50% and 70% with the remainder of the cellulose being in amorphous disordered arrangements [3]. Hemicelluloses are also polysaccharides, and are composed of combinations of monosaccharides, which include β -D Mannopyranose, β -D Galactopyranose, β -D xylopyranose and several others [3]. Hemicelluloses have a linear backbone, possess branches and have a lower degree of polymerization relative to cellulose [1-3]. As a result, they do not crystallize as readily and are amorphous in nature [4]. Lignin is a highly branched amorphous polymer and is composed of phenylpropane units consisting of coniferyl alcohol and sinapyl alcohol [3].

Within a wood cell, (known as a tracheid in softwood and a fiber in hardwood), cellulose is arranged in tightly packed partially crystalline strands known as microfibrils [2]. Deposits of amorphous hemicelluloses and lignin surround these microfibrils forming a matrix [2]. This resulting composite material (cellulose microfibrils, hemicelluloses and lignin) is arranged in cell wall layers within a wood cell [2]. Figure 1 shows a general representation of a wood cell showing cell wall layers.

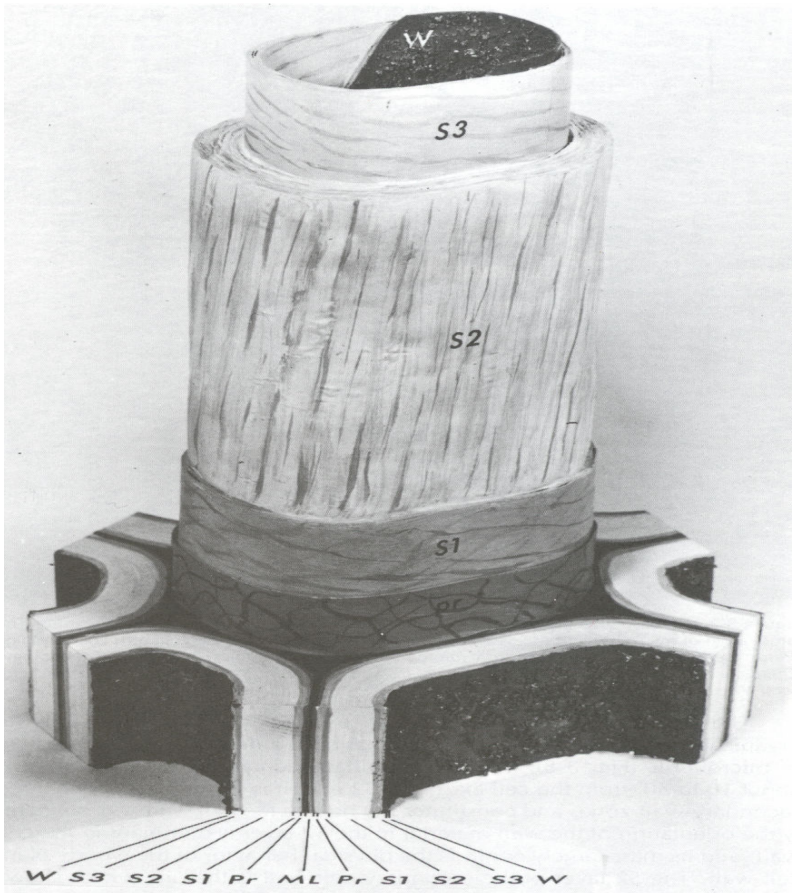

Figure 1 General Representation of a Wood Cell Showing Cell Wall Layers [2]

Although this is a representation of a softwood tracheid, Panshin and De Zeeuw [2] discussed that such a generalization can also be applicable to hardwood fibers. As shown in Figure 1, cell walls are separated by a middle lamella (Ml) composed of pectin. The cell well itself is composed of a primary wall (Pr), a secondary wall consisting of three layers (S_1, S_2 and S_3 layers) and a warty layer (W) that lines the lumen. In the primary wall, cellulose microfibrils are arranged randomly [2]. In the secondary wall, specifically the S_2 layer, cellulose microfibrils are arranged in a helical matrix about the vertical axis of the wood cell [2]. Of all the cell wall layers, the S_2 layer is the largest and is considered to be the component of the cell wall that dictates the properties of the

resulting fiber used in papermaking [1, 4]. In addition, this is the cell wall layer that contains the most cellulose [2, 3]. As shown in Figure 2, cellulose is most prevalent in the S_2 layer and to a lesser extent in the thin S_1 and primary wall layers.

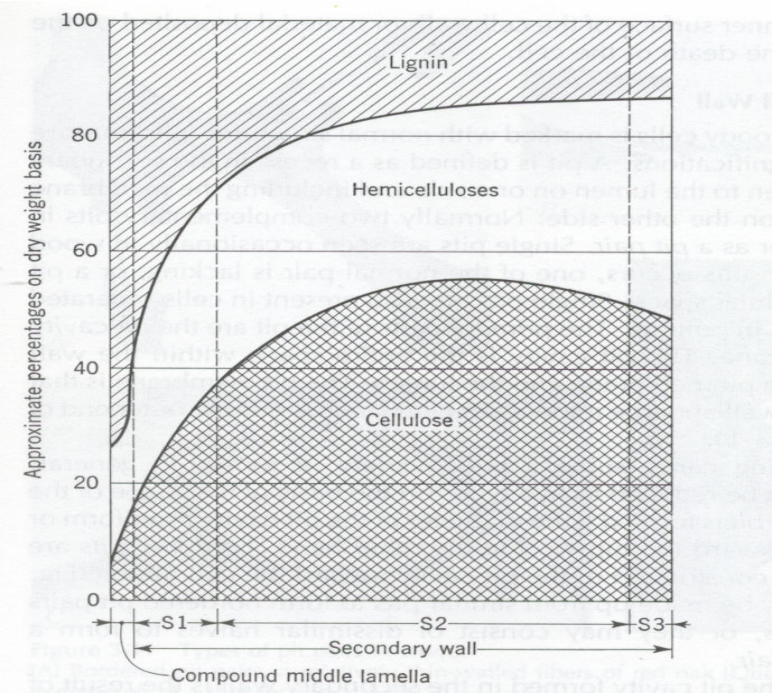

Figure 2 Distribution of Cellulose, Hemicelluloses and Lignin Within Cell Wall Layers [2]

Even though hemicelluloses and lignin are present within the wall of a wood cell and therefore the resulting fiber, the primary load-bearing component is considered to be cellulose, especially at lower S_2 fibril angles [1, 5]. Therefore, the fundamental deformation behavior of paper should show similarities and relate to the behavior of cellulose, cellulosic materials and other similar polymers. However, it is not implied that hemicelluloses and lignin are not influential. They are the composite matrix material surrounding the cellulose microfibrils and therefore act to distribute load. They also have

a significant influence in deformation if load is applied transverse to the orientation of the microfibrils. As a result, the effect hemicelluloses and lignin have on deformation behavior can not be disregarded within mechanical pulp fibers. In fibers produced from a chemical pulping process, as is the case with much of the previous research on tensile creep in paper, the lignin and to lesser extent hemicelluloses are greatly reduced, especially if the pulp is also bleached [3, 4]. Use of a bleached chemical pulp in a creep study makes it possible to eliminate the lignin contribution towards deformation and reduces the impact of hemicelluloses.

2.2 Generalized Deformation Behaviors

2.2.1 Elastic, Plastic and Viscous Behaviors

Before reviewing the creep behavior of paper and polymeric materials in general, it is necessary to cover and define some general deformation behaviors and terminology referred to throughout this thesis. The first of these discussed is elastic behavior. If a material is said to behave elastically, it means there will be an instantaneous strain upon application of a stress; there is no time dependence in the deformation [6]. As a result, if this stress remains and is held constant, the amount of strain will remain the same. When the stress is removed, the material will fully recover, and return to its original state [6-8]. In many materials, elastic deformation is linear, meaning an increase in stress will result in a proportional increase in strain [6]. However, this is not a requirement of elastic behavior. Rubber has been shown to possess elastic behavior that is non-linear [7]. Within this thesis, elastic behavior is referred to as time independent deformation (or strain) that is fully recovered upon removal of the stress. Linearity is not inplied unless it

is specifically mentioned. Most materials, including polymeric materials, will exhibit a degree of elastic behavior which is most prevalent at low applied stresses [6]. Figure 3 illustrates a stress-strain curve showing elastic behavior.

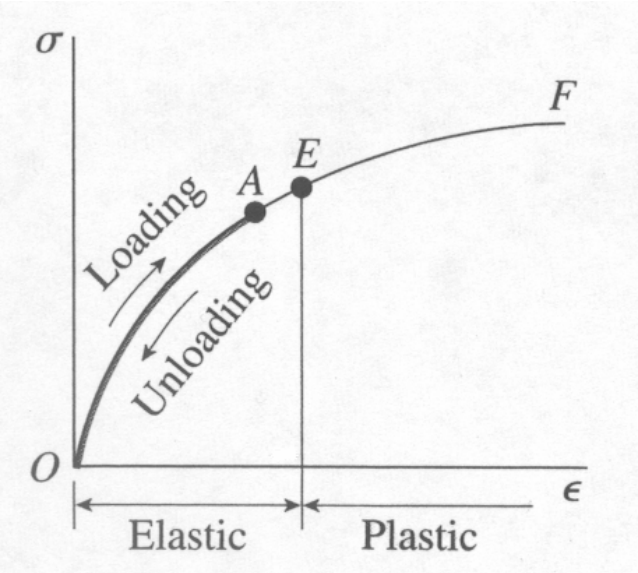

Figure 3 Stress-Strain Curve Showing Elastic Behavior [7]

As shown in Figure 3, a material is stressed to point A, resulting in an elastic strain. Upon removal of that stress, the material retraces the deformation path and fully recovers. Also indicated on Figure 3 is point E, which separates the stress-strain curve into two regions, one elastic and one plastic. Once a threshold stress is surpassed, referred to as the elastic limit (point E on Figure 3), some of the resulting strain will not fully recover, it becomes permanent [6-8]. This permanent deformation is referred to as plastic deformation [6-8]. As with elastic behavior, plastic behavior is considered to be time independent, although some dependence may be observed [6]. Figure 4 shows a stress-strain curve where the elastic limit is exceeded and plastic strain results.

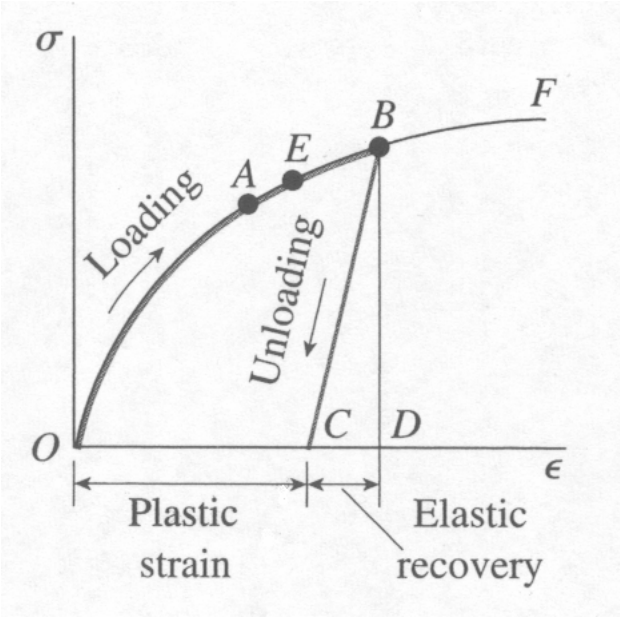

Figure 4 Stress-Strain Curve Showing Both Elastic and Plastic Behavior [7]

In Figure 4, a material is stressed beyond the elastic limit to point B. This results in both elastic and plastic strain. Upon removal of the applied stress, the elastic strain recovers and the plastic (permanent) strain remains. Often, plastic behavior is commonly discussed and more appropriate when referring to the deformation behavior of metals [8]. As a result, plastic behavior is only discussed on a limited basis within this thesis with regard to the deformation behavior of paper and polymeric materials. This is because the permanent deformation associated with polymeric materials such as paper possesses time dependence, which cannot be ignored [6, 8]. In the cases where elastic limits and plastic behavior are referred to, the terms are only used to differentiate regimes of deformation and do not imply time independence. When stress is below the elastic limit, deformation is said to be fully recoverable (or in the elastic region) and when stress is above the elastic limit, deformation is said to be partially recoverable (or in the plastic region).

The last general deformation behavior discussed is viscous behavior. Viscous behavior is a type of deformation that is characteristic of fluids [8, 9]. Like plastic behavior, viscous behavior results in a permanent deformation (or flow) [6, 8, 9]. Unlike plastic behavior, a material that exhibits a viscous behavior has a deformation (or flow) with a significant time dependence [6, 8, 9]. If a stress is applied to a viscous material such as a fluid, the material will flow as long as the stress is applied [6, 8, 9]. Furthermore, the higher the applied stress, the greater the rate of flow [8, 9]. Although, viscous behavior is characteristic of a fluid, it can be an important component of the deformation of solid materials, especially in polymeric materials (i.e., paper).

2.2.2 Viscoelastic Behavior

Within paper and other polymeric materials, it is not adequate to classify their deformation behavior simply as elastic, plastic or viscous. Rather, polymeric materials are considered to fall in the class of viscoelastic materials [6, 8, 10, 11]. Other than paper, this includes plastics, wood, natural and synthetic fibers, organic polymers, concrete and metals at high temperature [6, 8]. Viscoelastic behavior explains the deformation behavior of a material that possesses the characteristics of both an elastic and viscous material [6, 8, 11, 12]. As a result, when a stress is applied to a viscoelastic material, it will exhibit a combination of elastic strain (recoverable and time independent), viscous strain (permanent and time dependent), and delayed elastic strain (recoverable and time dependent) [6, 8, 11, 12]. Delayed elastic behavior is a true combination of elastic and viscous behaviors and is unique to a viscoelastic material [8]. Figure 5, Figure 6, Figure

7, and Figure 8 illustrate the deformation behaviors that are characteristic of a material that exhibits a viscoelastic response.

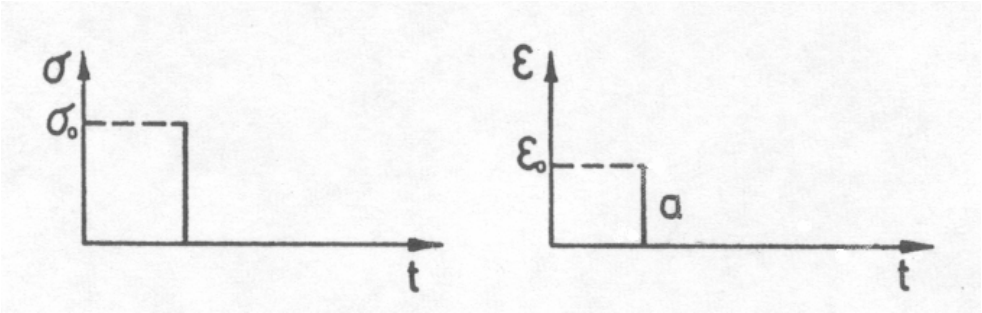

Figure 5 Deformation Behaviors of a Viscoelastic Material: (a) elastic behavior [6]

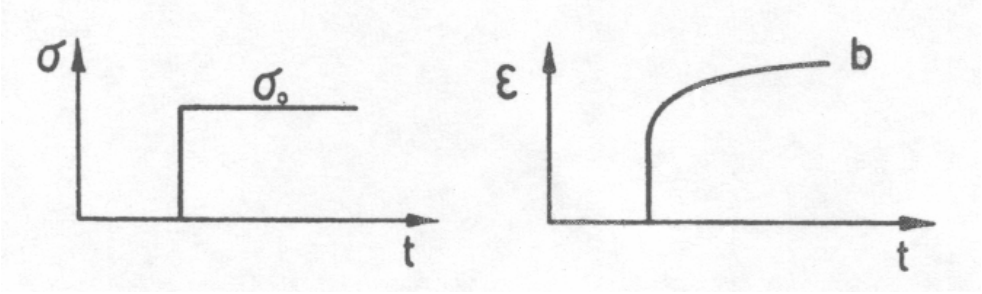

Figure 6 Deformation Behaviors of a Viscoelastic Material: (b) creep behavior [6]

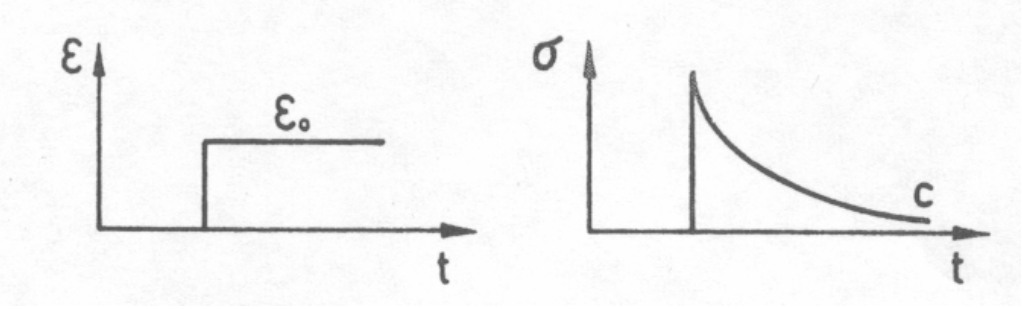

Figure 7 Deformation Behaviors of a Viscoelastic Material: (c) stress relaxation behavior [6]

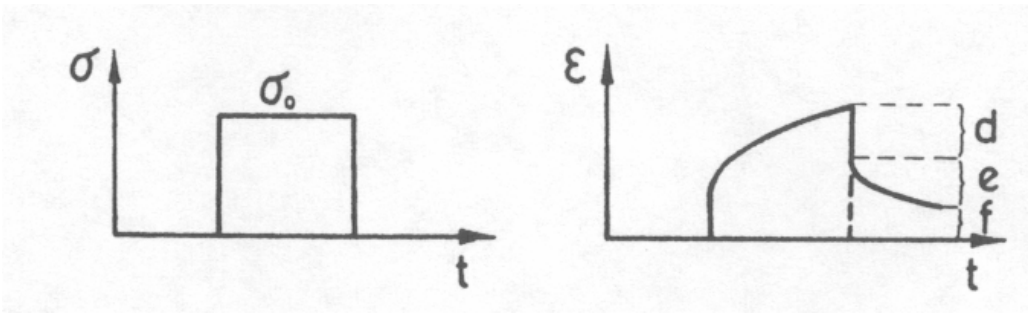

Figure 8 Deformation Behaviors of a Viscoelastic Material: (d) elastic recovery, (e) delayed elastic recovery, (f) permanent deformation [6]

As shown in Figure 5, if a stress is applied to a viscoelastic material, there will be an initial elastic strain. If this stress is held constant for a period of time, there will be a time dependent increasing strain as shown in Figure 6. This is referred to as creep and is the focus of the main body of work within this thesis. A complement to creep is illustrated in Figure 7 where strain is held constant and stress decreases with time. This is referred to as stress relaxation. In Figure 8, a creep curve is again shown with its subsequent recovery curve. This recovery behavior results from the removal of the applied stress. As shown in the figure, there will be an immediate elastic recovery (d), a delayed elastic recovery (e) and a permanent deformation (f). It is apparent that the creep that occurred prior to the removal of the applied stress involved both delayed elastic and viscous strain.

Most materials, including polymeric materials, behave as non-linear viscoelastic materials. Only when applied stresses and times are low, can these materials be approximated as linear viscoelastic [6]. In fact, when times are very low (close to moment when stress was applied), a viscoelastic material can almost be approximated as linear elastic [6]. At higher stresses and times, these same materials will show their non-

linear viscoelastic character [6]. The effect of increasing time and stress results in more non-linear strain. This means that stress and strain can no longer be accurately approximated as linearly proportional to each other.

2.2.3 Description and Characterization of Creep Behavior

As a result of being viscoelastic, polymeric materials will exhibit creep behavior. Creep behavior is characterized as a time dependent deformation (strain) upon application of a constant stress [6, 8, 11, 12]. As this applied stress is increased, so does the amount of creep. Often, most creep testing is conducted under a constant load, but this is considered to be a close approximation of constant stress under low strains [6]. That said, stress does change during straining if a constant load is applied. Therefore, initial applied stress is often referred to within this thesis to describe the creep behavior of a material where testing was conducted under a constant load.

Creep behavior can be described and characterized in many different ways. Figure 9 shows an illustration of a creep curve at one initial applied stress level and shows the components of creep deformation.

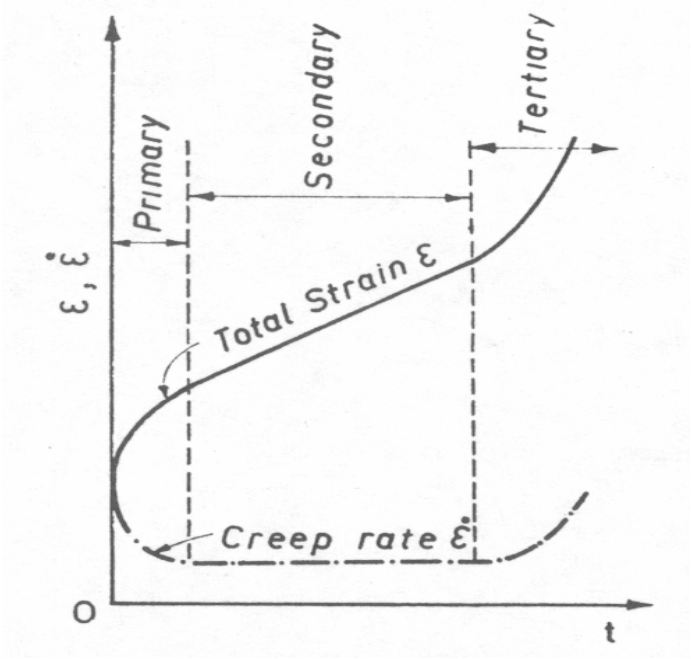

Figure 9 Illustration of a Creep Curve Showing the Components of Creep Deformation [6]

Figure 9 is a creep curve where strain is plotted versus time. In addition, strain rate is plotted versus time. In polymeric materials such as paper, total creep strain can be broken down into four components of strain. These are initial elastic strain, primary creep, secondary creep and tertiary creep. These terms are often used to describe creep behavior in metals where initial elastic strain is the instantaneous strain that occurs during initial loading, primary creep is where the creep rate is a function of time and decreases as time increases, secondary creep is where the creep rate is steady state (or nearly steady state), and tertiary creep displays an increase in creep rate close to the failure of the material [6, 13]. Initial elastic strain and primary creep are fully recoverable, while secondary creep and tertiary creep are non-recoverable [6, 13].

When considering polymers such as paper, Coffin [13] points out that secondary creep is not steady state as it is in metals, rather it is a function of time where creep rate

decreases as time increases. As a result, primary creep and secondary creep are only differentiated by their recoverability, where primary creep is recoverable and secondary creep is non-recoverable. Hence, strain rate time dependence is not considered as a factor in defining creep components within this thesis. Furthermore, Figure 9 is not intended to imply that components of creep occur one after another. While initial elastic strain and tertiary creep may occur only at the beginning and end of creep respectively, primary and secondary creep are often considered to occur simultaneously [6, 8, 11-13]. The separation of creep between primary and secondary on Figure 9 refers to the end of any significant primary creep and the beginning of a regime where secondary creep is dominant.

As creep in polymeric materials is non-linear, creep can also be related to compliance and expressed in master creep curves. In a linear material, total strain from creep is determined by taking the product of a time dependent proportionality constant and initial applied stress. In creep behavior this proportion is known as compliance. Equation 1 shows the relation where total strain from creep, ε, is the product of compliance, J(t), and initial applied stress, σ_o.

$$\varepsilon = J(t)\sigma_o$$

Equation 1 Linear Creep Relation Where Compliance is a Function of Time [6, 11, 13]

As a result, if a creep curve is divided by initial applied stress, the resulting plot would be creep compliance versus time. If a material is linear, no matter what the initial applied stress, the creep compliance versus time curve will be the same. This is shown in

Figure 10 (a) and (b). If creep behavior is non-linear, creep compliance versus time will not collapse onto the same curve as shown in Figure 10 (c). Creep compliance is no longer a function of time, but is also a function of initial applied stress. Equation 2 shows a simple relation where creep compliance is now a function of initial applied stress and time.

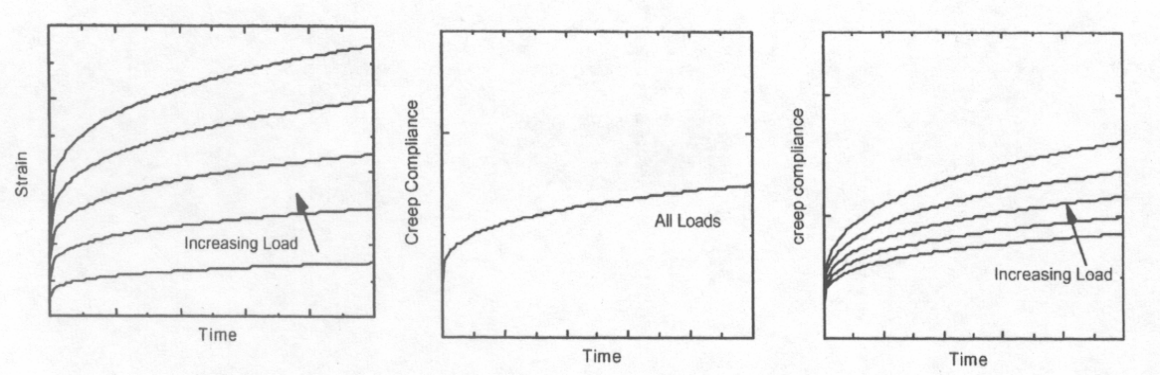

Figure 10 (a) Total Strain from Creep versus Time at Several Initial Applied Stresses, (b) Creep Compliance versus Time for a Linear Material, (c) Creep Compliance versus Time for a Non-Linear Material [13]

$$\varepsilon = J\left(t, \sigma_o\right)\sigma_o$$

Equation 2 Non-Linear Creep Relation Where Compliance is a Function of Time and Initial Applied Stress [13]

In order to better understand the non-linear creep behavior in polymers (including paper), a master creep curve can be created. If the creep compliance versus time curves in Figure 10 (c) are shifted in time so they overlap, they result in the "master creep curve" shown in Figure 11. The larger the time shift, the more non-linear the creep behavior is. Furthermore, by forming a master creep curve, it shows that the effect of increased initial

applied stress results in the predictable shifting of increased creep to a shorter time. The master creep curve also allows the time-scale at one stress to be extended by measuring the creep at several higher applied stresses.

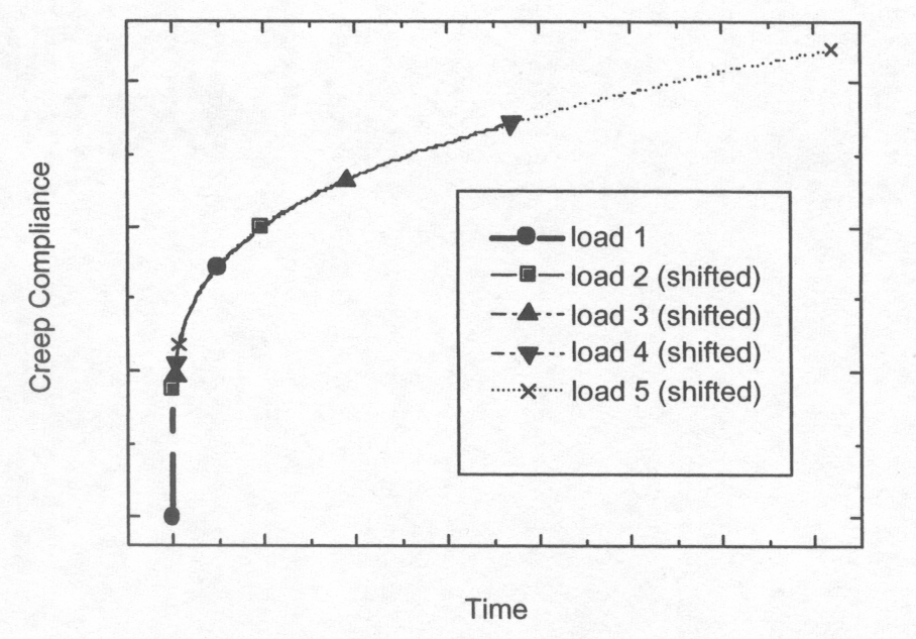

Figure 11 Illustration of a Master Creep Curve Where the Data Points Show the Beginning and End of Each Creep Compliance Curve [13]

Due to the slow rate of creep, it is often more practical to compare creep strain with log time rather than the real time. Figure 12 shows an example of creep curves plotted versus log time at various initial applied stresses. Using this type of plot allows for an easier comparison of creep behavior over a large time scale. A drawback to using this type of curve is the separation between primary and secondary creep regimes is no longer visible. Similar to real time plots, master creep curves can also be generated in log time.

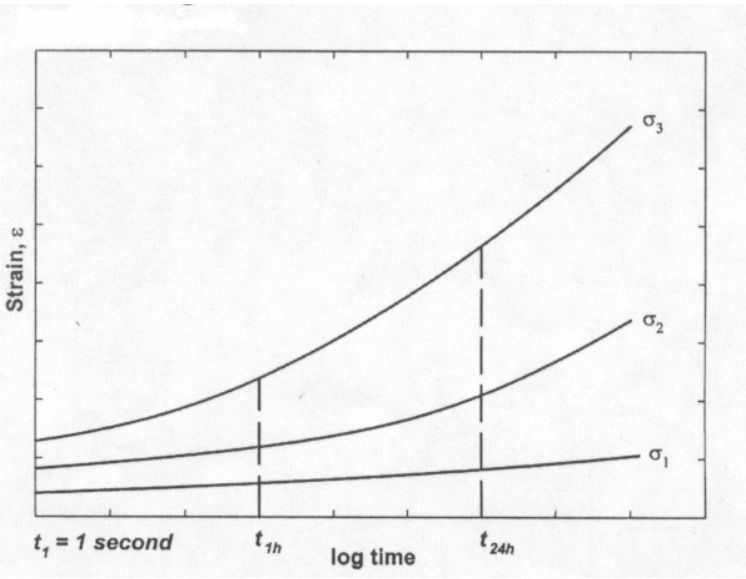

Figure 12 Illustration of Creep Curve Showing Total Strain from Creep versus Log Time [14]

All of the previous creep curves shown are plots of total strain from creep (or creep compliance) versus time (or log time). Another way to describe and characterize creep behavior is by using isochronous stress-strain curves. Isochronous stress-strain curves are generated by plotting total strain from creep versus initial applied stress at various snapshots of time [13-17]. Figure 13 shows examples of creep data being presented in the form of isochronous stress-strain curves. Notice that in each curve, time is held constant.

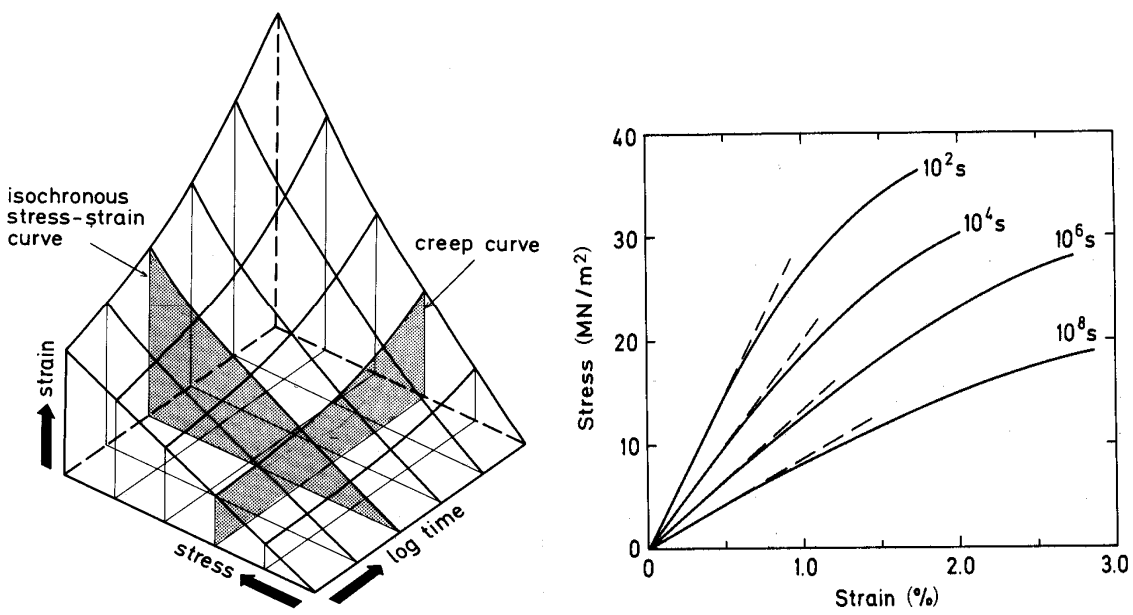

Figure 13 Examples of Creep Data Expressed in the Form of Isochronous Stress-Strain Curves [15]

Panek et al. [14] and Soremark et al. [18] considered the use of isochronous stress-strain curves as an effective way to analyze, simplify and present creep data in paper and refer to others who have effectively used these curves in polymeric materials. They are also effective in making comparisons with stress-strain behavior from other types of material testing techniques, such as stress-strain curves generated under a constant strain rate.

There are also several other ways creep behavior can be analyzed, but the ones discussed in this section are the only ones referred to in the remainder of this thesis. Specifically, isochronous stress-strain curves and creep versus log time curves are used in the presentation and analysis of the results presented in Chapters 5-8.

2.3 Creep Behavior in Polymeric Materials

2.3.1 Polymer Creep Behavior and Mechanism

In the previous section, it was discussed that there are many ways to describe and characterize deformation behaviors and specifically viscoelastic creep. These methods are often used to simplify discussion of the mechanisms involved in the creep behavior of paper. Before discussing that, it is first necessary to review the creep behavior of polymeric materials. This is necessary because the fibers that compose paper are themselves composed of natural polymers. Specifically, the primary load-bearing component in a papermaking fiber is cellulose and is a linear chain molecule arranged in a partially crystalline molecular network, meaning it contains amorphous disordered regions and crystalline regions [1]. In addition, hemicelluloses and lignin, which are also present in a papermaking fiber, are amorphous as well [4, 10].

The previous section discussed that creep can be broken down into four components. These are initial elastic strain, primary creep, secondary creep, and tertiary creep. Of those, tertiary creep is not considered here, as it is deformation that only occurs just prior to failure. As discussed by Coffin [13], paper exhibits a negligible amount of tertiary creep and is therefore not a significant contributor towards the total strain due to creep. Further justification of this will be presented in Chapter 6.

The first component of creep considered is the initial elastic strain. When Meredith [19] referred to the elasticity associated with polymeric materials, he discussed that linear chain molecules and the molecular network of which they are arranged will instantaneously strain upon application of a stress. When this stress is removed, the strain will instantaneously fully recover. In terms of the polymers papermaking fibers are

composed of, initial elastic strain involves the instantaneous straining of cellulose chains and of the molecular (partially crystalline) network of which they are arranged. In addition to the cellulose, the branched hemicelluloses chains and lignin, and the amorphous molecular networks of which they are arranged, will also exhibit an instantaneous straining that contributes to the initial elastic strain.

With regard to primary creep and secondary creep, the mechanism associated with their strain is often related to potential (or reaction rate) theory [12, 19-23]. The basis for this is the work of Eyring [24] who described viscosity using reaction rates and potential barriers. The theory says that in order for flow (strain) to occur, a potential barrier must be overcome [11, 19-21, 23]. The addition of stress acts to shift this barrier to where the energy required to overcome it becomes less in one direction [11, 19-21, 23]. This causes a bias and allows the flow (strain) of molecular segments within the polymer to preferentially occur. Figure 14 shows an illustration of potential barriers in the unstressed and stressed state.

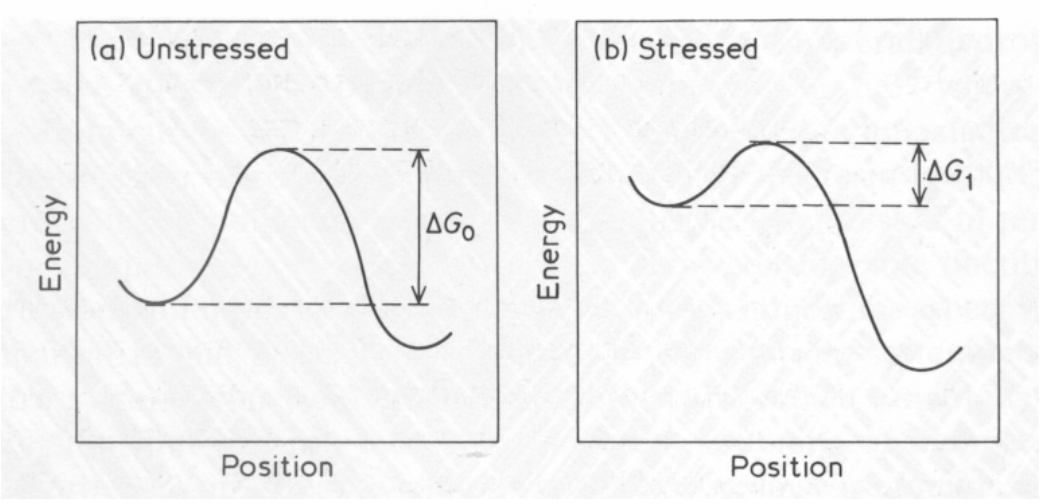

Figure 14 Illustration of Potential Barriers for Flow (Strain) of Polymers: (a) Unstressed, (b) Stressed [11]

As shown in Figure 14 (a), the energy required for a molecular segment to 'jump' the barrier and move to new location within the polymer molecular network is ΔG_o. In the unstressed state, the likelihood of this barrier being overcome is equal in both directions. As a result, a molecular segment is just as likely to jump across the barrier and move to a new location in the opposite direction. If the polymeric material is stressed, the potential barrier will shift as shown in Figure 14 (b). The energy required for molecular segments to jump to a new location will be less in the direction of the stress. This new energy is labeled ΔG_1 on Figure 14 (b). As shown in the figure, it is now less likely that a molecular segment will jump across the barrier in the opposite direction.

Mathematically, molecular segments jumping across a potential barrier and moving to a new location can be related to a strain rate based on an Arrhenius reaction rate [11, 12, 19, 21]. Equation 3 shows an Arrhenius rate equation for the frequency, n_o, of molecular segments jumping the potential barrier and moving to a new location in the unstressed state.

$$n_o = \frac{kT}{h}\exp\left(-\frac{\Delta G_o}{kT}\right)$$

Equation 3 Frequency of Molecular Segments Jumping a Potential Barrier in the Unstressed State Calculated from an Arrhenius Rate Equation [11, 21]

In Equation 3, h is Planck's Constant, k is the Boltzmann Constant and T is absolute temperature. If a stress is applied to the polymeric material, the potential barrier will shift. As a result the frequency, n_f, of molecular segments jumping the potential

barrier and moving to a new location in the direction of the applied stress is given by Equation 4.

$$n_f = \frac{kT}{h}\exp\left(-\frac{\Delta G_o - 0.5\sigma_o v}{kT}\right)$$

Equation 4 Frequency of Molecular Segments Jumping the Potential Barrier in the Direction on an Applied Stress [11, 21]

In Equation 4, the energy required to jump the potential barrier in the direction of the applied stress, ΔG_o, is reduced by one-half of the product of the applied stress, σ_o, and the volume of the empty space, v, that the molecular segment is moving to. In Figure 14 (b), ΔG_1 is equal to ΔG_o minus $0.5\sigma_o v$. By solving Equation 3 for kT/h and substituting into Equation 4, a simplified Equation 5 results.

$$n_f = n_o \exp\left(\frac{\sigma_o v}{2kT}\right)$$

Equation 5 Frequency of Molecular Segments Jumping the Potential Barrier in the Direction of the Applied Stress in a Simplified Form [11, 21]

Similarly, the frequency of molecular segments jumping the potential barrier and moving to a new location in the direction opposite to the applied stress can be found. Equation 6 shows the frequency, n_b, of molecular segments jumping the potential barrier and moving to a new location in the direction opposite to the applied stress. The resulting equation is similar to Equation 5, but the term in the exponential is negative.

$$n_b = n_o \exp\left(-\frac{\sigma_o v}{2kT}\right)$$

Equation 6 Frequency of Molecular Segments Jumping the Potential Barrier in the Direction Opposite to the Applied Stress [11, 21]

The flow rate of the net movement of molecular segments in the direction of the applied stress is equal to the difference between the frequency of molecular segments jumping in either direction times the volume of the empty space. Equation 7 illustrates this where Q is flow rate.

$$Q = v\left(n_f - n_b\right) = v n_o \left[\exp\left(\frac{\sigma_o v}{2kT}\right) - \exp\left(-\frac{\sigma_o v}{2kT}\right)\right]$$

Equation 7 Flow Rate Molecular Segments upon Application of a Stress [11, 21]

The strain rate (time dependent strain of primary and secondary creep) is found by dividing Equation 7 by the volume of the molecular segment, V. Equation 8 and a simplified Equation 9 illustrates this, where dε/dt is strain rate.

$$\frac{d\varepsilon}{dt} = \frac{v n_o}{V}\left[\exp\left(\frac{\sigma_o v}{2kT}\right) - \exp\left(-\frac{\sigma_o v}{2kT}\right)\right]$$

Equation 8 Strain Rate of a Polymeric Material Based on Potential Theory [11, 21]

$$\frac{d\varepsilon}{dt} = \frac{2vn_o}{V}\sinh\left(\frac{\sigma_o v}{2kT}\right)$$

Equation 9 Strain Rate of a Polymeric Material Based on Potential Theory (Simplified Form) [11, 21]

Overall, potential theory, as an explanation for time-dependent deformation (creep) stems from the premise that there must be empty volumes or voids within the molecular network [11, 19, 21]. These voids are necessary so molecular segments can jump a potential barrier and flow (strain) upon application of stress [11, 19, 21]. If a polymeric material is crystalline, there will not be as many voids due to the well-organized structure. As a result, the amount of flow in crystalline regions should be insignificant relative to amorphous regions where disorder persists and voids are present. Findley [20] discussed the tendency for crystalline polymers to be more creep resistant. Therefore, this theory is often applied to polymeric materials whose molecular network contains amorphous regions [11, 19, 21-23]. While, the initial elastic response results in strain from both the crystalline and amorphous regions of a polymeric material, time-dependent deformation (primary and secondary creep) occurs primarily within the amorphous regions of the molecular network. Within papermaking fibers, primary and secondary creep originates from the amorphous regions of the cellulose molecular network, and from the fully amorphous networks of the hemicelluloses and lignin (if present) [10, 17].

Understanding that primary and secondary creep can both be explained using potential theory, there is still a difference between them. Primary creep is recoverable and secondary creep is non-recoverable strain. This relates specifically to the type of

deformation that is occurring within the polymer molecules. Meredith [19] discussed primary creep behavior as a delayed elastic response within the amorphous regions in the molecular network of a polymer. More specifically, Alfrey [25] discussed primary creep as flow resulting from the uncurling of molecular chains within the amorphous regions of a polymer network. In terms of papermaking fibers, primary creep strain would be the uncurling of cellulose chains within the amorphous region of the cellulose molecular network. Uncurling of the amorphous hemicelluloses and lignin (if present) also occurs and contributes.

For secondary creep, Alfrey [25] discussed that this permanent time-dependent deformation involves the sliding of molecular segments past one another within the amorphous region of the molecular network. Tobolsky and Erying [23] similarly discussed the flow of molecular segments and the breaking of network bonds. In terms of papermaking fibers, secondary creep strain would be due to the sliding of cellulose chain segments past one another within the amorphous regions of the molecular network. The flow of amorphous hemicellulose segments and lignin (if present) would also contribute.

Overall, the work of Olsson and Salmén [26] offered support to the rationale that these molecular mechanisms are part of the explanation for primary and secondary creep strain. Using mid-IR spectroscopy, Olsson and Salmén [26] found that the data suggested an increase in orientation or stretching of cellulose molecules and the indications of sliding between cellulose chains in paper. Although, they did not attribute these observations specifically to primary creep strain and secondary creep strain, increase of orientation could be attributed to primary creep strain and sliding of molecular chains could be attributed to secondary creep strain. This would be consistent with what Alfrey

[25] discusses as the mechanisms behind primary and secondary creep strain in high molecular weight polymers.

2.3.2 Factors Influencing Polymer Creep Behavior

Other than stress and time, there are several other important factors that will influence the amount of creep in a polymeric material. These factors are strongly influenced by the structure of the polymer network. Findley [20] discussed the aspects of polymer structure with regard to creep mechanisms in plastics. In a polymeric material, Findley [20] referred to the presence of primary and secondary bonds. The primary bonds are the intramolecular bonds of the polymer molecule itself (i.e. covalent bonds), while the secondary bonds are weaker polar and van der Waals bonds that connects a network of these polymer molecules. Findley [20] discussed that since primary bonds are much stronger than the secondary bonds, the primary bonds are not significant in allowing flow to occur relative to the secondary bonding. Therefore, the structure of the network, be it crystalline or amorphous, will have a significant impact on its deformation behavior. Findley [20] discussed that if polymers are more crystalline, the density of the polymer will increase and there will be greater forces holding it together (i.e., secondary bonding). In addition, mobility will be greatly reduced as crystalline regions have less empty volumes into which molecular segments can flow. As a result, crystalline regions hinder flow (strain) within a polymeric material [20]. Ferry [27] showed this and discussed that the creep compliance of a highly crystalline polymer is lower than that of an amorphous polymer. Findley [20] discussed that polymeric materials composed of linear chain molecules are more creep resistant due to their ability to form crystalline regions. If bulky

atoms or side groups are attached to these linear chains, this further decreases mobility and increases creep resistance. The previous section alluded to this with regard to time dependent deformation (creep) being attributed to flow within the amorphous regions of a polymeric material [11, 19, 21-23]. In the amorphous regions, there is more disorder and as a result, more empty volume and a lesser degree of strong secondary bonding [20].

In addition to the overall molecular structure of the polymer, considerations must be given to what influence temperature and moisture have on creep behavior. Due to the presence of amorphous regions within a polymeric material, there will be a degree of temperature sensitivity [11, 17]. Ferry [27] showed and discussed that at sufficiently low temperatures, amorphous polymers behave similarly to crystalline polymers due to the lack of empty spaces (volumes) within the polymer network, resulting in lack of mobility of molecular segments. When the temperature is increased, the amorphous regions of a polymeric material will begin to flow (strain) more readily [11]. This was previously revealed in Equation 9 (derived from potential theory) where an increased temperature results in a higher primary and secondary creep rate. Furthermore, it has been shown in paper that an increase in temperature will also lower the elastic modulus [10, 17, 28, 29]. In terms of creep, a lower elastic modulus would result in an increase in initial elastic strain. If temperature is increased enough, the amorphous regions will reach the glass transition temperature [11, 17]. At and above this temperature, the polymer becomes more liquid in nature and empty volumes dramatically increase from the expansion, allowing easier flow of molecular segments upon application of stress [11].

In terms of the polymeric materials within a papermaking fiber, cellulose, hemicelluloses, and lignin are partially or completely composed of amorphous regions.

Therefore, there is a large sensitivity to temperature. Salmén and Back [28, 29] have shown that paper will exhibit a more compliant stress-strain behavior as temperature is increased. They further discussed that this effect is not as dramatic in pulps where the yield is low (i.e., chemical pulps where lignin is removed and hemicellulose content is lower). This is due to smaller amounts of amorphous polymers present to reduce elastic modulus and increase time-dependent deformation as temperature is increased [29]. Figure 15 shows an illustration of temperature dependence on stress-strain behavior in paper.

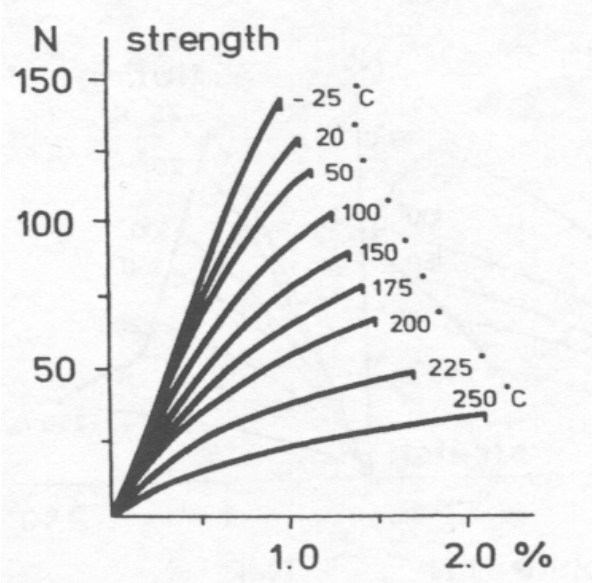

Figure 15 Illustration of Temperature Dependence on the Stress-Strain Behavior of Paper [29]

As shown in the Figure 15, a temperature increase from –25ºC to 250ºC resulted in a decrease in elastic modulus (as shown by the initial slope of the stress-strain curve) and a more compliant overall stress-strain behavior. Further exacerbating the effects of temperature, is the influence of moisture. The addition of moisture to a polymer with

amorphous regions will act as a plasticizer [10, 17]. Findley [20] discussed that water absorbs into the amorphous regions of a polymeric material effectively increasing the amount of empty spaces and disrupting secondary bonding. As a result, the material will become more compliant and exhibit more creep [17, 20]. Furthermore, the addition of moisture, lowers the glass transition temperature and softens the material [17]. In paper, Salmén and Back [28] and Benson [30] show that increased moisture strongly influences the elastic modulus and stress-strain behavior of the material as the moisture results in the softening of the amorphous components of the cellulose, hemicelluloses, and lignin within the fiber. Figure 16 shows an illustration of moisture dependence on the stress-strain behavior of paper.

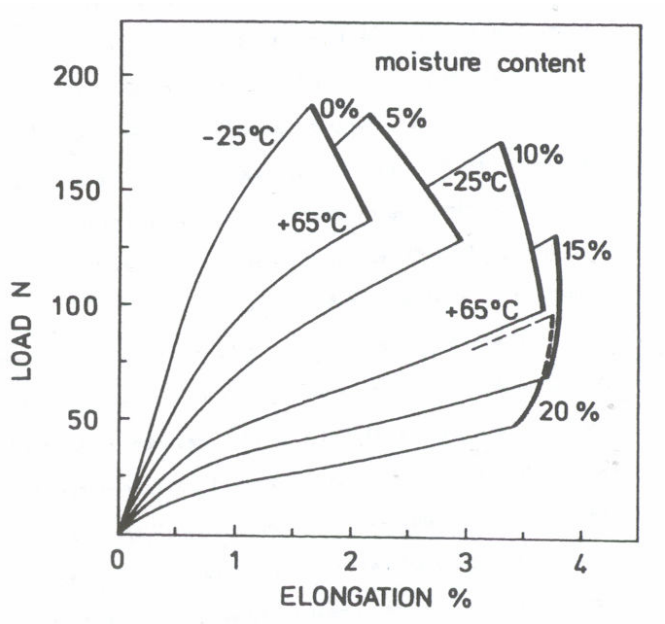

Figure 16 Illustration of Moisture Dependence on the Stress-Strain Behavior of Paper [28]

In Figure 16, an increase in moisture content from 0% to 20% resulted in a dramatic decrease in elastic modulus and increase in the compliance of the stress-strain curve. The figure also shows that if moisture content is increased, a lesser temperature would be required to achieve a similar (less compliant) behavior compared to that observed at lower moisture content.

2.4 Tensile Creep Behavior in Paper and Fibers

The previous section discussed the creep behavior of polymeric materials. Specifically, this focused on polymeric materials that were composed of amorphous or partially amorphous molecular networks. This section focuses on the more specific case of creep behavior in paper and the fibers that compose it. As with other polymeric materials, creep in paper can occur in tension or compression. That said, much of the fundamental research conducted in paper was done in tension. This was due to the ease of the tensile creep measurement versus compression. The problem with compressive creep testing is buckling of the material, which must be accounted for in the analysis. Coffin [13] and Vorakunpinij [31] both discussed the multitude of test methods that have been employed in such an analysis. It is apparent that by measuring the creep behavior of paper in compression, introduction of additional variables that mask the actual fundamental creep response may occur. Therefore, a complete understanding of the creep behavior of paper in tension should be researched prior to adding the additional complexity associated with compression testing. The research presented within this thesis follows that reasoning and only tensile creep studies were conducted. Therefore, the

subsequent sections of this literature survey focuses on tensile creep behavior in paper and fibers. Unless otherwise specified, all reference to creep refers to tensile creep.

Unlike other materials, the research on creep in paper is limited prior to 1950 [32]. Studies by Rance [33], Steenberg [34] and Mason [35] looked at creep behavior in paper prior to 1950 and found, that much like polymeric materials, paper exhibited instantaneous elastic strain, delayed-elastic strain (primary creep) and permanent strain (secondary creep). Their work, while significant was limited and far from complete as they focused on viscoelastic behavior in paper in general, not creep specifically. As Van den Akker [32] points out, one interesting result from the study of Rance [33] was that no matter the initial applied stress and the resulting creep strain rate, the paper failed at the same ultimate strain. This result was the first to show evidence that the failure of paper under creep does not necessarily trend with the strain rate and that deformation behavior and failure behavior are not necessarily coupled.

After 1950, more focus was placed on the creep behavior in paper. The most significant of the work was that conducted by Brezinski [36, 37]. Using an α-cellulose pulp (free of hemicelluloses and lignin), he conducted a thorough study on the creep behavior of paper over a range of initial applied stresses and moisture contents. His work is discussed throughout the remainder of this literature survey and is used, in part, to substantiate the overall conclusions made from this thesis. Brezinski [36, 37] showed similar to previous researchers, that creep in paper behaves like a polymeric material and exhibits an instantaneous elastic strain, a delayed-elastic strain (primary creep) and a permanent strain (secondary creep).

Brezinski [36, 37] discussed several responses to increased initial applied stress on creep behavior in paper. The first and most obvious is as initial applied stress increases, the total strain from creep increases. He further breaks this down and discusses that instantaneous elastic strain will increase as initial applied stress is increased. He also discusses that an increase in initial applied stress will cause delayed elastic strain (primary creep) to increase and terminate at a faster rate. Likewise, permanent strain (secondary creep) will be more significant as higher initial applied stresses are used. He also observed that delayed elastic strain (primary creep) and permanent deformation (secondary creep) will be more prevalent and may exceed instantaneous elastic strain at longer times.

When analyzing creep behavior, Brezinski [36, 37] presented much of his data in the form of strain versus log time plots. As shown in Figure 17, creep is plotted at five different initial applied stress levels with test durations of up to ten days.

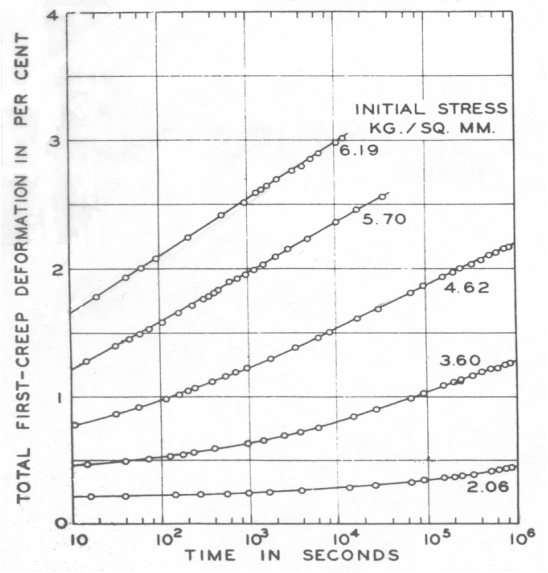

Figure 17 Total Strain from Creep versus Log Time at a Range of Initial Applied Stresses [36]

As shown in Figure 17, creep behavior in paper is linear with log time at high initial applied stresses and times (where secondary creep is more prevalent). By showing this, Brezinski [36, 37] was able to conclude that not only does primary creep strain rate possess time dependence, but secondary creep strain rate must also possess a time dependence. If secondary creep in paper was steady state like metals, creep strain would be linear with time, not with log time, at high initial applied stresses and times. As Coffin [13] commented, creep behavior in polymeric materials do not possess a steady state secondary creep strain rate.

Furthermore, Brezinski [36, 37] generated creep compliance curves from the data in Figure 17 by dividing the creep strain by the initial applied stress. These curves are shown in Figure 18.

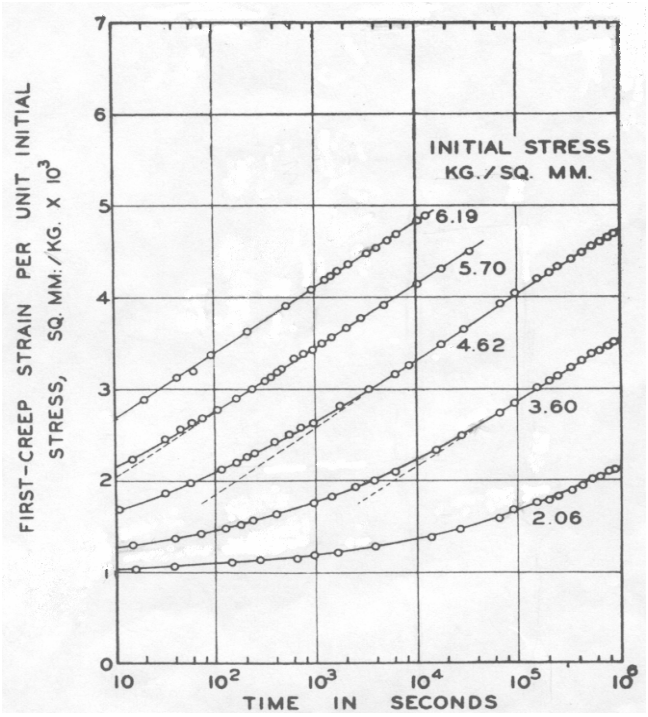

Figure 18 Creep Compliance versus Log Time at a Range of Initial Applied Stresses [36]

From Figure 18, it can be seen that creep behavior in paper is non-linear, as the creep compliance curves do not overlap. Brezinski [36, 37] observed this and found paper behaved like polymeric materials (such as nylon) and a master creep curve could be formed as a result. He shifted the compliance curves in Figure 18 in log time until they overlapped to create the master creep curve shown in Figure 19. He noted that not only could master creep curves be formed, but that the shift in log time required to overlap creep compliance curves was linearly proportional to the initial applied stress.

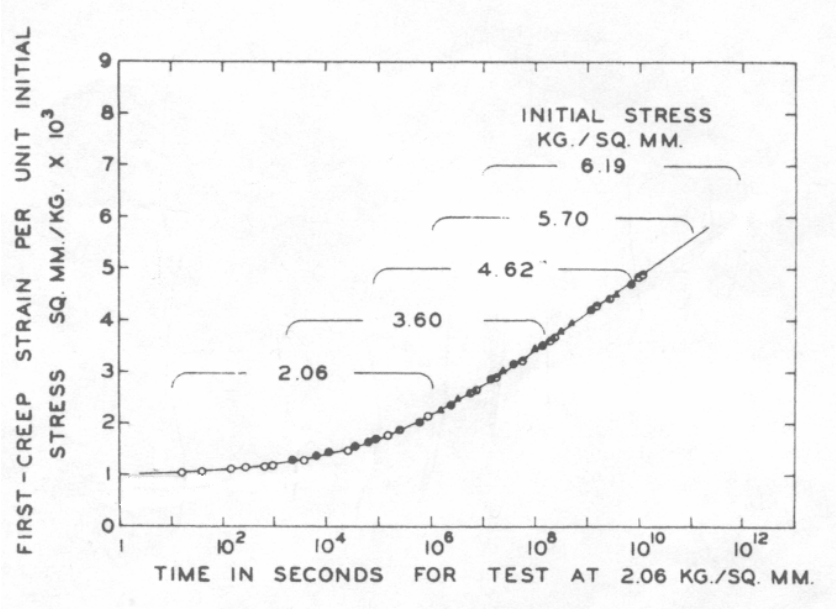

Figure 19 Master Creep Curve for Paper [36]

While the work shown in the previous figures was conducted at 50% RH, Brezinski [36, 37] also conducted creep studies at a range of humidities. Not surprisingly, he showed that as the relative humidity (moisture content) is raised, the amount of strain from creep increases as well. This is consistent with the reaction of a polymeric material when the moisture content is raised and plasticization of amorphous regions occurs.

Figure 20 shows creep curves at a range of relative humidities. In the figure, the initial applied stress used was equivalent to 55% of the 50% RH tensile strength of the paper.

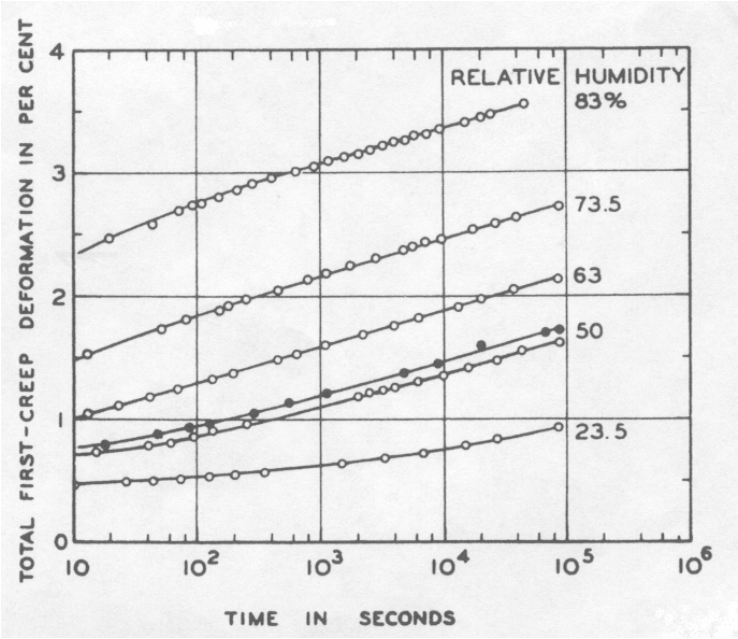

Figure 20 Total Strain from Creep versus Log Time at a Range of Relative Humidities [36]

Overall, Brezinski [36, 37] came to the conclusion that the creep behavior in paper showed tendencies which were consistent with molecular creep mechanisms. Brezinski [36, 37] also observed that by changing the level of wet pressing or the refining level of the fibers, that creep behavior would also change. As a result, his work did not resolve the debate as to whether or not the creep deformation seen in paper occurs as a result of fiber creep or from macroscopic influences (the sheet structure). More specifically, he did not resolve the debate as to whether or not the breakage of bonds between the fibers was the cause of creep in paper.

This was not resolved until Hill [38, 39] studied the creep behavior of individual fibers. Specifically, he studied the creep behavior of short leaf pine fibers that had undergone a holocellulose pulping process in which all lignin was removed. The results from his study correlated well with the results of Brezinski [36, 37]. Hill [38, 39] was able to demonstrate that fibers exhibited an instantaneous elastic strain, a delayed elastic strain (primary creep) and a permanent strain (secondary creep). Similarly, the response to initial applied stress was consistent with the results of Brezinski [36, 37], including a secondary creep strain rate that was time dependent. In addition, the creep response exhibited a non-linear behavior and a master creep curve could be formed. Figure 21 illustrates creep compliance curves versus log time. Figure 22 shows the master creep curve that resulted from the shifting of the creep compliance curves in Figure 21.

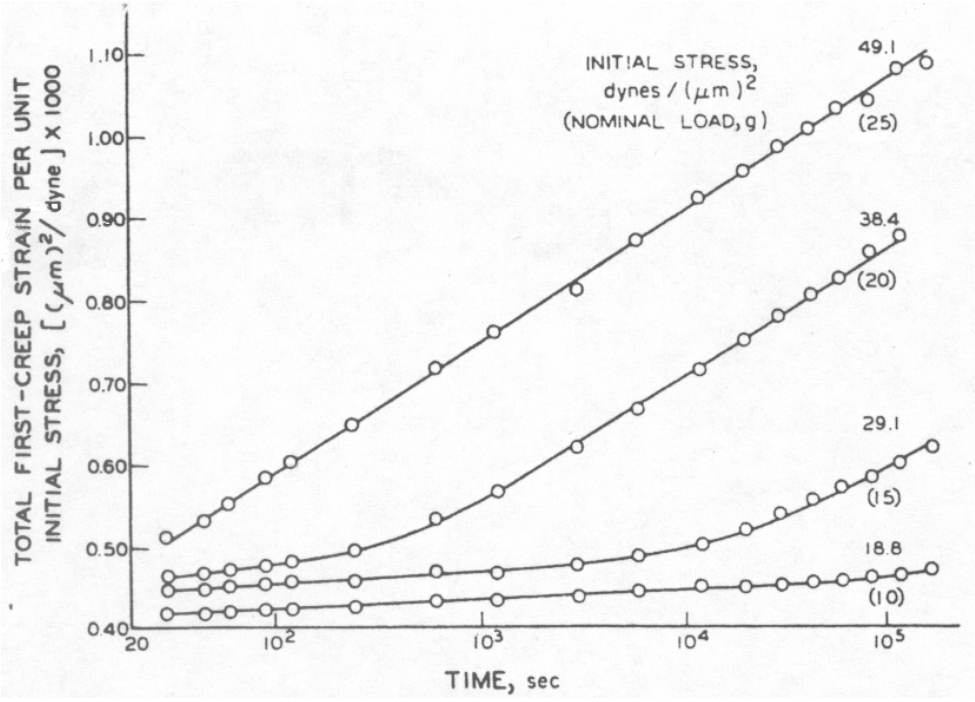

Figure 21 Creep Compliance versus Log Time for Individual Fibers [38]

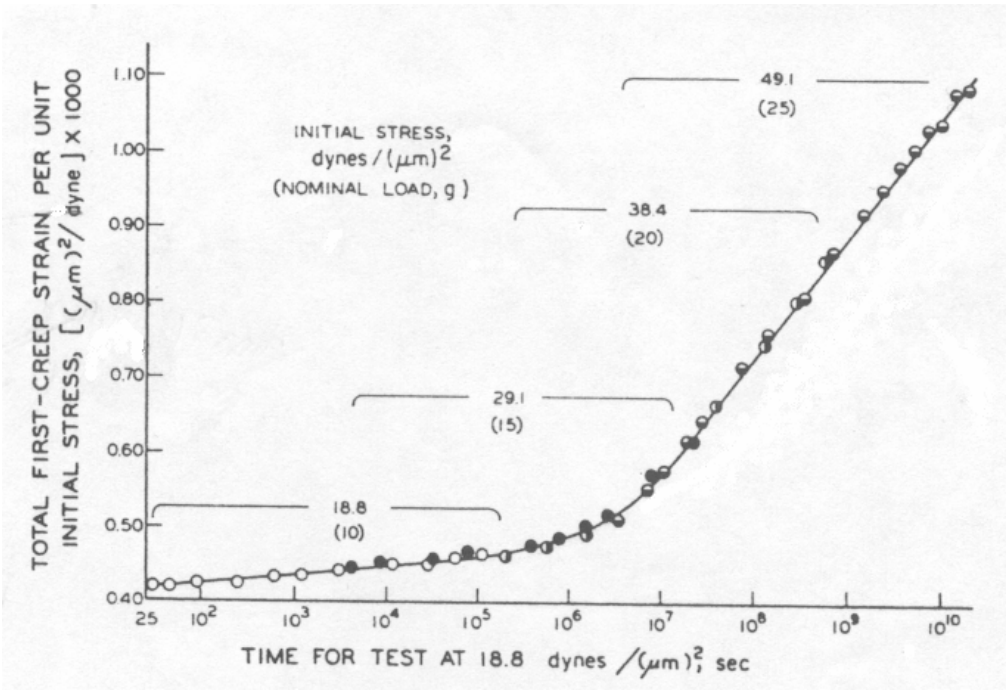

Figure 22 Master Creep Curve for Individual Fibers [38]

Hill [38, 39] also discussed possible structural changes within the fibers as a result of creep. He discussed that the amorphous regions within a fiber would exhibit configuration changes and move slightly, and suggested that this was recoverable strain. He also discussed that when secondary bonds within the molecular network are broken, larger scale movements can occur resulting in permanent strain. This is consistent with what Olsson and Salmén [26] found in paper using mid-IR spectroscopy. This is also consistent with what Alfrey [25] discussed as the molecular deformation mechanisms involved in the primary and secondary creep of high molecular weight polymers.

Overall, Hill [38, 39] showed that because fibers creep, the innate creep behavior of paper cannot be attributed to the sheet structure (i.e., the breakage of bonds). This is substantiated by the close resemblance to the results of Brezinski [36, 37]. This is why Brezinski [36, 37] found trends consistent with molecular creep mechanisms in

describing creep behavior in paper. The results of Hill [38, 39] do not suggest that the sheet structure has no influence on creep behavior. It simply implies that sheet structure can influence the inherent creep behavior that originates within the fibers. Brezinski [36, 37] showed this to be true when he altered bonding in paper by changing the level of wet pressing and refining. Specifically, his work indicated that increased bonding decreased creep.

2.5 Bonding Influence on Paper Properties

2.5.1 Fundamentals of Bonding

Of all the factors, other than the fiber structure, that can influence creep behavior in paper, it could be argued that bonding is the most important. Prior to discussing the research that has been conducted with regard to the role of bonding in creep behavior of paper, it is necessary to first discuss the fundamentals of bonding in paper in general. Seth and Page [40] discussed that bonding is important in distributing stress between fibers. The more bonding that is present, the more efficiently stress is distributed throughout the fibers in the paper. Page [41] and Van den Akker [32] discussed the importance of bonding in failure behavior, such as tensile strength. Also, Seth and Page [40] showed bonding is important with regard to deformation behavior and its influence on elastic modulus and stress-strain response.

Typically, when paper is formed, it is done in a wet-laid process (water is used as a forming medium). As water is removed, a fibrous mat (paper) forms as fibers are drawn closer together and bond with the aid of surface tension forces [4, 42, 43]. This is commonly referred to as the Campbell effect [4, 42, 43]. According to Clark [42], this

bonding is classified as predominantly cohesive, meaning when fibers come together and form paper, they are connected (bonded) together without the presence (aid) of other "adhesive" materials. When additives are used to aid in bonding, then bonding of fibers can also include a portion that can be classified as adhesive. These additives include cross linkers and strength additives. When fibers are bonded together, the mode by which they are bonded can include chemical bonds, intermolecular van der Waals bonds, and entanglement (or diffusion) of polymer chains [4]. With regard to chemical bonding, this can include hydrogen bonding and covalent or ionic bonds if additives are incorporated into the paper [4].

Within the literature, a significant number of researchers have concluded that hydrogen bonding is the dominant mode by which fibers are bonded within paper [4, 42, 44, 45]. In paper, hydrogen bonding is a strongly attractive force between hydroxyl containing polar molecules and water. Nissan and Sternstein [45] and Nissan [44] were strong proponents of inter-fiber bonding dominated by hydrogen bonding due to the presence of hydroxyl groups within the cellulose and hemicelluloses that compose fibers. These hydroxyl groups are polar in nature and will be drawn together to form a bond that is considerably stronger than van der Waals bonding [42]. This bonding is further assisted by the presence of water (a polar molecule) that can also hydrogen bond with fibers and act as a bridge between them [42]. As water is removed and surface tension forces draw fibers closer to together, fibers can eventually hydrogen bond with each other [42].

While Nissan and Sternstein [45] and Nissan [44] proposed that hydrogen bonding is the dominant mode of bonding of fibers to form paper, other work has shown that diffusion related processes can play an important role in bonding as well. McKenzie

[46] discussed that under normal papermaking conditions, diffusion related processes can play an important role in bonding. Essentially, bonding can occur due to the flowing (diffusion) of amorphous regions within the fibers and subsequent intermingling as fibers are pressed together. In order for this diffusion to occur, the amorphous hemicelluloses within the fiber must be above their glass transition temperatures allowing for easy flow. Goring [47] has shown that under normal papermaking conditions, the moisture conditions that exist are such that hemicelluloses are above their glass transition temperatures and are plasticized. Byrd [48, 49] and Takamura [50] discussed the importance of such a mode of bonding and show its presence to be real and significant in forming interfiber bonds in press drying applications.

While it is important to have knowledge of the inherent makeup of an interfiber bond, it is not necessary to know these exact details to analyze how bonding influences deformation and failure behavior. Typically, when analyzing these behaviors, the main concern is to look at bonding more generally and determine how much bonding there is, how strong these bonds are, and how they react under stress. Overall, when looking at deformation and failure behavior in paper, bonding influences are often characterized in terms of relative bonded area (RBA) and specific bond strength.

Relative bonded area is the ratio of the amount of bonded fiber surface area to the total fiber surface area [51]. It can be measured directly using microscopy methods as the work of Page et al. [52] shows. Most commonly though, relative bonded area is measured indirectly using light scattering techniques. This is based on the work of Parsons [53] who first used light scatter to measure the relative bonded area of paper using the Kubelka-Munk Theory; as relative bonded area decreases, light scatter increases.

Although, there is still debate to whether this method gives an accurate measure of relative bonded area, the work of Haselton [54] showed that light scatter correlated well with BET surface area measurements. Ingmanson and Thode [55] also discussed that relative bonded area calculated from light scatter may not be that different from the actual bonded area in paper. Debate aside, relative bonded area measurements made through light scatter offer a way to demonstrate differences in bonded area. If light scatter for two samples are different, the relative bonded areas are also different as long as fiber properties remain constant. This is important in determining how relative bonded area influences deformation behavior, specifically creep.

In addition to relative bonded area, the strength of the bonds is also important. Commonly, the strength of bonds is quantified as specific bond strength. Specific bond strength refers to the ratio of the shear strength of the bond to the area of that bond [4, 56]. There are numerous approaches to characterize the specific bond strength of bonds within paper which include in-plane measurements of individual bonds (by pulling two bonded fibers apart) and various out of plane measurements (both failure measurements and ultrasonic techniques) [56-58]. Overall, there is no accepted way to measure specific bond strength, but such testing techniques can give a relative measure of specific bond strength so differences in bonding can be compared between paper samples. Similar to light scatter, if a chosen out of plane testing technique shows different results, it implies specific bond strength is also different as long as fiber properties and relative bonded area remain constant. This is true even though the mode of failure in an out of plane test is not in shear. This is important in determining how specific bond strength influences deformation behavior, specifically creep.

2.5.2 Influence of Bonding on Creep

Although research by Hill [38, 39] found that fibers are the structural element from which creep behavior originates, it is still unclear how bonding of fibers may influence this behavior. This is due to the limited and incomplete body of literature regarding the role of bonding in creep. The first important research in this area was conducted by Brezinski [36, 37]. He showed that as wet pressing and level of refining were increased, higher initial applied stress levels were required to get the same amount of strain after 24 hours of creep testing. This implied that as bonding is improved either through wet pressing (densification) or refining (making more conformable fibers), that creep decreases. Figure 23 shows isochronous stress-strain curves at 24 hours at a range of wet pressing and refining levels. Referring to the curve numbers shown in Figure 23, curves 47, 48 and 50 represent paper produced from pulp refined to 775 ml freeness and wet pressed at 0.07 MPa, 0.34 MPa and 2.76 MPa respectively. Curves 23 and 36 represent paper produced from pulp refined to 620 ml freeness and wet pressed at 0.34 MPa, and 1.38 MPa respectively. Curve 55 represents paper produced from pulp refined to 420 ml freeness and wet pressed at 0.34 MPa.

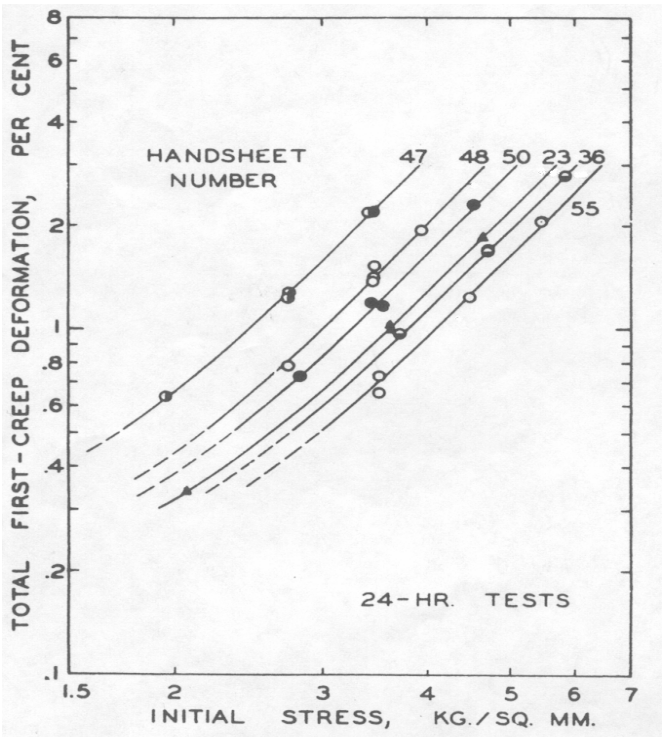

Figure 23 Isochronous Stress-Strain Curves at 24 Hours at a Range of Wet Pressing and Refining Levels [36]

What can be observed from Figure 23 is that it appears that the shape of the isochronous stress-strain curve remains relatively constant and only shifts with improvements in bonding through wet pressing and refining. Furthermore, as bonding is improved, it appears to have less of an impact on creep deformation. That is, improvements in bonding reduce creep deformation more dramatically when there is not a significant amount of bonding to start with. This is easily seen in Figure 23 where increased wet pressing decreased creep deformation dramatically between curves 47 and 48 and less so between 48 and 50.

Similarly, Parker [59] showed that as bonding is improved through wet pressing, creep will decrease. His work also showed that as bonding is increased, it plays a decreasing role in creep deformation behavior. Figure 24, Figure 25 and Figure 26 show

creep curves at three different wet pressing levels (0.34 MPa, 1.70 MPa and 6.80 MPa respectively).

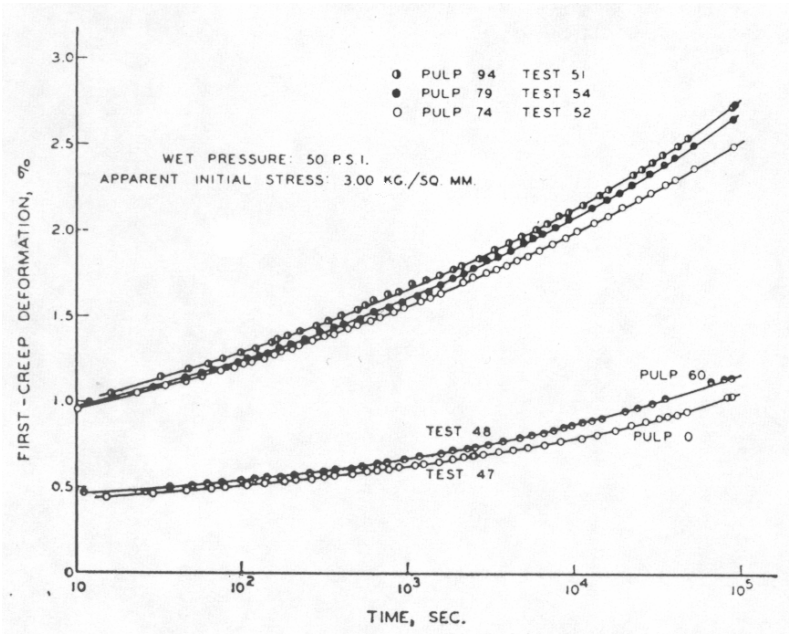

Figure 24 Creep Curves of Parker [59] at 0.34 MPa

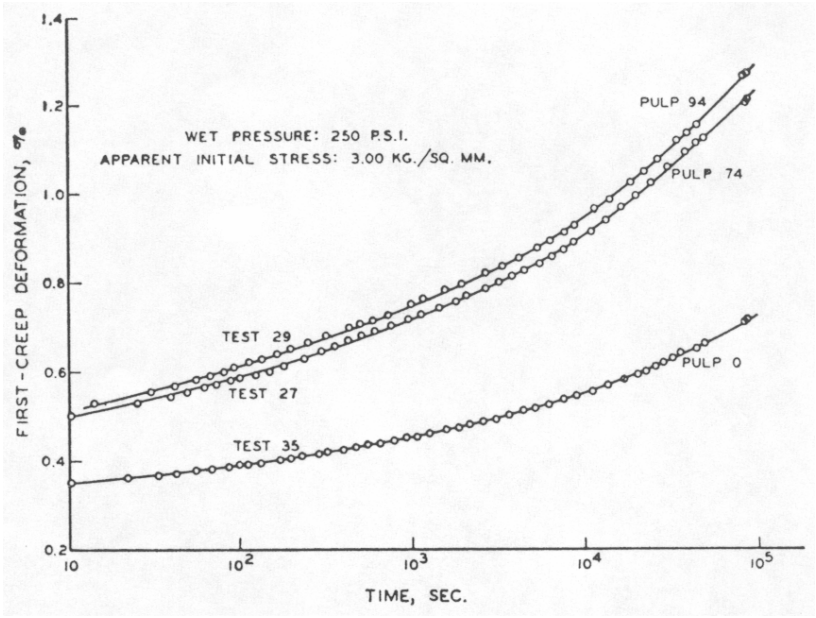

Figure 25 Creep Curves of Parker [59] at 1.70 MPa

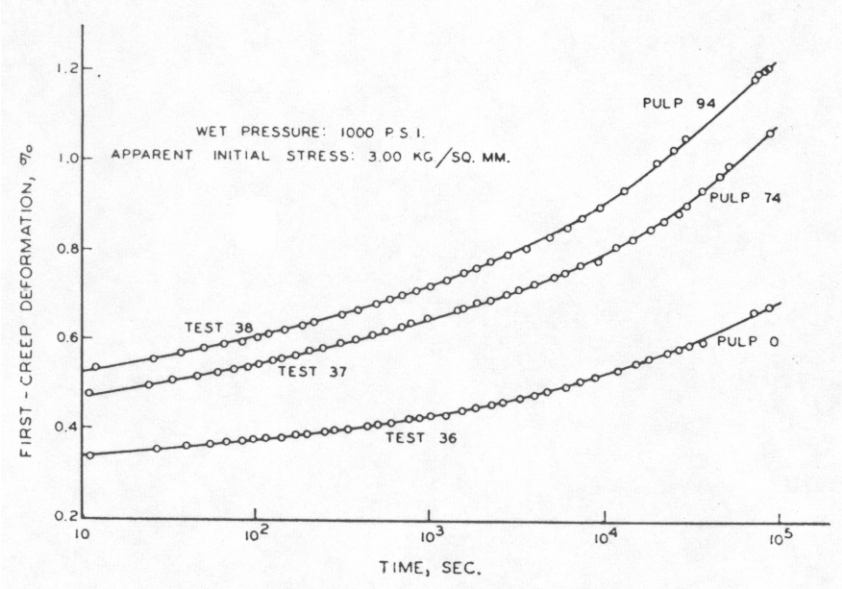

Figure 26 Creep Curves of Parker [59] at 6.80 MPa

Focusing on pulp 0 in Figure 24, Figure 25, and Figure 26, creep deformation is significantly affected when bonding is improved through wet pressing from 0.34 MPa to 1.70 MPa. On the other hand, creep deformation is not affected when wet pressing is further increased from 1.70 MPa to 6.80 MPa. Similar results are shown with pulp 74 and pulp 94. Parker [59] proposed that as bonding is improved, a paper could be made where the total strain from creep results only from the fibers and is not influenced by the bonds.

Schulz [60, 61] showed that increased levels of wet straining (straining the sheet while wet and making that strain permanent through restrained drying) leads to a decrease in creep behavior. He hypothesized that wet straining has the affect of changing the way stress is distributed within the paper structure. In other words, wet straining makes paper more efficient in distributing stress, causing a drop in creep behavior. Figure 27 shows creep curves at several different levels of wet straining.

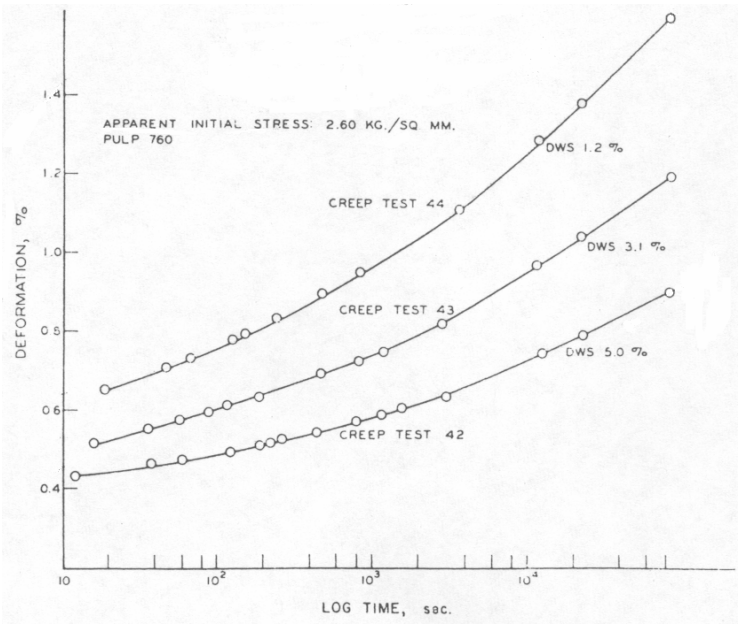

Figure 27 Creep Curves at Several Different Levels of Wet Straining [61]

Figure 27 illustrates that creep at 5.0% wet straining is less than creep at 3.1 % wet straining. What is important is that this result occurred even though the amount of bonding in the 5.0% wet strained paper was less than in the 3.1% wet strained paper. Schulz [60, 61] discussed this and concluded that decreases in bonding can be overcome by improvements in the stress distribution within the paper. Only when bonding and the ability to form a uniform stress distribution is significantly compromised will wet straining increase creep deformation. Unfortunately, it is unclear if improvement of stress distribution is the dominant reason for this decrease in creep. For example, fiber kinks and micro-compressions could be pulled out or amorphous regions of the fiber could be flowing, causing a strain hardening effect. Furthermore, Schulz [60, 61] did not explore how bonding itself could improve or degrade the stress distribution within paper.

Another result Schulz [60, 61] demonstrated was that failure behavior and deformation behavior do not always trend with each other. In several cases, it was shown

that tensile strength decreased as a result of bonded area loss and creep behavior actually improved. This result indicates that the role of bonding and its influence on failure behavior should not be used as a means to make conclusions on how bonding influences deformation behavior.

With regard to relative bonded area change, Sanborn [62, 63] showed that light scatter increased as strain during creep increased. This implies that there is some relative bonded area loss during creep deformation. It does not, however, imply that creep deformation is caused by bond breakage, only that bond breakage occurs concurrently. Sanborn [62, 63] did not present any evidence suggesting what role, if any, the loss in relative bonded area was playing in creep deformation. Figure 28 illustrates the change in relative bonded area versus strain from creep. In the figure, change in relative bonded area is characterized by measuring changes in light scatter.

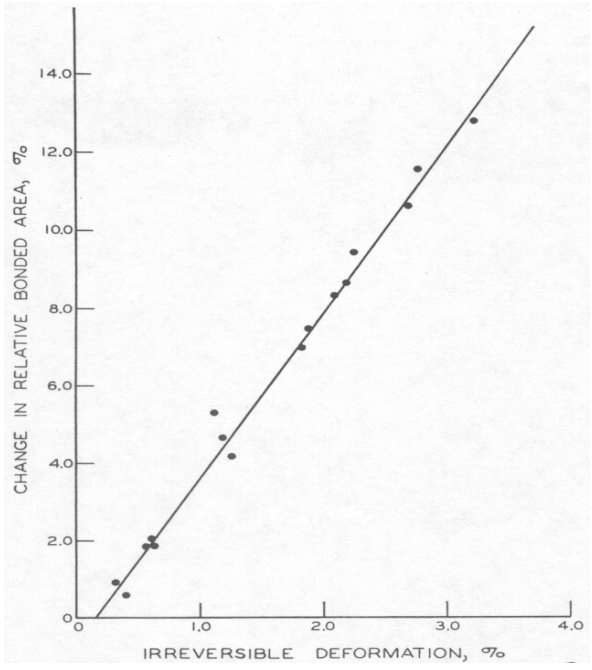

Figure 28 Change in Relative Bonded Area versus Strain from Creep [62]

While Figure 28 demonstrates that bonded area loss occurs as a linear proportion to strain from creep, Byrd [64] showed in his research that light scatter decreased as strain during creep testing increased. His data implies relative bonded area is increasing during creep deformation. However, in this case, the decrease in light scatter may have occurred because bonded area loss was so small, it could not overcome error in measurement on the effect of fibers being drawn into optical contact from lateral contraction due to longitudinal straining.

2.5.3 Influence of Bonding on Stress-Strain Behavior

Overall, there are no definitive answers and some possible contradictions in the existing body of literature regarding creep behavior and bonding. By comparison, the role of bonding with regard to elastic modulus, stress-strain behavior, and tensile strength have been extensively researched. Such research could be beneficial toward finding correlations with creep behavior.

Page [41] elucidated through development of an empirical model, "The Page Equation", that tensile strength in paper can be altered by changing relative bonded area and specific bond strength. Equation 10 shows 'The Page Equation" where T_s is tensile strength, Z is zero-span tensile strength, A_f is average fiber cross section, ρ is fiber density, g is acceleration due to gravity, b_s is the specific bond strength, P is the perimeter of the fiber cross section, L is fiber length, and RBA is relative bonded area.

$$\frac{1}{T_s} = \frac{9}{8Z} + \frac{12A_f \rho g}{b_s PL(RBA)}$$

Equation 10 Empirical Relation to Determine the Tensile Strength of Paper, "The Page Equation" [41]

As shown in Equation 10, tensile strength is a function of fiber strength and a bonding index. If specific bond strength and relative bonded area are increased enough, the bonding index (the second term of Equation 10) approaches zero and the resulting tensile strength is theoretically a function of only fiber strength determined by its zero-span tensile strength. Although Page [41] developed this equation, it was well known prior to this development that bonding was an important factor when considering the tensile strength of paper [65]. With regard to deformation behavior, such as stress-strain behavior, the role of bonding was not as well known until more recently.

Seth and Page [40] conducted one of the most complete research studies on stress-strain behavior in paper. They generated paper sheets at different levels of bonding through variation in wet pressing, refining, and the addition of additives. They showed that in some cases, bonding would have a significant influence on deformation behavior. In other cases they found that bonding would have no effect. Specifically, Seth and Page [40] were able to prove that if they decreased the specific bond strength of paper (with a debonder) or increased specific bond strength (with a bonder), the elastic modulus and the shape of the stress-strain curve would remain constant as long as there was an adequate level of bonding to maintain a fully efficient loaded structure; a structure where changing bonding no longer influences the deformation of paper. The only differences in the overall behavior produced by such changes were different strains to failure and tensile

strengths. Seth and Page [40] also measured changes in light scatter and found a loss of relative bonded area after sheet straining. They showed that relative bonded area decreased at differing rates depending on the treatment applied. The debonder treated sheets had the highest rate of loss followed first by the sheets with no treatment and finally by the bonder treated sheets. Figure 29 illustrates stress-strain curves where deformation behavior is the same and failure behavior is different.

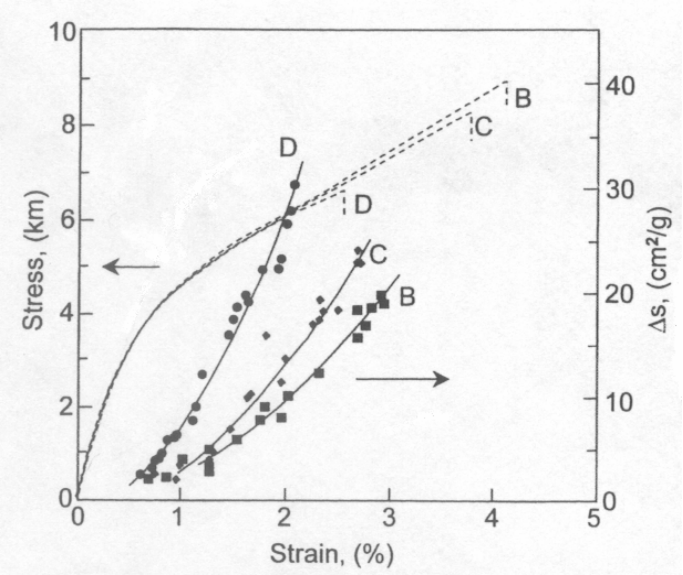

Figure 29 Stress-Strain and Bonded Area Loss Curves for Fully Efficient Loaded Structures [66]

In Figure 29, deformation is not affected by bonding even though the initial levels of bonding are different and the subsequent bonded area losses occurred at differing rates. Seth and Page [40] clearly demonstrated that bonding can reach a level in some cases where it no longer affects the deformation behavior in paper. Below this level, Seth and Page [40] showed that bonding will have an influence, and such paper structures are referred to as inefficient loaded structures.

Upon further analysis of papers that are defined as inefficient loaded structures, Seth and Page [40] introduced the concept of the efficiency factor. Their premise, based on their results, was that deformation behavior within paper originates within the fibers and an efficiency factor can be used to account for the influence of bonding regardless of whether the deformation behavior is elastic or plastic. Specifically, they proved that if stress-strain curves for paper made from the same fibers did not overlap, they could be made to overlap by dividing the stress component of the stress-strain curve by an efficiency factor. The efficiency factor was calculated by dividing the elastic modulus of the more compliant stress-strain curves (inefficiently loaded structures) by the elastic modulus of the least compliant, efficiently loaded, stress-strain curve. Equation 11 gives the definition of φ, the efficiency factor, where E_f is the elastic modulus of a fully efficient loaded structure and E_i is the elastic modulus of the inefficient loaded structure. An efficiency factor of 1.00 indicates that bonding has no influence on stress-strain behavior.

$$\varphi = \frac{E_i}{E_f}$$

Equation 11 Calculation to Determine Efficiency Factor

In the work of Seth and Page [40], the efficiency factor was calculated by using the elastic modulus determined from the slope of the stress-strain curve in the elastic region. Seth and Page [40] were able to demonstrate that the entire stress-strain curve of inefficiently loaded structures, both elastic and plastic regions, would superimpose upon

application of efficiency factors. Simply put, deformation behavior in the plastic region followed an elastically derived efficiency factor and this held true as long as bond breakage was not extreme enough to reduce the efficiency factor during straining. Figure 30 shows an example of stress-strain curves before and after application of efficiency factors.

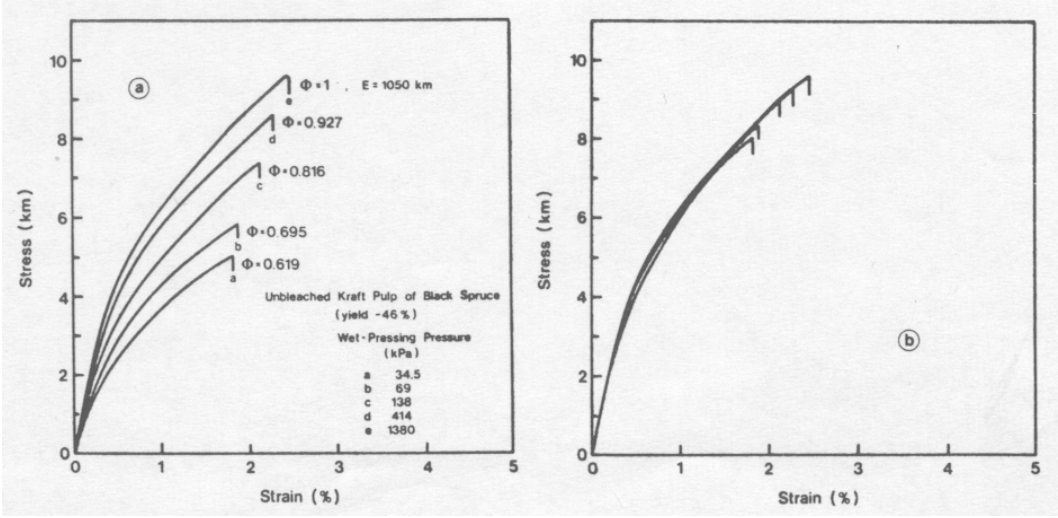

Figure 30 Stress-Strain Curves (a) Without Efficiency Factors Applied (b) With Efficiency Factors Applied [40]

In Figure 30 (a), the stress-strain curves do not overlap because bonding is influencing the deformation behavior. When efficiency factors are applied as in Figure 30 (b), the stress-strain curves are scaled to remove the influence of bonding and collapse onto a common stress-strain curve; the stress-strain curve of a fully efficient loaded structure where bonding has no influence. While Figure 30 demonstrates efficiency factors can be applied to paper with different levels of wet pressing, Seth and Page [40]

also proved it to work for paper with different refining levels and treatments with debonding and strength additives.

In addition to stress-strain experiments, Page et al. [67] conducted microscopic studies where direct observations of bonded area changes during straining were done. Upon analysis of microscopic data, Page et al. [67] found that a vast majority of the bonds they analyzed showed little or no loss in bonded area and few exhibited full failure during a stress-strain deformation test. Figure 31 is a histogram of the bonded area loss within paper as a result of stress-strain testing. In the figure, results were gathered from papers produced from pulp valley beaten at 0, 10 and 30 minutes and plate (restrained) dried.

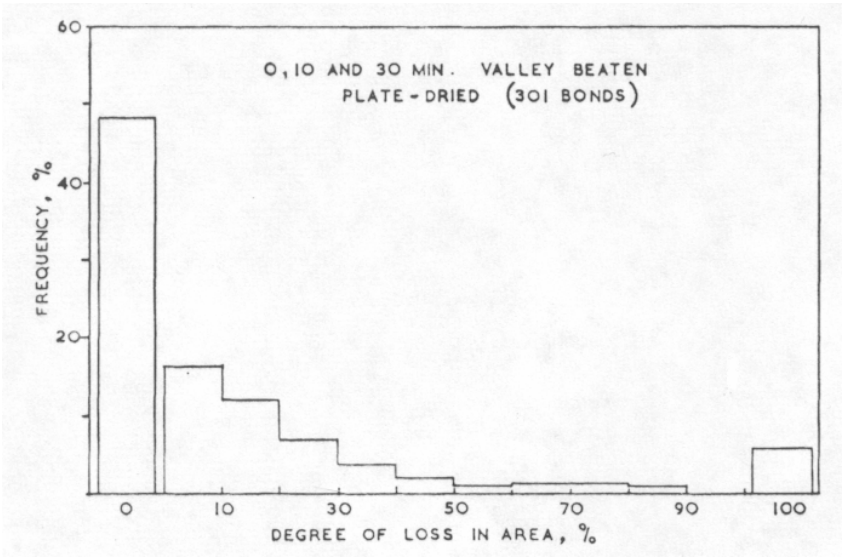

Figure 31 Histogram Showing Distribution of Bonded Area Loss [67]

According to Figure 31, most of the bonds exhibit a bonded area loss of less than 10% with very few showing full bond breakage. Furthermore, Page et al. [67] observed

that bonded area loss, when it did occur, propagated from the perimeter (or edge) of the bond. In more recent publications, Page [66, 68] determined that the reason this occurred was because bonds are under the highest level of shear stress at their perimeters. He concluded that bonded area loss is a strain-induced phenomenon and there is no connection between bond breakage and stress-strain behavior. This is substantiated by what was observed by Seth and Page [40], where deformation behavior remained unaffected even though rate of bonded area loss was significantly different. This behavior is also true for inefficient loaded structures as only the initial level of bonding affects its stress-strain behavior. If bonded area loss were to affect an inefficient loaded structure, an efficiency factor could not be applied, as it would drop during straining. Further evidence of this can be observed in the work of Steenberg [34]. He pointed out that the elastic modulus of paper remains unchanged over the course of straining, indicating bonded area loss is not influencing the behavior. Figure 32 illustrates this, where elastic modulus remains constant (as indicated by the approximately parallel initial deformation paths upon applying and reapplying stress) at various points along the stress-strain curve.

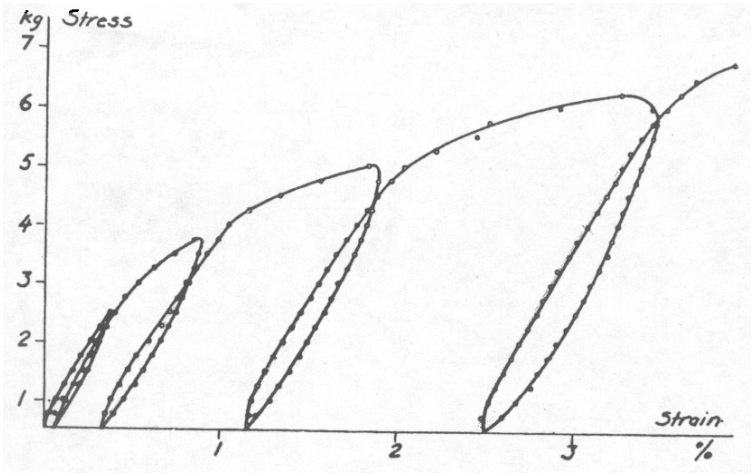

Figure 32 Stress-Strain Curve Showing Elastic Modulus Remaining Constant [34]

2.6 Modeling of Tensile Creep Behavior in Paper

2.6.1 Empirical Creep Models

There are many ways to model creep behavior, with no general method or approach being any more correct than the other. As a result, the choice of what type of model to use can be based on personal preference or necessity. One such approach is to develop an empirical model to predict creep behavior. An empirical model does not draw from material properties or from the fundamental behavior of the material. Rather, a purely mathematical relationship is developed to predict creep behavior. These models can range in complexity based on the behavior of the material and the accuracy desired. Within this thesis, tensile creep in paper under a uniaxial stress is the focus and is therefore the focus of this modeling section.

Among the most well known empirical models for creep behavior, Norton and Bailey utilized simple power law functions to predict the creep behavior of metals [6]. Drawing from Norton and Bailey, Nutting showed such a power law relation to be effective in predicting the creep behavior of plastics [6]. While these models are all simple, the complexity can be increased by incorporating logarithmic and trigonometric functions, and integral forms to obtain greater predicting accuracy. Equation 12 presents the Norton power law creep model, where strain is predicted at a defined creep time. Equation 13 presents the Bailey power law creep model assuming strain equals zero at time equals zero and Equation 14 presents the Nutting power law creep model. In all the equations, ε is the creep strain, σ is stress, A, b and c are constants and t is time. In order to fit the empirical models to a material, such as a metal or plastic, the constants are adjusted.

$$\varepsilon = A\sigma^{b}$$

Equation 12 Norton Power Law Creep Model for Metals [6]

$$\varepsilon = A\sigma^{b}t$$

Equation 13 Bailey Power Law Creep Model for Metals [6]

$$\varepsilon = A\sigma^{b}t^{c}$$

Equation 14 Nutting Power Law Creep Model utilized in Plastics [6]

Focusing on paper, there is a limited amount of modeling from which to draw with regard to tensile creep. As far as empirical models are concerned, Brezinski [36, 37] utilized simple exponential and logarithmic functions to describe the results from his work. He stated that at short times and low initial applied stress levels, creep behavior followed an exponential trend. He referred to this as exponential creep and discussed this as creep that is fully recoverable. At longer times and high initial applied stress levels, creep behavior followed a logarithmic trend. Brezinski [36, 37] referred to this as logarithmic creep and commented that this creep is not fully recoverable. The work of Hill [38, 39] with single fiber tensile creep utilized the same rationale focusing on creep behavior following a logarithmic trend. Equation 15 presents the relation Brezinski [36, 37] used to describe exponential creep under a constant initial applied stress. Equation 16 shows the relation Brezinski [36, 37] and Hill [38, 39] used to describe logarithmic creep under a constant initial applied stress. In these equations ε equals creep strain, t is time and A, b, C, D and F are constants used to fit the models to the creep of the paper or

fiber. These constants have to be changed every time initial applied stress, humidity or temperature is changed, even if the paper or fibers are not changed.

$$\varepsilon = At^{b} + C$$

Equation 15 Exponential Creep Model for the Tensile Creep of Paper [36, 37]

$$\varepsilon = D \log t + F$$

Equation 16 Logarithmic Creep Model for the Tensile Creep of Paper [36-39]

The work of Pecht et al. [69] employed a more complex empirical equation to describe tensile creep based in part on the work of Brezinski [36, 37]. He developed a universal equation rather than using an exponential function to model creep at low initial applied stresses or short times and a logarithmic function to model creep at high initial applied stresses or long times. It was also capable of being used to form master creep curves. Equation 17 shows this empirical model where ε is creep strain, σ_o is initial applied stress, σ_r is the reference stress, t is time, E is elastic modulus and A, b, c and t_o are constants. In the equation, reference stress refers to the initial applied stress that is the basis for the master creep curve. The other constants are used to fit the model to the creep behavior of the paper.

$$\varepsilon = \frac{\sigma_o}{E} + A\sigma_o \log\left[1 + \left(\frac{t10^{b(\sigma_o - \sigma_r)}}{t_o}\right)^c\right]$$

Equation 17 Pecht et al. [69] Empirical Model for Tensile Creep in Paper

Further work by Pecht and Johnson [70] expanded upon the model shown in Equation 17 to take moisture changes into account. Panek et al. [14] also proposed an empirical equation with significant complexity. It was derived specifically to predict isochronous creep curves, and utilizes hyperbolic tangent functions. Equation 18 presents this relation where ε is creep strain, σ_o is initial applied stress, t is time, t_1 is reference time and a_1, a_2, a_3, and b are constants. As shown in Equation 18, this equation is used to determine initial applied stress and would be cumbersome to invert and solve for creep strain.

$$\sigma_o = \left[a_1 \tanh\left(\frac{a_2\varepsilon}{a_1}\right) + a_3\varepsilon \tanh\left(\frac{a_2(100\varepsilon)^2}{a_3}\right)\right]\left(\frac{t}{t_1}\right)^{-b}$$

Equation 18 Panek et al. [14] Empirical Model to Predict Isochronous Stress-Strain Curves

2.6.2 Rheological Creep Models

Other than empirical models, a more physically descriptive approach can be utilized to describe creep behavior. Rather than arbitrarily deriving a mathematical relation to predict creep behavior, a model is developed focusing on the material properties and its inherent deformation mechanism. Again, there are many approaches

that can be taken in modeling, and choice of what type of model to use is often based on convenience. As this is so, only the models that relate to tensile creep behavior in paper under a uniaxial stress are reviewed here.

In paper and polymeric materials, rheological models are one such approach that is used to predict creep behavior. In fact, with regard to existing tensile creep models in paper, other than the empirical models previously discussed, a significant portion of the remainder are rheological in nature. In rheological models, each component of the total strain (initial elastic strain, primary creep and secondary creep) can be isolated and represented by a combination of springs and dashpots. These spring and dashpot elements are representations of the behavior of the material's inherent mechanistic (fundamental) response. As a result, the constants used in rheological models can have physical meanings which are related to the physical properties of the material. Figure 33 shows illustrations of a spring and a dashpot element.

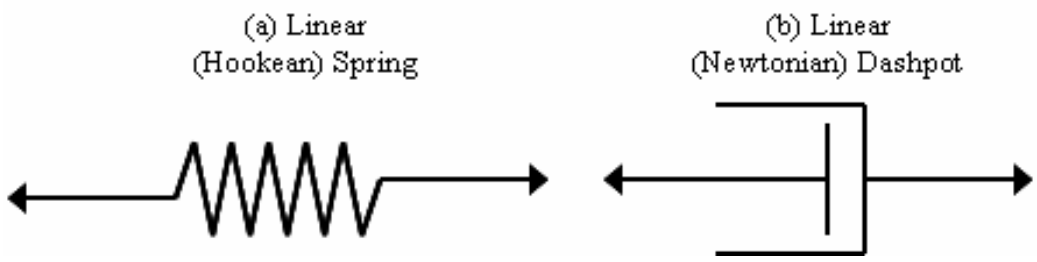

Figure 33 Representations used in Rheological Models: Spring Element (a) and Dashpot Element (b)

A linear spring is Hookean and is represented by Equation 19. Equation 19 is Hooke's law where σ_o is initial applied stress, ε is strain and E is elastic modulus. When a stress is applied to a spring element, the resulting strain is time independent and

recoverable [11, 12, 20]. A linear dashpot is Newtonian and is represented by Equation 20. Equation 20 shows this is two forms, one in terms of strain rate, dε/dt, and one in terms of strain, ε. In the equations, σ_o is initial applied stress, t is time and η is viscosity. If a stress is applied to a dashpot, the resulting strain is time dependent and permanent [11, 12, 20]. When spring and dashpot elements are combined, the characteristics of both elements interact and can be used to model viscoelastic behaviors such as creep [11, 12, 20].

$$\varepsilon = \frac{\sigma_o}{E}$$

Equation 19 Linear (Hookean) Spring Element Relation [11, 12, 20]

$$\frac{d\varepsilon}{dt} = \frac{\sigma_o}{\eta} \qquad \varepsilon = \frac{\sigma_o t}{\eta}$$

Equation 20 Linear (Newtonian) Dashpot Element Relations [11, 12, 20]

The work of Mason [35] discussed using several types of rheological models to describe creep in paper, including the use of a Maxwell Model (spring in series with a dashpot) depicted in Figure 34 (a), a Voigt Model (spring in parallel with a dashpot) depicted in Figure 34 (b) and a Burger's Model (Maxwell Model in series with a Voigt Model) depicted in Figure 34 (c).

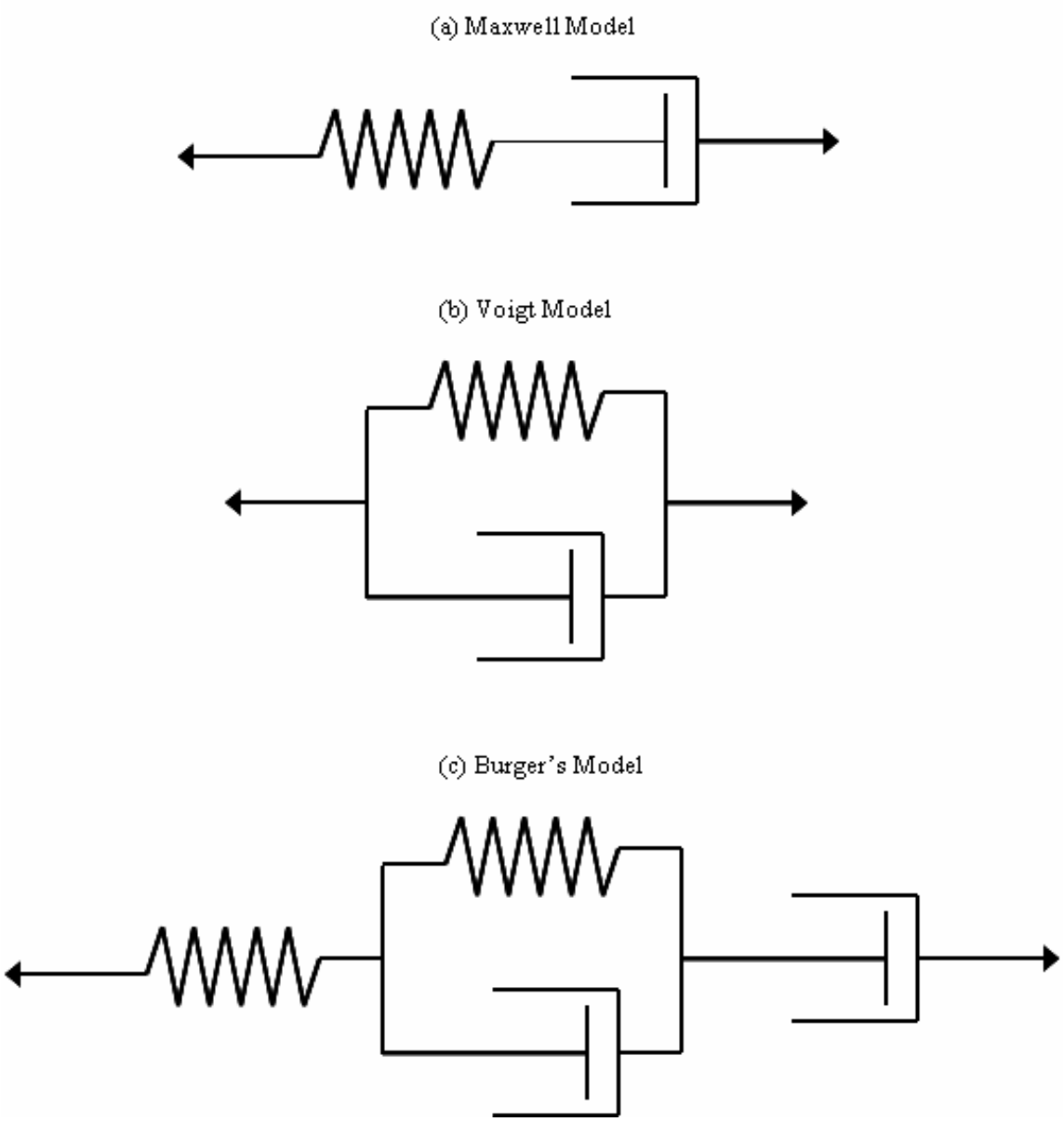

Figure 34 Illustrations of Rheological Models discussed by Mason [35]

In a Maxwell Model, when a stress is applied, there will be an instantaneous strain, and a time dependent strain response [11, 12, 20]. When stress is removed, there will be an instantaneous recovery and a permanent strain [11, 12, 20]. In modeling creep, it would represent the initial elastic and secondary (steady-state) creep responses of a linear viscoelastic material (the first and second terms respectively in Equation 21). Equation 21 shows the relation for a Maxwell Model where ε is strain, σ_o is initial applied stress, t is time and η_m and E_m are viscosity and elastic modulus parameters respectively. In the Maxwell Model, the spring and dashpot elements experience the same stress. As a result, the strains due to each element are not generally equal to one another.

$$\varepsilon = \frac{\sigma_o}{E_m} + \frac{\sigma_o t}{\eta_m}$$

Equation 21 Maxwell Model Relation [35]

In a Voigt Model, when stress is applied there will be a time dependent strain response, where strain rate decreases as time increases [11, 12, 20]. When stress is removed, there will be a time dependent recovery [11, 12, 20]. In modeling creep, it would represent the primary (transient) creep response of a linear viscoelastic material. Equation 22 shows the relation for a Voigt Model where ε is strain, σ_o is initial applied stress, t is time and η_v and E_v are viscous and elastic parameters respectively. In the Voigt Model, the spring and dashpot elements experience the same strain. As a result, the stresses experienced in each element are not generally equal to one another.

$$\varepsilon = \frac{\sigma_o}{E_v}\left[1 - \exp\left(\frac{-E_v t}{\eta_v}\right)\right]$$

Equation 22 Voigt Model Relation [35]

If the Voigt Model and Maxwell are connected, as shown in Figure 34 (c), a Burger's Model results and initial elastic strain, primary creep and secondary creep can be predicted separately (the first, second and third terms in Equation 23 respectively). Equation 23 shows this relation where Equation 21 and Equation 22 are added together.

$$\varepsilon = \frac{\sigma_o}{E_m} + \frac{\sigma_o}{E_v}\left[1 - \exp\left(\frac{-E_v t}{\eta_v}\right)\right] + \frac{\sigma_o t}{\eta_m}$$

Equation 23 Burger's Model Relation [35]

More complicated rheological models can also be used or more elements can be added in series. The work of Pommier et al. [71] is an example of this where he used two Voigt Models in series with a Maxwell Model to describe creep behavior. Again all of these models use linear (Hookean) springs and linear (Newtonian) dashpots and hence yield a relationship where stress and strain have a linear relationship. In paper, stress and strain have a non-linear relationship and the use of a rheological model based on elements with linear behaviors has inherent limitations on its accuracy, especially as strain increases. In addition, if the secondary creep component of strain is represented by a single dashpot, the result is a time independent strain rate, which is not representative of tensile creep in paper.

In order to account for the non-linear stress-strain relationship, Coffin [13] developed a non-linear tensile creep model. While the Coffin model is empirical in nature, it does contain rheological elements. Specifically, he uses a spring element to represent initial elastic strain and uses a function very similar to a Voigt Model to account for primary creep. He also uses a non-linear dashpot to represent secondary creep which employs a logarithmic function. This is likely based on the work of Brezinski [36, 37]. This function allows secondary creep rate to decrease as time increases. In addition, Coffin [13] drew from the work of Seth and Page [40] and employed an efficiency factor, in the model. Overall, the model provides a reasonable prediction of the creep data from Brezinski [36, 37] and can generate master creep curves. Equation 24 shows the relation Coffin [13] derived where σ_o is initial applied stress, ε is strain, φ is efficiency factor, t is time, ε_p is plastic strain and E, A, B, a_o, b_o, α and β are material parameters.

$$\varepsilon = \frac{\sigma_o}{\varphi E}\left[1 + A\left(1 - \exp\left(-a_o x t^a\right)\right) + B\ln\left(b_o y t + 1\right)\right]$$

$$x = \exp\left(\frac{\alpha\beta\sigma_o}{\varphi}\right) \qquad y = \exp\left(\frac{\beta\sigma_o}{\varphi} - \frac{E\varepsilon_p}{\sigma_o B}\right)$$

Equation 24 Tensile Creep Model Developed by Coffin [13]

Other than Coffin [13], Agbezuge [72] introduced a non-linear rheological model to describe the stress-strain behavior of xerographic papers. He used a 3-parameter rheological model in which a linear spring was in parallel with a linear spring and non-linear dashpot in series. Agbezuge [72] found that the model was effective in predicting

the stress-strain curve. He made the model non-linear by replacing the linear (Newtonian) dashpot with a non-linear Eyring dashpot. A drawback to using the model for predicting creep behavior is it does not have a secondary creep component and assumes full recovery of strain. Sedlachek [73] utilized that same approach as Agbezuge [72] and found that it was also effective in predicting the creep behavior of single fibers. Both of these authors draw from the work of Halsey et al. [21] who were responsible for one of the earliest uses of the Eyring dashpot. They developed a 3-parameter rheological model where a linear spring in parallel with a Maxwell Model was modified by replacing the linear dashpot with a non-linear Eyring dashpot. Later Holland et al. [22] did the same thing to the Burger's Model where both linear dashpots were replaced with non-linear Eyring dashpots. This 4-parameter model provided greater utility than the 3-parameter model as it separated initial elastic strain, primary creep and adds a secondary creep parameter. In this model both linear were replaced with non-linear Eyring dashpots.

The Eyring dashpot is non-linear dashpot that can be used to relate the creep deformation mechanism to potential (or reaction rate) theory. Potential theory was discussed previously, in Section 2.3.1 with regards to explaining the creep behavior and deformation mechanism of polymeric materials. The dashpot was first introduced by Tobolsky and Eyring [23] in 1943. Equation 25 shows the relation for the Eyring dashpot, where $d\varepsilon/dt$ is creep strain rate, σ_o is initial applied stress, and A_e and B_e are material parameters. This equation is the same as Equation 9 where A_e replaces $2kT/v$ and B_e replaces $2vn_o/V$.

$$\frac{d\varepsilon}{dt} = B_e \sinh\left(\frac{\sigma_o}{A_e}\right)$$

Equation 25 Non-Linear Eyring Dashpot Relation [23]

Halsey et al. [21] and Holland et al. [22] applied the Eyring dashpot to polymeric materials that contain amorphous (disordered) regions. The primary load bearing component in a papermaking fiber is cellulose and is a linear chain molecule arranged in a partially crystalline network, meaning it contains amorphous disordered regions [1]. In addition, hemicelluloses and lignin, which are also present in a papermaking fibers are amorphous [3, 4, 10]. As a result, use of the Eyring dashpot is particularly applicable to the modeling of paper and papermaking fibers. In combination with linear spring elements in a rheological model, the Eyring dashpot can be used to suggest an explanation for creep deformation on a molecular level.

2.7 Accelerated Creep Behavior in Paper

2.7.1 Description and Characterization of Accelerated Creep Behavior

The work of Brezinski [36, 37] showed that creep behavior in paper is highly sensitive to moisture content. His work indicated that as the relative humidity (moisture content of paper) is raised, the amount of strain from creep increases as well. This was discussed in a previous section and is illustrated in Figure 20. When Brezinski [36, 37] conducted these experiments, they were conducted under a constant relative humidity, meaning the moisture content of the paper was unchanged throughout the entire creep test. Under real environmental conditions, relative humidity rarely remains constant. As a

result, studies in creep behavior in paper under a changing relative humidity environment were necessary and first researched by Byrd [64, 74, 75].

Byrd [64, 74, 75] observed that when paper is exposed to a cyclic humidity environment, it will exhibit more creep strain than if the same paper were exposed to a constant humidity environment at the highest humidity experienced in the cyclic humidity environment. This is commonly referred to as accelerated creep or mechano-sorptive creep. This result was likely not a revelation to Byrd [64, 74, 75] as this behavior was also observed by Armstrong and Christensen [76, 77] in wood. Furthermore, accelerated creep can occur in many modes of deformation, including bending, tension and compression. Within this thesis, accelerated creep in bending and compression will not be discussed. Therefore, unless otherwise specified all reference to accelerated creep is in tension. Figure 35 shows an illustration of accelerated creep behavior in paper.

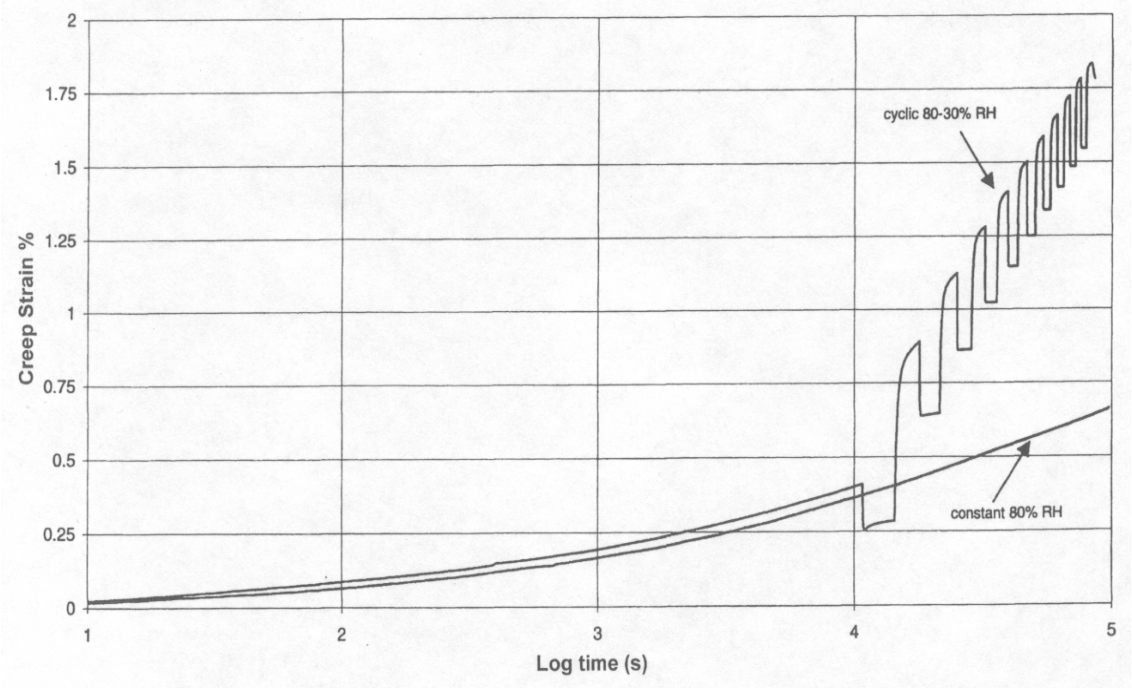

Figure 35 Illustration of Accelerated Creep Behavior in Paper [78]

In Figure 35, there are two creep curves where equal initial applied stresses were used. In the first curve, relative humidity is held to a constant 80% for the entire duration of the creep test. In the second curve, relative humidity is held to a constant 80% until log 4 seconds then cycled between 30% and 80% relative humidity ten times. As shown in Figure 35, once relative humidity is cycled, the creep strain exceeds the constant humidity creep strain curve quite dramatically. This behavior is consistent with a material that can experience accelerated creep. If there were no accelerated creep, cycling relative humidity between 30% and 80% would not have resulted in a creep curve greater than the constant humidity creep curve at 80% relative humidity. Rather, it would have decreased to a level between that which would be obtained for constant humidity creep tests at 30% and 80% relative humidity.

Furthermore, Wang [79, 80] showed this behavior is not a phenomenon limited to paper or wood and can occur in synthetic polymeric materials such as Kevlar fibers and composites. This is not surprising as many synthetic polymers have sensitivity to moisture just as paper and wood do. Overall, understanding accelerated creep behavior is of interest in many types of materials and has drawn particular attention in paper. It has been extensively researched and modeled to ascertain and explain the mechanism behind the phenomenon. This type of work has been the focus of much of the creep research in paper over the last 35 years.

2.7.2 Proposed Accelerated Creep Mechanisms

Many different viewpoints on the underlying mechanisms behind accelerated creep have been proposed. For materials in general, Wang [79] reviewed several

accelerated creep mechanisms that include hydrogen bonding and slip planes. He commented that while hydrogen bonding disruption during moisture cycling can lead to an increase in strain, it does not explain the role of material structure in the mechanism. Slip planes, which occur in compression and bending experiments, do not explain why accelerated creep occurs in tension experiments or at low stresses. Wang [79] also mentioned other mechanisms such as transient or redistributed stresses, increases in free volume causing an increase in molecular mobility, differential swelling, and crystallite rotation.

With respect to paper, there have been a number of explanations proposed since Byrd [64, 74, 75] conducted his studies. As a result, there are differing opinions with regard to the accelerated creep mechanism. In a recent review, Coffin [13] discussed these possible mechanisms in paper, including increase in free volume, formation of dislocations, bond breakage and moisture sorption. Based on the available research, the review disproved many of these mechanisms and proposed moisture sorption as the mechanism behind accelerated creep. In this mechanism, bond breakage does not play a role in creep behavior beyond its role in constant humidity creep behavior. Specifically, this is the mechanism proposed by Habeger and Coffin [78, 81, 82]. They propose as humidity is changed, moisture diffuses into the sheet causing a moisture gradient to form. Given enough time, the gradient will disappear, but once humidity is changed again, a new moisture gradient will be created. As moisture greatly influences the properties and behavior of fibers (elastic modulus and hygroexpansion), a moisture gradient will lead to an uneven stress distribution. Furthermore, if humidity is cycled, the moisture gradient and uneven stress distribution will cycle as well. Combined with the non-linear

deformation behavior of paper, this uneven stress distribution leads to increased creep behavior under cyclic humidity conditions. Figure 36 illustrates how a moisture gradient (moisture profile) can cause an uneven stress distribution (stress profile) when relative humidity is cycled.

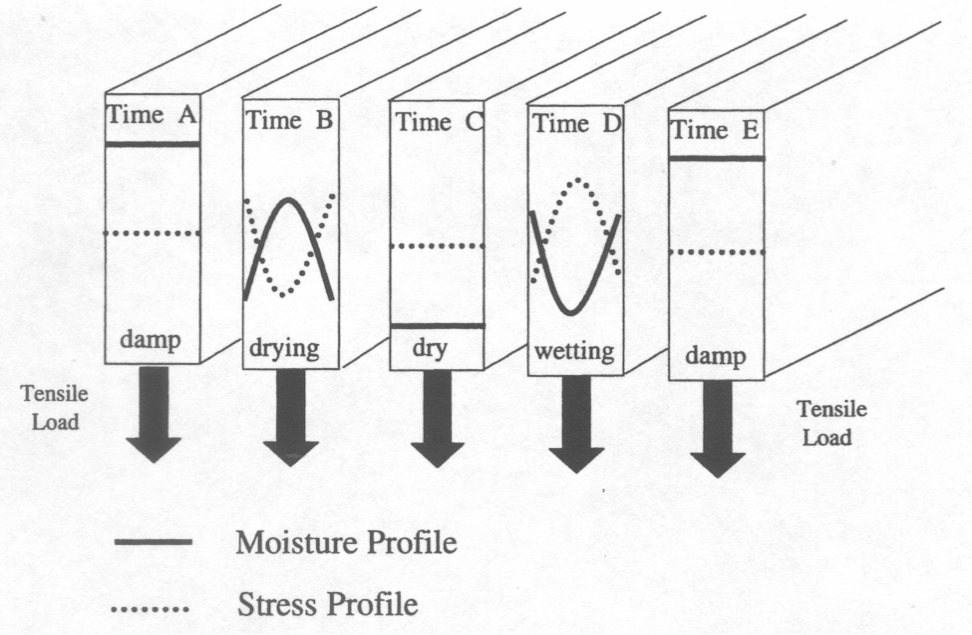

Figure 36 Moisture and Stress Profiles During a Relative Humidity Cycle [78]

Material heterogeneity can act to amplify this effect as differences in elastic modulus and hygroexpansivity already exist. This was shown by Coffin and Habeger [83] as multi-ply sheets made with different furnishes resulted in increased accelerated creep. Alfthan [84-87] pointed out that material heterogeneity also exists within a fiber network as anisotropic fiber swelling (hygroexpansivity) over bonded segments can lead to stress concentrations and more creep during moisture sorption.

In fact, Alfthan [84-87] focused primarily on the material heterogeneity portion of the Habeger and Coffin [78, 81, 82] mechanism with regards to accelerated creep. Through his modeling work, he showed that moisture sorption will cause anisotropic swelling at fiber crossings and lead to the formation of stress concentrations at, and around, bonded segments. This provided insight into possible details of the moisture sorption mechanism. Furthermore, Alfthan [84-87] assumed a no slip condition at the fiber-fiber bonds and proposed the extra strain associated with accelerated creep occurs or originates preferentially within the fibers at and around bonded segments. A no slip condition at the bonds implies that stress is only being transferred through the fiber network bonds. Accepting the no slip condition, any actual bonded area loss cannot be a contributor to accelerated creep. Any bonded area loss must be seen as a consequence of strain, not a cause of strain. While it could be argued from the work of Alfthan [84-87] that the mere presence of bonding in a fiber network contributes toward accelerated creep, the results of this study support the assertion that the primary mechanism is heterogeneity (the anisotropic nature of the fibers), not bonding.

A differing viewpoint on the accelerated creep mechanism is proposed by Haslach [88-90]. He contended that bonding, more specifically bonded area loss, plays an important role in accelerated creep. Evidence to support this is given by Sedlachek [73]. He showed that individual fibers do not exhibit an accelerated creep behavior. It would seem logical to conclude that if fibers do not show accelerated creep, the mechanism behind accelerated creep must involve bonds. A counter argument is that proposed by Habeger et al. [91]. They explain the results of Sedlachek [73] using their own accelerated creep mechanism. Individual fibers do not show accelerated creep because

sorption occurs so quickly, moisture gradients and therefore stress gradients do not have a chance to form or persist in single fibers. They contend, if sorption time could be increased or ramp time and cycle time could be sufficiently reduced, individual fibers would exhibit accelerated creep. Furthermore, Habeger et al. [91] pointed out the work of Sedlachek [73] does show it is "on the verge" of accelerated creep as it shows more creep than the average between the constant humidity curves at the moisture extremes.

Although, the evidence suggested that the mechanism of Habeger and Coffin [78, 81, 82] is likely the explanation for accelerated creep, disagreement remains. This is due to the limited availability of experimental data with regard to bonding and accelerated creep. In fact, there are no adequate studies that specifically focus on bonding and its role in accelerated creep. Byrd [64] is the only researcher who investigated bonding and accelerated creep. In his work, Byrd [64] showed that light scatter increased during accelerated creep testing. This indicated that bonded area was decreasing during accelerated creep. Combined with his data for constant humidity creep where he showed that light scatter decreased (discussed in Section 2.5.2), those who favor a bond breakage explanation of accelerated creep use this as strong supporting evidence. That said, it is unclear whether this bond breakage is the cause of accelerated creep, or an effect. Page [66, 68] pointed out in his work with stress-strain behavior, that bonded area loss is a strain-induced phenomenon and is a result produced by straining, not a cause. Within this thesis, additional studies shed light onto the true role of bonding in accelerated creep.

CHAPTER 3: PROBLEM ANALYSIS & THESIS OVERVIEW

Within this thesis, the main objective was to better discern the role bonding has in the tensile creep behavior of paper. The literature survey presented in the previous chapter discussed the most relevant information and research with respect to this area of study. This was used so an appropriate experimental program could be devised to expand the knowledge base in this area of bonding and its role in tensile creep behavior.

In the previous chapter, it was stated that paper is a material composed of a network of bonded fibers. These fibers are composed of semi-crystalline and wholly amorphous naturally occurring polymeric materials (cellulose, hemicelluloses and lignin). As a consequence of their composition, the fibers will exhibit deformation behaviors consistent with polymeric materials that also possess an amorphous molecular structure. Specifically, this type of polymeric material will creep when a constant load is applied to it. The creep behavior will exhibit an initial elastic strain response, primary creep and secondary creep. Primary creep is recoverable creep, while secondary creep is permanent. Unlike metals, secondary creep rate in polymeric materials is not considered to be time independent. Furthermore, deformation behavior of polymeric materials will show dependence on temperature and moisture. As a result, increasing temperature or moisture will result in an increase in creep deformation.

Fundamental studies on paper and fibers have shown creep behavior originates within the fiber, but that bonding also plays a role, that is not entirely clear. It has been shown that if bonding (relative bonded area and specific bond strength) is improved through wet pressing and refining, creep deformation in paper will decrease. Studies have

also suggested that subsequent improvements in bonding show a diminishing return effect. That is, improving bonding when it is already high will not yield as marked a decrease in creep as when the bonding is improved from an initially low level. Other creep studies have shown that bonded area decreases during straining, but it is unclear whether the loss of bonded area affects creep strain or is simply caused by it.

With regards to other deformation behaviors in paper such as stress-strain behavior, the role of bonding is better defined. In stress-strain behavior it has been shown that once bonding (relative bonded area and specific bond strength) reaches a certain level, further improvements no longer influence the deformation, they only increase failure stress and strain. At this level of bonding, paper is referred to as a fully efficient loaded structure; a structure where deformation is controlled by the fibers and bonds are effectively distributing the stress between these fibers. At lower levels of bonding, it has been shown bonding will have an influence on deformation because the sheet structure is inefficient; the bonds are not effectively distributing stress throughout the sheet structure. In this regime, both bonding and the fibers influence deformation behavior. Furthermore, efficiency factors can be calculated from the elastic modulus data of inefficient sheets to show the extent to which bonding is influencing deformation. Upon application of these efficiency factors, the influence of bonding can be removed to generate a stress-strain curve with the same deformation behavior as a fully efficient stress-strain curve. With regards to bonded area loss, it was shown that sheets can have the same deformation behavior while showing a differing amount and rate of bonded area loss. This indicates that bonded area loss is a strain induced phenomenon pertaining to stress-strain behavior; bonded area loss is a consequence of strain, not a cause of it.

In terms of modeling, there are a limited number of empirical and rheological models that can be drawn from to predict and explain tensile creep deformation in paper. In polymeric materials, potential or reaction rate theory has been used to describe the mechanism behind creep behavior. This has been successfully incorporated into rheological models to predict the deformation behavior of plastics, textiles and papermaking fibers.

In accelerated creep in paper, the role of bonding has not been thoroughly researched. The only available research in this area shows that bonded area loss occurs during accelerated creep deformation. It is unclear whether this bonded area loss is causing deformation or it is just a consequence of it as with stress-strain behavior. As the role of bonding under constant humidity conditions is not fully defined, it is hard to determine the role of bonding in a cyclic humidity environment because there is no baseline for comparison.

Based on the available literature, it was clear the role of bonding in tensile creep behavior in paper needed to be better defined. As a result, the following four research areas are summarized.

1. There is not a complete understanding of how the amount of bonding (relative bonded area and specific bond strength) in paper influences creep deformation. While studies have shown bonding has an influence, it has not been completely characterized, defined or understood.

2. With regards to modeling, the role of bonding has not been fully analyzed. It has not been shown that bonding influence can be specifically isolated, accounted for and incorporated into a mathematical model which is based on the fundamental deformation mechanisms of the polymeric components that comprise the fibers.
3. In addition to the amount of bonding present within paper, it has not been defined whether loss of bonded area during straining is influential in creep behavior or a consequence of strain as with stress-strain behavior.
4. The role of bonding in accelerated creep has not been experimentally explored. It has only been theoretically considered in terms of proposing possible deformation mechanisms. Once the role of bonding is defined, the mechanism behind accelerated creep can be more fully described.

The remainder of this thesis addresses these four research areas. As each one of these areas of study are significant undertakings, there is a separate results chapter for each of them. Specifically, the remainder of this thesis comprises an overall experimental methods section (Chapter 4), four results chapters (Chapters 5-8), an overall conclusions section (Chapter 9) and a recommendations for future work section (Chapter 10). Chapters 5-8, while incorporated into this thesis, were written in such a manner so they could be read as stand-alone publication papers. In each of these chapters, there is an abstract, relevant literature survey and experimental section as well as a results, discussion, and conclusion specific to the research area addressed. Chapters 5-8 can be read separately without reading any other portion of the thesis. The overall conclusions

section (Chapter 9) sums up the conclusions drawn from each of the previous four results chapters.

Chapter 5 addresses research area #1. In this chapter, tensile creep behavior of paper is analyzed at differing levels of bonding (relative bonded area and specific bond strength). This chapter defines the role of bonding in the creep behavior of paper and draws comparisons to stress-strain behavior. It also discusses the importance of bonding in analyzing the deformation behavior of paper at a range of bonding levels. Chapter 5 also partially addresses research area #3 by looking at bonded area loss during straining. Chapter 5 has been published by DeMaio and Patterson [92] in a similar format. This is the most important chapter within this thesis as the findings in this chapter are necessary to adequately resolve the remaining research areas addressed in Chapters 6-8.

Chapter 6 addresses research area #2. Two models are developed which take into account the role of bonding in the tensile creep behavior of paper. The first of which is a simple empirical model that draws upon mathematical relationships known to fit well with creep behavior. The second is a descriptive rheological model developed based on the deformation mechanisms of the polymeric components of the fibers. In both models, bonding is isolated and accounted for based on the findings of Chapter 5.

Chapter 7 addresses research area #3. Although, Chapter 5 looked at bonded area loss and creep deformation, Chapter 7 conducts a more in depth microscopic analysis. The results from this chapter are compared with stress-strain behavior as part of the analysis. Chapter 7 has been submitted and accepted for publication by DeMaio et al. [93] in a similar format

Chapter 8 addresses research area #4. Using the results of Chapter 5 as a baseline, the role of bonding in accelerated creep behavior is analyzed and defined. Implications of these findings are discussed with regard to possible accelerated creep mechanisms in paper. Chapter 8 has been submitted and accepted for publication by DeMaio and Patterson [94] in a similar format.

CHAPTER 4: EXPERIMENTAL MATERIALS AND PROCEDURES

4.1 Pulp and Preparation

NIST standard reference material 8495 Northern Softwood Bleached Kraft Pulp was used in this study. It is a once dried pulp composed of 68% white spruce (*picea engelmannii*), 32% lodgepole pine (*pinus contorta*) and a trace of balsam fir (*abies balsamea*) manufactured at the Grande Prairie Pulp Mill in Alberta, Canada [95]. The pulp arrived in dry lap sheets in hermitically sealed packages and had remained sealed for approximately 15 years. Upon opening the sealed packages, the moisture content of the pulp was found to be 7.5% after conditioning at 23°C and 50% RH for 24 hours.

Prior to refining, the pulp was hand torn (into approximately 5 cm x 5 cm pieces) and soaked in deionized water for 24 hours. It was then disintegrated in a Noram Disintegrator at 5% consistency for 10,000 revolutions. The disintegrated pulp was then refined using the Valley Beater method with reference to Tappi Standard T 200 sp-01 [96]. With the exception of two specified cases, all the pulp for this study was refined at a charge of 300 O.D. grams per batch (diluted to 19.2 L with deionized water) for 30 minutes. The batch size is lower than specified in the test method to eliminate loss of pulp over the side walls of the Valley Beater during refining.

The final pulp Canadian standard freeness was targeted at 400 ml (with actual measured values ranging between 386 ml and 407 ml). Canadian standard freeness was measured following Tappi Standard T 227 om-04 [96] using a “new model” freeness tester manufactured in 1985. All freeness testers manufactured after 1967 are considered

to be “new models” [96]. Table 1 shows the physical characteristics of the pulp after refining in a Valley Beater to a targeted 400 ml Canadian standard freeness.

Table 1 Physical Characteristics of Refined Pulp

Physical Characteristics	FQA Measurements
Coarseness (mg/m)	0.143
Length Weighted Fines (%)	0.99
Average Length- Length Weighted (mm)	2.12
Average Curl- Length Weighted	0.047

Overall, the pulp was specifically selected and prepared in such a manner to create long, straight, conformable fibers that would easily bond. This is confirmed by the results shown in Table 1, measured using an Optest FQA (Fiber Quality Analyzer). The pulp selected for this study has a low coarseness, making it conformable and easily bondable. The Valley Beater refining method, chosen based on the comments of Page [97], has created a pulp with little fines, good fiber length and low curl. Page [97] stated that a low consistency refining method will remove curl, nodes, slip planes and microcompressions in pulp. Such phenomena will reduce tensile strength and elastic modulus within paper [97-100]. This pulp was diluted to 1.50% solids pulp slurry and stored between 2°C and 4°C until it was needed.

4.2 Additives

4.2.1 Bonding Agent (Bonder)

In addition to the pulp, several additives were utilized in this study. Prior to making handsheets, the pulp slurry could be treated with one or more of these additives

based on requirements for that set of handsheets. The first additive is a bonding agent or bonder. In this study, it was desired to be able to increase the specific bond strength of the paper without influencing other characteristics, such as formation and relative bonded area. Use of a bonder was necessary to accomplish this and based on the work of Leech [101], locust bean gum was selected. Leech [101] found that locust bean gum was effective in increasing specific bond strength while having minimal affects on formation and relative bonded area. This is also the same additive used by Seth and Page [40] in their study of the stress-strain curve in paper. Locust bean gum is a galacto-mannan polysaccharide derived from the Carob tree (*ceratonia siliqua*) and is readily adsorbed onto the surfaces of cellulose fibers [102]. This creates more opportunity for bonding, as locust bean gum is a branched polysaccharide.

The locust bean gum used in this study was derived from the seeds of the Carob tree and arrived in powdered form from Sigma Aldrich. Therefore, it was diluted in deionized water to a 1.00% weight by volume solution and refrigerated between 2°C and 4°C until use. When bonder was used, enough pulp slurry to make one handsheet was diluted to 0.50% solids and dosed with 0.45% by pre-diluted weight of bonder and mixed for one minute. The dosage of 0.45% was arrived at by using the Leech [101] data as a starting point and adjusting through experimentation.

4.2.2 Debonding Agent (Debonder)

In this study, it was not only desired to be able to increase the specific bond strength of the paper, but also decrease it without significantly affecting other properties. Use of a debonding agent or debonder was necessary to accomplish this and a cationic

quaternary ammonium surfactant was selected. The charge of the surfactant is determined by the hydrophilic head of the molecule. A cationic surfactant was chosen because the head of the molecule should adsorb onto the surface of the fibers (which are anionic). As a result, the hydrophobic tails of the surfactant will stick out from the fiber surfaces. It is proposed that this will act to reduce the effectiveness of bonding by blocking fiber-fiber interaction.

In this study, Croda AS-55 Cationic surfactant was chosen. It arrived in a very viscous form and was subsequently diluted in deionized water to a 1.00% weight by volume solution and refrigerated between 2°C and 4°C until use. When debonder was used, enough pulp slurry to make one handsheet was diluted to 0.50% solids and dosed with 0.11% by pre-diluted weight of debonder and mixed for one minute. The dosage of 0.11% was arrived at through experimentation.

4.2.3 Black Dye

In addition to altering the specific bond strength of paper with the use of bonders and debonders, it was also necessary to be able to dye fibers for the microscopic analysis portion of this study (Chapter 7). In order to visualize bonded areas under a light microscope, it is necessary to dye a portion of the fibers black. The reason for this will be discussed later in this chapter. The dye chosen for this was Chlorazol Black. This is the same dye that was used by Page et al. [52] and Page [103] and was shown to be quite effective in his study of bond visualization. This dye was also chosen by Lowe et al. [104] in more recent studies.

In this study, Chlorazol Black was added to the 1.50% pulp slurry at a 0.20% by weight dosage and allowed to soak for 24 hours. Once soaking was complete, the pulp slurry was washed exhaustively with deionized water until wash water was free of color. At that point, it was safe for the dyed black fibers to be mixed with un-dyed fiber and have bonder or debonder added according to the procedures previously discussed.

4.3 Handsheets

To make handsheets, the pulp slurry (either dyed or un-dyed) was diluted from 1.50% solids to 0.50% solids with deionized water. Once diluted, enough pulp slurry is measured out to make one handsheet of 90 g/m^2 on an oven dry basis. The pulp slurry is treated with either debonder or bonder based on prior discussed procedure or receives no treatment. The slurry was formed into a handsheet using a 21 cm x 21 cm Noble and Wood handsheet mold where deionized water was used as dilution water. A 100 mesh Noble and Wood stainless steel screen was used as the forming wire. Tappi handsheets were deemed impractical and not used in this study as larger sheets were necessary for creep testing. Figure 37 shows images of the Noble and Wood handsheet forming equipment consisting of the handsheet mold, plunger, rolling pin and screen used as the forming wire.

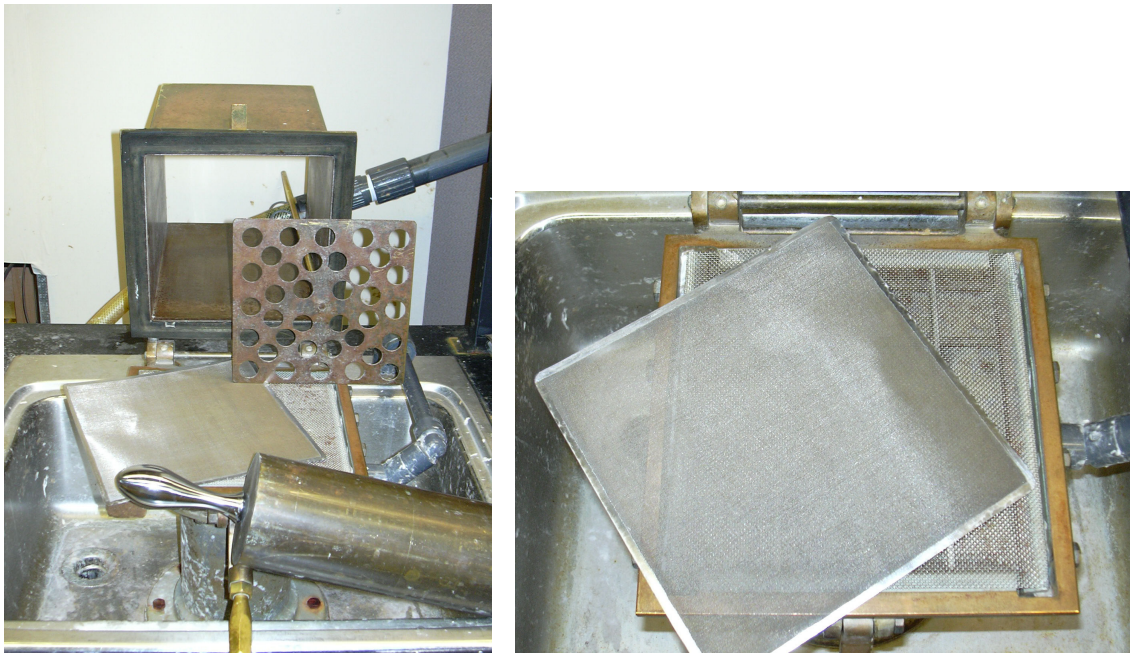

Figure 37 Noble and Wood Handsheet Forming Equipment Images

Sheets were wet pressed at 1.03 MPa, 0.17 MPa, or at 0.07 MPa. They were pressed using a manual hydraulic press. Sheets were pressed for five minutes, followed by a blotter change and pressed again at the same level for two minutes. Gloss plates were not used. Handsheets were dried on a drum dryer at 0.14 MPa steam pressure for 5 minutes. These sheets were fully restrained against the surface of the drum with a tensioned felt. Once dry, all sheets were immediately bagged and placed in a 23°C and 50% RH room for conditioning prior to testing. Sheets were conditioned for a minimum of 24 hours and remained in this conditioned environment throughout subsequent testing.

4.4 Physical Testing

4.4.1 Grammage, Caliper and Apparent Density

Once handsheet conditioning was complete, a comprehensive battery of physical testing was conducted. The first set of tests conducted were grammage, caliper and apparent density. First, all handsheets were cut into 180 mm x 180 mm squares thereby removing all outer edges. Using a Mettler Scale and following Tappi Standard T 410 om-02 [96], handsheet grammage was measured. A hard caliper measurement was made using an Emveco 200A electronic micro-gauge following Tappi Standard T 411 om-05 [96]. From grammage and caliper data, apparent density was calculated by dividing grammage by caliper. Density is referred to as apparent because paper is highly porous. Two sheets of paper with the same amount of fiber can have largely different apparent densities based on how consolidated the sheets are (how porous they are). Also the measurement of paper thickness is not straightforward and can be dramatically different depending on the method used to measure it.

4.4.2 Non-Destructive Testing

Following grammage, caliper, and apparent density measurements, several non-destructive physical properties measurements were made. These include ultrasonic modulus measurements, formation measurements, and light scatter measurements. Ultrasonic modulus measurements were made using the Institute of Paper Science and Technology (IPST) In-Plane Ultrasonic Modulus Tester. It uses sound waves to measure the elastic behavior of paper without destroying the sample. This is done by utilizing Newton's Second Law and measuring the velocity of sound through paper sent from a

transmitter to a receiver of known distance. The work of Mann et al. [105], as well as Baum et al. [106] offer additional detail and insight regarding the theory behind and inner workings of the ultrasonic modulus measurement. In this study, longitudinal in-plane ultrasonic moduli were measured by propagating a longitudinal wave through the paper at 100 kHz. The receiver and transmitter were connected to a Mitsubishi robotic arm that was controlled by a computer based data acquisition system. This system also recorded and calculated ultrasonic modulus values. Figure 38 shows images of the IPST In-Plane Ultrasonic Modulus Tester, which includes a view of the robotic arm and a close up of the transmitter and receiver.

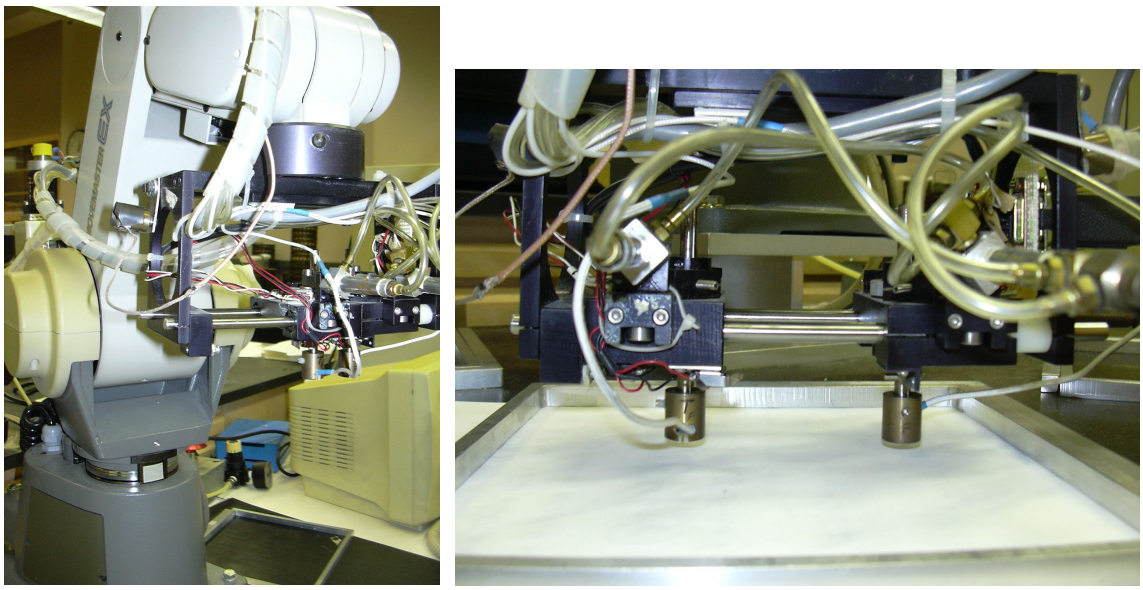

Figure 38 IPST In-Plane Ultrasonic Modulus Tester Images

Formation was tested using a MB Video Formation Tester. It works by placing a paper sample over a light box and measuring the variation in the amount of light that is transmitted through it on a small scale. This light is measured by a high resolution digital

video camera and an image of the paper is sent to a computer based data acquisition system. Based on the amount of light that transmits through the paper, the localized variation in mass can be discerned; an area higher in mass will transmit less light than an area low in mass. Based on the variation in light transmitted through the paper, a relative formation number is calculated. If this number is high, the amount of light transmitted through the paper is highly variable. Therefore, there is a high degree of mass variation in the sheet and poor formation (many areas with flocculations accompanied by many areas with light spots). If the formation number is low, the opposite would be true (a more uniform appearance in the paper). This method of measuring formation takes the subjectivity out of the formation measurement. In this study, formation was measured to confirm that the sheets have similar formation numbers so this would not be factor in the analysis of results.

The last non-destructive test conducted for this study was light scatter. Light scatter measurements can be used as a relative measure of bonding in paper. Justification for using light scatter as a measure of relative bonded area in paper has previously been demonstrated by Parsons [53] and Haselton [54]. Light scatter is calculated using Equation 26, and measuring R_o (the reflectance of a single layer of paper against an ideal black background), R_∞ (the reflectance of multiple layers of the same paper where the addition of additional layers will not change the reflectance), and w (the grammage of the paper).

$$LS = \frac{0.5}{bw} \ln\left(\frac{x+1}{x-1}\right)$$

$$a = 0.5\left(\frac{1}{R_\infty} + R_\infty\right) \qquad b = 0.5\left(\frac{1}{R_\infty} - R_\infty\right) \qquad x = \frac{1 - aR_o}{bR_o}$$

Equation 26 Light Scatter Calculation for Paper [96]

Equation 26, where LS is light scatter, is based on the Kubelka-Munk Theory and can be found with more information in Tappi Standard T1214 sp-02 [96]. In this study, light scatter values were calculated based on measurements of R_o, and R_∞ from a BNL-3 Opacimeter. The Opacimeter utilizes 572 nm light directed towards the paper sample at a 15 degree angle. The choice of light wavelength and angle were made to reduce absorption and surface gloss effects on the measurements.

4.4.3 Destructive Testing

Following the non-destructive testing, a series of destructive tensile tests were carried out. These consisted of zero-span tensile testing, z-directional tensile testing and tensile testing. Zero-span tensile strength was measured following Tappi Standard T 231 cm-96 [96]. The only significant deviation from the standard is that 90 g/m^2 sheets were used as opposed to 60 g/m^2 sheets. In this study, a Pulmac TS-100 Zero Span Tensile Tester was used. The gap between the clamps was set to zero and zero-span tensile strength was measured and displayed on a digital readout. Zero-span tensile strength was

measured to confirm that all of the sheets made regardless of treatment have the same fiber properties so this would not be factor in the analysis of results.

Z-directional tensile strength was measured following Tappi Standard T 541 om-05 [96]. In this study, a TMI Model 84-22 Z-directional Tensile Tester was used. Results from testing were recorded by the machine and displayed on a digital readout. As no direct measurements of specific bond strength were made in this thesis, an alternative method needed to be used. Differences in z-directional tensile strength can be used as a relative indication of bonding within paper. This is possible because the fiber contribution to z-directional tensile strength is minimal as fibers are not aligned in the z-direction of the sheet. If relative bonded area measured through light scatter is held constant, differences in z-directional tensile strength can be attributed to differences in specific bond strength [56].

In-plane tensile strength was measured following Tappi Standard T 494 om-01 [96]. The only significant deviation from the standard is that the spacing between the jaws was 140 mm as opposed to 180 mm. Tensile testing was conducted at this lower span to compare better with creep testing, which also was conducted at a 140 mm span. In this study, an Instron Model 1122 Tensile Tester was used. It was controlled by a computer based data acquisition system using Instron Series IX software. In addition to tensile strength measurements, strain at failure measurements and stress-strain curves were recorded by the computer system.

4.5 Creep Testing

4.5.1 Constant Humidity Testing

Constant humidity creep testing was conducted using the IPST tensile creep tester under a constant 23 °C and 50% RH condition. Samples were cut into 170 mm x 25 mm wide strips and mounted in the clamps using a jig assembly to assure proper alignment and dimension of the test strip. A thin layer of Miller-Stephenson Epoxy 907 was applied to the surfaces of the clamps to act as an adhesive with the paper. Once the strips were mounted into clamps, the free length of the test strip was reduced from 170 mm to 140 mm. These strips were conditioned in the jig for 24 hours at 23 °C and 50% RH to allow the epoxy to set prior to any application of load.

Once the epoxy had set, strips were removed from the jig (with clamps adhered to the test strips on the bottom and top) and placed into the tensile creep tester where load was applied. A series of different magnitude dead loads (initial applied stress levels) were evaluated. Displacements and failure times were recorded using linear variable displacement transducers (LVDT sensors) with the output signals sent to a computer based data acquisition system. In addition, the creep tester was equipped with a bubble column and dry air supply so the computer system could control the humidity as well. This gave better humidity control and greatly reduced the possibility of humidity fluctuations adversely affecting the test results. Computer control of relative humidity was based off measurements of an HMP233 Vaisala humidity and temperature transmitter. Light scatter of creep test strips were measured prior to and after creep deformation testing according to the previously discussed light scatter procedure. Figure

39 shows images of the IPST tensile creep tester with a close up of the mounted strips inserted into the tester.

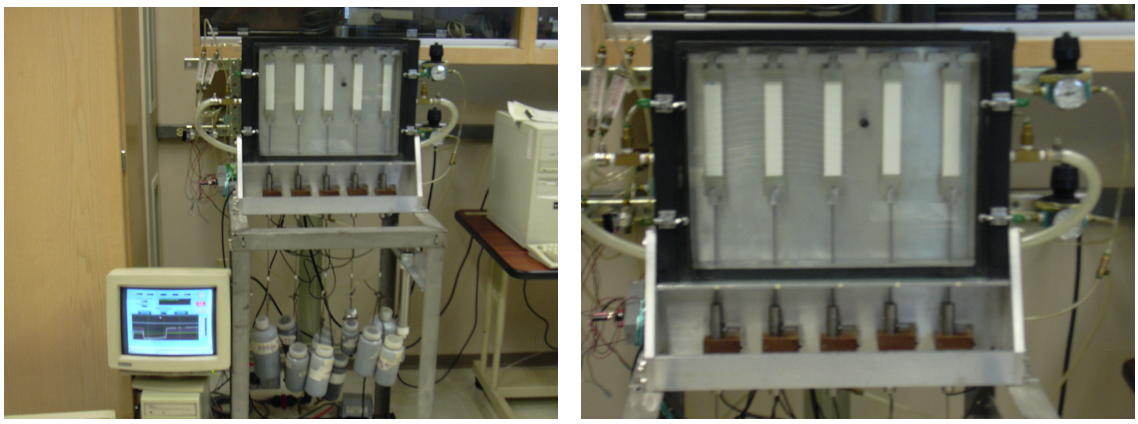

Figure 39 IPST Tensile Creep Tester Images

4.5.2 Accelerated Creep Testing

As previously mentioned, the IPST tensile creep tester is able to control humidity, making it possible to test paper at differing humidity levels and under cyclic humidity conditions. This type of testing was conducted for the accelerated creep portion of the study (Chapter 8). In all cases, a single dead load (2.68 N/mm initial applied stress) was used as the only concern was with moisture effects, not load. Instead of 23 °C and 50% RH, constant humidity creep testing was conducted as 23 °C and 25% RH as well as 23 °C and 75% RH. Because relative humidity is at 50% when test strips are removed from the jigs, test strips are placed in the creep tester and conditioned for an additional 24 hours at 23 °C at the desired constant humidity level (either 25% RH or 75% RH). Therefore, strips spent 24 hours in the jig and an additional 24 hours in the creep tester prior to load application.

Cyclic humidity testing was conducted by applying the tensile dead load for three hours at 23 °C and 50% RH followed by cycling the relative humidity 10 times between 25% RH and 75% RH. One cycle consisted of a 1 minute ramp to 25% RH, maintaining the relative humidity at 25% for one hour, followed by a 5 minute ramp from 25% RH to 75% RH, and maintaining the relative humidity at 75% for 1 hour. By starting the accelerated creep test sequence at 50% RH, the additional 24 hours conditioning in the creep tester was eliminated. If the cyclic humidity testing began at a relative humidity other than 50%, then an additional 24 hours of conditioning would have been necessary at the desired starting relative humidity level. Again, light scatter of the creep test strips were measured prior to and after creep deformation testing according to the previously discussed light scatter procedure to measure changes in relative bonded area.

4.6 Microscopy

A portion of this study involved the microscopic analysis of bonded area prior to and after creep testing (Chapter 7). To conduct this work, a light microscope system available at IPST was used. The light microscope is a Leica DM-IRM Inverted Reflected Light Microscope equipped with a 40X Leica objective. Using this objective and adjusting the magnification to the desired levels, images are seen magnified 600X. Images seen through the objective are photographed using a Hamamatsu ORCA-ER Digital Camera. Images are sent to a computer based data acquisition system (SimplePCI), which allows for image storage and analysis. The light source used is a 50 watt metal halide lamp employing monochromatic light at a wavelength of 547 nm ±10 nm. The entire system, with the exception of the computer is placed atop a damping table

to minimize blur in the acquired images due to vibration. Figure 40 shows images of the light microscope system and a close-up of the objective used. This entire system resides in a temperature and humidity controlled room at 23 °C and 50% RH.

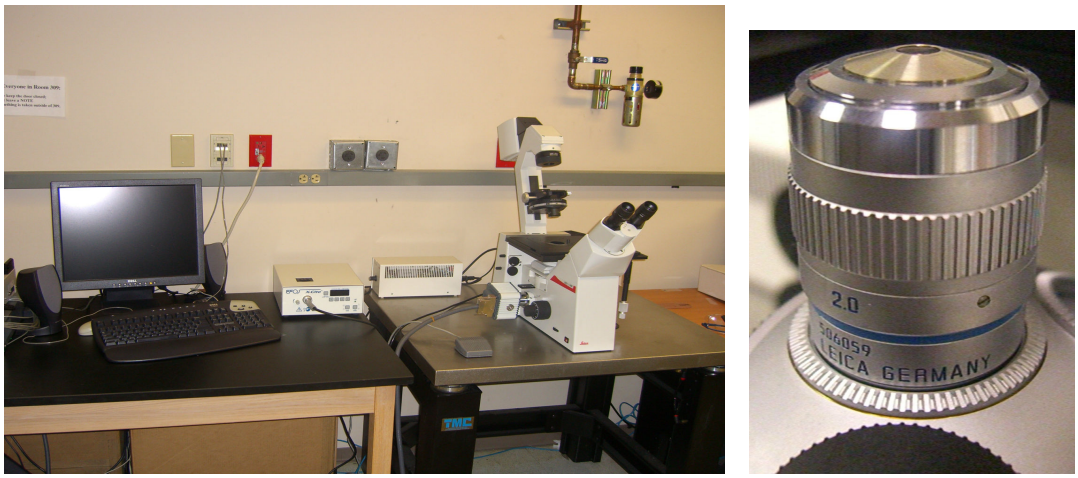

Figure 40 Light Microscope System and Objective Images

In order to image bonded areas under the light microscope, it was necessary that a certain percentage of the fiber in the handsheets used in this analysis be black. The procedure for creating black fibers and the dye used were outlined earlier in the chapter. Based on the work of Page et al. [52] and Page [103], who also visualized bonded area using light microscopy, the proper ratio of fibers in the sheet should be approximately 70% dyed, 30% un-dyed. In this work, it was found through experimentation, that 85% dyed, 15% un-dyed worked best for the furnish type used.

The reason a portion of the fibers need to be dyed and a portion un-dyed is related to the scattering of light. Dyed fibers will appear dark under the microscope because they will absorb all the incident light. On the other hand, un-dyed fibers will either scatter light of allow light to transmit through depending on surface interfaces. Light will scatter if the un-dyed fiber interfaces with air. Light will transmit through if the

interface is with another fiber. If a dyed fiber lies below an un-dyed fiber to create a fiber-fiber interface, the portion of the un-dyed fiber in contact with the dyed fiber will appear dark, while the rest of the fiber appears light. This dark spot is the bonded area between the two fibers. To improve contrast, between un-dyed and dyed fibers, images are viewed in cross polars. Viewing in cross polars refers to transmitting the incident light to the fibers in one orientation and viewing the returning scattered light in a different orientation. All light in other orientations are filtered out by polarizers.

In this study, images of bonded areas are taken before and after creep testing to analyze the behavior of the bonds during long-time straining. This was accomplished by marking areas where images were taken before creep testing and relocating them after creep testing. Changes in bonded areas and angles of the fiber crossings were measured before and after creep testing using the SimplePCI computer software used to acquire the image from the digital camera. Angle change was determined by drawing a line down the central axis of each fiber forming an intersection and measuring the angle relative to the direction of the applied stress. Bonded area changes were calculated by tracing bonded areas on each pre-creep and post-creep image. Figure 41 shows an image (at 600X magnification) of several fiber crossings with visible dark bonded areas. In the image, an un-dyed fiber is bonded with several Chlorazol Black dyed fibers which lie below the un-dyed fiber.

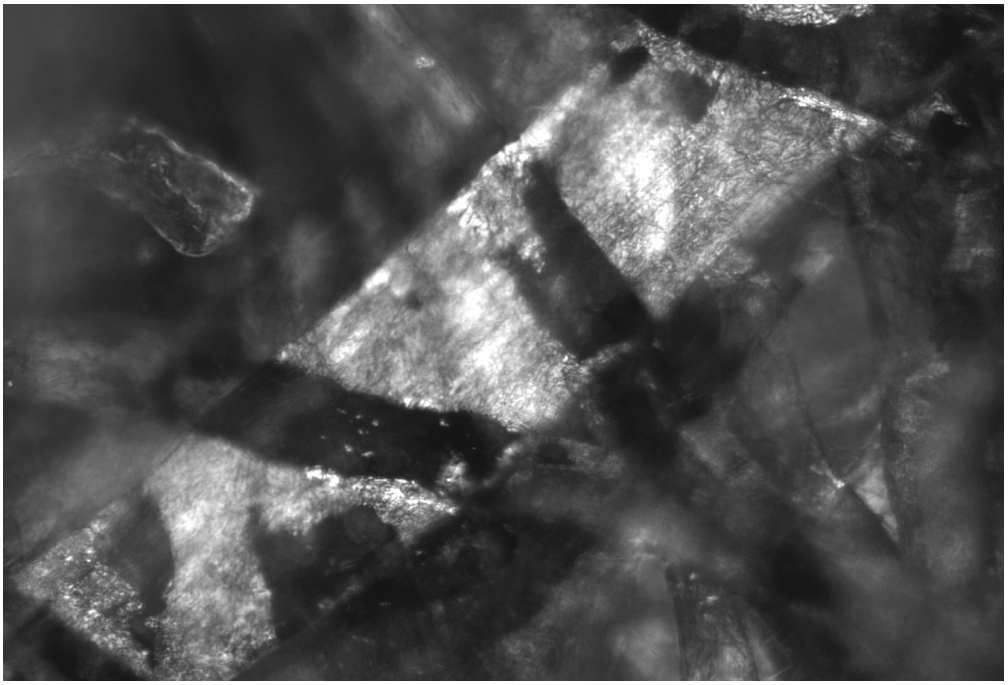

Figure 41 Representative Image of an Un-Dyed Pulp Fiber Bonded to Several Chlorazol Black Dyed Fibers (600X)

CHAPTER 5: INFLUENCE OF BONDING ON THE TENSILE CREEP BEHAVIOR OF PAPER

5.1 Abstract

In this study, two sets of sheets were made with differing levels of specific bond strength and relative bonded area. The sheets of one set were wet pressed using a high press load and the other sheets were wet pressed using a low press load. Within each set, the sheets were treated with either a debonder or a bonder or received no treatment. Creep behavior data showed that creep curves for the debonder, bonder, and untreated sheets were the same for the sheets wet pressed at the high press load and different for the sheets wet pressed at the low press load. Creep failure time was influenced by the treatments in both the high and low load wet pressed sheets; sheets treated with debonder failed first and the sheets treated with bonder failed last. It was concluded that at high levels of bonding as is the case with the high load wet pressed sheets, differences in specific bond strength due to the treatments do not influence creep deformation because bonding is at a level where the sheets are efficiently loaded structures. The low load wet pressed sheets showed differences in creep deformation when specific bond strength was changed with treatments because bonding was at a lower level where the sheets were inefficiently loaded. As the loading efficiency of the paper structure is improved through increased bonding (either by increasing specific bond strength or relative bonded area), an efficiently loaded structure can be achieved where bonding no longer affects deformation. This allows creep behavior to reach a minimum level which is dictated solely by the fibers. An efficiency factor can be used to describe deformation behavior where an efficiency of "1" indicates an efficiently loaded structure and lower values indicate a less

than fully efficient structure, one in which bonding influences deformation behavior. In this study, efficiency factors were used to scale the low load wet pressed sheet results and several sets of lesser refined and pressed sheets (thereby "removing" bonding influence) and the data superimposed onto the high load wet pressed sheet results.

5.2 Introduction

Although research by Hill [38, 39] found that fibers are the structural element from which creep behavior originates in paper, it is still unclear exactly how bonding of these fibers may influence this behavior. Beginning with the research of Byrd [64, 74, 75] the focus of creep research shifted to accelerated creep without fully understanding the role of bonding. This has resulted in a limited base of available research regarding bonding and creep in the literature.

Brezinski [36, 37] showed that as wet pressing and level of refining were increased, higher initial applied stress levels were required to get the same amount of strain after 24 hours of creep testing. This implied that as bonding is improved either through wet pressing (densification) or refining (making more conformable fibers), that creep decreases. Parker [59] also showed that as bonding is improved through wet pressing, creep will decrease. His work also showed that as bonding is increased, it plays a decreasing role in creep deformation behavior. Schulz [60, 61] showed that increased levels of wet straining leads to a decrease in creep behavior. He hypothesized that wet straining has the affect of changing the way stress is distributed within the paper structure. In other words, wet straining makes paper more efficient in distributing stress, causing a drop in creep behavior. Unfortunately, it is unclear if this is the dominant

reason for the drop in creep behavior. For example, fiber kinks and micro-compressions could be pulled out causing a strain hardening effect.

With regard to relative bonded area change, Sanborn [62] showed that light scatter increased as strain during creep testing increased. This implied that there is some relative bonded area loss during creep testing. It does not, however, imply that creep deformation was caused by bond breakage, only that bond breakage occurs concurrently. On the other hand, Byrd [64] showed in his research that light scatter decreased as strain during creep testing increased. His data implied relative bonded area was increasing during creep deformation. A most probable explanation is that there was minimal relative bonded area loss and the decrease in light scatter was due to fibers being drawn into optical contact from lateral contraction and longitudinal straining.

Overall, there are no definitive answers and some possible contradictions in the existing body of paper creep literature. By comparison, the role of bonding with regard to elastic modulus, stress-strain behavior and tensile strength has been extensively researched. Page [41] showed through development of an empirical model, "The Page Equation", that tensile strength in paper can be altered by changing relative bonded area and specific bond strength. In addition, Seth and Page [40] were able to show that when decreasing specific bond strength (with a debonder) or increasing specific bond strength (with a bonder), elastic modulus and the shape of the stress-strain curve remained constant as long as there was an adequate level of bonding to maintain a fully efficient loaded structure, a structure where changing bonding no longer influences the deformation of paper. The only differences in the overall behavior produced by such changes were different strain to failures and tensile strengths. Seth and Page [40] also

measured changes in light scatter and found a loss of relative bonded area after sheet straining. They showed that relative bonded area decreased at differing rates depending on the treatment applied. The debonder treated sheets have the highest rate of loss followed first by the sheets with no treatment and finally by the bonder treated sheets.

In addition, Seth and Page [40] introduced the concept of the efficiency factor. Their premise is that deformation behavior within paper originates within the fibers and an efficiency factor can be used to show the influence of bonding regardless of whether the deformation behavior is elastic or plastic. Specifically, they showed that if stress-strain curves for paper made from the same fibers did not overlap, they could be made to overlap by dividing the stress component of the stress-strain curve by an efficiency factor. The efficiency factor was calculated by dividing the elastic modulus of the more compliant stress-strain curves (inefficiently loaded structures) by the elastic modulus of the least compliant, efficiently loaded, stress-strain curve. Elastic modulus was determined by finding the slope of the stress-strain curve in the elastic region. Seth and Page [40] were able to show that the whole stress-strain curve, both elastic and plastic portions, would superimpose. Simply put, deformation behavior in the plastic region followed an elastically derived efficiency factor and this held true as long as bond breakage was not severe enough to reduce the efficiency factor during straining.

5.3 Experimental

5.3.1 Pulp and Preparation

NIST standard reference material 8495 Northern Softwood Bleached Kraft Pulp was used in this study. The pulp arrived in dry lap sheets in a hermitically sealed

package. The pulp had remained sealed for approximately 15 years. Unless otherwise specified, the pulp was refined in a Valley Beater at a charge of 300 O.D. grams per batch for 30 minutes. The final pulp Canadian Standard Freeness was targeted at 400 ml. The pulp was prepared in such a manner to create straight, conformable fibers that would easily bond. Prior to making handsheets, the pulp slurry was treated with either a debonder or a bonder or received no treatment. The debonder used was a cationic surfactant (Incrosoft AS-55), from Croda, while the bonder used was locust bean gum, from Sigma-Aldrich. Bonder and debonder were added to the pulp slurry and mixed for 1 minute at dosages of 0.45% and 0.11% by weight, respectively.

5.3.2 Handsheets

Handsheets were made using a 210 mm x 210 mm Williams handsheet mold. A 100 mesh screen was used as the forming wire. The handsheets made from the treated pulp slurries were targeted to have an oven dry basis weight of 90 g/m^2. Sheets were wet pressed at either 1.03 MPa, 0.17 MPa or at 0.07 MPa, depending on sample set. Sheets were pressed for five minutes, followed by a blotter change and pressed again at the same level for two minutes. Gloss plates were not used. Handsheets were dried on a drum dryer under full restraint at 0.14 MPa steam pressure for 5 minutes. All sheets were immediately bagged and placed in a 23°C and 50% RH room for conditioning prior to testing. The process used insured that for each press load (1.03 MPa, 0.17 MPa, and 0.07 MPa), sheets were produced with similar calipers and densities and most importantly similar relative bonded areas. Wet pressing acts to consolidate the sheet, thereby altering the caliper, density, and relative bonded area of the sheet. The sheets pressed at low loads

had a lower relative bonded area than those pressed at high loads. The addition of bonder and debonder does not alter the relative bonded area, but instead increases or decreases the specific bond strength. Given equal relative bonded area and different specific bond strengths, overall bonding is altered. Therefore, with each group of sheets, there were sheets with enhanced, degraded, and unchanged levels of specific bond strength.

5.3.3 Physical and Creep Testing

Extensive physical testing was conducted including, handsheet grammage, hard caliper, ultrasonic velocities, formation, light scatter, zero-span tensile strength, z-directional tensile strength, and in-plane tensile strength. In-plane tensile measurements were made using an Instron tester with jaw spacing of 140 mm to be consistent with creep testing spans. Stress-strain curves were recorded for each of the in-plane tensile tests. Although no direct measurement of specific bond strength is made in this study, differences in z-directional tensile strength will indicate a change in specific bond strength when relative bonded area remains constant. Within each set of handsheets, density was held constant and thereby relative bonded area was also held constant, by careful control of refining, pressing and drying.

Creep testing was conducted using the IPST tensile creep tester under a constant 23 °C and 50% RH condition. Samples were cut into 170 mm x 25 mm wide strips, mounted and conditioned for 24 hours at 23 °C and 50% RH condition prior to application of load. The free length of the samples after mounting was 140 mm. A series of different magnitude dead loads (initial applied stress levels) were evaluated. Displacements and failure times were recorded using linear variable displacement

transducers (LVDT sensors) with the output signals sent to a computer based data acquisition system. Light scatter of creep test strips were measured prior to and after creep deformation testing to measure relative bonded area change. The basis for using light scatter as means to measure changes in relative bonded area in paper has previously been demonstrated [53, 54].

5.4 Results

5.4.1 High Load Wet Pressed Sheets

The first of two sets of results presented are for sheets treated with debonder, nothing (control), or bonder that were wet pressed at high load (1.03 MPa) resulting in high density, highly bonded sheets. Table 2 shows the physical testing results for these sheets.

Table 2 Physical Testing Results from the High Load Wet Pressed Sheets

Sheet Treatment	Grammage (g/m^2)	Hard Caliper (mm)	Apparent Density (g/cm^3)	Formation Number	Ultrasonic Modulus (km^2/s^2)
Debonder	96.0	0.118	0.814	32.8	10.6
Control	95.8	0.117	0.819	33.8	10.8
Bonder	95.7	0.115	0.832	33.4	10.9
Variation	0.3%	2.6%	2.2%	1.8%	2.8%

Sheet Treatment	Light Scatter (m^2/g)	Z-Tensile (N/mm^2)	Tensile (N/mm)	Failure Strain (%)	Zero-Span (N/mm)
Debonder	21.4	0.672	9.12	3.39	15.5
Control	20.5	0.798	10.2	3.84	15.8
Bonder	19.8	0.927	10.7	3.99	16.0
Variation	8.1%	37.9%	17.3%	17.7%	3.2%

The data from physical testing presented in Table 2 show that sheets treated with debonder and bonder did not show significant differences from the control with regard to grammage, hard caliper, formation, and zero-span tensile strength. Deformation behavior, as indicated by the ultrasonic elastic modulus data in Table 2 and stress-strain curves shown in Figure 42 were similar for all three sets. The differences in the sheets were in z-directional tensile strength, tensile strength, and strain to failure, caused predominantly by differences in specific bond strength. A small influence due to variation in relative bonded area (indicated by light scatter differences and slight apparent density differences) cannot be ruled out. The z-directional tensile strength in the bonder treated sheets would have been even higher if it were not for the contribution due to failure of the tape used to conduct the test. Figure 42 shows that sheets treated with debonder were the weakest, while the sheets treated with bonder were the strongest and illustrates how deformation between the three sets of sheets remains similar, only differing in the failure point.

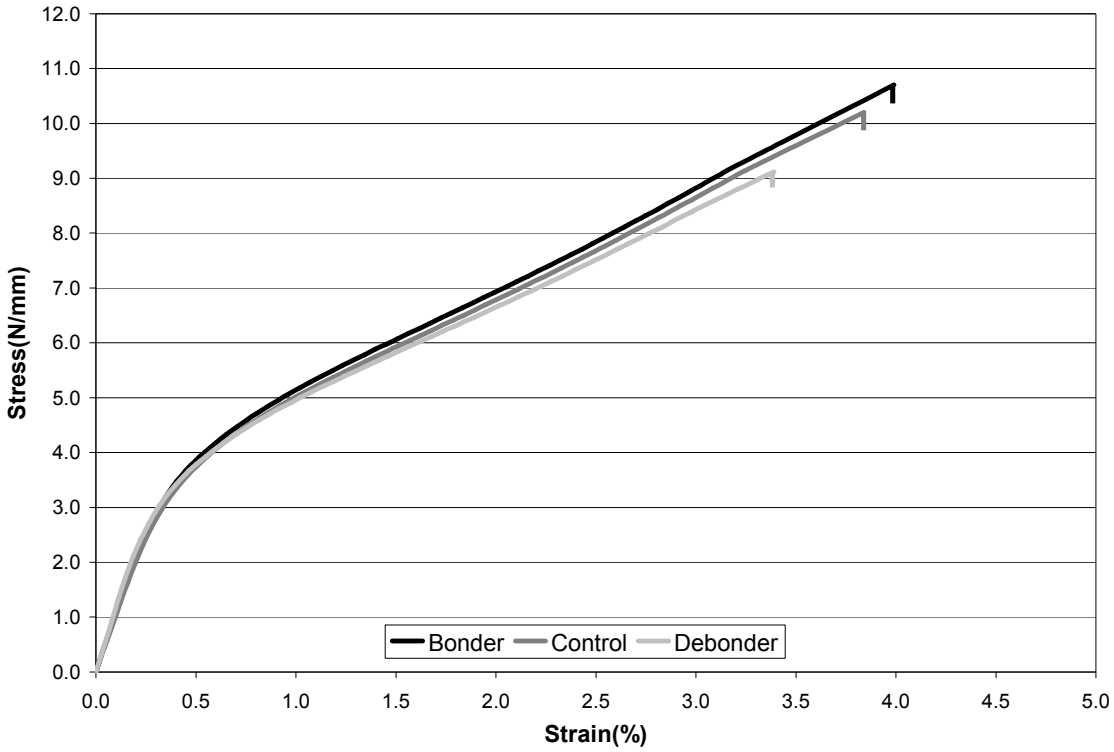

Figure 42 Stress-Strain Curves from Instron Tensile Testing of High Load Wet Pressed Sheets

These results demonstrate that it is possible to create three sets of handsheets with similar deformation behavior and differing specific bond strengths. These results also confirm the work of Seth and Page [40] where at high levels of bonding, a fully efficient paper structure can be created where elastic modulus plateaus and differences in specific bond strength do not affect deformation behavior, but do influence failure behavior. According to Seth and Page [40] , the elastic modulus of a fully efficient randomly oriented sheet should be approximately one-third of the fiber modulus. These results are consistent with that relationship according to data listed by Seth and Page [40] for black spruce fibers; a fiber source similar to the fibers used within this thesis. That said, to get a

true assessment, the modulus of the fibers within this thesis would need to be measured and compared to the elastic modulus results of the paper.

Creep behavior results follow the same trend with regard to deformation as the elastic modulus data and stress-strain behavior. This would indicate that even though the time duration for a creep test is much longer than that of a stress-strain measurement, its influence was not a factor. Overall, as illustrated in Figure 43, the creep curves generated at several different initial applied stress levels show good overlap and fall within the standard error bars, indicating they have creep behaviors that cannot be differentiated from each other.

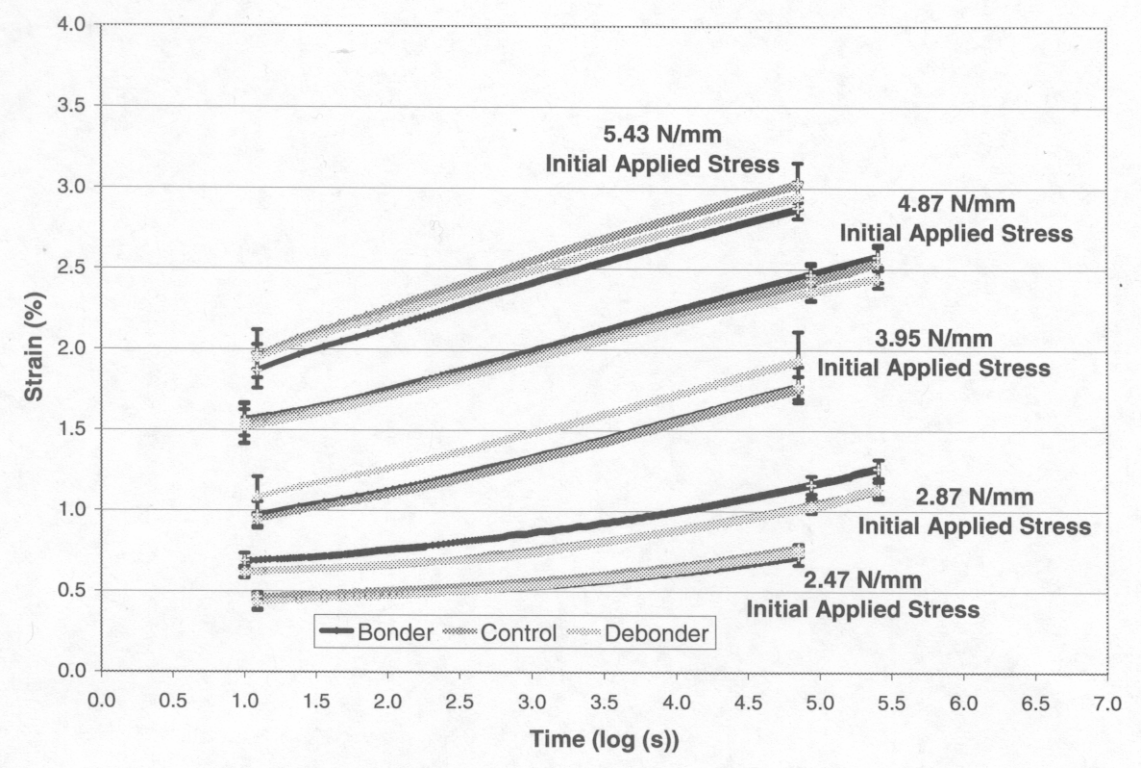

Figure 43 Creep Curves from High Load Wet Pressed Sheets

Further proof for this is obtained by constructing isochronous stress-strain curves from the data. Isochronous stress-strain curves, plotting strain versus the initial applied stress at various snapshots in time, are another way of comparing creep data. In Figure 44, strain after 10 seconds and 24 hours of creep testing are plotted versus initial applied stress. As illustrated in Figure 44, the isochronous stress-strain curves derived from the creep curves in Figure 43 for the debonder, control, and bonder sheets do not show any significant difference between the cases. The curves overlap and fall within the standard error bars. The data was fit with power function trend lines with R^2 values all greater than 0.97. This is contrary to the expectation that the bonder treated sheets would be the least compliant and the debonder treated sheets would be the most compliant.

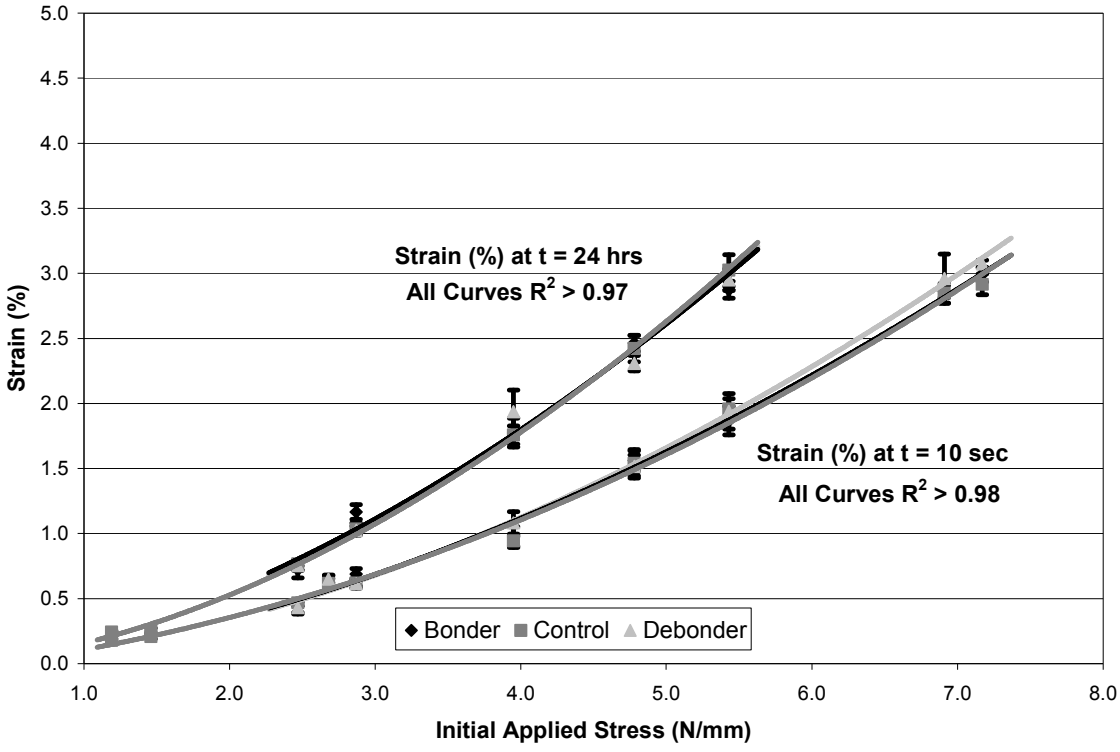

Figure 44 Isochronous Stress-Strain Curves from Creep Testing of High Load Wet Pressed Sheets

Furthermore, light scatter data indicated that the loss of relative bonded area occurred at differing rates. Figure 45 shows that at a given level of strain, the bonder treated sheet showed the smallest change in light scatter and debonder treated sheet the greatest. In order to more easily illustrate these differences in relative bonded area loss versus strain, the data points were fit with a second order polynomial function, all of which gave R^2 values greater than 0.90. Overall, this data indicated that creep behavior remains unaffected at high levels of bonding despite differences in specific bond strength and rate of relative bonded area decrease.

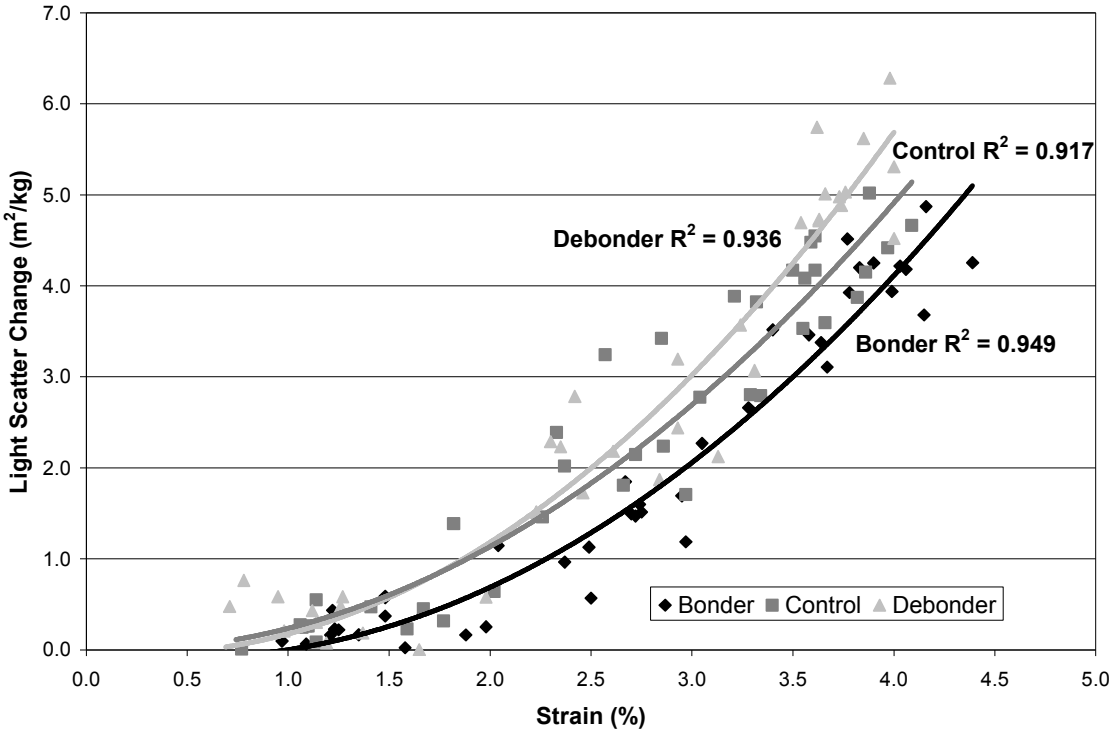

Figure 45 Light Scatter Change versus Strain From Creep Testing of High Load Wet Pressed Sheets

Additional creep testing was done at a higher initial applied stress level with the intent of causing failure, allowing a more detailed analysis of the behavior. Figure 46 illustrates the failure points and light scatter change versus time for debonder, control and bonder treated sheets.

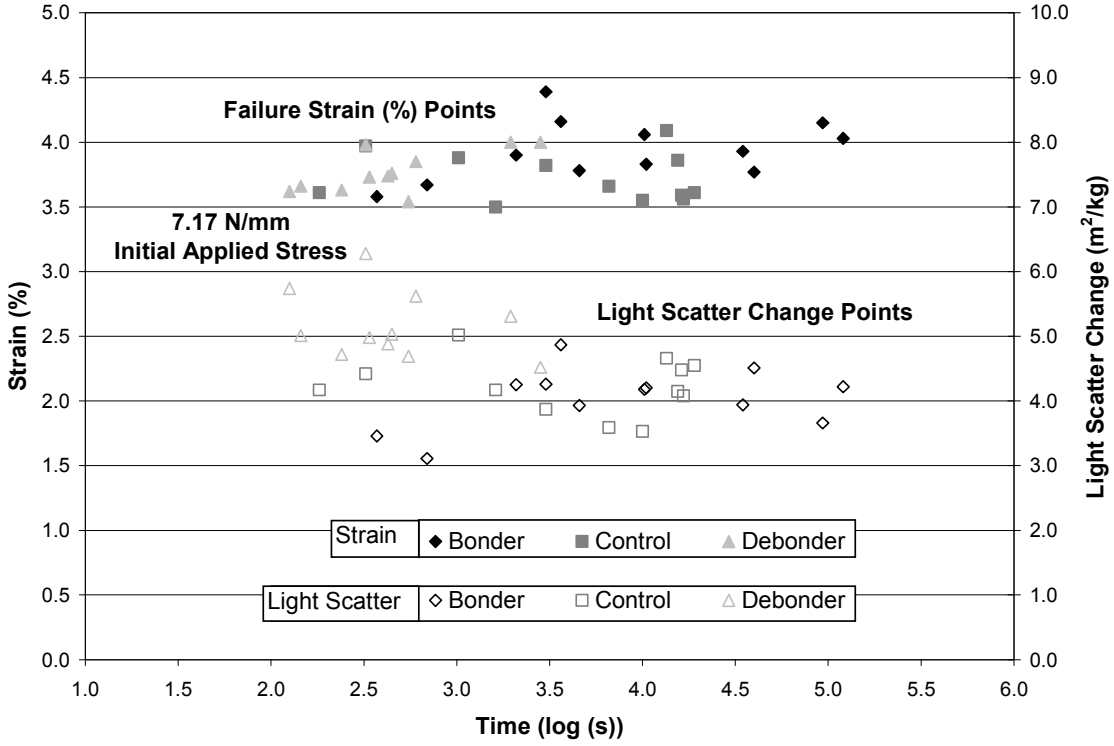

Figure 46 Creep Testing Failure Strain and Light Scatter Change versus Time for High Load Wet Pressed Sheets

The debonder treated sheets failed much sooner than the bonder treated sheets with the control failure points scattered in between. Average failure strain is not significantly different in the bonder treated sheets versus the control and debonder sheets. Light scatter change indicates that there is the greatest loss in relative bonded area with

the debonder treated sheets and the change occurs fastest in those sheets. Table 3 summarizes the data illustrated in Figure 46.

Table 3 Failure Strains, Times and Light Scatter Changes for High Load Wet Pressed Sheets

Sheet Treatment	Failure Strain (%)	Failure Time (log(s))	Failure Time (min)	Light Scatter Change (m^2/g)
Debonder	3.77	2.86	12.1	5.16
Control	3.73	3.94	144	4.22
Bonder	3.94	4.43	449	4.04
Variation	5.6%	54.9%	>>100%	27.7%

As indicated by the percentage differences in Table 3, there are large differences in failure time and light scatter change between the three differently treated sets of sheets. The bonder treated sheets last over an order of magnitude longer than the debonder treated sheets. The debonder treated sheets have an almost 30% higher change in light scatter than the bonder treated sheets. Overall, the creep behavior data are consistent with Seth and Page [40]. The creep curves and isochronous stress-strain curves indicate that creep behavior is the same for sheets wet pressed at high load, despite differences in specific bond strength. The differences in specific bond strength manifests itself only by a change in failure behavior and change in light scatter.

5.4.2 Low Load Wet Pressed Sheets

The second set of results presented here are sheets treated with debonder, nothing (control), or bonder and wet pressed at low load (0.17 MPa), resulting in lower density

and less bonded sheets than the highly pressed case. Table 4 shows the physical testing results for these low load wet pressed sheets.

Table 4 Physical Testing Results from the Low Load Wet Pressed Sheets

Sheet Treatment	Grammage (g/m^2)	Hard Caliper (mm)	Apparent Density (g/cm^3)	Formation Number	Ultrasonic Modulus (km^2/s^2)
Debonder	95.2	0.145	0.657	31.7	9.73
Control	94.9	0.143	0.664	31.8	10.2
Bonder	95.0	0.141	0.674	31.3	10.6
Variation	0.3%	2.8%	2.6%	1.3%	8.9%

Sheet Treatment	Light Scatter (m^2/g)	Z-Tensile (N/mm^2)	Tensile (N/mm)	Failure Strain (%)	Zero-Span (N/mm)
Debonder	27.6	0.474	8.57	3.54	15.4
Control	26.9	0.567	9.18	3.59	15.7
Bonder	26.1	0.631	10.2	3.85	15.3
Variation	5.7%	33.1%	19.0%	8.8%	2.6%

As with the high load wet pressed case, the data from physical testing presented in Table 4 showed that sheets treated with debonder and bonder did not show significant differences from the control with regard to grammage, hard caliper, formation, and zero-span tensile strength. The major noticeable difference between the low load wet pressed sheets and the high load wet pressed sheets is that the low load wet pressed sheets have more bulk than the high load wet pressed sheets. This is seen by comparing the sheet apparent densities from Table 2 and Table 4. Deformation behavior, as indicated by the ultrasonic elastic modulus data in Table 4 and stress-strain curves illustrated in Figure 47 were more dissimilar for all three sets than in the case of high load wet pressed sheets. Light scatter in the low load wet pressed sheets is higher, indicating a lower relative

bonded area than the high load wet pressed sheets. The same differences as with the high load wet pressed sheets existed with regards to z-directional tensile strength, tensile strength and strain to failure. Sheets treated with debonder were the weakest, while the sheets treated with bonder were the strongest.

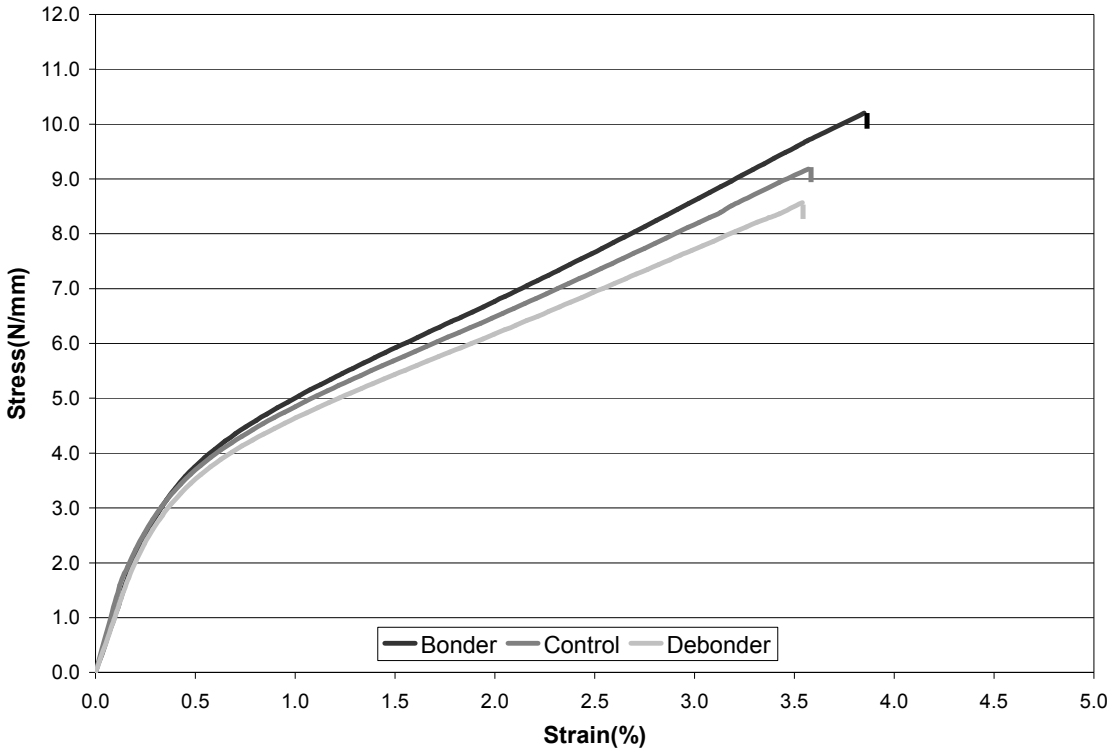

Figure 47 Stress-Strain Curves from Instron Tensile Testing of Low Load Wet Pressed Sheets

Overall, the low load wet pressed sheets have lower moduli, more compliant stress-strain curves, and are weaker than the high load wet pressed sheets. These results also relate to the work of Seth and Page [40]; at lower levels of bonding, an inefficient paper structure is created where elastic modulus has not reached a plateau, and

differences in specific bond strength and relative bonded area do affect deformation and failure behavior.

Creep behavior results again follow the same trend with regard to deformation as the elastic modulus data, and stress-strain behavior. Overall, as illustrated in Figure 48, the creep curves generated at several different initial applied stress levels show poor correlation as the curves do not overlap and do not have overlapping standard error bars. In all cases, the bonder treated sheets are the least compliant and debonder treated sheets are the most compliant.

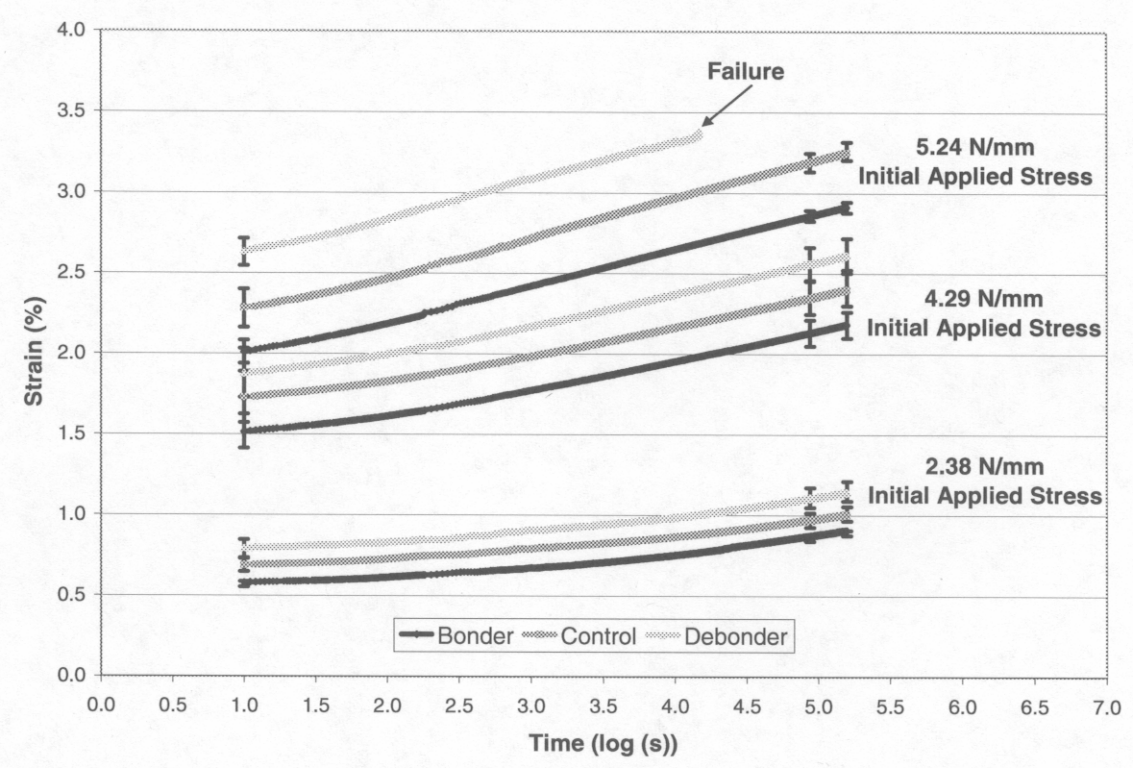

Figure 48 Creep Curves from Low Load Wet Pressed Sheets

Again, isochronous stress-strain curves can be generated from the creep data to further illustrate differences in the creep behavior. In the Figure 49, strain after 10

seconds and 24 hours of creep testing are plotted versus initial applied stress. As illustrated in Figure 49, the isochronous stress-strain curves derived from the creep curves in Figure 48 for the debonder, control and bonder sheets show that the creep behavior is different between the cases. Again, the bonder treated sheets are the least compliant and the debonder treated sheets are the most compliant. The curves do not overlap or fall within the standard error bars. All data were fit with power function trend lines, all with R^2 values greater than 0.96.

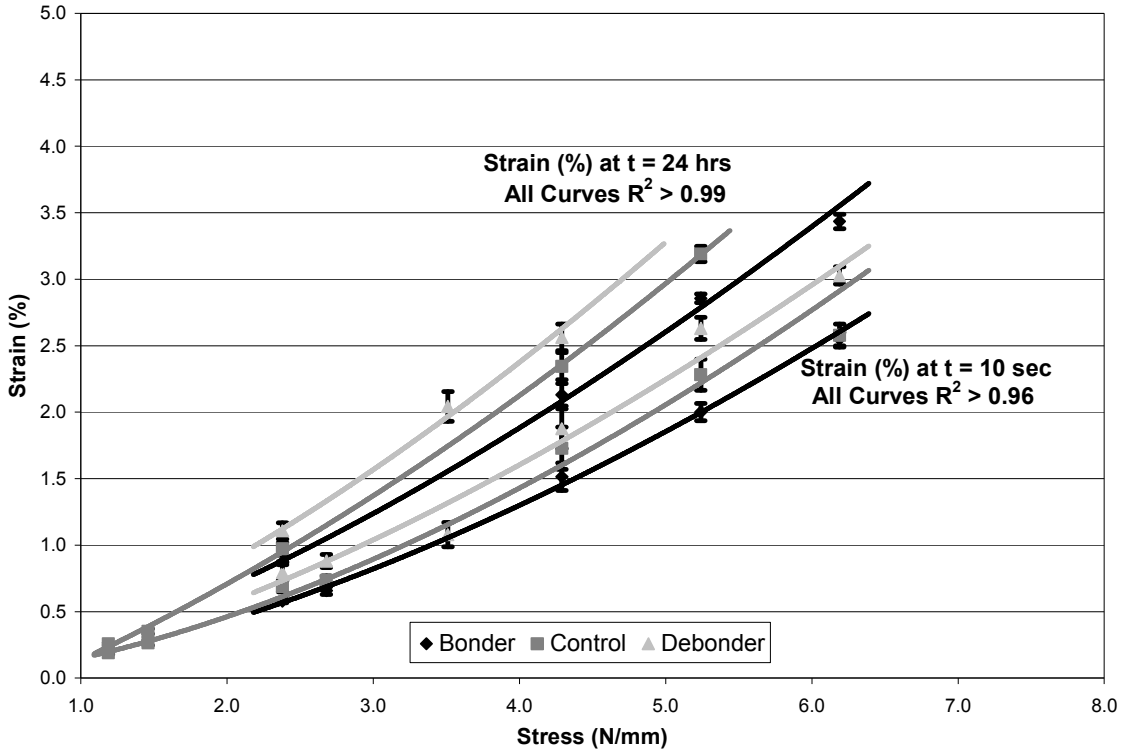

Figure 49 Isochronous Stress-Strain Curves from Creep Testing of Low Load Wet Pressed Sheets

As with the high load wet pressed sheets, light scatter data indicate that the loss of relative bonded area occurred at differing rates. Figure 50 shows that at a given level of

strain, the bonder treated sheet exhibit the smallest change in light scatter and debonder treated sheet the greatest. In order to more easily illustrate these differences in relative bonded area loss versus strain, the data points were fit with a second order polynomial function, which gave R^2 values all over 0.80. Overall, the change in relative bonded area is smaller for the low load wet pressed sheets than the high load wet pressed sheets. This is due to the fact that there is less initial relative bonded area in the low load wet pressed sheets versus the high load wet pressed sheets. Therefore, a small change in light scatter amounts to a much larger percentage of relative bonded area loss in the low load wet pressed sheets.

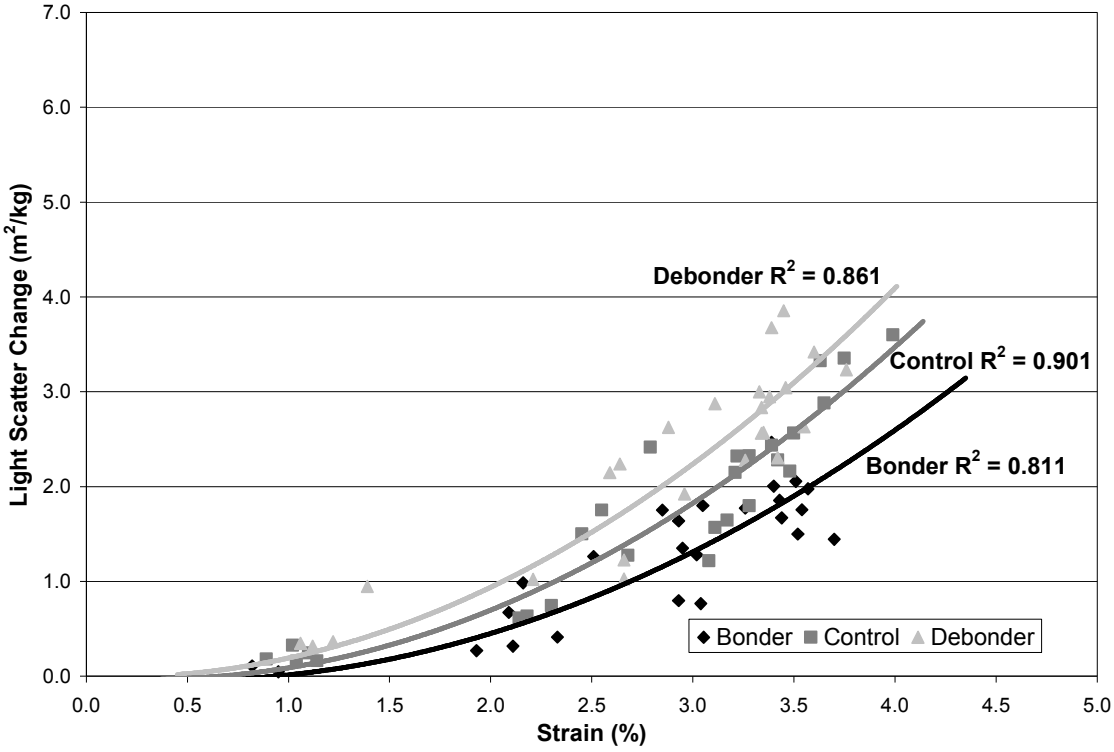

Figure 50 Light Scatter Change versus Strain From Creep Testing of Low Load Wet Pressed Sheets

Additional creep testing was also done at a higher initial stress levels with the intent of causing failure, allowing a more detailed analysis of the behavior. Figure 51 illustrates the failure points and light scatter change versus time for debonder, control and bonder treated sheets.

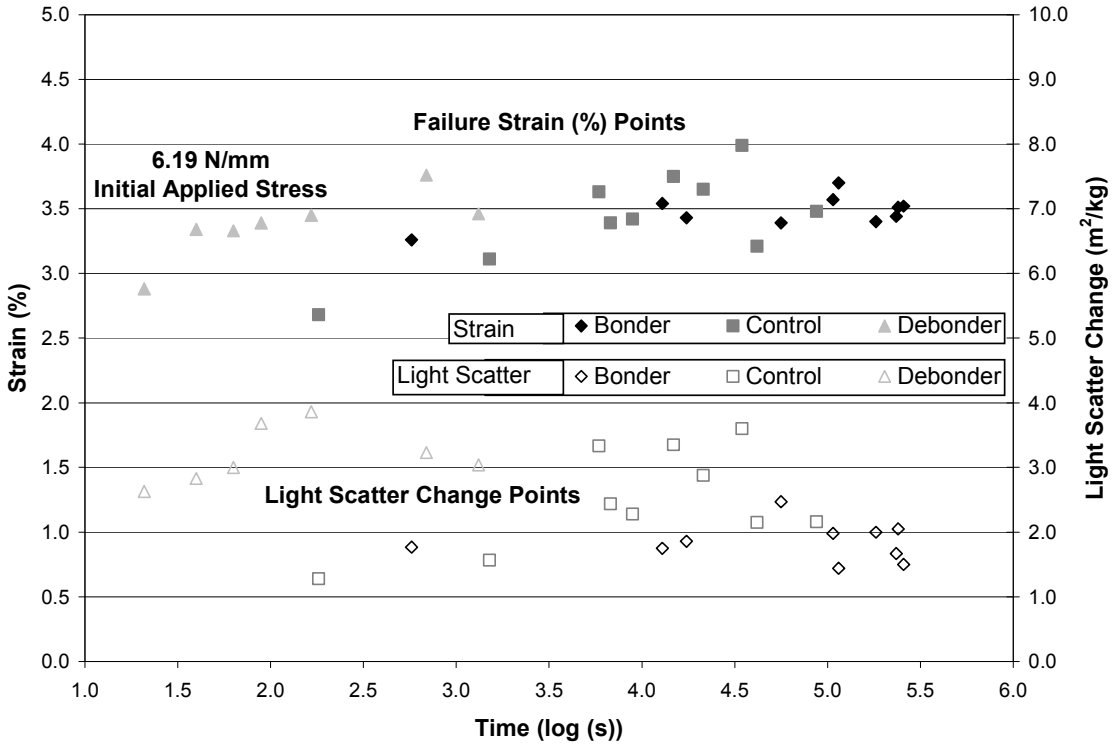

Figure 51 Creep Testing Failure Strain and Light Scatter Change versus Time for Low Load Wet Pressed Sheets

The debonder treated sheets fail much sooner than the bonder treated sheets with the control failure points scattered in between. Average failure strain is not significantly different in the bonder, control, and debonder sheets although they all are lower than the failure strains from the high load wet pressed sheets. Light scatter change indicates that there is the greatest loss in relative bonded area with the debonder treated sheets and the

change occurs fastest in those sheets. Table 5 summarizes the data illustrated in Figure 51.

Table 5 Failure Strains, Times and Light Scatter Changes for Low Load Wet Pressed Sheets

Sheet Treatment	Failure Strain (%)	Failure Time (log(s))	Failure Time (min)	Light Scatter Change (m^2/g)
Debonder	3.37	2.53	5.69	3.18
Control	3.43	4.35	371	2.50
Bonder	3.48	5.09	2040	1.85
Variation	3.3%	102%	>>100%	71.9%

Table 5 shows that there are large differences between the three sheet types in failure time and light scatter change. The bonder treated sheets last over two orders of magnitude longer than the debonder treated sheets. The debonder treated sheets show an over 70% increase in light scatter change from the bonder sheets. Overall, the creep curves and isochronous stress-strain curves of the three sheet types indicate that creep behavior is different for the low load wet pressed sheets.

5.5 Discussion

5.5.1 Deformation Behavior

As paper reaches higher levels of bonding, relative bonded area, and specific bond strength will reach or surpass a point where only fiber deformation controls paper deformation behavior. This occurs because a sufficient amount of bonding exists within the paper structure to effectively distribute load throughout the fiber network. The load distribution paths provided by the bonds are redundant in the amount of relative bonded

area and specific bond strength. Therefore, individual bonds cannot control creep deformation. This can be considered to be a fully efficient structure. If a bonder is added to paper where bonding has already reached or surpassed this point, the increase in specific bond strength will not result in a change in creep behavior. If a debonder is added to paper and it does not reduce specific bond strength to a point where bonding is below this point, creep behavior will also remain unchanged. This can be correlated to work by Seth and Page [40] where they demonstrated the elastic modulus and stress-strain curve in paper remained unchanged at differing levels of specific bond strength as long as the paper's structure remained fully efficiently loaded. This was the case with the high load wet pressed sheets from this study.

If paper remains at a low level of bonding as was the case with the low load wet pressed sheets in this study, the combination of relative bonded area and specific bond strength will be at a point where bonding will influence the paper deformation. This occurs because not enough bonding exists within the paper structure to effectively distribute load through the fiber network. If a debonder is added to paper, specific bond strength will decrease, acting to further deteriorate the paper's ability to effectively distribute load through the fiber network during deformation. This will lead to increased creep behavior. This type of paper structure would be considered an inefficiently loaded structure. A bonder would act to increasingly improve the paper's ability to distribute load effectively, decreasing creep behavior. Eventually, enough bonder could conceivably be added to increase specific bond strength enough to result in a fully efficient structure.

5.5.2 Efficiency Factor and Deformation

When Seth and Page [40] introduced the concept of the efficiency factor, they hypothesized that deformation originates within the fibers and bonding could influence deformation and be related to an efficiently loaded structure by means of an efficiency factor, a common efficiency factor that could be used for both elastic and viscoelastic deformation behavior. By using the efficiency factor to scale the stress magnitude, stress-strain curves with different efficiencies were superimposed on one another. This removed the effect of bonding. This was attempted with the data from this study. First, an attempt was made to superimpose all of the stress-strain curves generated from the low load wet pressed sheets and high load wet pressed sheets. Figure 52 shows the stress-strain curve before efficiency factors were applied.

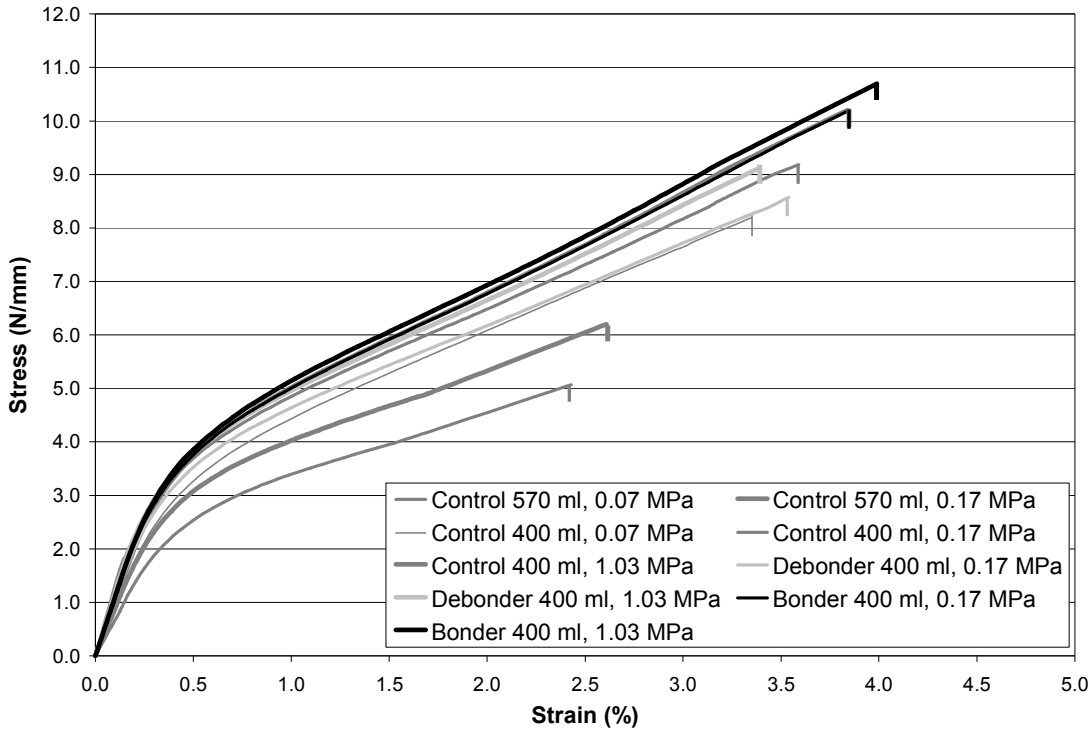

Figure 52 Stress-Strain Curves for All Sheet Conditions

Figure 52 shows the three low load wet pressed stress-strain curves (debonder, control, bonder treated), the three high load wet pressed stress-strain curves (debonder, control, bonder treated), and three additional stress-strain curves (untreated-controls) at lower pressing and refining levels. Sheet treatments, freeness values, and press loads are indicated in Figure 52 and all subsequent figures and tables for the purpose of differentiation. Upon applying efficiency factors, the curves superimpose as shown in Figure 53. The efficiency factors used were approximated, to best superimpose the curves. These efficiency factors are compared to the efficiency factors calculated from the ultrasonic elastic modulus results later in this section.

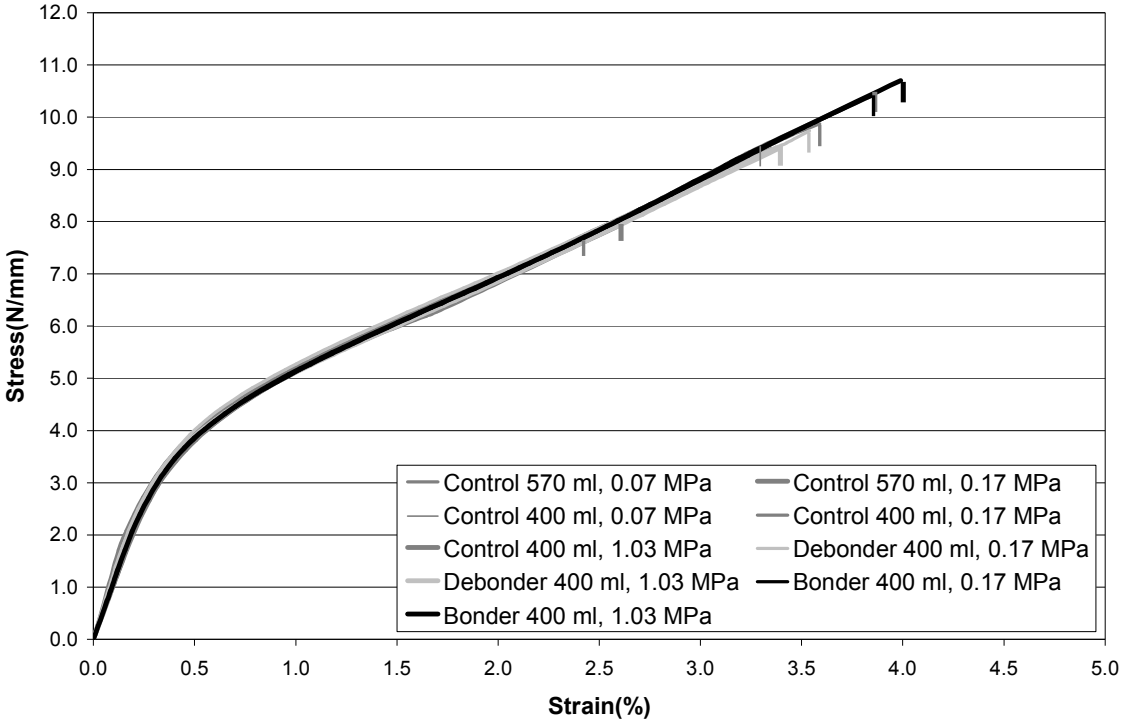

Figure 53 Stress-Strain Curves for All Sheet Conditions with Efficiency Factors Applied

The curves all superimpose indicating that none have severe enough bonding loss during straining to reduce the efficiency factor. In other words, damage to the sheet is not severe enough to affect the deformation behavior during straining. It also confirms the work of Seth and Page [40]. The creep behavior data in Figure 54 show the isochronous stress-strain curves for the three low load wet pressed cases (debonder, control, bonder treated), the three high load wet pressed cases (debonder, control, bonder treated), and three additional isochronous stress-strain curves (untreated-controls) at lower pressing and refining levels.

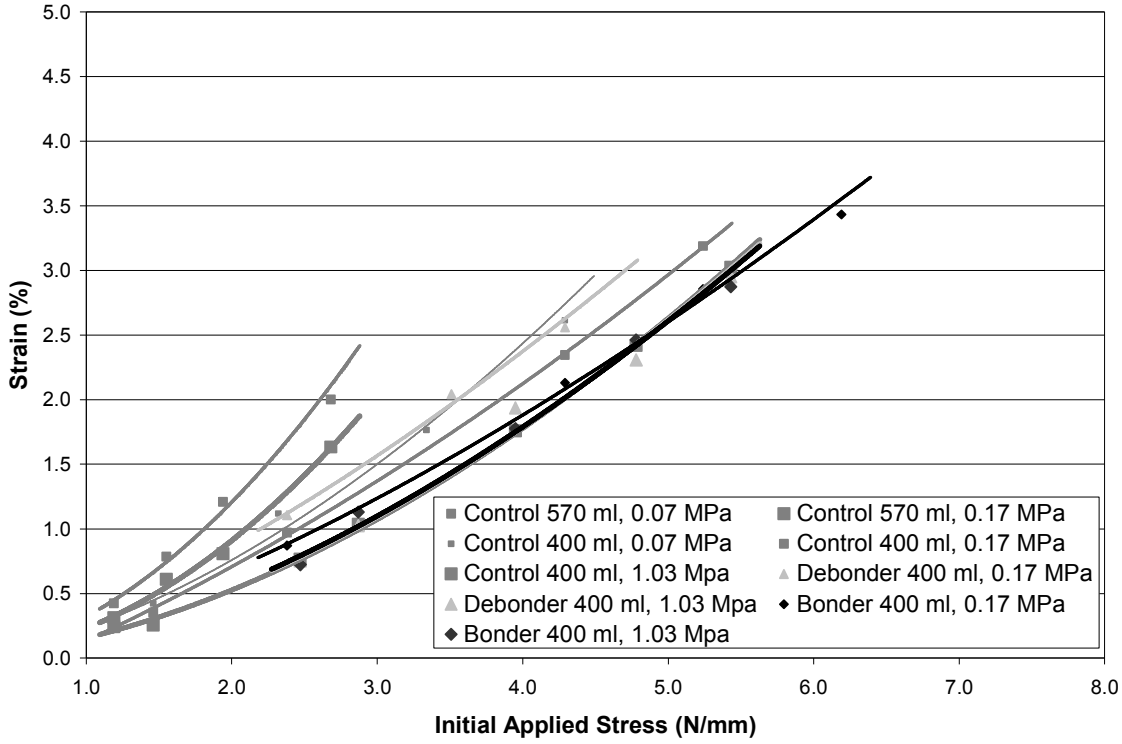

Figure 54 Isochronous Stress-Strain Curves for All Sheet Conditions

If efficiency factors are applied, the data points can be superimposed unto a common curve as shown in Figure 55. The data was fit to a power function trend line with an R^2 value of 0.990. Again, the efficiency factors used were approximated to best superimpose the isochronous stress-strain data.

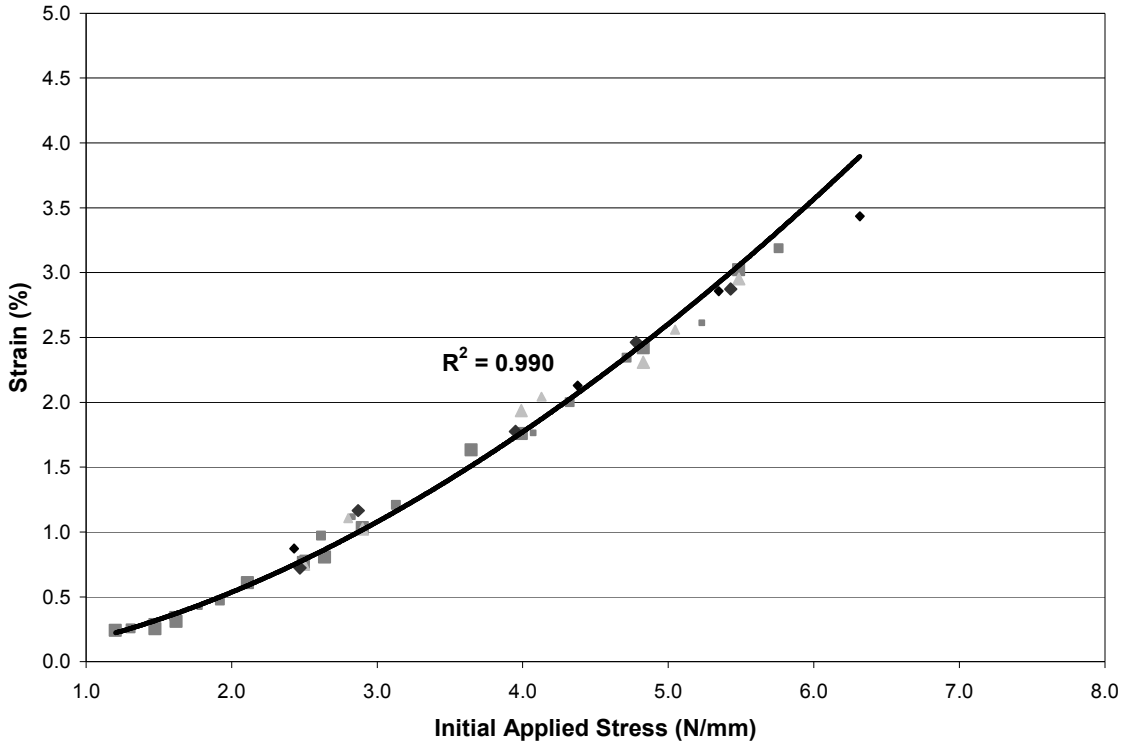

Figure 55 Isochronous Stress-Strain Curves for All Sheet Conditions with Efficiency Factors Applied

Overall, the efficiency factors approximated to superimpose the stress-strain curves from Instron testing (shown in Figure 53) and the isochronous stress-strain data from creep testing (shown in Figure 55) were consistent with each other. Figure 56 shows the efficiency factors approximated for the isochronous stress-strain curves versus the efficiency factors approximated for the stress-strain curves.

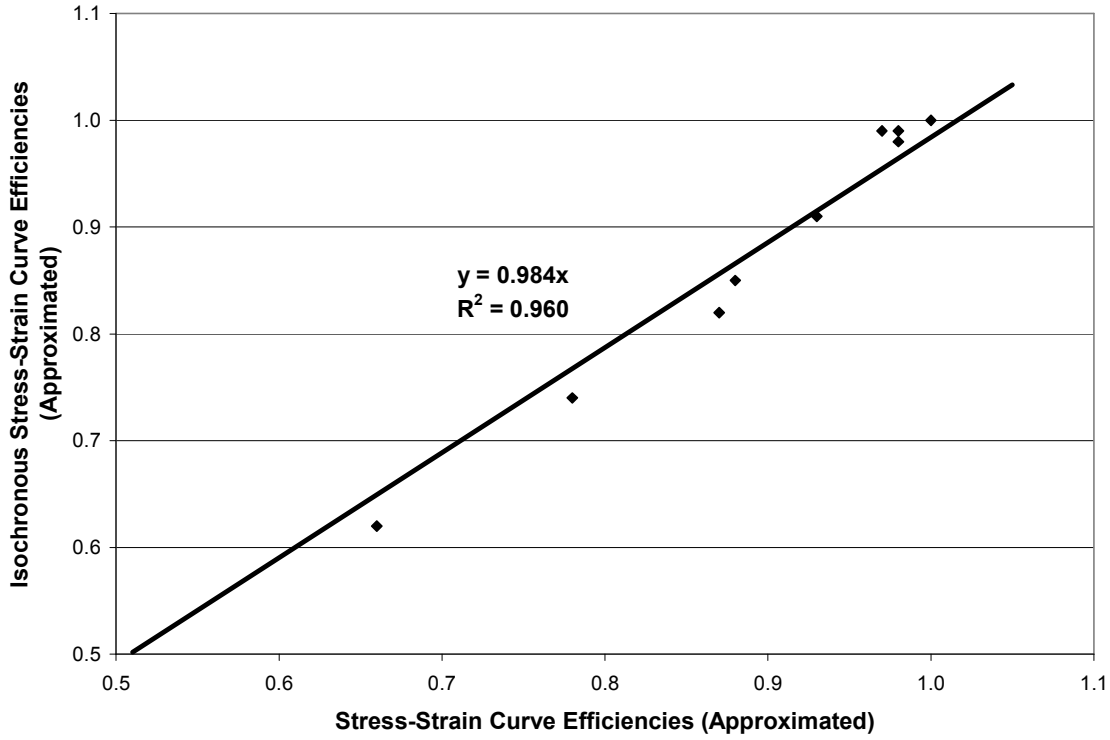

Figure 56 Isochronous Stress-Strain Curve Efficiency Factors versus Stress-Strain Curve Efficiency Factors

Figure 56 shows the slope of the linear trend line at 0.984 with an R^2 of 0.960 indicating a one to one relationship between the efficiencies used to overlap isochronous stress-strain curves from creep testing and stress-strain curves from physical testing. This data indicates the isochronous stress-strain curves generated from 24 hours of creep deformation and the stress-strain curves generated from a less than 20 second Instron test can have common efficiency factors applied to them, meaning bond breakage was not significant enough to reduce the efficiency factor for the creep behavior results. However, these creep results do not prove that efficiency factor does not decrease over longer creep testing durations where damage to the sheet may occur from the decrease of bonding. Nevertheless, efficiency factors can be applied to the creep data to make them

superimpose and these factors are consistent with the Instron stress-strain curve efficiency factors. In addition, efficiency factors were calculated using the ultrasonic modulus data in Table 2 and Table 4. Figure 57 shows these calculated efficiency factors from the ultrasonic modulus data versus the efficiency factors approximated to superimpose the stress-strain curves from Instron testing (shown in Figure 53) and the isochronous stress-strain curves from creep testing (shown in Figure 55).

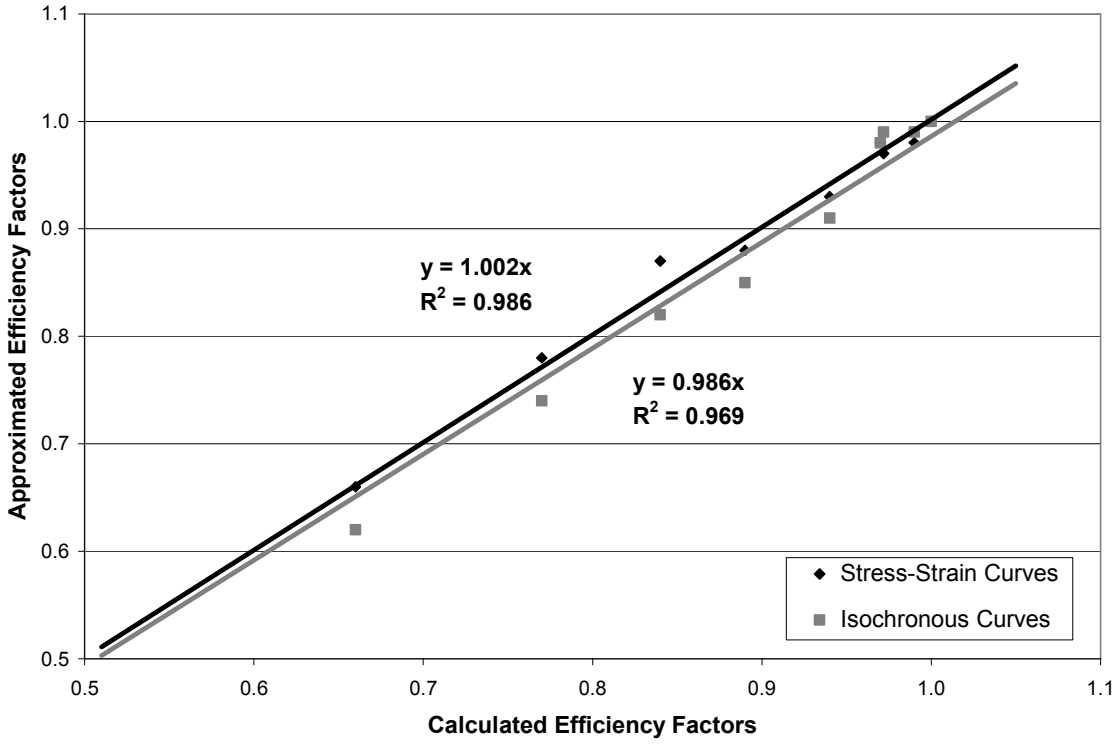

Figure 57 Approximated Efficiency Factors versus Calculated Efficiency Factors

Figure 57 indicates that there is good agreement as the slopes of both trend lines exhibit a one to one relationship between calculated efficiencies from ultrasonic modulus data versus the approximated stress-strain curve efficiencies (line slope of 1.002 and R^2

of 0.986), and the approximated isochronous stress-strain curve efficiencies (line slope of 0.986 and R^2 of 0.969). This first indicates good consistency between physical testing results and creep testing results. Having three sets of data (ultrasonic elastic modulus, stress-strain curves from Instron testing, and isochronous stress-strain curves from creep testing) relate so well as indicated in Figure 56 and Figure 57 is excellent considering all possible sources of error. This also indicates that efficiency factors, calculated using Equation 11 and ultrasonic modulus data, can be shown to still apply to deformation behavior that is neither elastic nor rate independent in behavior, supporting Seth and Page [40]. Table 6 shows the efficiency factor data used to generate Figure 56 and Figure 57.

Table 6 Calculated Efficiency Factors From Ultrasonic Modulus Data and Approximated Efficiency Factors for Stress-Strain Curves and Isochronous Stress-Strain Curves

Sheet Treatment	Ultrasonic Modulus Data	Stress-Strain Curves	Isochronous Stress-Strain Curves
Control 570 ml, 0.07 MPa	0.66	0.66	0.62
Control 570 ml, 0.17 MPa	0.77	0.78	0.74
Control 400 ml, 0.07 MPa	0.84	0.87	0.82
Debonder 400 ml, 0.17 MPa	0.89	0.88	0.85
Control 400 ml, 0.17 MPa	0.94	0.93	0.91
Bonder 400 ml, 0.17 MPa	0.97	0.98	0.97
Debonder 400 ml, 1.03 MPa	0.97	0.97	0.99
Control 400 ml, 1.03 MPa	0.99	0.98	0.99
Bonder 400 ml, 1.03 MPa	1.00	1.00	1.00

Further evidence that efficiency factors can apply towards creep behavior comes from data reported by Brezinski [36, 37]. Figure 58 shows isochronous stress-strain curves from a series of sheets made at differing wet pressing and refining levels; wet

pressing levels ranging from 0.07 MPa to 5.52 MPa and refining levels that gave a pulp freeness ranging from 425 ml to 775 ml. All data for these sheets are labeled by their freeness value and pressing level in the subsequent figures and table.

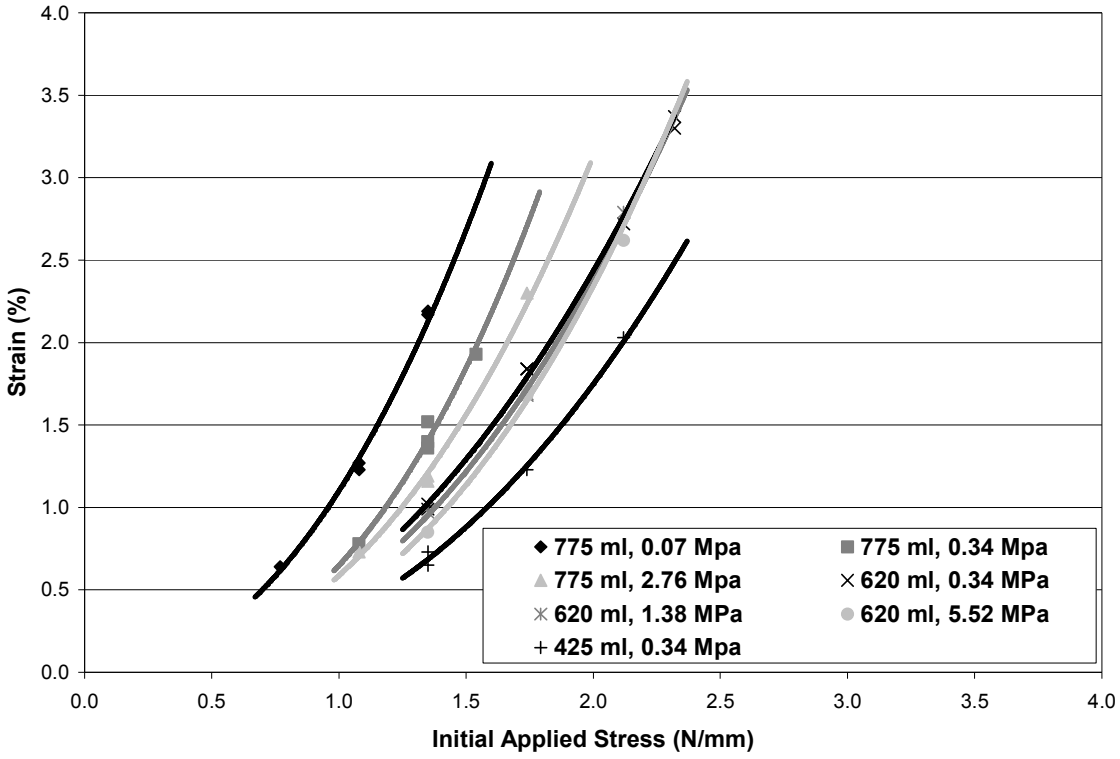

Figure 58 Brezinski [36, 37] Isochronous Stress-Strain Curves

Upon applying approximated efficiency factors, the data points all fall unto a common isochronous creep curve as seen in Figure 59. This curve was generated using a power function trend line with an R^2 of 0.991. The Brezinski [36, 37] data are more dramatic than the data from this study as there was greater spread between the isochronous stress-strain curves.

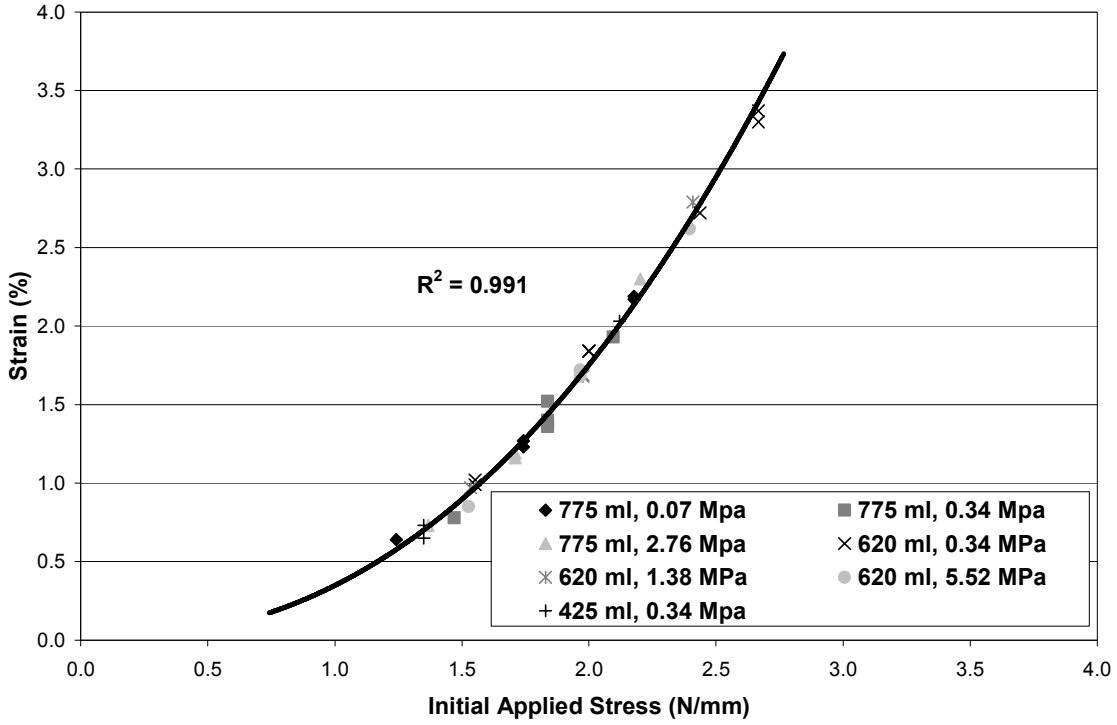

Figure 59 Brezinski [36, 37] Isochronous Stress-Strain Curves with Efficiency Factors Applied

Overall, the efficiency factors approximated to superimpose the isochronous stress-strain data of Brezinski [36, 37] (shown in Figure 59) were consistent with the efficiency factors calculated from his modulus data. Figure 60 shows the efficiency factors approximated for the isochronous stress-strain curves versus the efficiency factors calculated from the modulus data of Brezinski [36, 37].

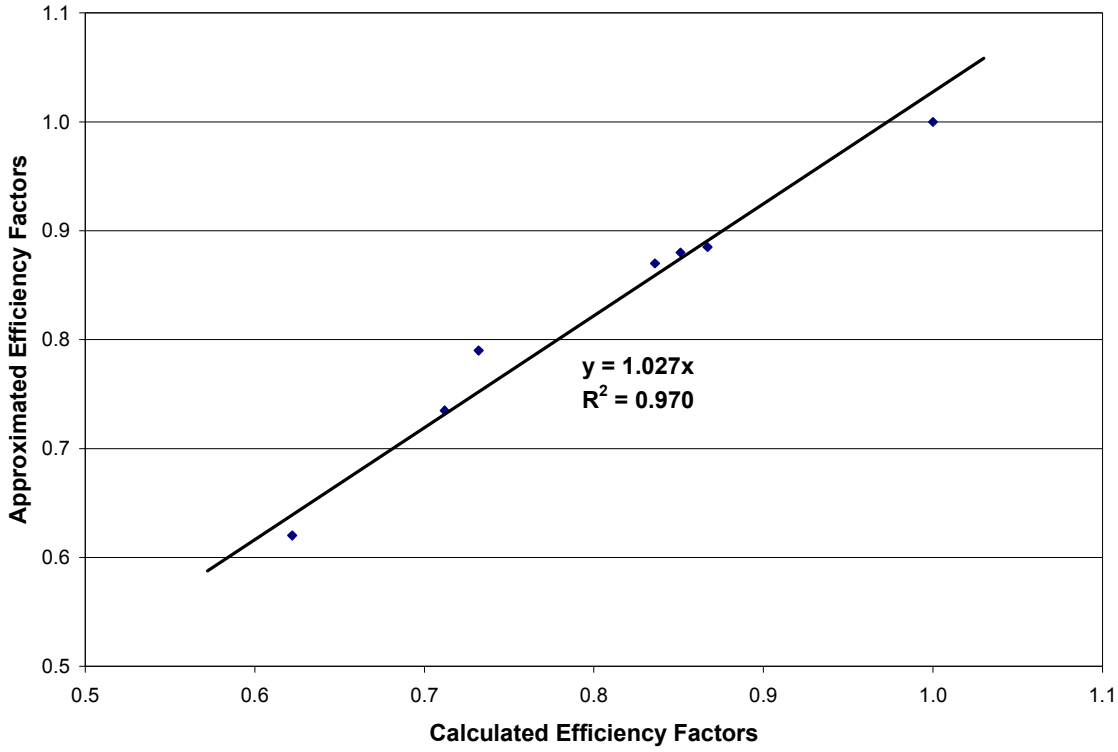

Figure 60 Approximated Efficiency Factors versus Calculated Efficiency Factors for Brezinski [36, 37] data

Figure 60 indicates that there is good agreement as the slope of the trend line indicates a one to one relationship between approximated efficiencies used to superimpose isochronous stress-strain data versus calculated efficiencies from modulus data (line slope 1.027 and R^2 of 0.970). The fact that these results trend so well together, especially with the inferiority of the laboratory equipment, is a testament to the work of Brezinski [36, 37]. Furthermore, the Brezinski [36, 37] data act to confirm that creep data other than what was obtained for this study (using different pulping and processing techniques) follow the same trend; a trend where efficiency factors can be applied to the data of inefficiently loaded structures to create a data set that mimics the behavior of an efficiently loaded structure. Again, these efficiency factors (calculated from modulus

data) were able to be effectively applied to deformation behavior that is neither elastic nor time independent. Table 7 shows the efficiency factor data used to generate Figure 60.

Table 7 Brezinski [36, 37] Modulus Data, Calculated Efficiency Factors from the Modulus Data and Approximated Efficiency Factors from Isochronous Stress-Strain Curves

Sheet Treatment	Modulus Data (N/mm)	Calculated Efficiency Factors	Approximated Efficiency Factors
775 ml, 0.07 MPa	276	0.62	0.62
775 ml, 0.34 MPa	316	0.71	0.74
775 ml, 2.76 MPa	325	0.73	0.79
620 ml, 0.34 MPa	371	0.84	0.87
620 ml, 1.38 MPa	378	0.85	0.88
620 ml, 5.52 MPa	385	0.87	0.89
425 ml, 0.34 MPa	444	1.00	1.00

5.5.3 Failure Behavior

With regard to creep failure time, it was influenced by bonding in both the low load wet pressed and high load wet pressed sheets. In a general sense, creep failure occurs when localized bond and fiber failure (damage) becomes significant enough to cause part of the structure to partially or completely stop bearing load. The remainder of the paper redistributes that load continually to compensate until it can no longer do so and fails. If a bonder is added to the paper, specific bond strength increases and the rate at which relative bonded area decreases during creep is diminished. As a result, the time when creep failure occurs is increasingly due to the fibers, as the decreased rate of relative bonded area loss makes localized bond failure a less influential cause. The higher

the specific bond strength or relative bonded area, the less influence bonding has on creep failure. If a debonder is added to the paper, the opposite would occur. Therefore, bonds would play an increasingly important role in the time of creep failure, acting to diminish it.

The results presented in Figure 46 and Figure 51 offer support to this rationale. They show that the creep failure time in the bonder treated sheets is higher than that of the debonder treated sheets. Furthermore, the rate of change and total loss in relative bonded area is lower in the bonder treated sheets. In other words, the creep failure of the bonder treated sheets occurs later, but with less change in relative bonded area. This shows that bonding had less influence on failure compared to the debonder treated sheets. If bonding had the same influence on creep failure time, the bonder treated sheets would have failed at a higher change in relative bonded area compared to the debonder treated sheets. The creep failure would have only been delayed due to the decreased rate of relative bonded area loss.

The Page Equation [41] offers an empirical explanation of how fiber strength and bonding influence the tensile strength in paper. This can be seen as a corollary to failure time in creep. Theoretically, according to the Page Equation [41], relative bonded area and specific bond strength could be increased past a point where bonding will have no influence on failure. At that point, failure would be initiated solely by the fibers. This could be called a “super” efficiently loaded structure. None of the sheets made in this study achieved that level of bonding.

5.5.4 Bonding Regimes

Based on the results from this study, it is clear that deformation behavior and failure behavior do not always trend with each other. Overall, one can imagine that paper can be placed in one of three regimes depending on the level of bonding. The first regime would be where bonding is at a level where deformation behavior and failure behavior are influenced. This would be considered an inefficiently loaded structure. This is what occurred in the low load wet pressed sheets where creep behaviors were different and failure times were different. The second regime would be where bonding is high enough where deformation behavior is unaffected but failure behavior is influenced. This would be considered an efficiently loaded structure. This is what occurred in the high load wet pressed sheets, where creep behaviors were the same and failure times were different. The third regime would be where bonding reaches a "super" efficiently loaded state and neither deformation behavior nor failure behavior would be influenced. Again, no sheets were made in this regime. A conceptual relationship between structural efficiency and bonding is shown in Figure 61.

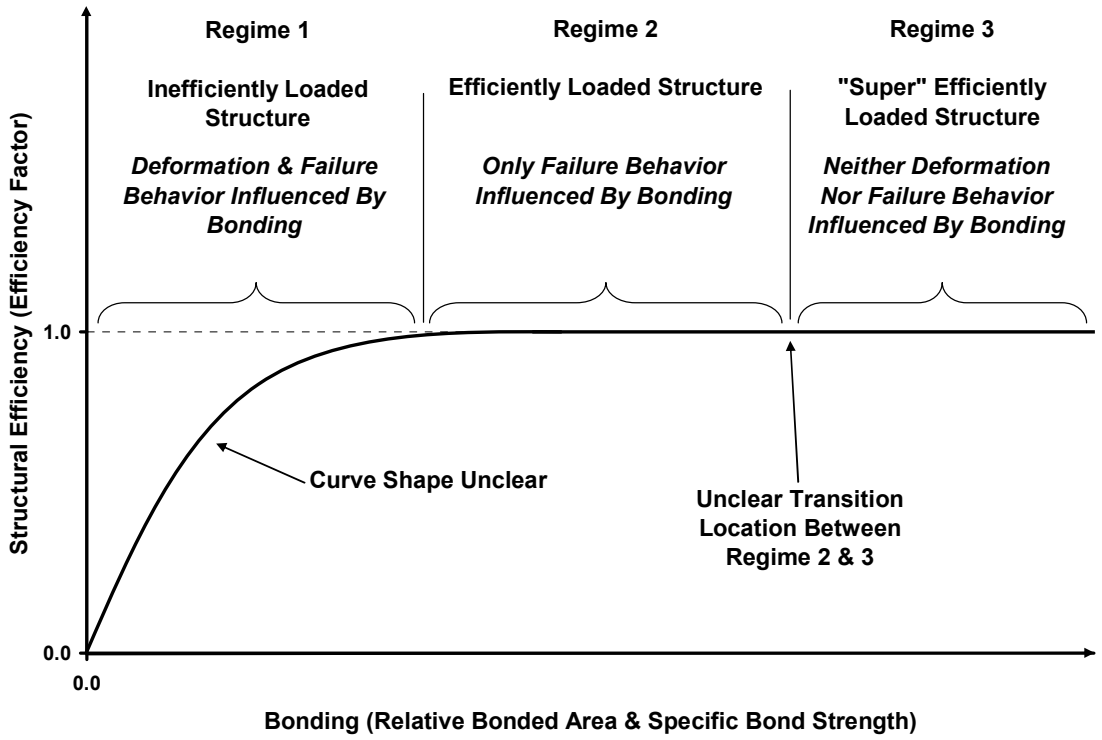

Figure 61 Conceptual Relationship Between Structural Efficiency and Bonding

With reference to Figure 61, two aspects of bonding and efficiency are unclear. First, it is unclear what the exact relationship between structural efficiency and bonding is when efficiency is less than one. Most likely, the curve on Figure 61 is a good approximation. It is likely that bonding has more of an influence on efficiency when it is close to "0" and has a diminishing influence as efficiency approaches "1". More lab work would need to be conducted to quantitatively determine the shape of this relationship. Furthermore, knowing that efficiency and bonding are related, it may be possible to predict the efficiency of paper based off the level of bonding within the sheet.

Second, it is unclear exactly where the fully efficient regime ends and "super" fully efficient regime begins. It should be possible to quantitatively determine this if more

laboratory work is done. This would most likely be accomplished by making high load wet pressed sheets with high levels of bonder.

5.6 Conclusions

Creep in paper will reach a minimum as higher and higher levels of bonding are achieved. This is because bonding can be improved until an efficiently loaded structure is created, a structure which can effectively distribute load. Once the point is passed where the paper structure becomes fully efficient, only creep failure time can be increased with increased levels of bonding. This substantiates the premise that a fully efficient structure is not influenced by bonding with regard to deformation behavior, only failure behavior. This correlates with what Seth and Page [40] saw with elastic modulus and stress-strain behavior.

In addition, it is possible to apply efficiency factors to the creep data of inefficiently loaded structures and create a data set that superimposes with creep data from an efficiently loaded structure. This efficiency factor can be calculated by relating elastic modulus data and still applies to the time dependent viscoelastic deformation seen with stress-strain behavior and creep behavior. The efficiency factor in effect relates how well the existing bonding allows the structure to effectively distribute load throughout the sheet; a structure where deformation originates within the fiber and bonding can only influence deformation at a less than fully efficient loaded condition. This relation will hold true as long as the efficiency factor does not decrease with strain due to excessive relative bonded area loss (sheet damage). This did not occur with the data in this study but has been shown to occur in work by Seth and Page [40].

Furthermore, it has been shown that differences or similarities in deformation behavior do not necessarily correspond to differences or similarities in failure behavior with regards to creep or other physical properties. Depending on which one of three regimes the bonding is in, it has been shown that it is possible to create sheets with differing levels of bonding (either in relative bonded area or specific bond strength) that have:

- The same deformation behavior and different failure behavior.
- Different deformation behavior and different failure behavior.
- While not achieved in this study, the same deformation behavior and the same failure behavior.

CHAPTER 6: EMPIRICAL AND RHEOLOGICAL MATHEMATICAL MODELING OF THE TENSILE CREEP BEHAVIOR OF PAPER

6.1 Abstract

An empirical model and a rheological model have been developed to predict the tensile creep behavior of paper under a uni-axial stress. Specifically, the focus of these models was to predict creep behavior in the form of isochronous stress-strain curves where only stress, time, and efficiency factor (effectiveness of bonding) are the variables used to predict strain. While the empirical model is meant to be simple, the rheological model is more detailed. As a result, it offers more insight into creep behavior (drawing from molecular creep mechanisms) and separates total strain from creep into initial elastic, primary creep, and secondary creep components. Both of the models are shown to be good predictors of isochronous stress-strain curves and were derived using the characteristics of the fibers. Inter-fiber bonding is taken into account through the use of an efficiency factor which represents how effectively bonding is distributing load throughout the fiber network of the paper. As a result, these models make it possible to easily predict the creep behavior of paper over a range of bonding levels; all that is needed is the creep data from paper at any one level of bonding. Then, using efficiency factors, the creep behavior of paper at any other level of bonding can be found. This will hold true as long as the fibers and the orientation of the fibers are not changed. The results from this chapter confirm that bonding influence in paper can be accounted for with an easily derived efficiency factor.

6.2 Introduction

In Chapter 5, it was found as paper reaches higher levels of bonding, relative bonded area and specific bond strength will reach or surpass a point where only fiber deformation controls paper deformation behavior. This occurred because a sufficient amount of bonding existed within the paper structure to effectively and evenly distribute load throughout the fiber network. This is considered to be a fully efficient loaded structure. At that point, any further increases in bonding will no longer affect creep behavior. The only improvement will be limited to failure behavior. Therefore, if deformation behavior is the only subject of concern, bonding is not a variable.

Furthermore, it was shown that efficiency factors can be used to account for the bonding influence on creep behavior when the level of bonding within the paper structure is less than fully efficient. These efficiency factors can be found based on a direct comparison of the deformations of fully efficient loaded structures versus inefficient loaded structures. Simply, efficiency factor can be calculated by dividing the inefficient loaded structure elastic modulus by the fully efficient loaded structure elastic modulus. Even though the efficiency factor is calculated using elastic modulus, it also predicts time-dependent deformation behavior (viscoelastic behavior). The results in Chapter 5 showed that the time duration of the deformation is not a variable that influences the efficiency factor.

Chapter 5 results illustrated that the efficiency factor was effective in accounting for the influence of bonding in creep behavior with both the data measured for this thesis and the data from Brezinski [36, 37]. Creep behavior of inefficiently loaded structures, presented using isochronous stress-strain curves, was shown to superimpose with creep

behavior of fully efficient loaded structures, when efficiency factors were applied to account for bonding. Seth and Page [40] were previously able to show that efficiency factors could be used to account for bonding and explain the differences in stress-strain behavior. Based on these results, the use of efficiency factor can be a powerful tool in the mathematical modeling of creep behavior in paper. The purpose of this chapter is to utilize efficiency factors and derive two mathematical models (one empirical and one rheological) to describe the tensile creep behavior of paper under a uni-axial stress.

Specifically, the focus of these models is to predict creep behavior in the form of isochronous stress-strain curves where only stress, time and efficiency factor are the variables used to predict strain. The use of isochronous stress-strain curves is favored within this thesis as an effective way to present creep data. These curves are generated by plotting total strain versus the initial applied stress at various snapshots in time. Panek et al. [14] and Soremark et al. [18] considered the use of isochronous stress-strain curves as an effective way to analyze, simplify, and present creep data and refer to others who have effectively used these curves to predict creep in polymers. With regard to the use of efficiency factor to account for bonding, the modeling work of Coffin [13] showed that such an approach is viable. Temperature and moisture are not variables considered within this chapter, although future works could be done to incorporate them. Within this chapter, the first model described is an empirical model, while the second is a rheological model that possesses physical meaning.

6.3 Empirical Model Predicting Tensile Creep in Paper

6.3.1 Background on Empirical Modeling

The first model introduced is an empirical model. The intent of this model is to predict the total strain seen during creep deformation using intial stress, time and efficiency factor as variables. The objective of this model is to allow easy prediction of isochronous stress-strain curves using as few constants as possible. The intent of the model is not to separate the total strain into its elastic, primary creep, and secondary creep components or to use knowledge of inherent material creep mechanisms, rather to predict the overall behavior of the paper.

There are a limited number of modeling examples that can be drawn upon with regard to tensile creep in paper. With focus on empirical models, Brezinski [36, 37] utilized simple exponential and logarithmic functions to describe the results from his work. He described that at short times and low initial applied stress levels, creep behavior followed an exponential trend. At longer times and high initial applied stress levels, creep behavior followed a logarithmic trend. The work of Hill [38, 39] with single fiber tensile creep utilized the same rationale, focusing on creep behavior following a logarithmic trend. While these models are simple, the drawback is they only use time as a variable, meaning the constants must be changed when initial applied stresses are changed.

The work of Pecht et al. [69] employed a more complex empirical equation to describe tensile creep based in part from the work of Brezinski [36, 37]. He developed a universal equation rather than using an exponential function to model creep at low initial applied stresses or short times and a logarithmic function to model creep at high initial applied stresses or long times. While this model can be used to predict master creep

curves, it is not favored due to its complexity. Rather than using this model to predict isochronous stress-strain curves, a simpler empirical model (with fewer constants) could be developed. Further work by Pecht and Johnson [70] expanded upon their model to take moisture changes into account. This is outside the scope of the modeling work within this chapter. Similarly, Panek et al. [14] also proposed an empirical equation with significant complexity. While this model was derived specifically to predict isochronous creep curves, the use of hyperbolic tangent functions makes it difficult to solve for strain. Furthermore, none of these models took bonding into account using efficiency factors. The influence of bonding was simply incorporated into the constants of the equations. Other, more descriptive models have been developed to describe tensile creep in paper and are described later, when the rheological model is presented.

6.3.2 Derivation of an Empirical Model

The empirical model predicts strain as a function of initial applied stress and time. For simplicity, this is done by multiplying a function of initial applied stress by a function of time. Equation 27 shows this relation, where ε is strain, σ_o is initial applied stress and t is time.

$$\varepsilon = f(\sigma_o)g(t)$$

Equation 27 Relation Showing Strain as a Function of Stress and Time for the Empirical Model

There are many empirical relations that can be used to represent the initial applied stress relationship with strain. These include exponential, hyperbolic, and power

functions. For this model, the relation chosen was a power function. The use of a power function to relate stress to strain has been used in the past by Norton and Bailey to predict creep in metals [6]. Similar power functions have also been used to predict creep in viscoelastic materials, such as plastics [6]. Equation 28 shows the power function used, where γ is a material constant.

$$f(\sigma_o) = \sigma_o^{\gamma}$$

Equation 28 Function of Initial Applied Stress for the Empirical Model

The time relationship with strain could also be a power function based on previous work by Nutting in predicting creep in viscoelastic materials [6]. With respect to paper, the logarithmic function of Brezinski [36, 37] was chosen instead. It was based on his observation that tensile creep in paper follows a linear relationship with log time at higher stresses and times. It was assumed that the exponential creep regime he proposed at low times and stresses is small and will not significantly impact the overall ability of this empirical model to predict isochronous stress-strain curves. Equation 29 shows the logarithmic function used, where α and β are material constants and t_r is a reference time constant. The reference time constant is set to the time scale which creep measurements are made. For example, if creep measurements are made in seconds, the reference time constant will equal one second.

$$g(t) = \alpha t_r \ln\left(\frac{t}{t_r} + 1\right) + \beta$$

Equation 29 Function of Time for the Empirical Model

By substituting Equation 28 and Equation 29 into Equation 27, an empirical model that relates initial applied stress and time to strain is obtained. This empirical model is shown in Equation 30.

$$\varepsilon = \sigma_o^{\gamma}\left[\alpha t_r \ln\left(\frac{t}{t_r} + 1\right) + \beta\right]$$

Equation 30 Empirical Model Relating Initial Applied Stress and Time to Strain

The final step required to complete this empirical model is to incorporate the efficiency factor into Equation 30. This was done by dividing the initial applied stress by an efficiency factor. By doing this, the efficiency factor can be thought of as a modifier of the initial applied stress. Recalling that the efficiency factor is less than or equal to 1, it accounts for how bonding reduces the initial applied stress necessary to achieve a given amount of strain in an inefficiently loaded structure. Equation 31 shows the final form of the empirical model, with efficiency factor φ, incorporated into the model.

$$\varepsilon = \left(\frac{\sigma_o}{\varphi}\right)^{\gamma}\left[\alpha t_r \ln\left(\frac{t}{t_r}+1\right)+\beta\right]$$

Equation 31 Final Form of Empirical Model Relating Initial Applied Stress, Time and Efficiency Factor to Strain.

What the final form of this empirical model yields is a simple calculation to solve for the total strain during creep and is well suited for predicting isochronous stress-strain curves. It only has three variables being initial applied stress, time, and efficiency factor. It contains a reference time constant that is defined by the time scale of the creep measurements. It also contains three material constants (α, β, γ), which can be found from direct comparison with experimental data. Although, this model is empirical, these constants can be related to material properties. The term γ is representative of the material's stress non-linearity with respect to strain. The terms α and β represent how compliant the material is as a function of time, where β represents the initial compliance at time equal to zero and α controls the rate of increase in the compliance as time increases. The influence of bonding is accounted for with the use of an efficiency factor. The remaining physical aspects of the paper, such as fiber type, fiber defects, formation, and orientation are accounted for through the three constants. If any of these parameters change, so will the constants.

6.3.3 Validation of the Empirical Model

In order to validate the empirical model shown in Equation 31, it must be compared to creep results obtained experimentally at varying sheet structure efficiencies. To do this, the experimental results presented in Chapter 5 will be used. The three

material constants (α, β, γ) are selected to provide the best model "fit" to the experimental results and remain unchanged for all initial applied stresses, times and efficiency factors. This was accomplished by fitting the constants to the creep data from the 400 ml freeness, 1.03 MPa wet pressed, bonder treated sheets. These sheets are fully efficient loaded structures and have an efficiency factor equal to 1.00, indicating bonding does not impact deformation behavior. Specifically, through an iterative process, constants were adjusted until the residual difference between the actual creep data and values the empirical model predicted was minimized. The reference time constant was set at one second as the experimental results presented in Chapter 5 were obtained in a seconds time scale. Table 8 shows the selected values and units for these constants.

Table 8 Values of Empirical Model Constants Used to Fit Experimental Results

Empirical Model Constants	Values	Units
α	0.000070	$(mm/N)^{1.73}/s$
β	0.00081	$(mm/N)^{1.73}$
γ	1.73	
t_r	1.0	s

Figure 62 and Figure 63 show isochronous stress-strain curves calculated using the empirical model in Equation 31 and the constants from Table 8. Data points (with standard error bars) from the actual creep results obtained from the 400 ml freeness, 1.03 MPa wet pressed, bonder treated, fully efficient sheets are also shown.

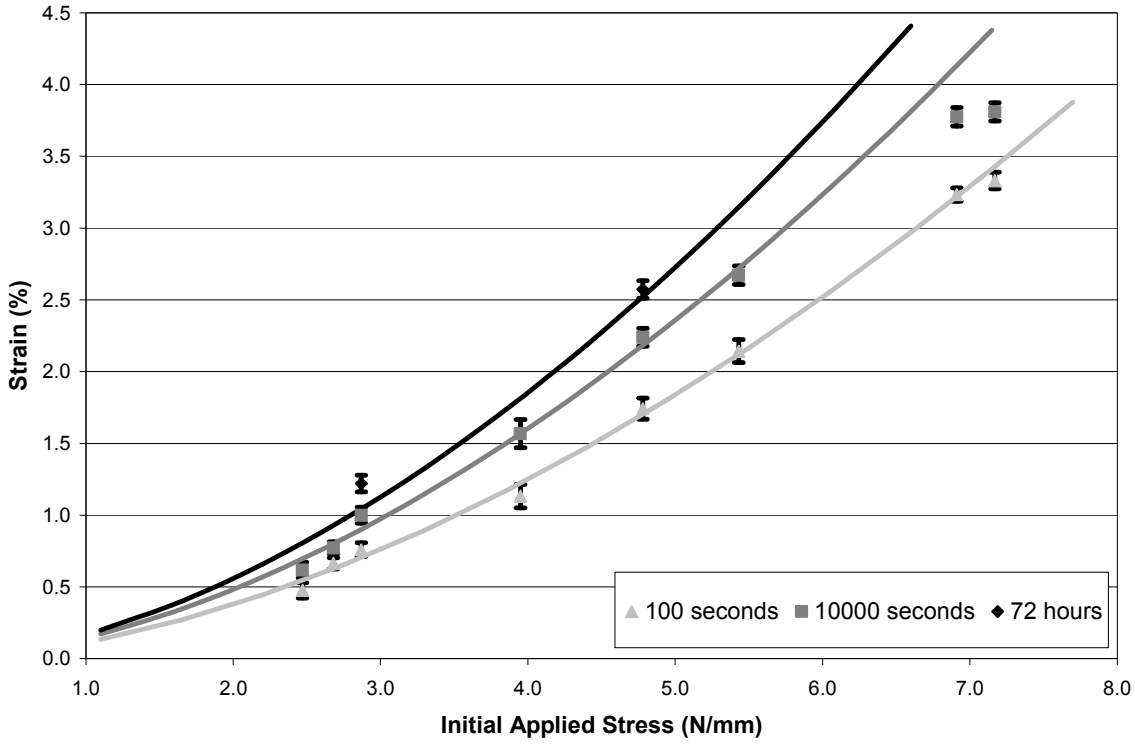

Figure 62 Predicted Isochronous Stress-Strain Curves for 400 ml Freeness, 1.03 MPa Wet Pressed, Bonder Treated Sheets at 100 seconds, 10000 seconds and 72 hours using the Empirical Model and an Efficiency Factor of 1.00

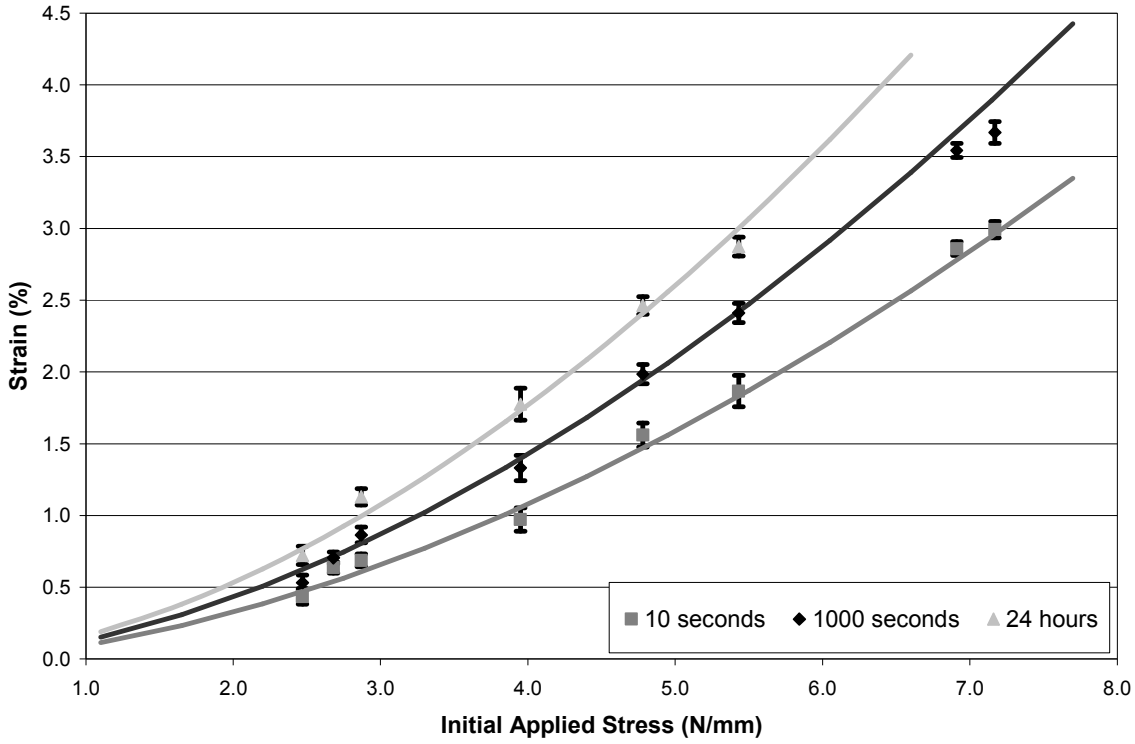

Figure 63 Predicted Isochronous Stress-Strain Curves for 400 ml Freeness, 1.03 MPa Wet Pressed, Bonder Treated Sheets at 10 seconds, 1000 seconds and 24 hours using the Empirical Model and an Efficiency Factor of 1.00

Figure 62 and Figure 63 show isochronous stress-strain curves at six different times. As the separation of individual isochronous stress-strain curves is not significant, these curves are separated into two figures in such a manner to more clearly illustrate the results. As indicated, the model correlates well to the experimental results. This signifies that the model is effective in predicting isochronous stress-strain curves when paper is a fully efficient loaded structure. Further comparisons of this model are necessary to point out correlations with creep results obtained from less than fully efficient loaded structures (i.e. efficiency factor is less than 1 and bonding impacts deformation behavior). Figure 64, Figure 65, Figure 66, Figure 67, Figure 68, and Figure 69 shows isochronous stress-

strain curves calculated using the empirical model in Equation 31 and the constants from Table 8. Data points (with standard error bars) from actual creep results obtained through experimentation are also illustrated. Again, data from Chapter 5 was used. Figure 64 and Figure 65 data were obtained from 400 ml freeness, 0.17 MPa wet pressed, control sheets with efficiency factors of 0.91. Figure 66 and Figure 67 data were obtained from 400 ml freeness, 0.17 MPa wet pressed, debonder treated sheets with efficiency factors of 0.85. Figure 68 and Figure 69 data were obtained from 570 ml freeness, 0.07 MPa wet pressed, control sheets with efficiency factors of 0.62.

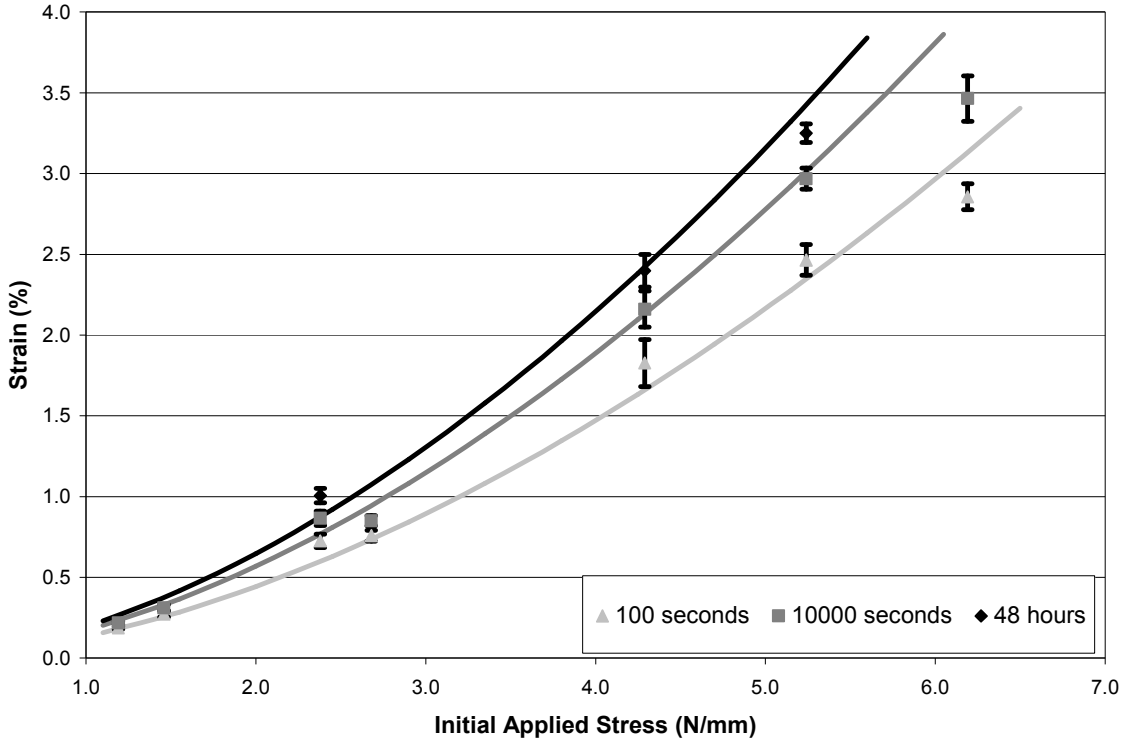

Figure 64 Predicted Isochronous Stress-Strain Curves for 400 ml Freeness, 0.17 MPa Wet Pressed, Control Sheets at 100 seconds, 10000 seconds and 48 hours using the Empirical Model and an Efficiency Factor of 0.91

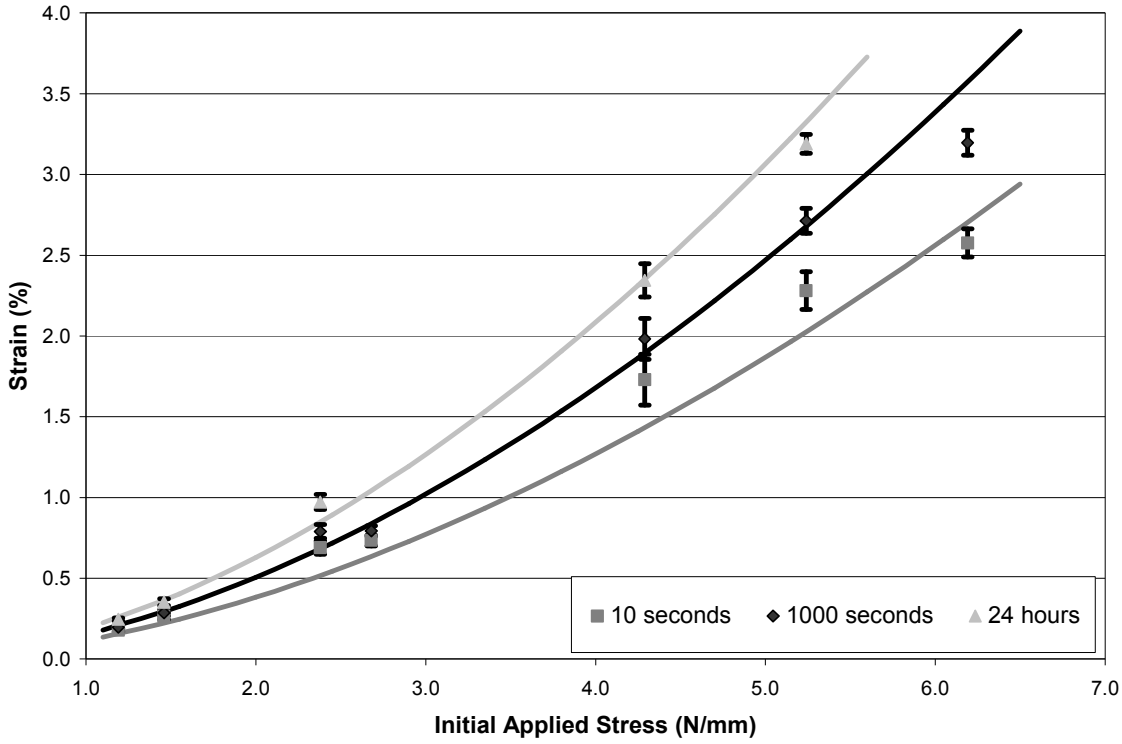

Figure 65 Predicted Isochronous Stress-Strain Curves for 400 ml Freeness, 0.17 MPa Wet Pressed, Control Sheets at 10 seconds, 1000 seconds and 24 hours using the Empirical Model and an Efficiency Factor of 0.91

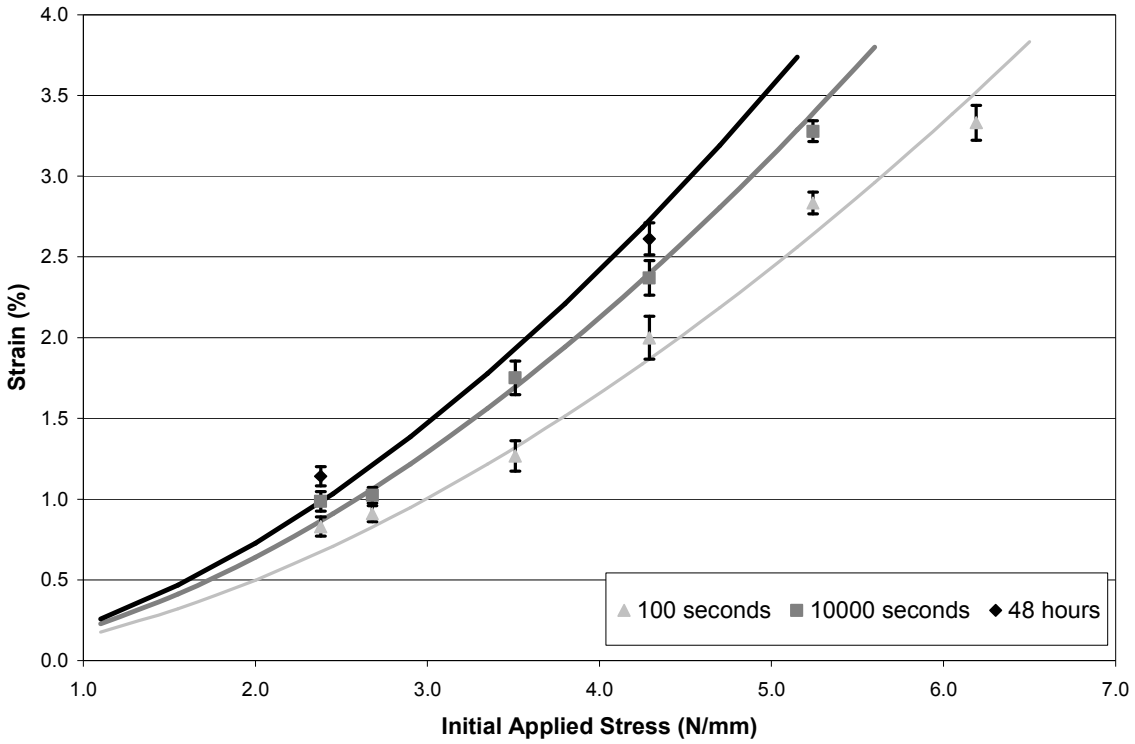

Figure 66 Predicted Isochronous Stress-Strain Curves for 400 ml Freeness, 0.17 MPa Wet Pressed, Debonder Treated Sheets at 100 seconds, 10000 seconds and 48 hours using the Empirical Model and an Efficiency Factor of 0.85

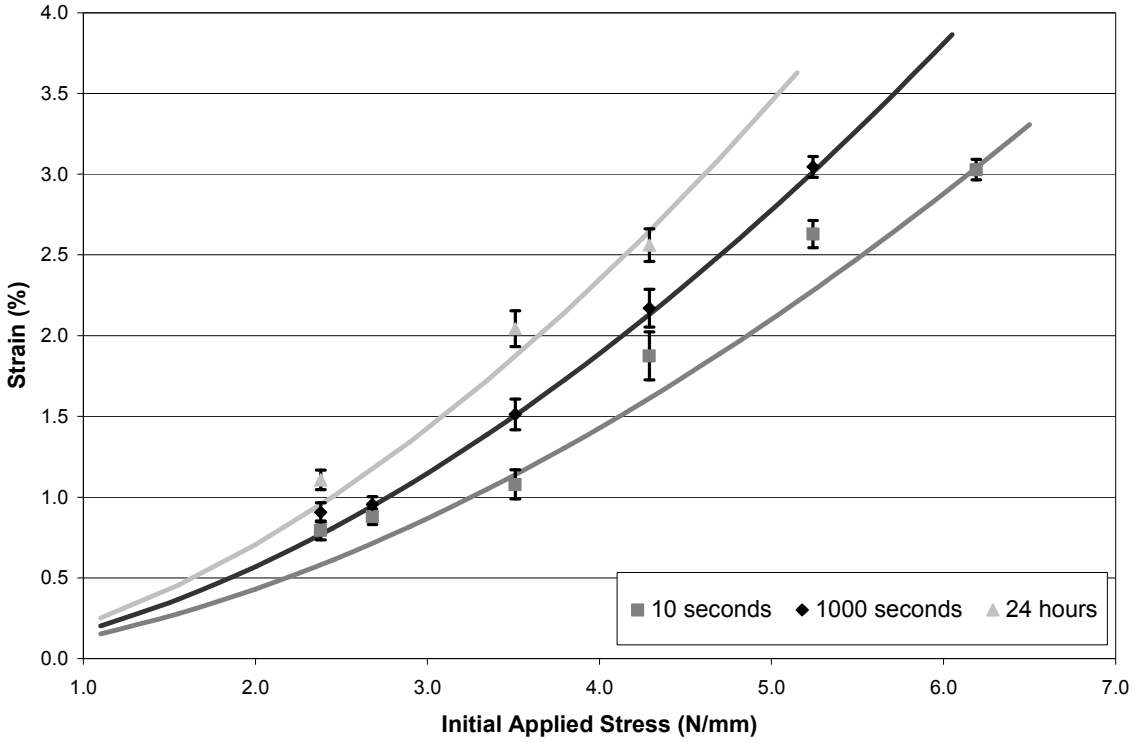

Figure 67 Predicted Isochronous Stress-Strain Curves for 400 ml Freeness, 0.17 MPa Wet Pressed, Debonder Treated Sheets at 10 seconds, 1000 seconds and 24 hours using the Empirical Model and an Efficiency Factor of 0.85

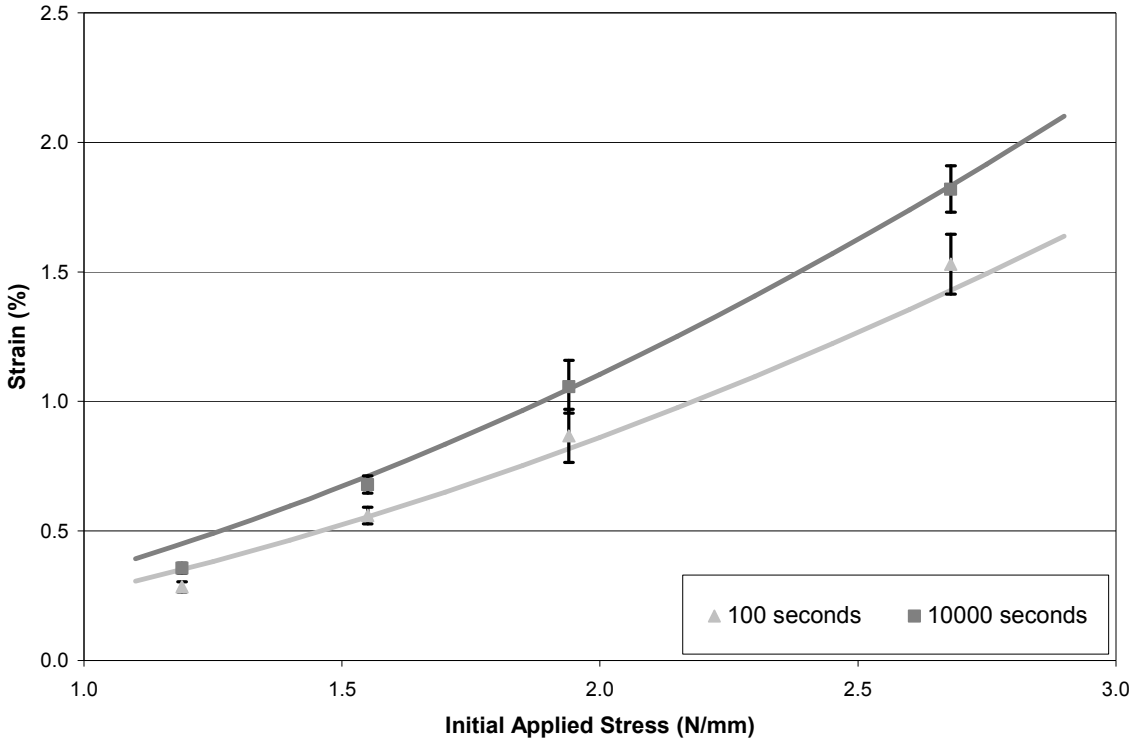

Figure 68 Predicted Isochronous Stress-Strain Curves for 570 ml Freeness, 0.07 MPa Wet Pressed, Control Sheets at 100 seconds, and 10000 seconds using the Empirical Model and an Efficiency Factor of 0.62

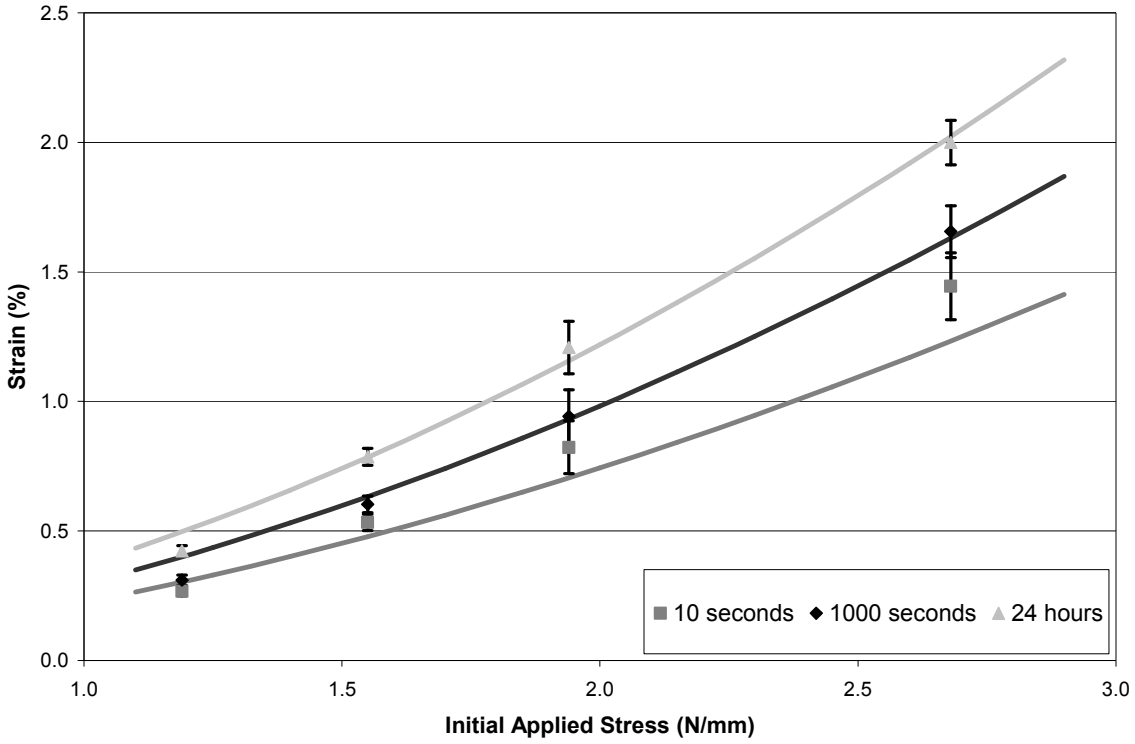

Figure 69 Predicted Isochronous Stress-Strain Curves for 570 ml Freeness, 0.07 MPa Wet Pressed, Control Sheets at 10 seconds, 1000 seconds and 24 hours using the Empirical Model and an Efficiency Factor of 0.62

As illustrated in Figure 64, Figure 65, Figure 66, Figure 67, Figure 68, and Figure 69, the model correlates well to the experimental results of the inefficiently loaded sheets. This indicates that an efficiency factor can be used in this model to account for the bonding influence on creep deformation. These efficiency factors are the same efficiency factors used to scale the isochronous stress-strain curves in Chapter 5 and are consistent with the efficiency factors calculated from the ultrasonic modulus data and stress-strain curve data as shown in Figure 56 and Figure 57.

While the model is effective in fitting the experimental results from this thesis, it is also important to consider how well it translates into other researcher's data. The

experimental results of Brezinski [36, 37] presented in Chapter 5 are used as further validation for the empirical model. The three material constants (α, β, γ) are again selected to obtain the best "fit" of the model to the experimental results and remain unchanged for all initial applied stresses, times, and efficiency factors. This was accomplished by fitting the constants to the creep data (as labeled in Chapter 5) from the 425 ml freeness, 0.34 MPa wet pressed sheets, with efficiency factors of 1.00. Specifically, through an iterative process, constants were adjusted until the residual difference between the actual creep data and values the empirical model predicted was minimized. The reference time constant is set at one second as the experimental results are in a seconds time scale. Table 9 shows the values and units for these constants.

Table 9 Values of Empirical Model Constants Used to Fit Experimental Results of Brezinski [36, 37]

Empirical Model Constants	Values	Units
α	0.00025	$(mm/N)^{2.46}/s$
β	0.00045	$(mm/N)^{2.46}$
γ	2.46	
t_r	1.0	s

If these constants are judged against the ones from Table 8, they suggest that the creep behavior measured by Brezinski [36, 37] is more non-linear as indicated by a higher value of γ and the rate of increase in compliance is higher as indicated by a higher α. Figure 70, Figure 71, Figure 72, and Figure 73 show isochronous stress-strain curves calculated using the empirical model in Equation 31 and the constants from Table 9. Data points from actual creep results obtained from Brezinski [36, 37] are also shown. These

results were obtained from sheets with a range of efficiencies. Using the labeling for sheets as in Chapter 5, Figure 70 data was obtained from the 425 ml freeness, 0.34 MPa wet pressed, fully efficient sheets used to find the material constants. Figure 71 data was obtained from 620 ml freeness, 1.38 MPa wet pressed sheets with efficiency factors of 0.88. Figure 72 data was obtained from 775 ml freeness, 0.34 MPa wet pressed sheets with efficiency factors of 0.74. Finally, Figure 73 data was obtained from 775 ml freeness, 0.07 MPa wet pressed sheets with efficiency factors of 0.62.

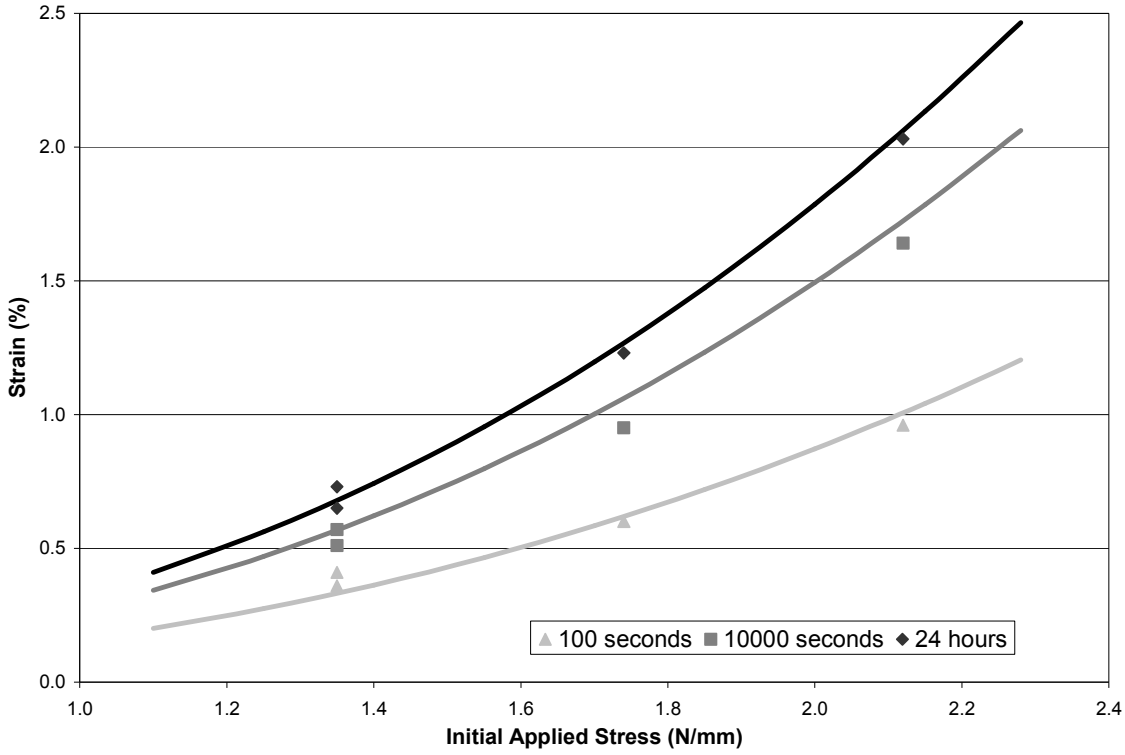

Figure 70 Predicted Isochronous Stress-Strain Curves for 425 ml Freeness, 0.34 MPa Wet Pressed Sheets at 100 seconds, 10000 seconds and 24 hours using the Empirical Model and an Efficiency Factor of 1.00

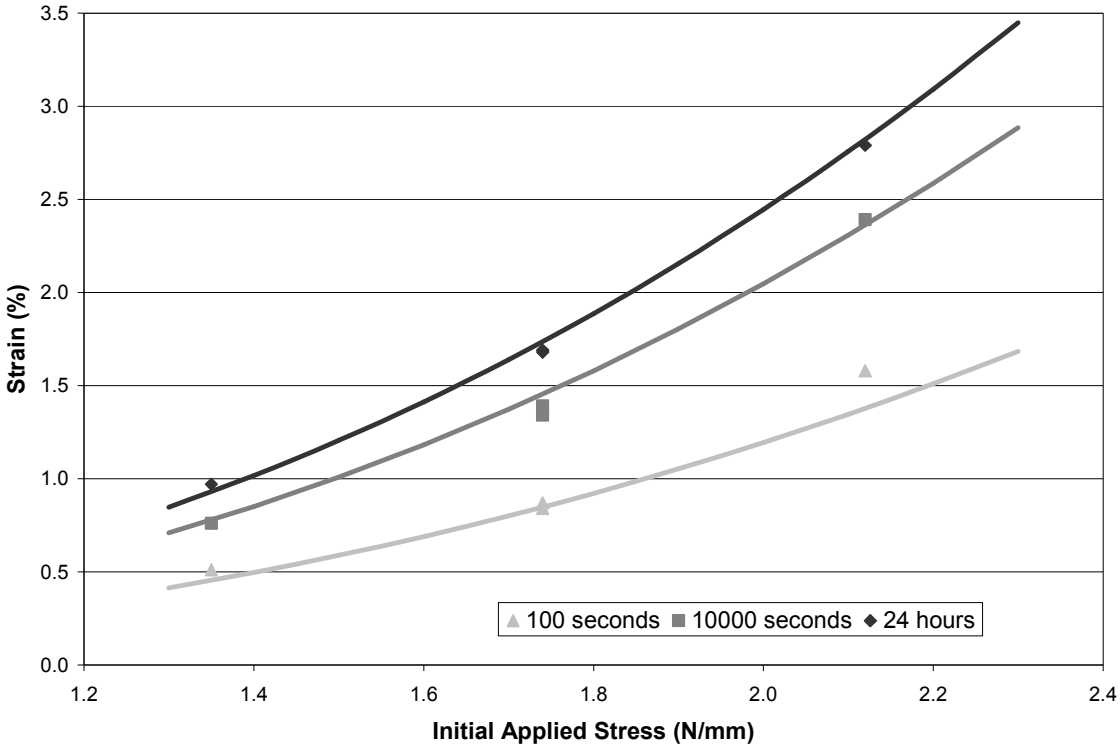

Figure 71 Predicted Isochronous Stress-Strain Curves for 620 ml Freeness, 1.38 MPa Wet Pressed Sheets at 100 seconds, 10000 seconds and 24 hours using the Empirical Model and an Efficiency Factor of 0.88

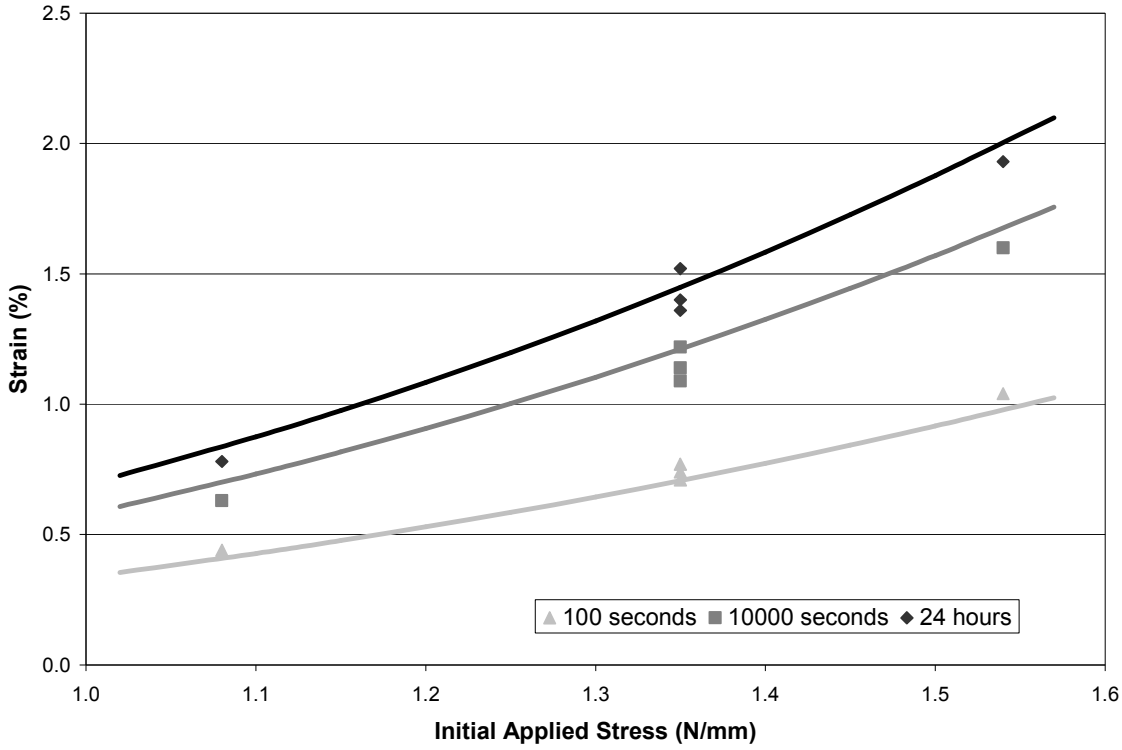

Figure 72 Predicted Isochronous Stress-Strain Curves for 775 ml Freeness, 0.34 MPa Wet Pressed Sheets at 100 seconds, 10000 seconds and 24 hours using the Empirical Model and an Efficiency Factor of 0.74

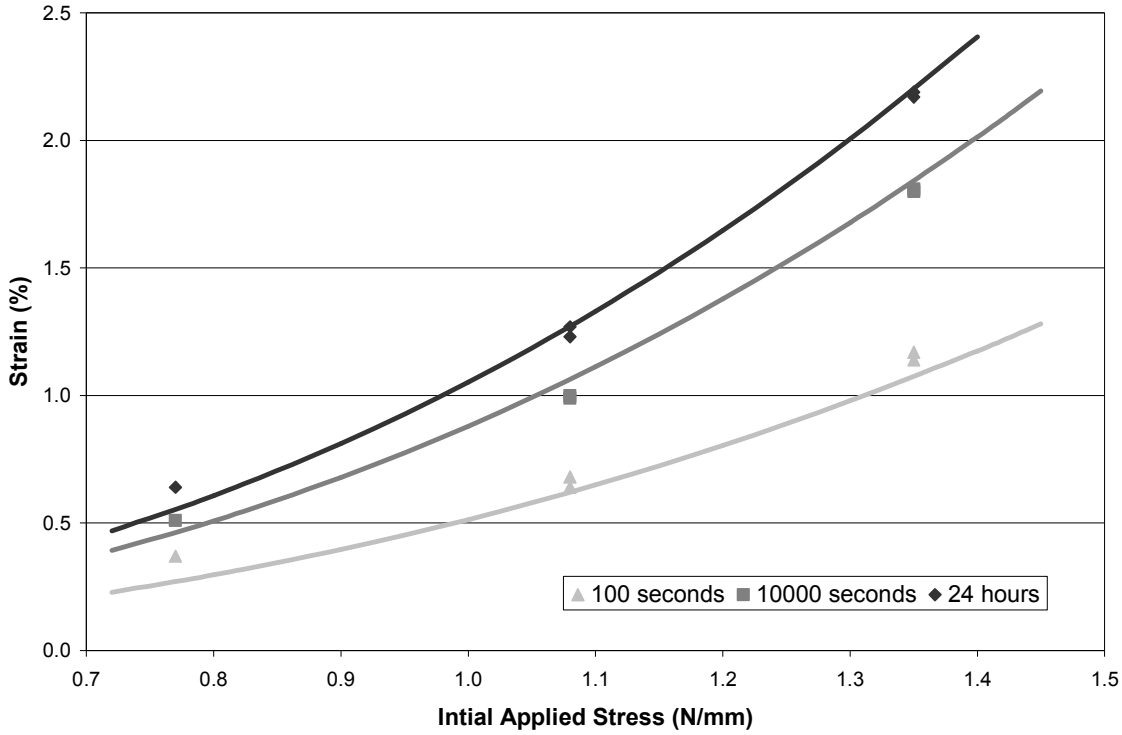

Figure 73 Predicted Isochronous Stress-Strain Curves for 775 ml Freeness, 0.07 MPa Wet Pressed, Sheets at 100 seconds, 10000 seconds and 24 hours using the Empirical Model and an Efficiency Factor of 0.62

Figure 70, Figure 71, Figure 72, and Figure 73 illustrate isochronous stress-strain curves at 3 different times. As shown, the model correlates well to the experimental results. As with the experimental results from Chapter 5, the model is effective in fitting isochronous stress-strain curves for the Brezinski [36, 37] experimental results. This again indicates that an efficiency factor can be used in this model to account for the bonding influence on creep deformation. These efficiency factors are the same efficiency factors used to scale the Brezinski [36, 37] isochronous stress-strain curves in Chapter 5 and are consistent with the efficiency factors calculated from modulus data as shown in Figure 60.

Overall, the empirical model proposed is accurate and simple. It is effective in fitting experimental results obtained for this thesis and from the work of Brezinski [36, 37] (who used a different furnish and pulping technique). Furthermore, in both cases the model allows bonding to be accounted for using an efficiency factor. Although, the model correlates well overall, it shows a tendency to under predict the strain at short times. This effect is amplified as the efficiency factor diminishes. This means that the model is not likely to be a good predictor of isochronous stress-strain curves when times are less than 10 seconds. This was expected as a logarithmic function was chosen in the model. Brezinski [36, 37] shows that this type of function is only effective at higher times and that a power law function is better at short times. Therefore, a modification of the model would be necessary if curves at these short times were desired.

Furthermore, the model does not separate the deformation into initial elastic, primary creep, and secondary creep components. As discussed previously, this empirical model was meant to be simple and only predict the total strain from uni-axial creep testing in tension. If a more descriptive understanding of creep behavior is desired, a different model must be employed. This is the intent of the model presented in the next section.

6.4 Rheological Model Predicting Tensile Creep in Paper

6.4.1 Introduction

The second model introduced is a rheological model. Similar to the empirical model, this model predicts the total strain seen during tensile creep deformation using stress, time, and efficiency factor as input parameters. As a result, this model also

predicts isochronous stress-strain curves. Unlike the empirical model, its derivation is not limited by a requirement for simplicity and should (as a result) provide more information about the creep behavior while providing comparable if not greater accuracy over a range of times, initial applied stresses, and efficiencies. Specifically, the proposed rheological model should offer insight into creep deformation and its underlying mechanism, and separate its total strain during creep into its elastic, primary creep, and secondary creep components.

In polymeric materials such as paper, total creep strain can be broken down into strain components. Commonly, these are referred to as initial elastic strain, primary creep and secondary creep. These terms are often used to describe creep behavior in metals where initial elastic strain is the "instantaneous" strain that occurs during initial loading, primary creep is characterized by a creep rate that is a function of time and decreases as time increases, and secondary creep is characterized by a creep rate that is independent (or nearly independent) of time [6, 13]. Initial elastic strain and primary creep are considered to be fully recoverable while secondary creep is non-recoverable [6, 13].

When considering polymers such as paper, Coffin [13] pointed out that secondary creep is not steady state as with metals, but is rather a function of time where creep rate decreases as time increases. As a result, primary creep and secondary creep are only differentiated by their recoverability, where primary creep is recoverable and secondary creep is non-recoverable. Hence, strain rate time dependence is not considered as a factor in defining creep components within this thesis and the rheological model within this chapter.

There also exists a component of creep called tertiary creep. This creep occurs as a material approaches failure and is characterized by a dramatic increase in creep rate. As discussed by Coffin [13], paper exhibits only a negligible amount of tertiary creep and it is therefore not considered in the derivation of the proposed rheological model. Evidence to support this is shown in Figure 74 where a 75% tensile strength load is applied to 400 ml freeness, 1.03 MPa wet pressed, bonder treated sheets from this thesis.

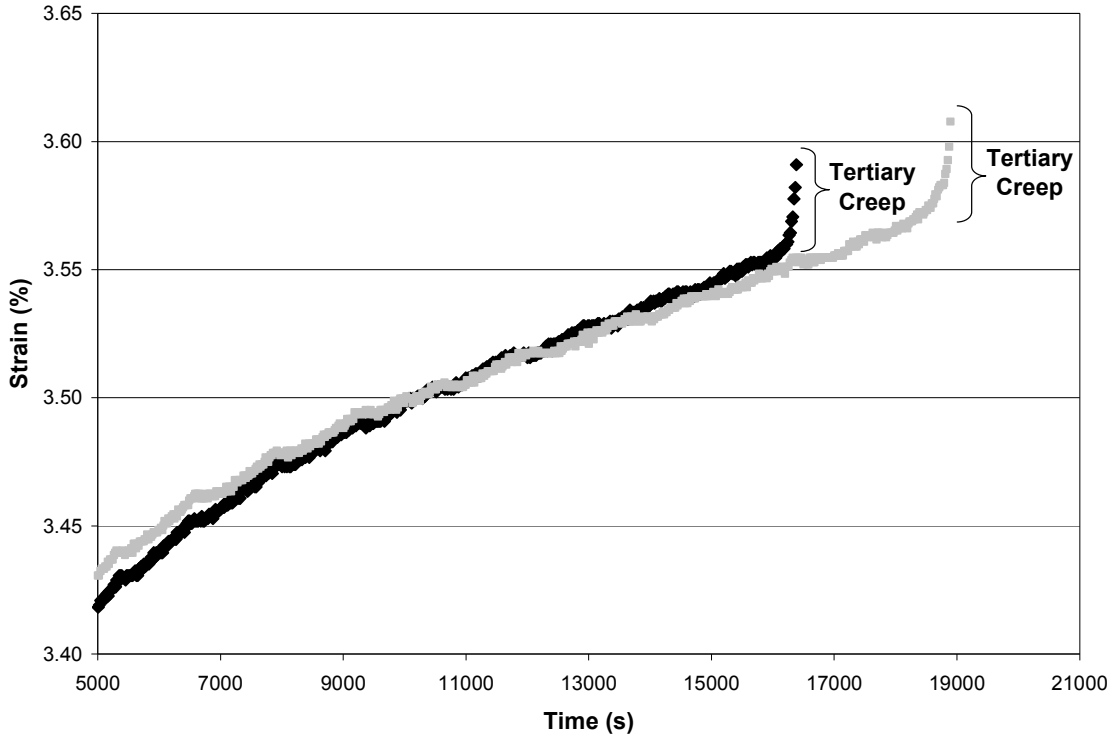

Figure 74 Tertiary Creep in 400 ml Freeness, 1.03 MPa Wet Pressed, Bonder Treated Sheets

The results in Figure 74 show examples of the largest amount of tertiary creep observed from the data gathered for this thesis. It is evident that tertiary creep does not play a significant role in the total creep as the tertiary creep from the most extreme

observed cases is less than 1 % of the total strain and did not occur until very close to failure, where the sheet structure is significantly compromised.

6.4.2 Background of Rheological Models

In this chapter, a rheological model is proposed in which each component of the total strain (initial elastic strain, primary creep, and secondary creep) is represented by springs and dashpots. This type of approach has been used in paper to model creep behavior in the past. The work of Mason [35] discussed using several types of rheological models to describe creep in paper, including the use of a Maxwell Model (spring in series with a dashpot), a Voigt Model (spring in parallel with a dashpot), and a Burgers Model (Maxwell Model in series with a Voigt Model). More recently, the work of Pommier et al. [71] used two Voigt Models in series with a Maxwell Model to describe creep behavior. These models used linear springs and linear dashpots and hence yield a relationship where stress and strain have a linear relationship. In paper, stress and strain have a non-linear relationship and the use of a rheological model based on elements with linear behaviors has inherent limitations on its accuracy. In addition, if the secondary creep component of strain is represented by a single dashpot, the result is a time independent strain rate, which is not representative of tensile creep in paper.

In order to account for the non-linear stress-strain relationship, Coffin [13] developed a non-linear tensile creep model. While the Coffin model is empirical in nature, it does contain rheological elements. Specifically, he uses a spring element to represent initial elastic strain and uses a function very similar to a Voigt Model to account for primary creep. He also uses a non-linear dashpot to represent secondary creep

which employs a logarithmic function. This is likely based on the work of Brezinski [36, 37]. This function allowed secondary creep rate to decrease as time increased. In addition, Coffin [13] employed an efficiency factor in the model and showed overall that it provides a reasonable prediction of the creep data from Brezinski [36, 37]. While this model was accurate and can predict master creep curves, it does not exclusively employ rheological elements.

Agbezuge [72] introduced a non-linear rheological model to describe the stress-strain behavior of xerographic papers. He used a 3-parameter rheological model where a linear spring was in parallel with a linear spring and non-linear dashpot in series. Agbezuge [72] found that the model was effective in predicting the stress-strain curve. He made the model non-linear by replacing the linear (Newtonian) dashpot with a non-linear Eyring dashpot. A drawback to using the model for predicting creep behavior is it does not have a secondary creep component and assumes full recovery of strain. Sedlachek [73] utilized the same approach as Agbezuge [72] and found that it was also effective in predicting the creep behavior of single fibers. Both of these authors draw from the work of Halsey et al. [21] who were responsible for one of the earliest uses of the Eyring dashpot. They developed a 3-parameter rheological model where a linear spring in parallel with a Maxwell Model was modified by replacing the linear (Newtonian) dashpot with a non-linear Eyring dashpot. Later Holland et al. [22] employed the same approach with the Burger's Model where both linear dashpots were replaced with non-linear Eyring dashpots. This 4-parameter model provided greater utility than the 3-parameter model as it separated initial elastic strain and primary creep as well as adding a secondary creep parameter.

The Eyring dashpot is a non-linear dashpot that can be used to relate the creep deformation mechanism to potential (or reaction rate) theory. The Eyring dashpot is based on an Arrhenius reaction rate where constants incorporate temperature, energy of activation, volume of flowing (molecular) segments, and the volume of empty or vacated spaces. The dashpot was first introduced by Tobolsky and Eyring [23] in 1943. The theory behind the model states that in order for flow or strain to occur, a potential barrier must be overcome. The addition of stress acts to shift this barrier to where the energy required to overcome it becomes less in one direction causing a bias and allowing flow or strain in the direction of the bias to occur. Halsey et al. [21] and Holland et al. [22] applied the Eyring dashpot to polymeric materials that contained amorphous (disordered) regions within their molecular networks. Molecular network refers to the arrangement of the molecules that compose the polymer (i.e. the arrangement of the molecular network is amorphous, crystalline, or partially crystalline). The primary load bearing component in a papermaking fiber is cellulose, a linear chain molecule arranged in a partially crystalline network (meaning it contains amorphous disordered regions) [1]. In addition, hemicelluloses and lignin, which are also present in papermaking fibers are amorphous [3, 4, 10]. As a result, use of the Eyring dashpot is particularly applicable to the modeling of paper and papermaking fibers. In combination with linear (Hookean) spring elements in a rheological model, the Eyring dashpot can be used to suggest an explanation for creep deformation on a molecular level.

The previous work employing the Eyring dashpot did not take into account several factors which are important to the accurate modeling of tensile creep in paper. Efficiency factors were not used to represent the level of bonding. Therefore, bonding

was taken into account only be altering the constants employed. Secondary creep rate was modeled as time independent. Consideration was not given to creep behavior at low initial applied stresses. These are stress levels that can be characterized as below the elastic limit on a stress-strain curve.

6.4.3 Derivation of the Rheological Model

The following derivation creates a rheological model with a series of springs and dashpots representing creep behavior. Since creep behavior in paper is non-linear, non-linear rheological elements must be incorporated into the model. Specifically, non-linear Eyring dashpots, discussed in the last section were used as opposed to linear (Newtonian) dashpots. Linear (Hookean) springs were used within the derivation as well. As with the empirical model, the proposed rheological model predicts strain as a function of initial applied stress, time and efficiency factor. It also separates the total creep strain into initial elastic strain, primary creep, and secondary creep components. As a result, the total strain from creep is represented by the sum of initial elastic strain, primary creep strain and secondary creep strain. This relation is shown in Equation 32 where ε is total strain from creep, ε_e is initial elastic strain, ε_1 is primary creep strain, and ε_2 is secondary creep strain. As with the empirical model, σ_o is initial applied stress and t is time.

$$\varepsilon = \varepsilon_e + \varepsilon_1 + \varepsilon_2$$

$$\varepsilon_e = f(\sigma_o) \qquad \varepsilon_1 = f(\sigma_o, t) \qquad \varepsilon_2 = f(\sigma_o, t)$$

Equation 32 Total Strain from Creep Shown as the Sum of Initial Elastic Strain, Primary Creep Strain and Secondary Creep Strain for the Rheological Model

As shown in Equation 32, initial elastic strain is only a function of the initial applied stress, where primary creep strain and secondary creep strain are functions of both initial applied stress and time. Drawing from the work of Holland et al. [22], the same four-parameter rheological model was selected as a starting point to represent the strains in Equation 32. Figure 75 shows a representation of this model, where the four-parameters are represented by two springs and two dashpots.

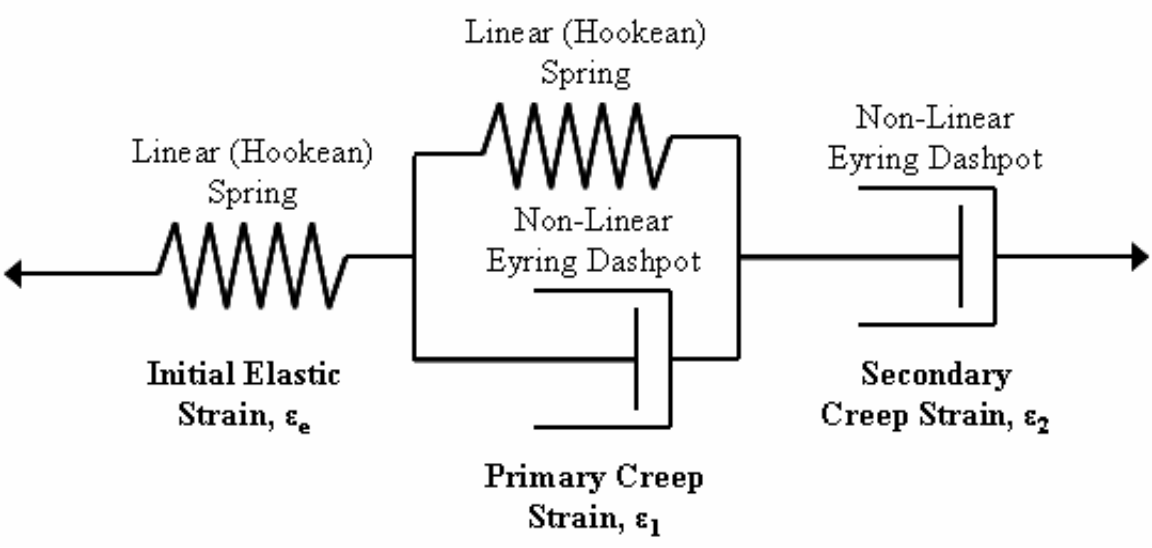

Figure 75 Four-Parameter Rheological Model Used to Model Tensile Creep Behavior in Paper

In Figure 75, initial elastic strain is represented by a linear spring, primary creep strain is represented by a linear spring in parallel with a non-linear Eyring dashpot, and secondary creep strain is represented by a non-linear Eyring dashpot. Equation 33 shows the relation for initial elastic strain, where initial elastic strain is represented by Hooke's Law, the relation used to represent a linear spring.

$$\varepsilon_e = \frac{\sigma_o}{E_e}$$

Equation 33 Linear Spring Element for Initial Elastic Strain Component of the Rheological Model

In Equation 33, E_e is the spring constant used to relate initial applied stress to initial elastic strain; it is the elastic modulus of the paper. Initial elastic strain is characterized by an immediate strain when a stress is applied to the paper. When this stress is removed, the strain will instantaneously and fully recover. If this deformation is thought of from a molecular standpoint, Equation 33 represents the initial elastic response of the cellulose chains and the molecular (partially crystalline) network of which they are arranged within the fiber. This is the same explanation put forth by Meredith [19], when he referred to the elasticity associated with partially crystalline polymeric linear chain molecules in general. In addition to the cellulose, the branched hemicelluloses chains and lignin (if present) as well as their amorphous networks will also contribute towards the initial elastic response. However, initial elastic strain cannot only be attributed to molecular mechanisms. Consideration also has to be given to the larger scale influences, such as fiber type, fiber defects, formation, and orientation. These variables also affect the value of E_e.

Primary creep strain (recoverable strain) is represented by a linear spring in parallel with a non-linear Eyring dashpot. When the spring and dashpot are connected in parallel, the strain and strain rate associated with each element are equivalent and represent the primary creep strain and primary creep strain rate respectively. Equation 34 shows the relation for the linear spring where σ_s is the stress on the spring, ε_1 is the

primary creep strain, and E_1 is the spring constant. Equation 35 shows the relation for the non-linear Eyring dashpot where σ_d is stress on the dashpot, $d\varepsilon_1/dt$ is the strain rate of the dashpot, and A_1 and B_1 are the dashpot constants.

$$\sigma_s = E_1\varepsilon_1$$

Equation 34 Linear Spring Element for the Primary Creep Strain Component of the Rheological Model

$$\sigma_d = A_1 \sinh^{-1}\left(\frac{1}{B_1}\frac{d\varepsilon_1}{dt}\right)$$

Equation 35 Non-Linear Eyring Dashpot Element for the Primary Creep Strain Component of the Rheological Model

While the strain and strain rate associated with each element are the same when connected in parallel, the stresses are not; each element bears a different portion of the applied stress. As a result, initial applied stress is found when Equation 34 and Equation 35 are combined. Equation 36 shows this and gives the final relation of a linear spring connected in parallel with a non-linear Eyring dashpot, where initial applied stress, σ_o, is a function of primary creep strain and primary creep strain rate.

$$\sigma_o = \sigma_s + \sigma_d$$

$$\sigma_o = E_1\varepsilon_1 + A_1 \sinh^{-1}\left(\frac{1}{B_1}\frac{d\varepsilon_1}{dt}\right)$$

Equation 36 Initial Applied Stress as the Sum of the Stresses Associated with the Linear Spring Element and Non-Linear Eyring Dashpot Element used as the Primary Creep Strain Components of the Rheological Model

Equation 36 is a differential equation and cannot be used directly to find primary creep strain as a function of initial applied stress and time. In order to find this, the differential equation must be solved to remove the strain rate component. Equation 36 is reorganized into Equation 37, showing a differential equation.

$$\frac{d\varepsilon_1}{dt} = B_1 \sinh\left(\frac{\sigma_o - E_1\varepsilon_1}{A_1}\right)$$

Equation 37 Differential Equation of the Linear Spring Element Connected in Parallel to a Non-Linear Eyring Dashpot Element for the Primary Creep Strain Component of the Rheological Model

Equation 37 is solved, resulting in Equation 38. The mathematics behind this particular solution is shown in Appendix B. Equation 38 shows primary creep strain as a function of initial applied stress and time where E_1, A_1, and B_1 are material constants.

$$\varepsilon_1 = \frac{1}{E_1}\left(\sigma_o - 2A_1 \tanh^{-1}\left[\tanh\left(\frac{\sigma_o}{2A_1}\right)\exp\left(-\frac{E_1 B_1 t}{A_1}\right)\right]\right)$$

Equation 38 Solution of the Differential Equation for the Linear Spring Element Connected in Parallel to a Non-Linear Eyring Dashpot Element for the Primary Creep Strain Component of the Rheological Model

According to Equation 38, as time increases, the initial applied stress will be borne completely by the spring element. As a result, the total amount of primary creep strain will be linearly related to initial applied stress given enough time. This is because the spring element is linear and controls the total amount of primary creep strain. The constant, E_1 comes from this spring element and is a material parameter that represents the total amount of primary creep strain that will occur. The constants, A_1 and B_1 come from the Eyring dashpot and are material parameters that control the delayed elastic behavior of the paper including the rate at which primary creep will progress and exhaust.

Meredith [19] discussed primary creep behavior as the delayed elastic response of the amorphous molecular network with respect to polymeric materials. More specifically, Alfrey [25] discussed primary creep as flow resulting from the uncurling of molecular chains within the amorphous regions of a polymer network. In terms of paper, primary creep strain would be the uncurling of cellulose chains within the amorphous region of the molecular network within a fiber. Uncurling of amorphous hemicelluloses and amorphous lignin (if present) would also occur. Within the Eyring dashpot, the B_1 constant includes the effects of temperature, energy of activation, volume of flowing (molecular segments), and the volume of empty or vacated spaces. The A_1 constant includes temperature and the volume of empty or vacated spaces. Again, consideration

also has to be given to the larger scale influences, such as fiber type, fiber defects, formation, and orientation. If any of these variables change, they will affect E_1, A_1 and B_1.

Secondary creep strain (permanent strain) is represented by a single non-linear Eyring dashpot. Equation 39 shows the relation for a non-linear Eyring dashpot where $d\varepsilon_2/dt$ is secondary creep strain rate, σ_o is initial applied stress and A_2 and B_2 are material constants.

$$\frac{d\varepsilon_2}{dt} = B_2 \sinh\left(\frac{\sigma_o}{A_2}\right)$$

Equation 39 Differential Equation of the Non-Linear Eyring Dashpot Element for the Secondary Creep Strain Component of the Rheological Model

Equation 39, when solved, yields a relationship in which secondary creep strain is non-linear with initial applied stress and secondary creep strain is linear with time. However, secondary tensile creep strain in paper is not linear with time. As shown by Brezinski [36, 37], secondary creep strain in paper is linear with log time. To account for this, Equation 39 is modified to incorporate a time dependence on secondary creep strain rate. This is shown in Equation 40, where a time term, $(t/t_r + 1)$ is incorporated into the Eyring dashpot relation.

$$\frac{d\varepsilon_2}{dt} = \left[B_2 \sinh\left(\frac{\sigma_o}{A_2} \right) \right] \frac{1}{t / t_r + 1}$$

Equation 40 Differential Equation of the Non-Linear Eyring Dashpot Element with a Time Term Incorporated for the Secondary Creep Strain Component of the Rheological Model

When the differential equation in Equation 40 is integrated, Equation 41 results. Equation 41 shows secondary creep strain as a function of initial applied stress and time where A_2 and B_2 are material constants and t_r is a reference time constant. Like the empirical model, the reference time constant is set to the time scale which creep measurements are made.

$$\varepsilon_2 = \left[B_2 \sinh\left(\frac{\sigma_o}{A_2} \right) \right] t_r \ln\left(\frac{t}{t_r} + 1 \right)$$

Equation 41 Particular Solution to the Differential Equation of the Non-Linear Eyring Dashpot Element with a Time Term Incorporated for the Secondary Creep Strain Component of the Rheological Model

According to Equation 41, as time increases, the rate of secondary creep will diminish. The constants, A_2 and B_2 are material parameters that represent the viscous behavior of the paper and the rate at which secondary creep will progress. Unlike the primary creep strain case, if initial applied stress is removed, the secondary creep strain will not recover, it is a permanent deformation. Alfrey [25] discussed secondary creep behavior as a permanent deformation involving the sliding of molecular segments past one another within the amorphous region of a molecular network. Tobolsky and Eyring

[23] similarly discussed the flow of molecular segments and the breaking of network bonds. In terms of paper, secondary creep strain would be the sliding of cellulose chain segments past one another within the amorphous regions of the molecular network within the fiber. The flow of amorphous hemicelluloses segments and lignin (if present) also contributes. Within the Eyring dashpot, the B_2 constant includes the effects of temperature, energy of activation, volume of flowing (molecular segments), and the volume of empty or vacated spaces. The A_2 constant includes temperature and the volume of empty or vacated spaces. Again, consideration also has to be given to the larger scale influences, such as fiber type, fiber defects, formation, and orientation. If any of these variables change, so will A_2 and B_2.

Overall, the work of Olsson and Salmén [26] offer support to the rationale behind the molecular mechanisms being part of the explanation describing primary creep and secondary creep strain. Using mid-IR spectroscopy, Olsson and Salmén [26] found that there appeared to be an increase in orientation or stretching of cellulose molecules and the indication of sliding between cellulose chains. Although they did not attribute these observations specifically to primary creep strain and secondary creep strain, increase of orientation could be attributed to primary creep strain and sliding of molecular chains could be attributed to secondary creep strain. This would be consistent with what Alfrey [25] discussed as the mechanisms behind primary and secondary creep strain.

Using Equation 33, Equation 38 and Equation 41, the total strain from creep can be predicted. These equations are incorporated into Equation 32 to yield a rheological model which predicts total strain from creep as the sum of initial elastic strain, primary creep strain, and secondary creep strain. This is shown in Equation 42.

$$\varepsilon = \frac{\sigma_o}{E_e} + \frac{1}{E_1}\left(\sigma_o - 2A_1 \tanh^{-1}\left[\tanh\left(\frac{\sigma_o}{2A_1}\right)\exp\left(-\frac{E_1 B_1 t}{A_1}\right)\right]\right) + \left[B_2 \sinh\left(\frac{\sigma_o}{A_2}\right)\right] t_r \ln\left(\frac{t}{t_r}+1\right)$$

Equation 42 Rheological Model Predicting Total Strain from Creep as the Sum of Initial Elastic Strain, Primary Creep Strain and Secondary Creep Strain

Equation 42 does not adequately account for creep behavior at low initial applied stresses, stresses below the elastic limit on a stress-strain curve. To resolve this, prior research into stress relaxation behavior in paper can be drawn upon. Johanson and Kubat [107] researched stress relaxation behavior in paper and found that it is possible for paper to bear a non-zero stress (now known as Kubat stress) without measurable relaxation. They proposed that the rate of stress relaxation becomes zero at or below this stress. As a result, Skowronski and Szwarcsztajn [108] concluded that paper would only react elastically below the Kubat stress. Similarly, Waterhouse [109] and Niskanen [16] stated that the Kubat stress must be overcome for any significant stress relaxation to occur. Niskanen [16] further discussed that stress relaxation may occur below the Kubat stress, but it is too slow to measure. Htun and de Ruvo [110, 111] and Htun [112] found that Kubat stress existed in paper that was dried under restraint and that this stress correlates to the (drying) stress generated within paper during restrained drying. In effect, the restrained drying process acts to harden the material so a certain stress must be exceeded for any significant time-dependent behavior to occur. Conversely, if paper is freely dried, the Kubat stress will be zero as no material hardening occurs. It is proposed that if such an activation stress exists for stress relaxation behavior, that it would also exist for creep

behavior. Like Niskanen [16], it is not argued that time-dependent deformation ceases to occur below such an activation stress, but a change in deformation behavior occurs near this stress where all deformation below it can be ignored. As a result, an activation stress, σ_k, is incorporated in to Equation 42, resulting in Equation 43.

$$\varepsilon = \frac{\sigma_o}{E_e} + \frac{1}{E_1}\left(\left\langle \sigma_o - \sigma_k \right\rangle - 2A_1 \tanh^{-1}\left[\tanh\left(\frac{\left\langle \sigma_o - \sigma_k \right\rangle}{2A_1} \right) \exp\left(-\frac{E_1 B_1 t}{A_1} \right) \right] \right) + \left[B_2 \sinh\left(\frac{\left\langle \sigma_o - \sigma_k \right\rangle}{A_2} \right) \right] t_r \ln\left(\frac{t}{t_r} + 1 \right)$$

Equation 43 Rheological Model Predicting Total Strain from Creep as the Sum of Initial Elastic Strain, Primary Creep Strain and Secondary Creep Strain (Incorporating an Activation Stress)

As shown in Equation 43, an activation stress is incorporated into the time-dependent components of the model (primary and secondary creep strain equations). Specifically, activation stress is subtracted from initial applied stress and placed within McCauley Brackets (values within these brackets less than zero are equal to zero). As a result, if initial applied stress is less than the activation stress, only the initial elastic strain component of the rheological model will contribute towards the total strain during a creep test. Hence, the model will predict strain as only instantaneous linear elastic strain below the activation stress. If this deformation is thought of from a molecular standpoint, the molecular network in which cellulose chains and hemicelluloses are arranged within a fiber can support a finite amount of stress before significant time-dependent uncurling or viscous flow of molecular segments occurs.

As with the empirical model, the final step required to complete this rheological model is to incorporate the efficiency factor into Equation 43. Dividing the initial applied stress by the efficiency factor does this. The efficiency factor accounts for how bonding reduces the initial applied stress necessary to achieve a given amount of strain in an inefficiently loaded structure. Equation 44 shows the final form of the rheological model, with efficiency factor, φ, incorporated into the model.

$$\varepsilon = \frac{\sigma_o}{\varphi E_e} + \frac{1}{E_1}\left(\left\langle \frac{\sigma_o}{\varphi} - \sigma_k \right\rangle - 2A_1 \tanh^{-1}\left[\tanh\left(\left\langle \frac{\sigma_o}{\varphi} - \sigma_k \right\rangle \frac{1}{2A_1}\right)\exp\left(-\frac{E_1 B_1 t}{A_1}\right)\right]\right) + \left[B_2 \sinh\left(\left\langle \frac{\sigma_o}{\varphi} - \sigma_k \right\rangle \frac{1}{A_2}\right)\right] t_r \ln(t+1)$$

Equation 44 Final Form of Rheological Model Predicting Total Strain from Creep as the Sum of Initial Elastic Strain, Primary Creep Strain and Secondary Creep Strain (Incorporating an Activation Stress and Efficiency Factor)

The final form of this rheological model yields a calculation well suited for predicting isochronous stress-strain curves. It has three variables, initial applied stress, time, and efficiency factor. It contains a reference time constant that is defined by the time scale of the creep measurements. It also contains seven material constants, which can be found from direct comparison with experimental data. It offers a greater insight than the empirical model as it separates strain into its initial elastic, primary creep, and secondary creep components. It also draws from the molecular deformation mechanisms of the partially crystalline cellulose chains, amorphous hemicelluloses, and lignin (if present) that compose a papermaking fiber.

6.4.4 Validation of the Rheological Model

As with the empirical model, it is necessary to validate the rheological model shown in Equation 44. It is compared to creep results obtained experimentally at varying efficiencies; the same experimental results used with the empirical model are used with the rheological model. These include the experimental results presented in Chapter 5 and the experimental results of Brezinski [36, 37]. First, the experimental results of Chapter 5 are used to validate the model. The seven material constants, σ_k, E_e, E_1, A_1, B_1, A_2, and B_2 are selected to "fit" the model to the experimental results and remain unchanged for all initial applied stresses, times, and efficiency factors. This was accomplished by fitting the constants to the modulus and creep data from the 400 ml freeness, 1.03 MPa wet pressed, bonder treated sheets. These sheets are fully efficient loaded structures and have an efficiency factor equal to 1.00, indicating bonding does not impact deformation behavior.

Specifically, activation stress, σ_k, was determined experimentally by finding the initial applied stress at which creep became insignificant. Activation stress can more accurately be found by measuring the drying stress of the paper; drying stress and activation stress are equivalent. Elastic modulus, E_e, was also determined experimentally by measuring the elastic modulus of paper. In order to determine the values of the remaining constants, the amount of primary creep and secondary creep must be found. Without recovery data, as is the case with these experimental data, it was assumed that all the strain occurring after 10000 seconds was secondary creep. Using this assumption, A_2 and B_2 were found through an iterative process and these constants were adjusted until the residual difference between the actual secondary creep data and the values the

rheological model predicted was minimized. By subtracting the secondary creep and instantaneous elastic strain from the total strain, the total amount of primary creep was found and set the E_1 constant. A_1 and B_1 were then found through an iterative process and these constants were adjusted until the residual difference between the actual primary creep data and the values the rheological model predicted was minimized. The reference time constant was set at one second as the experimental results presented in Chapter 5 were obtained in a seconds time scale. Table 10 shows the values and units for these constants.

Table 10 Values of Rheological Model Constants Used to Fit Experimental Results

Rheological Model Constants	Values	Units
σ_k	1.5	N/mm
E_e	960	N/mm
E_1	270	N/mm
A_1	0.085	N/mm
B_1	2.5E-08	1/s
A_2	4.6	N/mm
B_2	8.1E-04	1/s
t_r	1.0	s

Notice that the units for A_1 and B_1 (and A_2 and B_2) are such that their quotient results in the units of viscosity. This is not a coincidence; the relationship is commented on by Drosdov [12] when a rheological model incorporating an Eyring dashpot is simplified to a linear model.

Figure 76 and Figure 77 show isochronous stress-strain curves calculated using the rheological model in Equation 44 and the constants from Table 10. Data points (with

standard error bars) from the actual experimental creep results obtained from the 400 ml freeness, 1.03 Mpa wet pressed, bonder treated, fully efficient sheets are also shown.

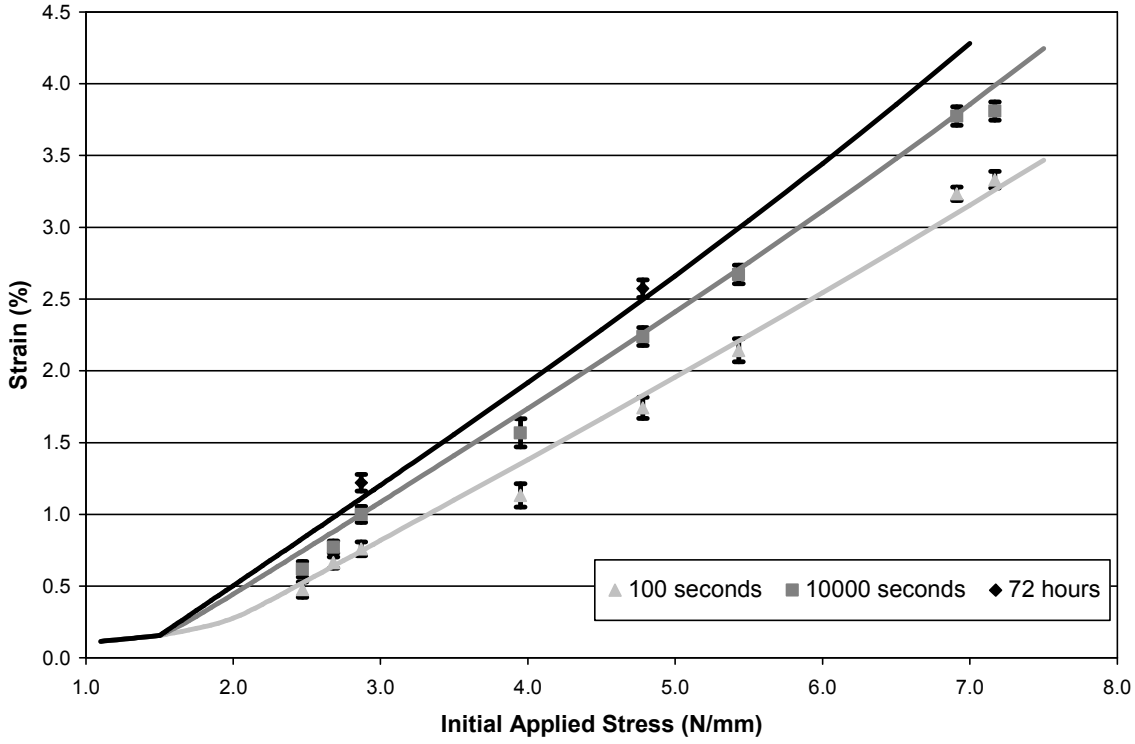

Figure 76 Predicted Isochronous Stress-Strain Curves for 400 ml Freeness, 1.03 MPa Wet Pressed, Bonder Treated Sheets at 100 seconds, 10000 seconds and 72 hours using the Rheological Model and an Efficiency Factor of 1.00

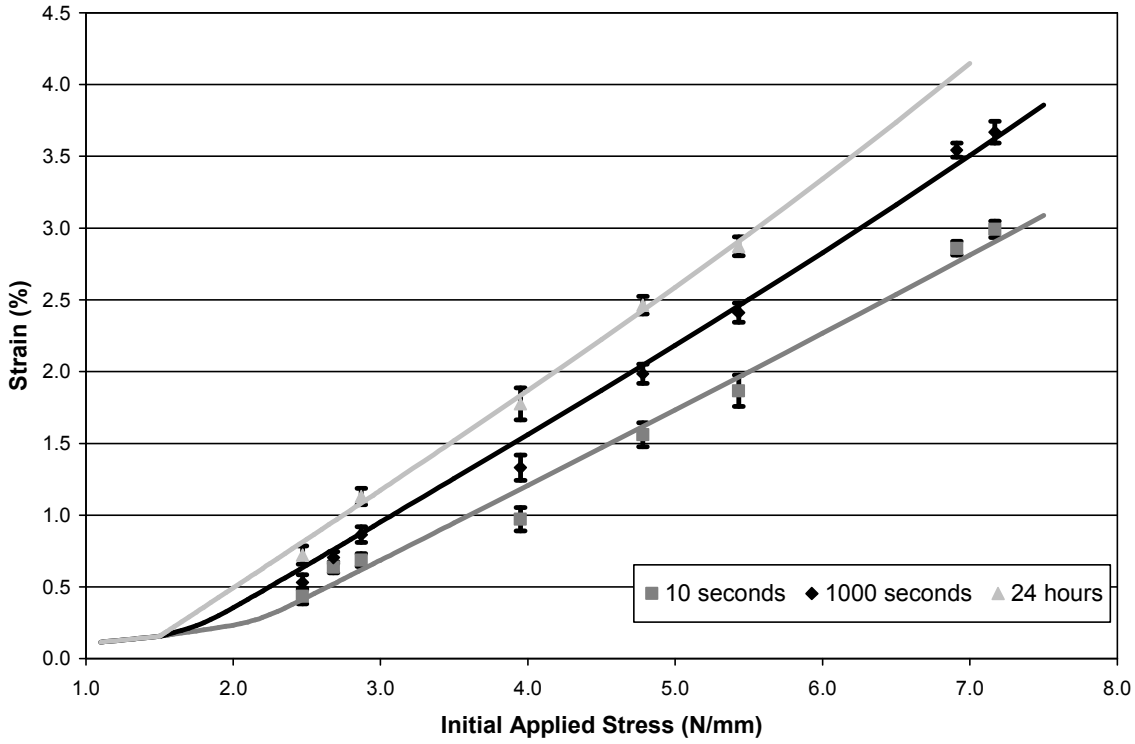

Figure 77 Predicted Isochronous Stress-Strain Curves for 400 ml Freeness, 1.03 MPa Wet Pressed, Bonder Treated Sheets at 10 seconds, 1000 seconds and 24 hours using the Rheological Model and an Efficiency Factor of 1.00

Figure 76 and Figure 77 show isochronous stress-strain curves at six different times. As with the empirical model, this model correlates well with experimental results. Further comparisons of this model are done with creep results from less than fully efficient loaded structures. Figure 78, Figure 79, Figure 80, Figure 81, Figure 82, and Figure 83 illustrate isochronous stress-strain curves calculated using the rheological model in Equation 44 and the constants from Table 10. Data points (with standard error bars) from actual creep results obtained through experimentation are also shown. Again, data from Chapter 6 was used. Figure 78 and Figure 79 data was obtained from 400 ml freeness, 0.17 MPa wet pressed, control sheets with 0.91 efficiency factors. Figure 80 and

Figure 81 data was obtained from 400 ml freeness, 0.17 MPa wet pressed, debonder treated sheets with 0.85 efficiency factors. Figure 82 and Figure 83 data was obtained from 570 ml freeness, 0.07 MPa wet pressed, control sheets with 0.62 efficiency factors.

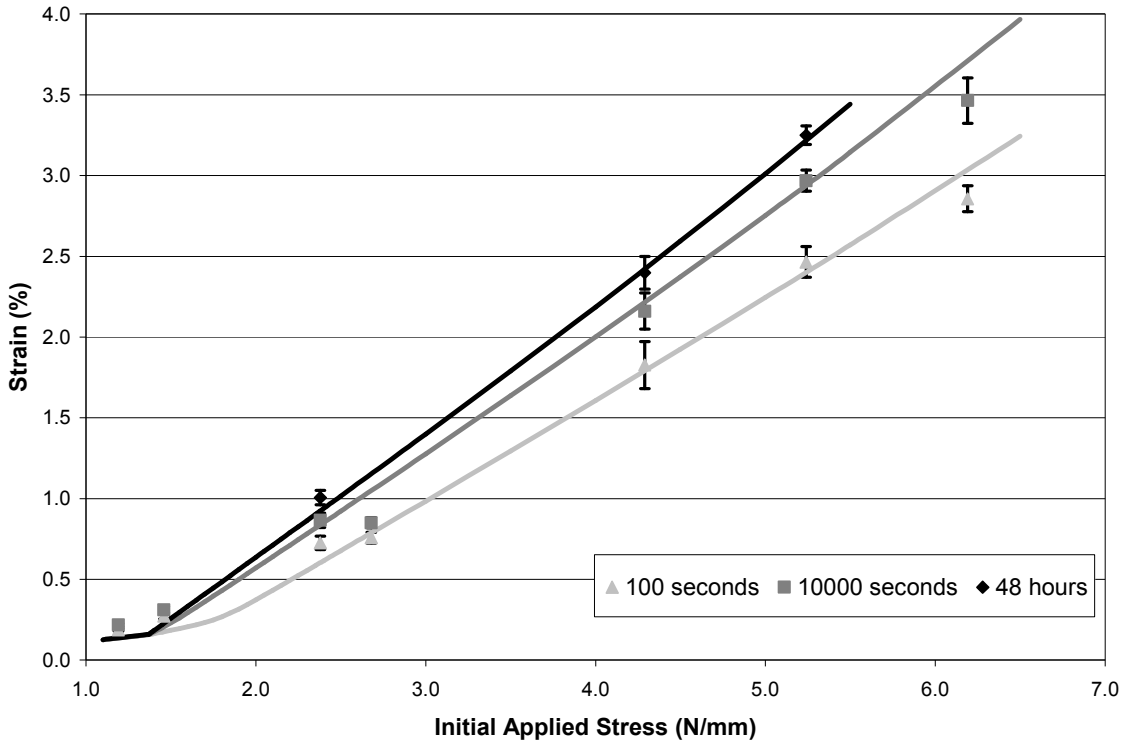

Figure 78 Predicted Isochronous Stress-Strain Curves for 400 ml Freeness, 0.17 MPa Wet Pressed, Control Sheets at 100 seconds, 10000 seconds and 48 hours using the Rheological Model and an Efficiency Factor of 0.91

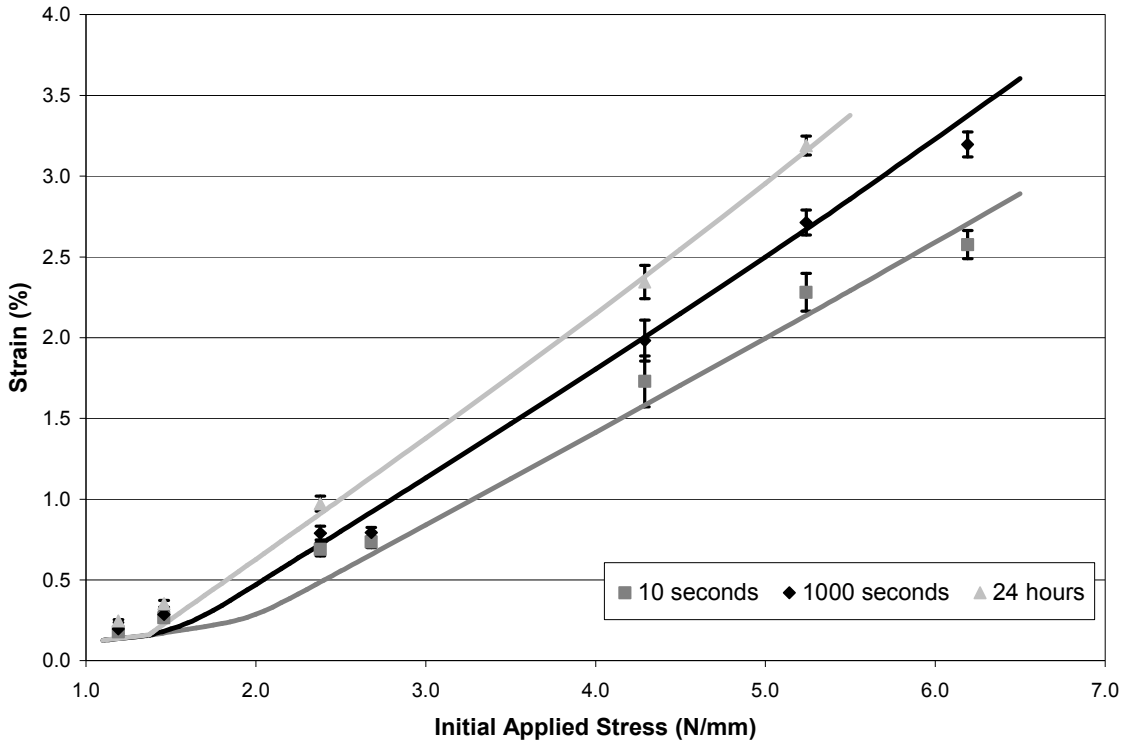

Figure 79 Predicted Isochronous Stress-Strain Curves for 400 ml Freeness, 0.17 MPa Wet Pressed, Control Sheets at 10 seconds, 1000 seconds and 24 hours using the Rheological Model and an Efficiency Factor of 0.91

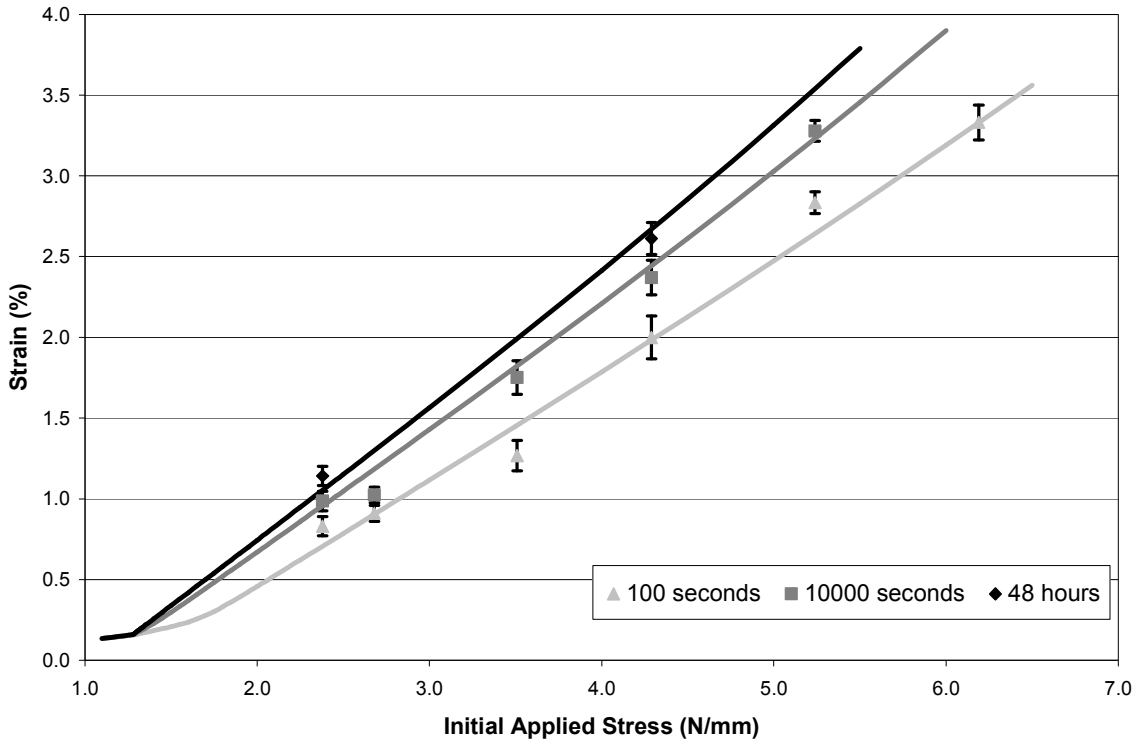

Figure 80 Predicted Isochronous Stress-Strain Curves for 400 ml Freeness, 0.17 MPa Wet Pressed, Debonder Treated Sheets at 100 seconds, 10000 seconds and 48 hours using the Rheological Model and an Efficiency Factor of 0.85

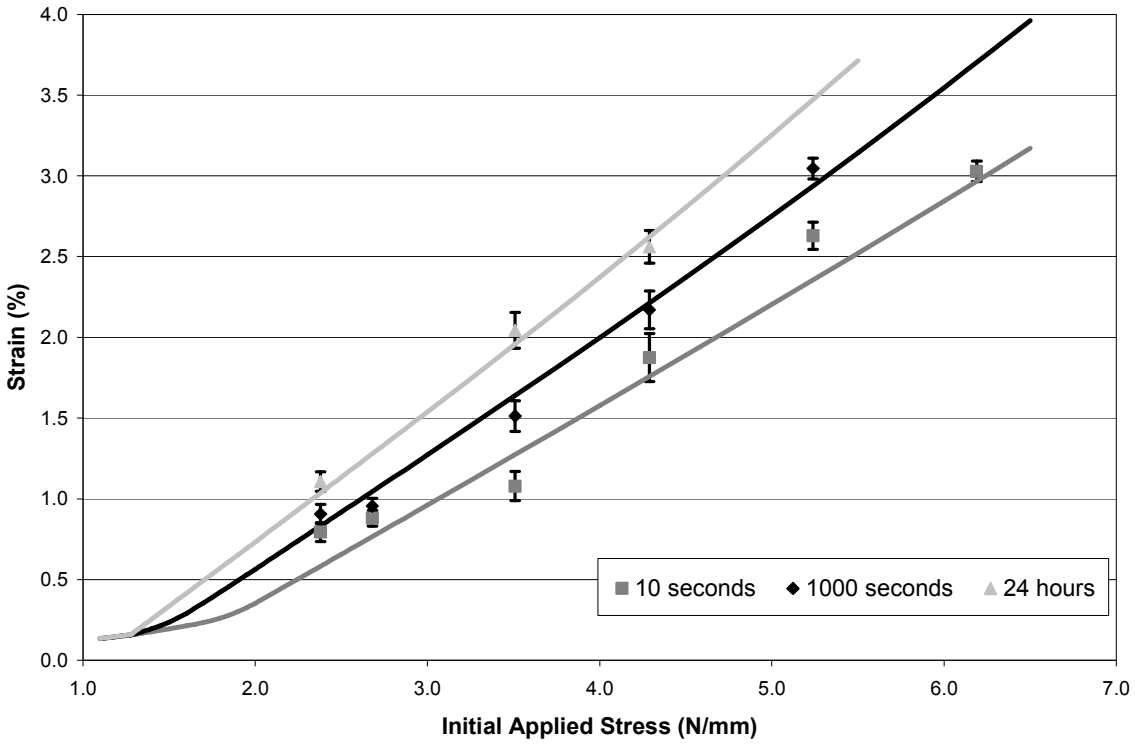

Figure 81 Predicted Isochronous Stress-Strain Curves for 400 ml Freeness, 0.17 MPa Wet Pressed, Debonder Treated Sheets at 10 seconds, 1000 seconds and 24 hours using the Rheological Model and an Efficiency Factor of 0.85

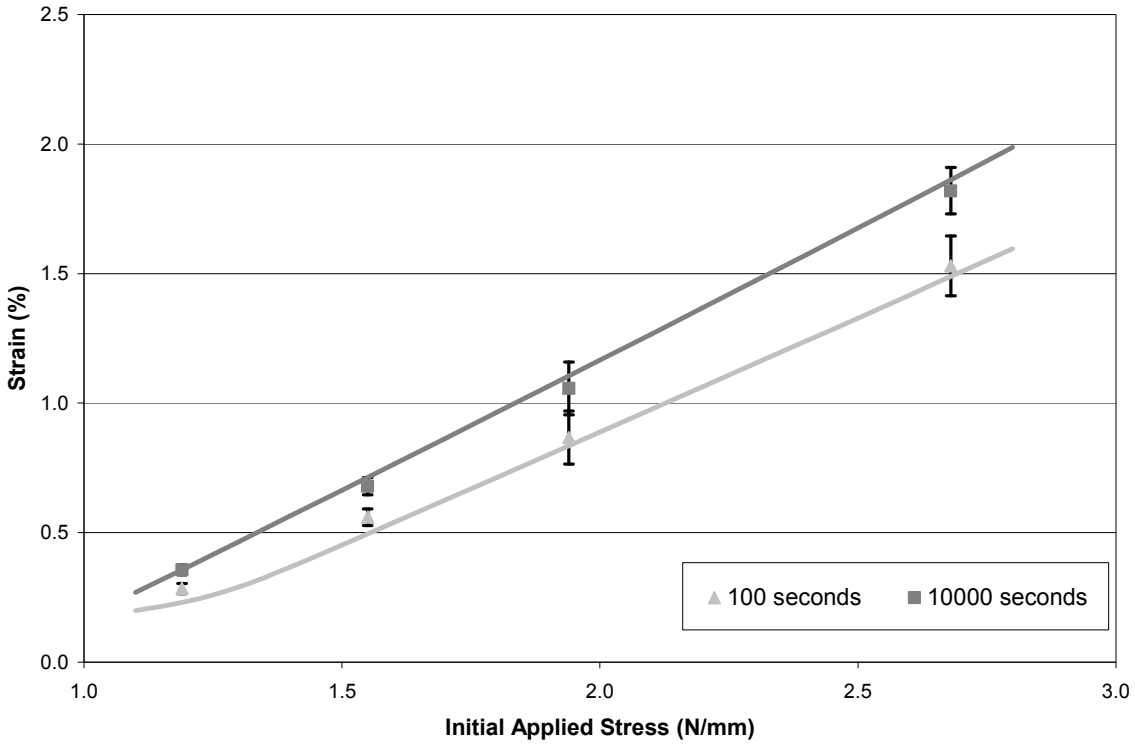

Figure 82 Predicted Isochronous Stress-Strain Curves for 570 ml Freeness, 0.07 MPa Wet Pressed, Control Sheets at 100 seconds and 10000 seconds using the Rheological Model and an Efficiency Factor of 0.62

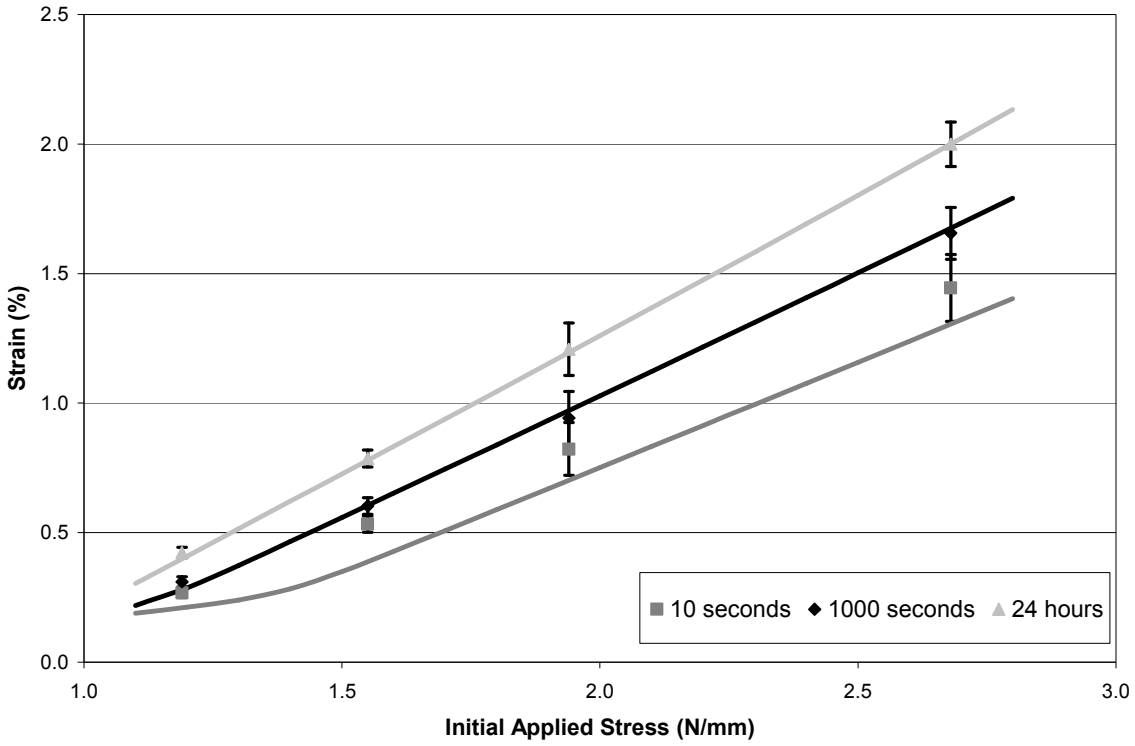

Figure 83 Predicted Isochronous Stress-Strain Curves for 570 ml Freeness, 0.07 MPa Wet Pressed, Control Sheets at 10 seconds, 1000 seconds and 24 hours using the Rheological Model and an Efficiency Factor of 0.62

As shown in Figure 78, Figure 79, Figure 80, Figure 81, Figure 82, and Figure 83, the model correlates well to the experimental results of the inefficiently loaded sheets. This shows that as with the empirical model, an efficiency factor can be used in this model to account for the influence of bonding on creep deformation.

As with the empirical model, the experimental results of Brezinski's [36, 37] are used as further validation of the rheological model. The seven material constants, σ_k, E_e, E_1, A_1, B_1, A_2, and B_2 are used to "fit" the model to the experimental results and remain unchanged at all initial applied stresses, times, and efficiency factors. This was

accomplished by fitting the constants to the creep data (as labeled in Chapter 5) from the 425 ml freeness, 0.34 MPa wet pressed sheets, with efficiency factors of 1.00.

Specifically, all the material constants for this data were found in the same fashion as with the experimental results from this thesis. The only exception is instead of having to determine the amount of primary creep and secondary creep by making an assumption, actual creep recovery data was used. As a result, the amount of primary creep and the E_1 constant did not have to be determined by subtracting the secondary creep and instantaneous elastic strain from the total strain. The reference time constant was set at one second as the experimental results are in a seconds time scale. Table 11 shows the values and units for these constants.

Table 11 Values of Rheological Model Constants Used to Fit Experimental Results of Brezinski [36, 37]

Rheological Model Constants	Values	Units
σ_k	0.9	N/mm
E_e	440	N/mm
E_1	360	N/mm
A_1	0.22	N/mm
B_1	1.3E-08	1/s
A_2	0.71	N/mm
B_2	3.9E-04	1/s
t_r	1.0	s

If these constants are judged against the ones from Table 10, they suggest that the creep behavior measured by Brezinski [36, 37] has a lower activation stress, σ_k, more instantaneous elastic strain and secondary creep, and less primary creep compared to the experimental results from this thesis. A greater instantaneous elastic strain is indicated by

the decreased elastic modulus, E_e. A lesser primary creep is indicated by a higher E_1 constant. With regard to the A_1 and B_1 constants, A_1 is higher, indicating a primary creep rate that is more linear with initial applied stress. B_1 is lower, indicating a slower rate in which primary creep will progress and eventually exhaust. Greater secondary creep is indicated by the A_2 and B_2 constants. A_2 is lower, indicating a more non-linear secondary creep behavior. In fact, A_2 is significantly lower than the A_2 constant used for the experimental results from this thesis. Due to this, B_2 is also lower, indicating at first glance a lesser secondary creep rate. This is not so because the decreased A_2 lessens the value of B_2 required to give a faster secondary creep rate. The reason this occurs is because A_2 and B_2 both share dependence on common parameters. These include the volume of the empty or vacated spaces within the molecular network of the fibers and temperature. This is also true for A_1 and B_1, but in this case, the differences in the primary creep rates were so large, the greater A_1 did not cause the value of B_1 to be higher than the B_1 constant used for the experimental results from this thesis.

Figure 84, Figure 85, Figure 86, and Figure 87 show isochronous stress-strain curves calculated using the rheological model in Equation 44 and the constants from Table 11. Data points from actual creep results obtained from Brezinski [36, 37] are also shown. These results were obtained from sheets with a range of efficiencies. Using the labeling for the sheets in Chapter 5, Figure 84 data was obtained from the 425 ml freeness, 0.34 MPa wet pressed, fully efficient sheets used to find the material constants. Figure 85 data was obtained from 620 ml freeness, 1.38 MPa wet pressed sheets with efficiency factors of 0.88. Figure 86 data was obtained from 775 ml freeness, 0.34 MPa

wet pressed sheets with efficiency factors of 0.74. Finally, Figure 87 data was obtained from 775 ml freeness, 0.07 MPa wet pressed sheets with efficiency factors of 0.62.

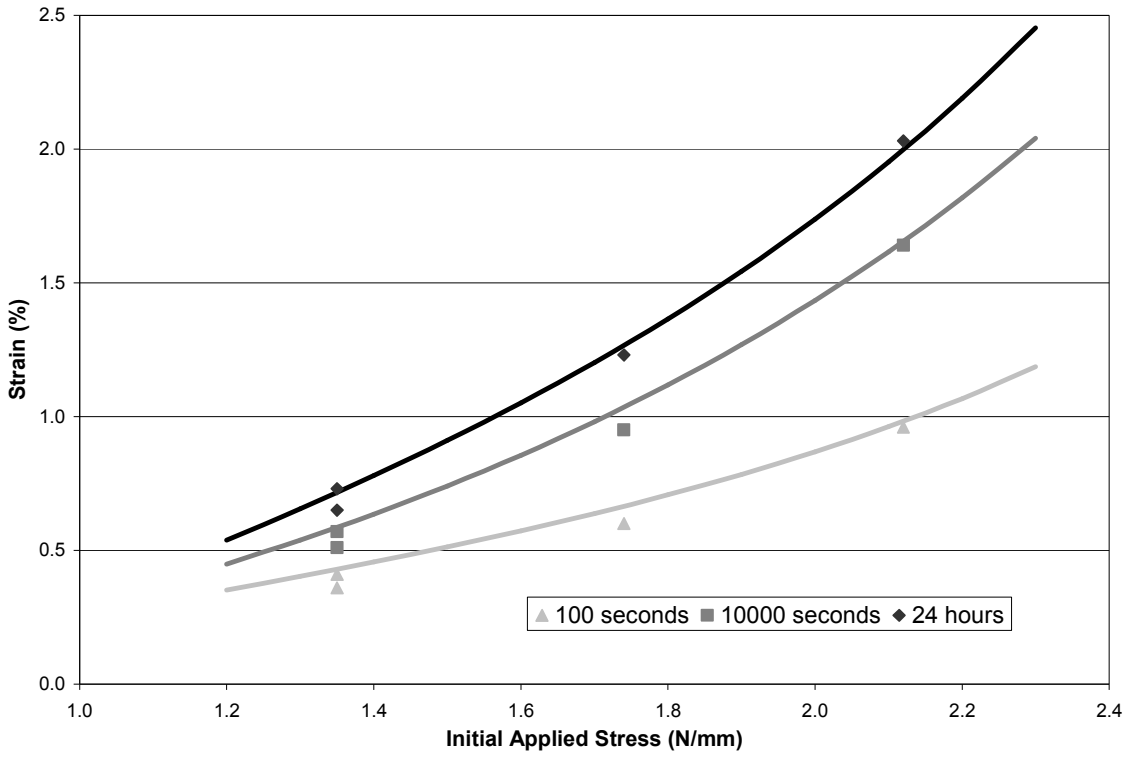

Figure 84 Predicted Isochronous Stress-Strain Curves for 425 ml Freeness, 0.34 MPa Wet Pressed Sheets at 100 seconds, 10000 seconds and 24 hours using the Rheological Model and an Efficiency Factor of 1.00

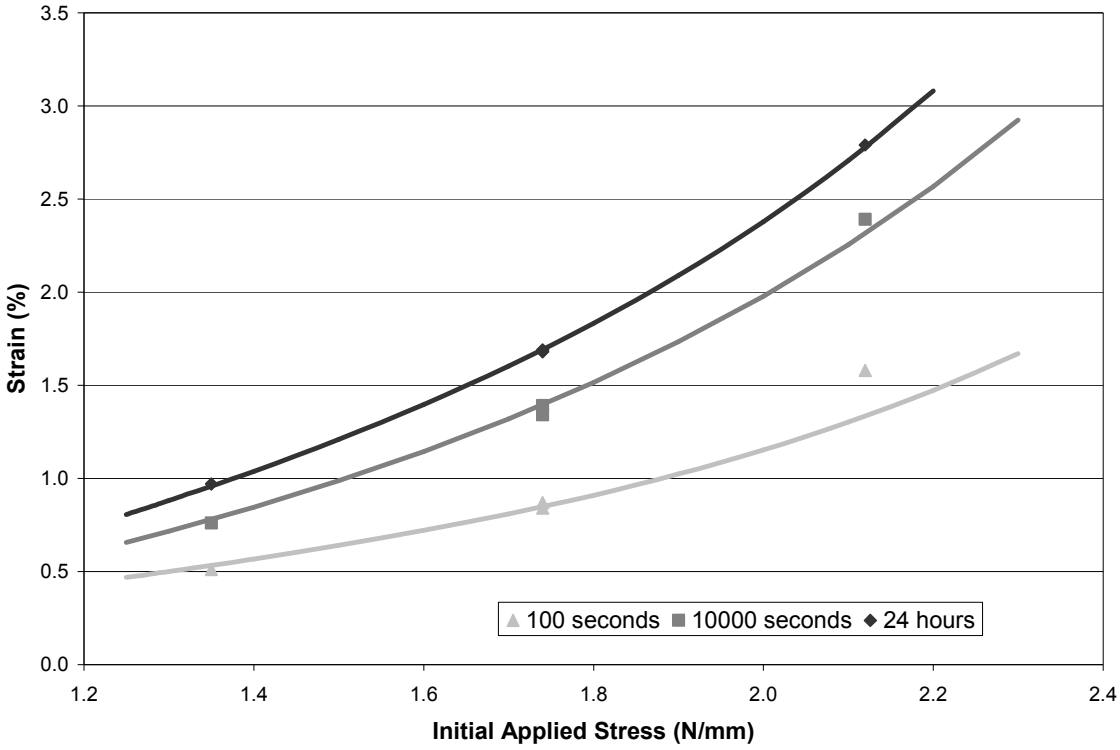

Figure 85 Predicted Isochronous Stress-Strain Curves for 620 ml Freeness, 1.38 MPa Wet Pressed Sheets at 100 seconds, 10000 seconds and 24 hours using the Rheological Model and an Efficiency Factor of 0.88

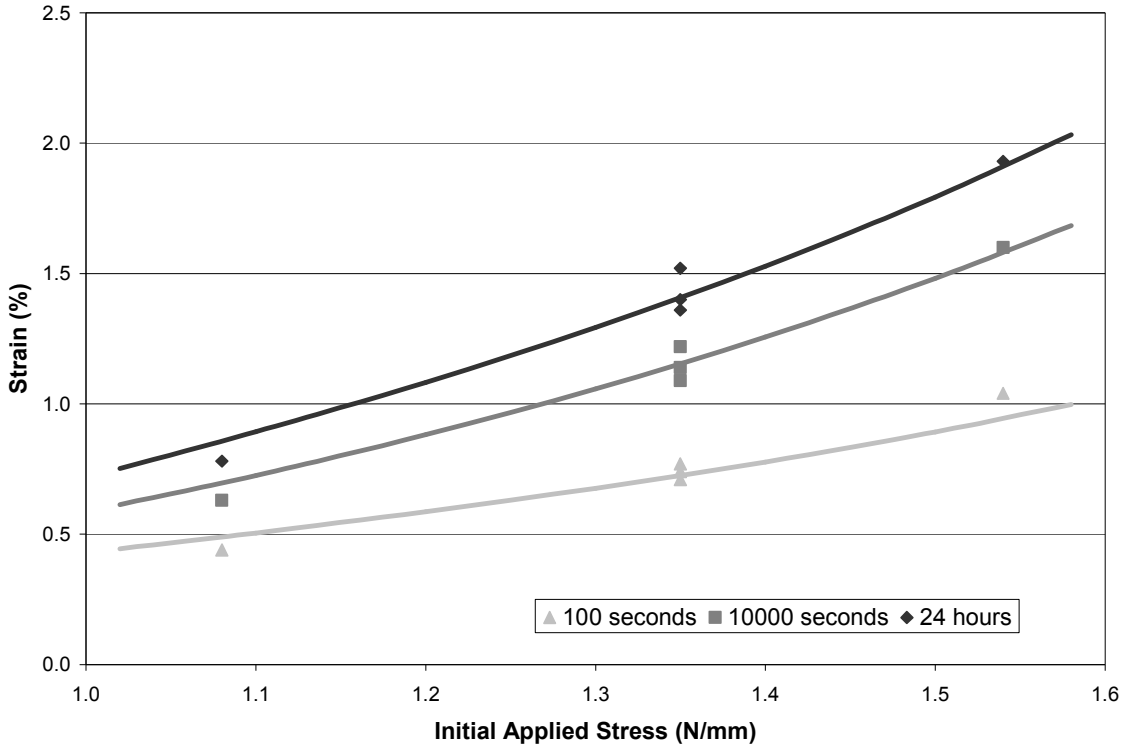

Figure 86 Predicted Isochronous Stress-Strain Curves for 775 ml Freeness, 0.34 MPa Wet Pressed Sheets at 100 seconds, 10000 seconds and 24 hours using the Rheological Model and an Efficiency Factor of 0.74

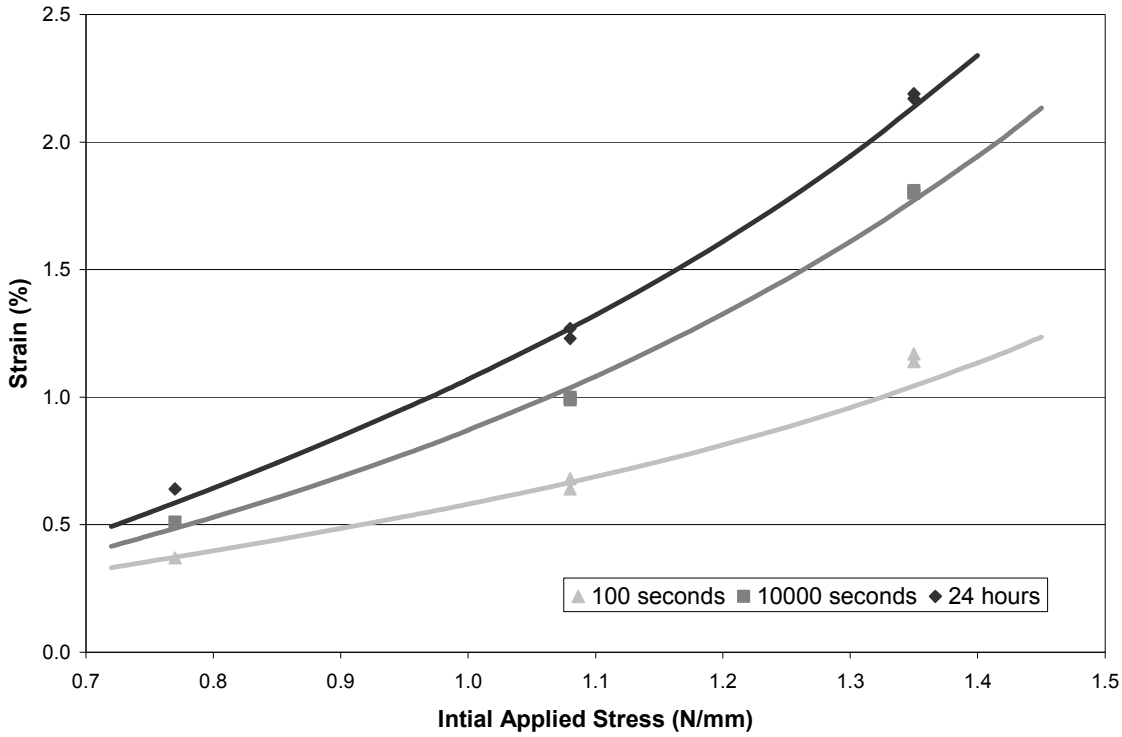

Figure 87 Predicted Isochronous Stress-Strain Curves for 425 ml Freeness, 0.07 MPa Wet Pressed Sheets at 100 seconds, 10000 seconds and 24 hours using the Rheological Model and an Efficiency Factor of 0.62

Figure 84, Figure 85, Figure 86, and Figure 87 show isochronous stress-strain curves at three different times. Overall, the proposed rheological model is accurate and effective in predicting experimental results obtained for this thesis and from the work of Brezinski [36, 37] (who used a different furnish and pulping technique). Furthermore, in both cases, the model allows bonding to be accounted for using an efficiency factor. Although it has seven constants (which are not as easily found as the empirical model constants), it offers the benefit of separating the strain into initial elastic, primary creep and secondary creep components. It also draws upon molecular mechanisms to explain the deformation.

Compared to the empirical model, the rheological model behaves somewhat differently. With the empirical model, strain follows a power law trend as stress is increased. With the rheological model, the behavior is similar to an elastic-strain hardened response. The elastic strain-hardened response is present based in part on the introduction of an activation stress within the model. This causes the isochronous stress-strain curves to behave in a linear elastic manner below a certain initial applied stress. This type of behavior can be seen in paper as Steenberg [34] showed it possible for an elastic-strain hardened response to occur in stress-strain curves almost 60 years ago. Furthermore, the model also allows the elastic limit to change as the time duration associated with the isochronous stress-strain curves is changed. At short times, the elastic limit is higher, and as time is increased, the elastic limit drops until it reaches the activation stress. The work of Johanson and Kubat [107] showed this type behavior with their stress-strain curve data and is also discussed by Skowronski and Szwarcsztajn [108]. In some cases, activation stress is zero because paper is freely dried or annealed. As a result, the elastic limit will go to zero as time is increased.

As with the empirical model, this model shows a tendency to under predict the strain at short times. The effect is amplified as the efficiency factor decreases. Similar to the empirical model, it will not be a good predictor of isochronous stress-strain curves when time is less than ten seconds. This model, like the empirical model does not take into account Brezinski's [36, 37] observation, that creep strain in paper shows a power law dependence with time at low times. Therefore, a modification of the model would be necessary if curves at these short times were desired. This could be accomplished by

making the secondary creep strain component of the model have a power law dependence with time instead of a logarithmic dependence.

6.5 Discussion and Conclusions

Overall, two models are presented within this chapter, one empirical and one rheological. Both of these models are good predictors of isochronous stress-strain curves for uni-axial tensile creep in paper using initial applied stress, time, and efficiency factor as variables. The empirical model is simple and contains only three material constants as well as a reference time constant, but does not offer any descriptive insight behind creep deformation. The rheological model is complex and contains seven material constants and a reference time constant. As a result, the complexity allows the model to not only predict isochronous stress-strain curves, but separates creep into initial elastic, primary creep, and secondary creep components while drawing upon molecular deformation mechanisms. Choice of which model is appropriate would depend mostly on need. The empirical model is beneficial if a rough estimate of creep deformation is desired without need for a descriptive understanding. The rheological model is beneficial if a descriptive understanding of the total strain from creep or a specific contribution towards this strain is desired (for example, permanent strain associated with secondary creep). In addition, this model through comparison of constants would be useful in determining how fiber modifications, formation changes, orientation changes, etc., are affecting specific aspects of creep behavior.

Whether the empirical model of rheological model is used, they both offer two powerful advantages toward predicting creep behavior, specifically isochronous stress-

strain curves. The first of these advantages is that since the constants in the models do not change, creep tests only need to be run for a short time to predict long-time isochronous stress-strain curves. With the empirical model, the constants could be found in as little as 10,000 seconds or just less than three hours. With the rheological model, more time is necessary, on the order of 24 hours. As a result, creep tests of under a day could be used to predict deformation over long periods of time. It is often impossible to conduct long-term creep tests with paper as temperature, humidity control, and intangibles can come into play.

Second, and most importantly, these models are derived drawing upon the characteristics of the fibers with bonding influence being accounted for using an efficiency factor. This is especially true for the rheological model, which draws from the deformation behavior of cellulose, hemicelluloses, lignin (if present), and the molecular network associated with each of these fiber components. Inter-fiber bonds (relative bonded area and specific bond strength) are taken into account through the use of an efficiency factor which represents how effectively bonding is distributing load throughout the fiber network of the paper. As a result, these models make it possible to predict the creep behavior at a range of bonding levels; all that is needed is creep data from paper at one level of bonding. Then, using efficiency factors, the creep behavior of paper at any other level of bonding can be found. This will hold true as long as fibers (either type or amount of defects), formation, and orientation (both fiber and drying orientation) are not changed. The results from this chapter confirm that bonding influence in paper can be accounted for with an easily derived efficiency factor.

CHAPTER 7: DIRECT OBSERVATIONS OF BONDING INFLUENCE ON THE TENSILE CREEP BEHAVIOR OF PAPER

7.1 Abstract

It has been shown, as sheet loading efficiency is improved through increased bonding (by increasing relative bonded area or specific bond strength), a fully efficient loaded structure can be achieved where further improvements in bonding become redundant and have no effect on creep behavior; deformation is dictated only by the characteristics of the fibers. In this study, fully efficient sheets were made at differing levels of specific bond strength by treating the sheets with a debonder or a bonder. Untreated control sheets were also prepared. Microscopic analysis of the bonded areas before and after creep testing was conducted. It was found that, although creep behavior was the same, the amount of bonded area loss was greater in the debonder treated sheets versus the bonder treated sheets. In addition, bonded area loss for all cases was skewed towards small bonded area losses with few bonds showing significant bonded area loss. Furthermore, observed bonded area losses were shown to originate from the edges (or perimeters) of the bonds. The overall conclusion from this study, as with previous studies of stress-strain behavior, is bonded area loss is a strain-induced phenomenon caused by deformation and is not connected with or the inherent cause of creep behavior. Although creep behavior can be shown to be affected by the initial level of bonding in an inefficient loaded structure, previous studies have shown subsequent bonded area loss during straining does not further influence (degrade) behavior.

7.2 Introduction

Creep is a characteristic behavior of a viscoelastic material which is undesirable in most paper applications. When paper is placed under a constant load, it will exhibit a time dependent deformation otherwise known as creep. Fundamental work by Brezinski [36, 37], Schulz [60, 61], Sanborn [62], Parker [59], and Hill [38, 39] laid the groundwork in constant humidity tensile creep behavior. The results presented in Chapter 5 studied the influence of bonding on constant humidity tensile creep behavior. Up until that point, there was a limited base of available research regarding bonding and creep behavior in paper [36, 37, 59, 62, 64]. The results from Chapter 5 showed that either decreasing specific bond strength with a debonder or increasing specific bond strength with a bonder had no effect on creep behavior. As long as there was an adequate level of bonding to maintain an efficiently loaded structure, load was effectively distributed throughout the sheet. The only difference in the overall behavior was that creep failure times were increased as specific bond strength was improved. It was concluded once paper reaches a fully efficient loaded state, redundancies in bonding exist and no longer influence creep deformation. These findings are in agreement with the conclusions of Coffin [13] and concur with what was found and concluded by Seth and Page [40] with short-time deformation behavior (elastic modulus and stress-strain behavior).

With regard to bonded area loss, Sanborn [62] showed that light scattering increased as the strain during creep increased. As a result, he showed that there is bonded area loss during creep deformation. It does not, however, imply that creep deformation is caused by bonded area loss, only that bonded area loss occurs concurrently. In later work, Byrd [64] showed that light scatter decreased during creep, implying an increase in

bonded area. However, in this case the decrease in light scatter may have occurred because bonded area loss was so small, it could not overcome error in measurement or the effect of fibers being drawn into optical contact from lateral contraction due to longitudinal straining. This contradictory data is resolved in the results from Chapter 5 where measurements in the change of light scatter before and after creep deformation are presented. It was found that at a given strain, sheets treated with debonder had a higher change in light scatter versus sheets treated with bonder. Bonded area was not only decreasing with creep, but decreasing at a faster rate when sheets were treated with debonder versus a bonder. While not an extraordinary result by itself, it becomes significant, because creep behavior remained unaffected. The work of Seth and Page [40] reported the same result with stress-strain curves.

Unfortunately, light scatter data do not definitively indicate how bonded area is changing during creep deformation. In order to determine this, direct observation of bonded area changes must be conducted to validate the findings of light scatter data with optical evidence. This would also offer insight into the bond failure mechanism as it relates to tensile creep behavior. No such study has been conducted prior to this with regard to creep behavior in paper. However, Page et al. [67] examined stress-strain behavior and found that a vast majority of the bonds they analyzed showed little or no loss in bonded area and few exhibited full failure. Furthermore, they observed that bonded area loss, when it did occur, propagated from the perimeter (or edge) of the bond. In more recent publications, Page [66, 68] determined that the reason this occurred was because bonds are under the highest level of shear stress on their perimeters. He concluded that bonded area loss is a strain-induced phenomenon and there is no

connection between bond breakage and stress-strain behavior. Since creep behavior is a highly time-dependant viscoelastic phenomenon, it is uncertain whether the conclusions of Page can be directly applied toward creep behavior. This chapter presents a method whereby bonded area behavior as a result of creep can be directly observed. It also presents results obtained using that method.

7.3 Experimental

7.3.1 Pulp and Preparation

NIST standard reference material 8495 Northern Softwood Bleached Kraft Pulp was used in this study. The pulp arrived in dry lap sheets in a hermitically sealed package. The pulp had remained sealed for approximately 15 years. The pulp was refined in a valley beater at a charge of 300 O.D. grams per batch for 30 minutes. The final pulp Canadian Standard Freeness was targeted at 400 ml. The pulp was prepared in such a manner to create straight, conformable fibers that would easily bond. Chlorazol Black, from Sigma-Aldrich, was added to the pulp slurry at a 0.20% by weight dosage and allowed to soak for 24 hours. Once soaking was complete, the pulp slurry was washed exhaustively with deionized water until wash water was free of color. Prior to making handsheets, the pulp slurry was treated with either a debonder or a bonder or received no treatment. The debonder used was a cationic surfactant (Incrosoft AS-55), from Croda, while the bonder used was locust bean gum, from Sigma-Aldrich. Bonder and debonder were added to the pulp slurry and mixed for 1 minute at dosages of 0.45% and 0.11% by weight, respectively.

7.3.2 Handsheets

Handsheets were made using a 210 mm x 210 mm Williams handsheet mold. A 100 mesh screen was used as the forming wire. The handsheets made from the treated pulp slurries were targeted to have an oven dry basis weight of 90 g/m^2. Sheets were wet pressed at 1.03 MPa and dried under full restraint on a drum dryer at 0.14 MPa steam pressure for 5 minutes. Sheets were pressed for five minutes, followed by a blotter change and pressed again at the same level for two minutes. Gloss plates were not used. All sheets were immediately bagged and placed in a 23°C and 50% RH room for conditioning prior to testing. The process used insured that the sheets were produced with similar calipers and densities and most importantly similar relative bonded areas. Wet pressing acts to consolidate the sheet, thereby altering the caliper, density, and relative bonded area of the sheet. The addition of bonder and debonder does not alter the relative bonded area, but instead increases or decreases the specific bond strength. Given equal relative bonded area and different specific bond strengths, the overall amount of bonding is altered. Therefore, within this group of sheets, there were sheets with enhanced, degraded and unchanged levels of specific bond strength.

7.3.3 Physical and Creep Testing

Extensive physical testing was conducted including handsheet grammage, hard caliper, ultrasonic velocities, formation, zero-span tensile strength, z-directional tensile strength, and in-plane tensile strength. In-plane tensile measurements were made using an Instron tester with jaw spacing of 140 mm to be consistent with creep testing spans. Stress-strain curves were recorded for each of the in-plane tensile tests. Although no

direct measurement of specific bond strength is made in this study, differences in z-directional tensile strength will indicate a change in specific bond strength when relative bonded area remains constant. Within each set of handsheets, density was held constant and thereby relative bonded area was also held constant by careful control of refining, pressing and drying. Creep testing was conducted using the IPST tensile creep tester under a constant 23 °C and 50% RH condition. Samples were cut into 170mm x 25 mm wide strips, mounted and conditioned for 24 hours at 23 °C and 50% RH prior to application of load. The free length of the samples after mounting was 140 mm. Two different magnitude dead loads (initial applied stress levels) were evaluated. These load levels were 2.50 N/mm and 4.09 N/mm respectively. Displacements and failure times were recorded using linear variable displacement transducers (LVDT sensors) with the output signals sent to a computer based data acquisition system.

7.3.4 Microscopy

Images of bonded areas were captured using a method similar to one developed by Page et al. [52]. Prior to creep testing, each strip was examined with a Leica DM-IRM inverted, reflected light microscope equipped with a Hamamatsu ORCA-ER digital camera and a 50 watt metal halide lamp. Pre-creep images were collected by illuminating each strip with polarized monochromatic light (λ=547±10 nm) to increase contrast between dyed and un-dyed fibers. After creep testing, the same techniques were utilized to capture images of the same areas. The orientation of the fibers and the shape of the bonds were used to verify the images were of the same area. Figure 88 shows a representative image of fiber crossings and bonded areas at 600X magnification.

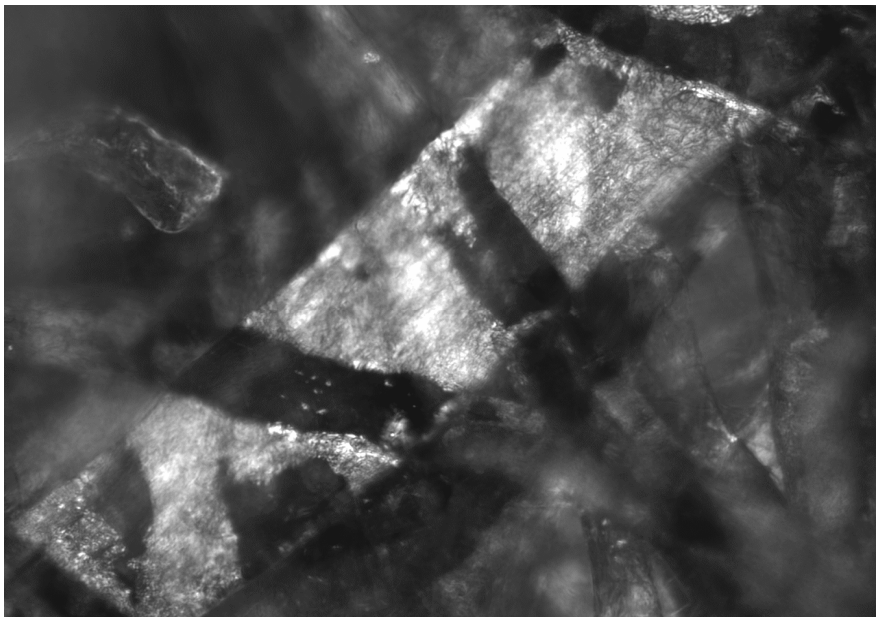

Figure 88 Representative Image of an Un-Dyed Pulp Fiber Bonded to Several Chlorazol Black Dyed Fibers (600X)

Changes in fiber orientation and bond area were measured using Simple PCI, an image analysis software package. Orientation was determined by drawing a line down the central axis of each fiber forming the intersection and measuring the angle relative to the direction of the applied stress. Simple PCI can be calibrated to measure image areas. Bond areas were traced on each pre-creep and post-creep image and a percent bond area change was calculated.

7.4 Results

7.4.1 Physical and Creep Testing Results

The results presented are for debonder, control, and bonder sheets that were wet pressed at high load (1.03 MPa) resulting in high density, highly bonded sheets. The intent of the high press load is to make sheets that are fully efficient loaded structures,

where the initial level of bonding does not influence deformation behavior and bonded area loss can be isolated for analysis. Table 12 shows the physical testing results from these sheets.

Table 12 Physical Testing Results of Debonder, Control, and Bonder Treated Sheets

Sheet Treatment	Grammage (g/m^2)	Hard Caliper (mm)	Density (g/cm^3)	Ultrasonic Modulus (km^2/s^2)
Debonder	97.6	0.144	0.678	10.7
Control	96.6	0.141	0.685	10.9
Bonder	96.5	0.139	0.694	11.0
Variation	**1.1%**	**3.6%**	**2.4%**	**2.8%**

Sheet Treatment	Z-Tensile (N/mm^2)	Tensile (N/mm)	Failure Strain (%)	Zero-Span (N/mm)
Debonder	0.473	7.97	2.93	16.0
Control	0.584	8.80	3.26	16.3
Bonder	0.852	10.3	4.22	16.7
Variation	**80.1%**	**29.2%**	**44.0%**	**4.4%**

The data from physical testing presented in Table 12 shows that sheets treated with debonder and bonder did not show significant differences from the control with regard to grammage, hard caliper, formation, and zero-span tensile strength. Deformation behavior, as indicated by the ultrasonic elastic modulus data in Table 12 and stress-strain curves shown in Figure 89 were similar for all three sets. The differences in the sheets were in z-directional tensile strength, tensile strength, and strain to failure, caused predominantly by differences in specific bond strength. A small influence due to variation in relative bonded area (indicated by slight apparent density differences) cannot

be ruled out. Figure 89 shows that sheets treated with debonder were the weakest, while the sheets treated with bonder were the strongest.

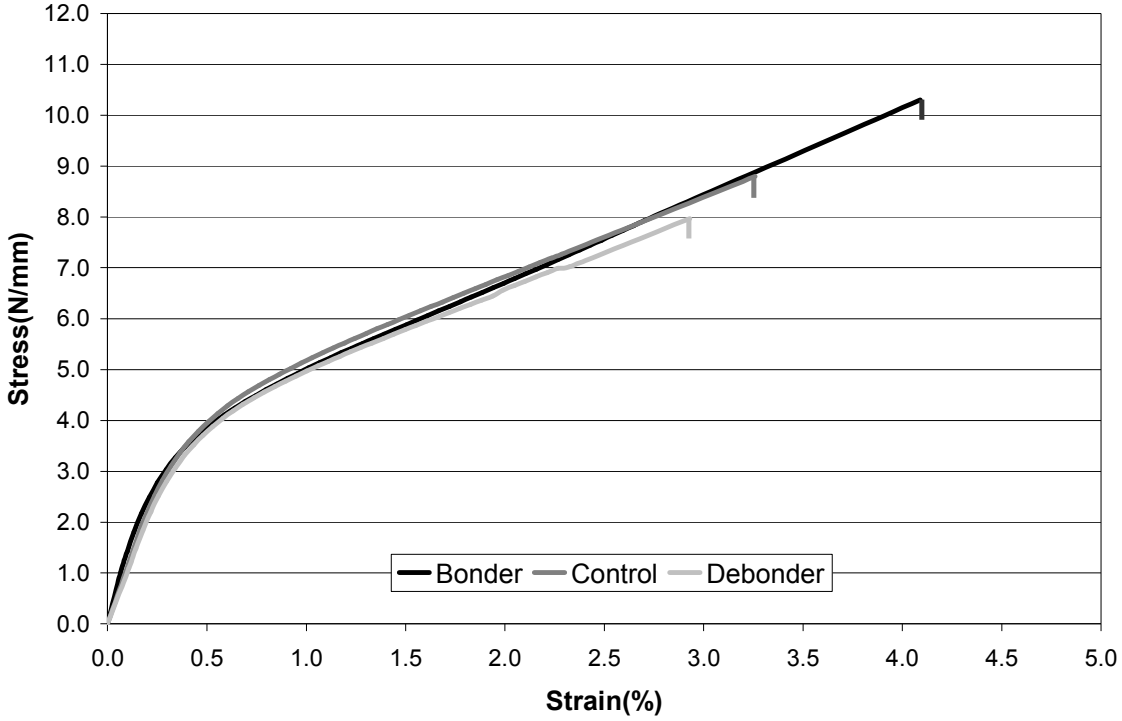

Figure 89 Stress-Strain Curves from Instron Tensile Testing for Debonder, Control, and Bonder Treated Sheets

These results are consistent with the past work of Seth and Page [40], and the results from Chapter 5. The data in Table 12 and Figure 89 confirm that high levels of bonding create a fully efficient loaded paper structure where elastic modulus has reached a plateau. Differences in specific bond strength do not affect deformation behavior, but do influence failure behavior. Overall, the physical testing results confirm that all sheet sets are fully efficient loaded structures.

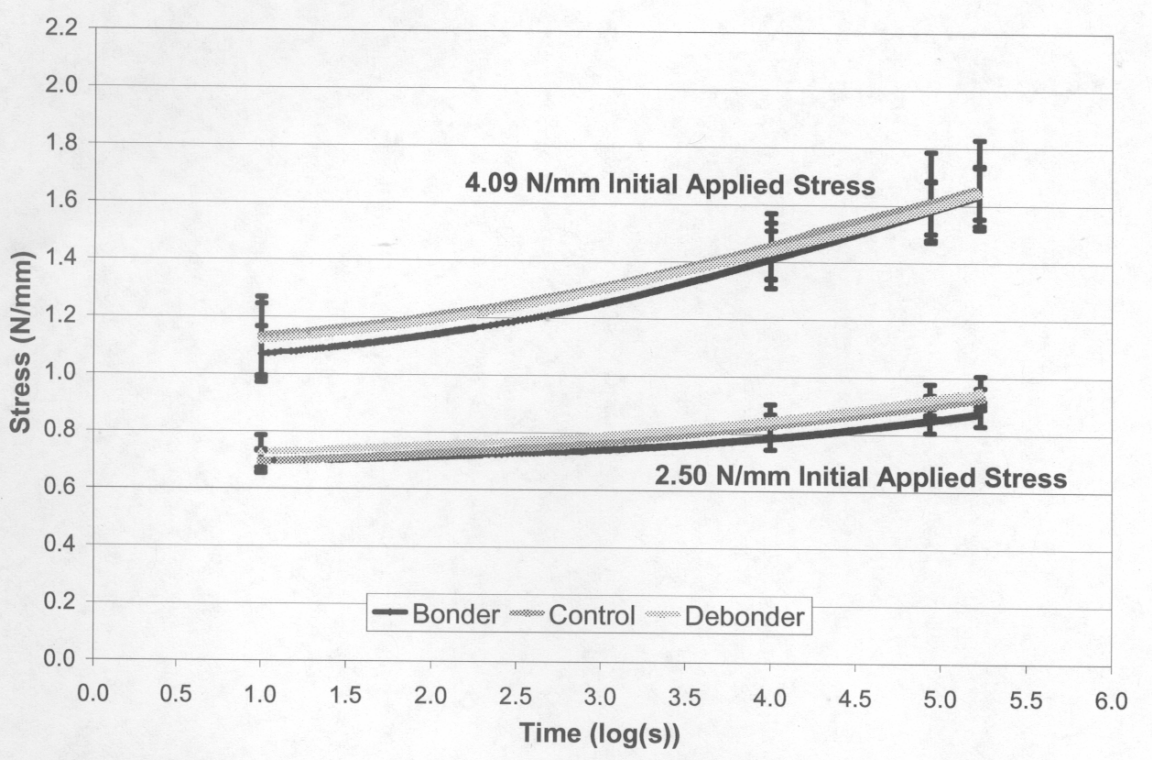

Figure 90 Creep Curves at High and Low Load Initial Applied Stress Levels for Debonder, Control, and Bonder Treated Sheets

The creep behavior results shown in Figure 90 follow the same trend as the physical testing data in Table 12 and Figure 89. The results show that the creep curves generated at both initial applied stress levels show good overlap and fall within the standard error bars, indicating they have creep behaviors that cannot be differentiated from each other. Again, this was expected as the results of Chapter 5 show similar results with fully efficient loaded sheets.

7.4.2 Microscopy Results

Before and after creep testing of the sheets at both initial applied stress levels, images of bonded areas were taken and analyzed for the debonder treated, control, and

bonder treated sheets. Table 13 shows the results from the image analysis of the 2.50 N/mm initial applied stress (low creep) and 4.09 N/mm initial applied stress (high creep) testing levels.

Table 13 Bonded Area Results from Microscopy Image Analysis for Debonder, Control, and Bonder Treated Sheets

Sheet Treatment	Bonds Analyzed	Average Initial Bonded Area (μm^2)	Low Creep Average Bonded Area Decrease	High Creep Average Bonded Area Decrease
Debonder	94	933	8.8 %	14.5 %
Control	62	880	4.5 %	8.7 %
Bonder	89	998	1.5 %	5.1 %
Variation		**13.4%**	**> 100%**	**>100%**

The sheets treated with debonder and bonder did not show significant differences from the control with regard to the average initial bonded areas. Furthermore, these average bonded areas are consistent with the work of Page et al. [67] who found an average bonded area of 932 μm^2 for a similar pulp type and refining level. More importantly, the data show that at the low and high creep testing levels, the average bonded area decreased by different amounts. The debonder treated sheets had the highest loss in bonded area and the bonder treated sheets had the lowest. The amount of bonded area loss was also relatively small. Even the debonder treated sheets at the high creep testing level showed less than a 15% average bonded area loss.

Based on these results and the fact that the creep behaviors of the debonder, control and bonder treated sheets are all the same, it is apparent that the deformation behavior is not influenced by the rate of bonded area loss. Figure 91 shows the average

bonded area loss versus strain for the debonder, control and bonder treated sheets. The data points do not overlap or fall within standard error bars. Lines were fit through the data points as a means to better illustrate differences in rate of bonded area loss. These lines were fit through the axis origin (0,0), as no bonded area loss will occur when strain is equal to zero.

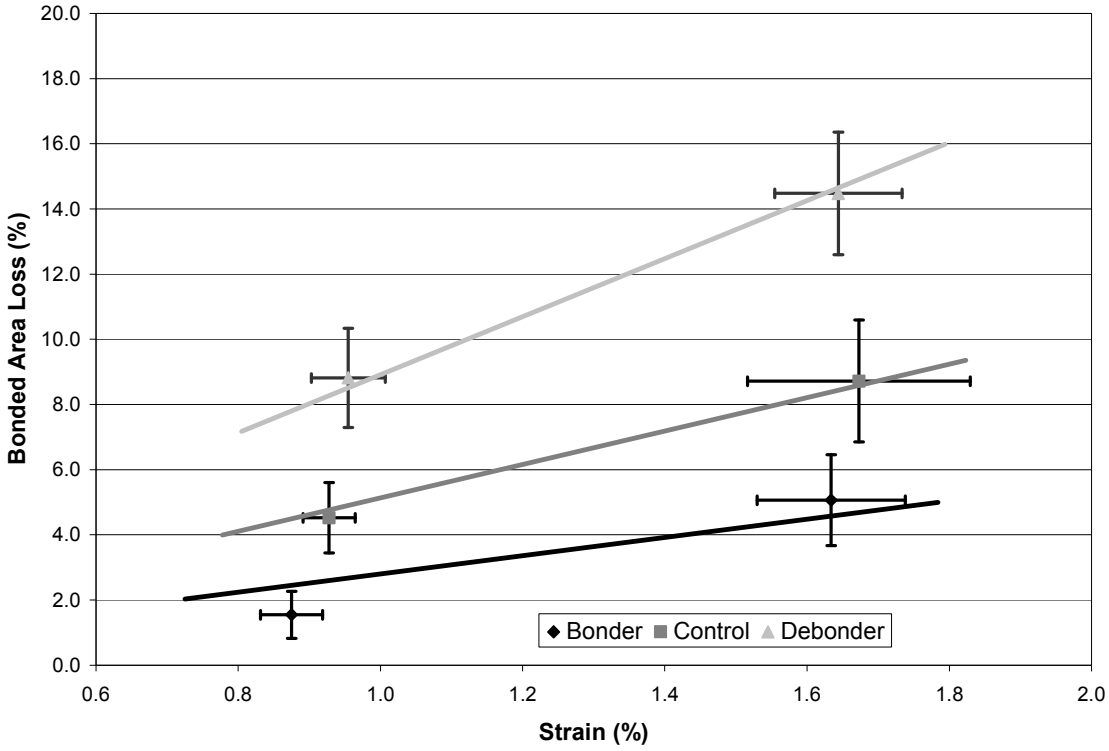

Figure 91 Average Bonded Area Loss versus Strain from Creep Testing for Debonder, Control, and Bonder Treated Sheets

Other than the observation of bonded area loss at different rates, several other observations were made from the microscopy analysis. First, the orientation of the fibers which were bonded did not show a measurable change as a result of creep testing. This indicates that the fibers did not move significantly in the direction of the applied stress.

Secondly, the overall level of bonded area loss was small and bond failure originated from the perimeters (or edges) of the bonded area. This is consistent with what Page et al. [67] observed. Figure 92, Figure 93, and Figure 94 show representative examples of what was observed at differing levels of bonded area loss. Dashed lines of the before creep bonded areas are superimposed onto the after creep images to better illustrate bonded area loss.

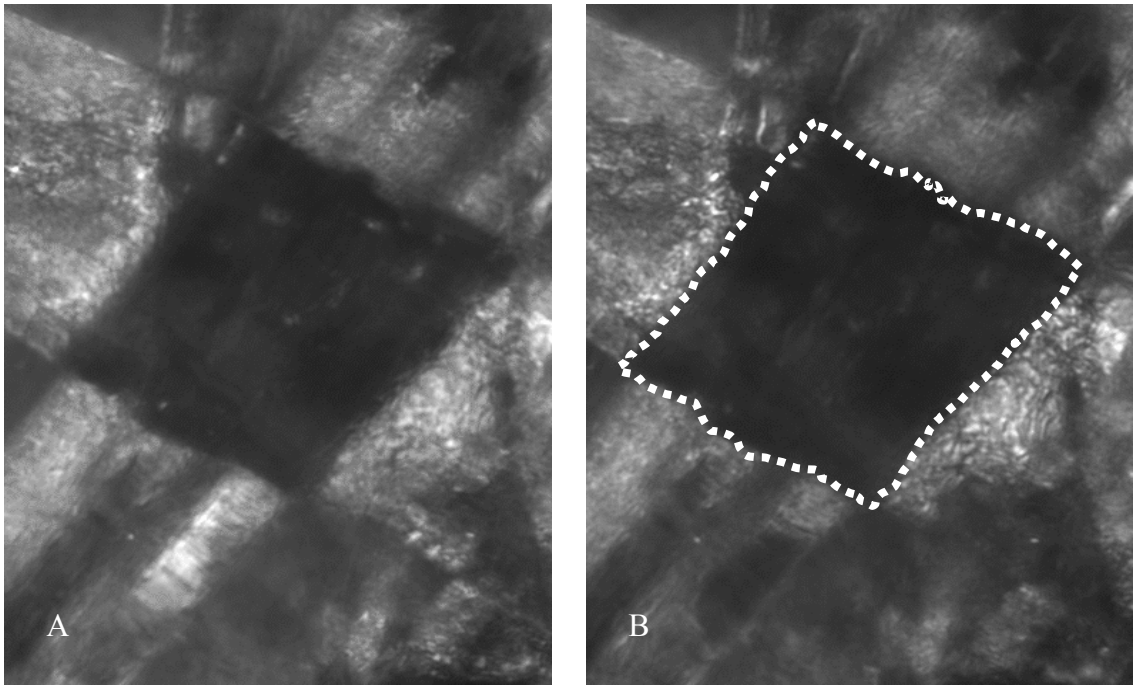

Figure 92 Before Creep (A) and After Creep (B) Images of a Bond Showing Approximately No Loss in Bonded Area (600X)

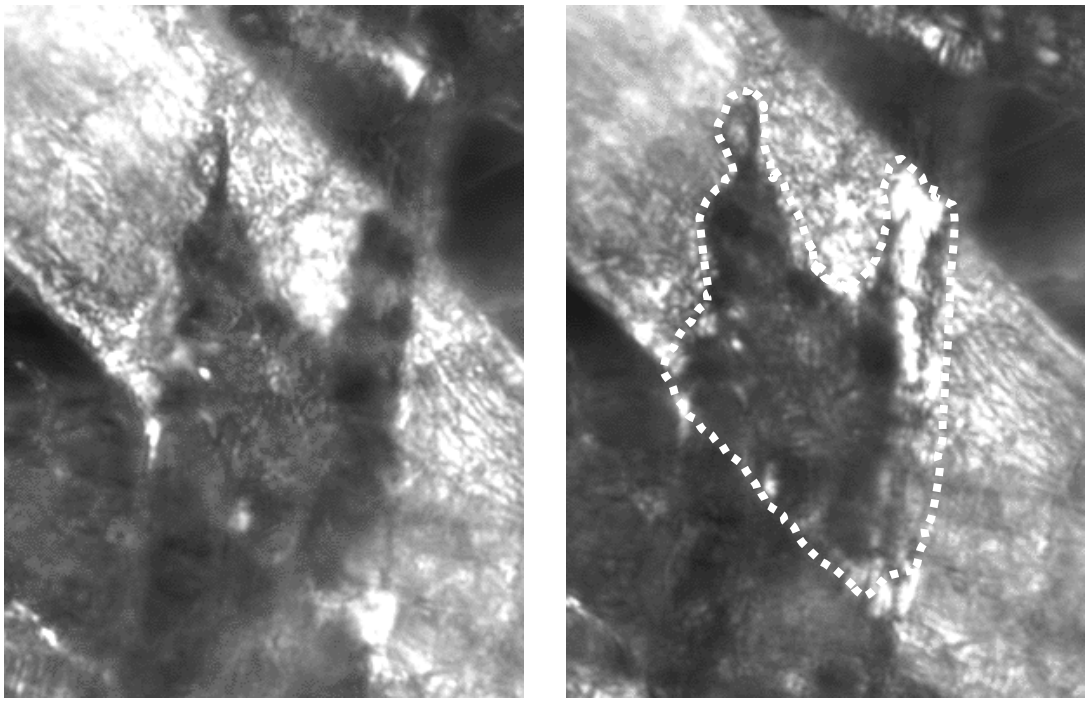

Figure 93 Before Creep (A) and After Creep (B) Images of a Bond Showing an Approximate 20% Loss in Bonded Area (600X)

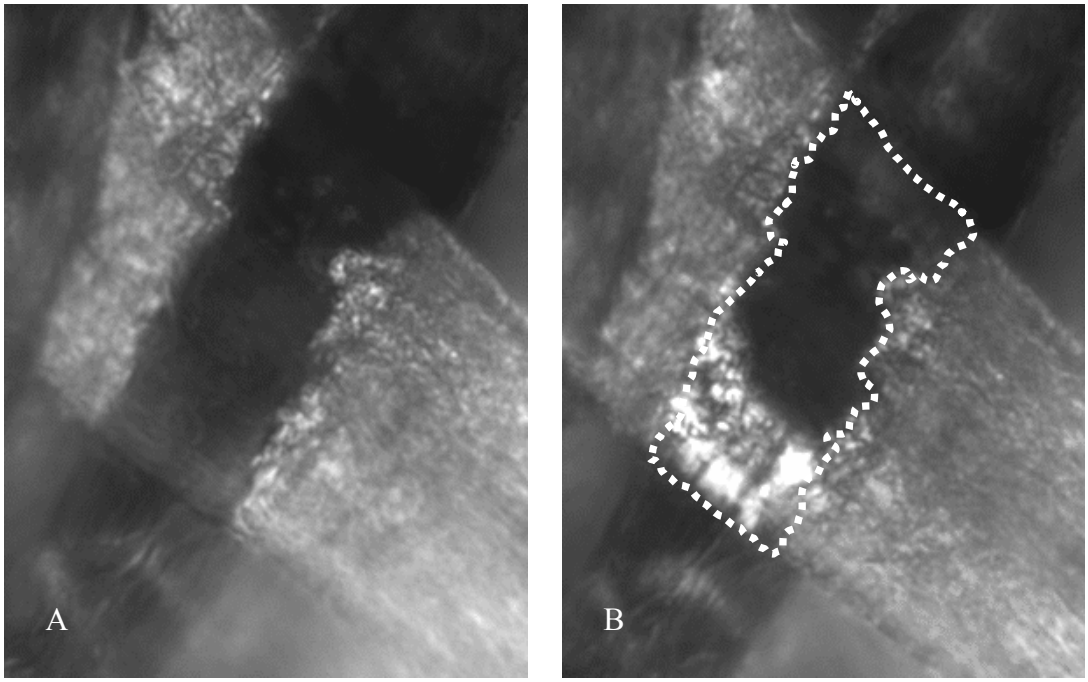

Figure 94 Before Creep (A) and After Creep (B) Images of a Bond Showing an Approximate 30% Loss in Bonded Area (600X)

Figure 92 shows approximately no loss in bonded area during creep. Figure 93 and Figure 94 show bonded area losses of approximately 20% and 30% respectively. In addition, the bonded area losses are seen from the edges of the bonds. This is typical of what was observed in this study. Overall, the amount of bonded area losses were predominantly observed between the extremes of what was illustrated in Figure 92 and Figure 93. Bonded area losses greater than 20% were far less common. Figure 8 shows a histogram of measured bonded area loss for sheets tested at high creeps loads.

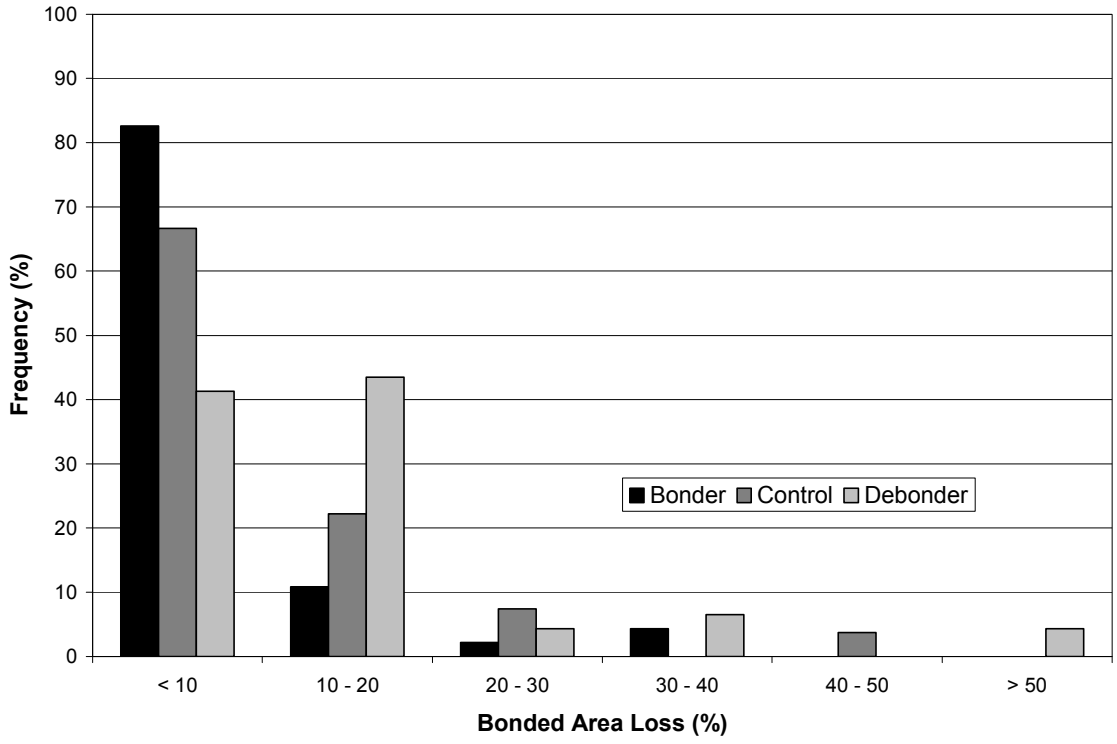

Figure 95 Histogram of Bonded Area Loss in High Creep Load Testing for Debonder, Control, and Bonder Treated Sheets

As Figure 95 shows, the amount of bonded area loss is not significant, even at the high creep load used in these tests. The data shows a histogram with a skewed

distribution towards many small bonded area losses. The skewness increases with specific bond strength; the sheets with bonder had the least amount of large bonded area loss and the debonder sheets had the greatest. Still, even the debonder treated sheets show greater than 80% of measured bonds have less than 20% bonded area loss. Figure 96 shows the results for low creep load testing where an even more skewed distribution towards less bonded area loss is present.

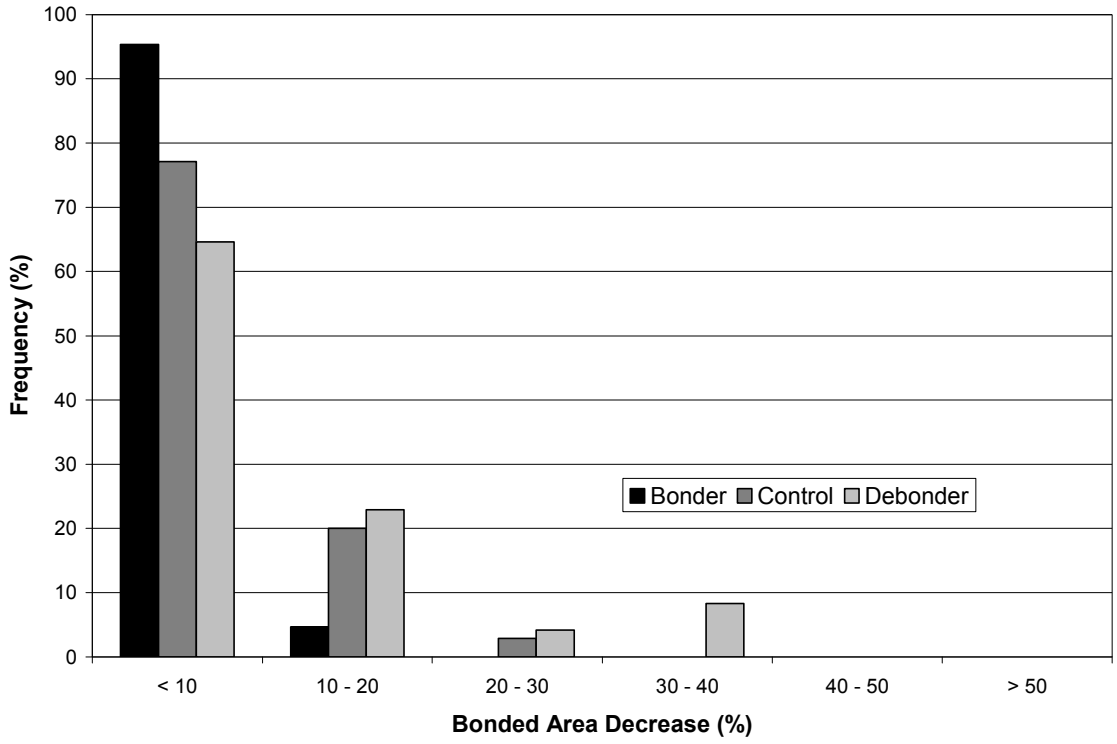

Figure 96 Histogram of Bonded Area Loss in Low Creep Load Testing for Debonder, Control, and Bonder Treated Sheets

As shown in Figure 96, greater than 95% of the bonded area loss for the bonder treated sheets is less than 10%. The debonder treated sheets shows greater than 65% of the bonded area loss being less than 10%. Overall, the type of bonded area loss

distributions seen in Figure 95 and Figure 96 are the same as the behavior Page et al. [67] observed with stress-strain behavior.

7.5 Discussion

Based on the results from this study, the data confirm that the initial level of bonding (both in relative bonded area and specific bond strength) and subsequent bonded area loss do not influence the creep behavior of paper when it is a fully efficient loaded structure. Although, the specific bond strengths of the debonder, control, and bonder treated sheets were different and the rate at which bonded area loss occurred was different (based on microscopy), the deformation behavior was not influenced. This confirms what was reported in Chapter 5 and correlates with what was seen with light scatter data.

The results strengthen the case that bonding is not the main controlling factor that determines creep behavior in paper. Rather, that distinction belongs to the fibers. In some cases, when paper is less than fully efficient, bonding will influence creep behavior due to lack of an effective stress distribution through the sheet. That said, the results from Chapter 5 on inefficiently loaded sheets found that even though the deformation was influenced by the initial level of bonding within the sheet, the subsequent loss in bonded area during creep testing did not further degrade behavior. Seth and Page [40] found this to be true in stress-strain behavior as well, and found that only when bonding is significantly low will loss in bonded area be significant enough to further influence deformation during straining. This led Page [66, 68] to the overall conclusion that bonded area loss does not necessarily influence deformation, but rather bonded area loss is a

strain-induced phenomenon (i.e., not a cause, but rather an effect of deformation). The results from this chapter and Chapter 5 confirm this result for creep behavior.

The level and type of bonded area loss in the sheets further substantiate this strain-induced conclusion. In this study the level of bonded area loss was small, even at the highest creep load with the debonder treated sheets. Furthermore, this loss originated from the edges of the bonded areas where, as Page [66] pointed out, the shear stresses are the highest. This is where the bonds would be affected first when fibers are strained. As a result, the level and type of bonded area loss does not lend itself towards a reduction in the overall ability of the bonds being able to distribute load effectively throughout the sheet.

7.6 Conclusions

A novel application of a known method was utilized to directly examine bonded area change as a result of creep. Prior to this study, it was known that creep behavior in a fully efficient loaded structure is not influenced by the initial level of bonding and subsequent loss of bonded area. It is now known why, as the average level of bonded area loss is small and skewed towards many bonds failing partially and very few failing significantly. As a result, the stress distribution in paper during creep should not be significantly disrupted and creep behavior will remain unaffected. Based on Page [66, 68] bonded area loss is a strain-induced phenomenon that is a caused by deformation and there is no connection between bonded area loss and stress-strain behavior. In this study, the same conclusion is made with regard to creep behavior. The deformation behavior in paper during creep is dictated solely by the fibers. Although, creep behavior can be

shown to be affected by the level of bonding in an inefficient loaded structure, the results in Chapter 5 show subsequent bonded area loss during straining does not further influence (degrade) behavior. This will hold true until an extreme case is achieved, where the initial level of bonding is so small any loss in bonded area would significantly disrupt the stress distribution within the sheet.

CHAPTER 8: INFLUENCE OF BONDING ON THE TENSILE CREEP BEHAVIOR OF PAPER IN A CYCLIC HUMIDITY ENVIRONMENT

8.1 Abstract

It has been shown, as paper structure is improved through increased bonding (by increasing relative bonded area or specific bond strength), a fully efficient loaded structure can be achieved. Once fully efficient, further improvements in bonding become redundant and have no effect on some paper deformation behaviors; deformation is dictated only by the characteristics of the fibers. Previous work has shown this to be true for elastic modulus and short time duration stress-strain behavior. In addition, Chapter 5 showed this to be true for constant humidity tensile creep behavior. In this study, the goal was to ascertain if cyclic humidity tensile creep behavior (known as accelerated creep) would follow the same trend. To accomplish this, sheets were made at differing levels of relative bonded area and specific bond strength. This was done by applying two different wet pressing levels (to alter relative bonded area) and using bonder and debonder (to change specific bond strength). It was found that accelerated creep behavior of paper sheets is no different than constant humidity creep behavior; changing bonding does not influence accelerated creep if the sheet has a fully efficient loaded structure. If the sheet structure is inefficiently loaded (there is no redundancy in bonding), accelerated creep will be affected by bonding. However, it is proposed that the only reason accelerated creep is influenced by bonding when inefficiently loaded is because constant humidity creep behavior determines the accelerated behavior and it is influenced, in this case, by bonding.

8.2 Introduction

When paper is exposed to a cyclic humidity environment, it will exhibit more creep strain than if the same paper were exposed to a constant humidity environment at the highest humidity experienced in the cyclic humidity environment. This behavior was first observed in paper by Byrd [64, 74, 75] over 30 years ago and by Armstrong [76, 77] in wood prior to that. Wang [79, 80] showed this behavior is not a phenomenon limited to paper or wood and can occur in synthetic materials such as Kevlar fibers and composites. Overall, understanding accelerated creep behavior is of interest in many types of materials and has drawn particular attention in paper. It has been extensively researched and modeled to ascertain and explain the mechanism behind the phenomenon.

As a result, many different view points on the underlying mechanisms behind accelerated creep have been proposed. For materials in general, Wang [79] reviewed several accelerated creep mechanisms which include hydrogen bonding and slip planes. He comments that while hydrogen bonding disruption during moisture cycling can lead to an increase in strain, it does not explain the role of material structure in the mechanism. Slip planes, which occur in compression and bending experiments, do not explain why accelerated creep occurs in tension experiments or at low stresses. Wang [79] also mentioned other mechanisms such as transient or redistributed stresses, increase in free volume causing an increase in molecular mobility, differential swelling, and crystallite rotation.

With respect to paper, Haslach [88-90] proposed a mechanism related to anisotropic swelling, the unwrinkling of bonded areas and bond breakage. Specifically, he discusses that partial or complete bond breakage occurs during moisture cycling which

leads to the increased creep associated with accelerated creep. More recently, in a review of accelerated creep, Coffin [13] discussed the possible mechanisms in paper, including increase in free volume, formation of dislocations, bond breakage, and moisture sorption. The review proposed moisture sorption as the mechanism behind accelerated creep. In this mechanism, increased creep associated with accelerated creep occurs because uneven stress distributions are created due to both the formation of moisture gradients and the inherent material heterogeneity of paper. The work of Alfthan [84-87] focused on material heterogeneity and proposes a mechanism by which anisotropic swelling of the bonded fiber segments lead to accelerated creep. Unlike the mechanism of Haslach [88-90], Alfthan [84-87] proposed that there is no bond breakage and that the mechanism behind accelerated creep is related to that proposed by Coffin [13]. Clearly, there still is debate regarding the role of bonding in accelerated creep. Surprisingly, there have been limited experimental studies conducted to ascertain the role of bonding in accelerated creep.

By comparison, the role of bonding with regard to elastic modulus, stress-strain behavior, and tensile strength has been extensively researched. Page [41] showed through development of an empirical model, "The Page Equation", that tensile strength in paper can be altered by changing relative bonded area and specific bond strength. In addition, Seth and Page [40] were able to show that when decreasing specific bond strength (with a debonder) or increasing specific bond strength (with a bonder), elastic modulus and the shape of the stress-strain curve remained constant as long as there was an adequate level of bonding to maintain a fully efficient loaded structure; this is a structure where changing bonding no longer influences the deformation of paper. The only differences in

the overall behavior produced by such changes were different strains to failure and tensile strengths. Seth and Page [40] also measured changes in light scatter and found a loss of relative bonded area after sheet straining. They showed that relative bonded area decreased at differing rates depending on the treatment applied. The debonder treated sheets have the highest rate of loss followed first by the sheets with no treatment and finally by the bonder treated sheets.

In addition, Seth and Page [40] introduced the concept of the efficiency factor. Their premise is that deformation behavior within paper originates within the fibers and an efficiency factor can be used to show the influence of bonding regardless of whether the deformation behavior is elastic or plastic. Specifically, they showed that if stress-strain curves for paper made from the same fibers did not overlap, they could be made to overlap by dividing the stress component of the stress-strain curve by an efficiency factor. The efficiency factor was calculated by dividing the elastic modulus of the more compliant stress-strain curves (inefficiently loaded structures) by the elastic modulus of the least compliant, efficiently loaded, stress-strain curve. Elastic modulus was determined by finding the slope of the stress-strain curve in the elastic region. Seth and Page [40] were able to show that the whole stress-strain curve, both elastic and plastic portions would superimpose. Simply put, deformation behavior in the plastic region followed an elastically derived efficiency factor and this held true as long as bond breakage was not severe enough to reduce the efficiency factor during straining.

Turning back to creep behavior, the results from Chapter 5 showed the influence of bonding on constant humidity tensile creep behavior. These results showed that either decreasing specific bond strength (with a debonder) or increasing specific bond strength

(with a bonder) had no effect on creep behavior as long as there was an adequate level of bonding to maintain an efficiently loaded structure. The only difference in the overall behavior was that creep failure times were increased as specific bond strength was improved. It was concluded once paper reaches a fully efficient loaded state, changes in bonding will no longer influence creep deformation. Once the point is passed where the paper structure becomes fully efficient, only creep failure time can be increased by increasing the level of bonding. These results, along with the findings of Seth and Page [40] substantiate the premise that a fully efficient structure can be created and it is not influenced by the degree of bonding with regards to deformation behavior. Only failure behavior changes with bonding for a fully efficient structure.

Chapter 5 showed it was possible to apply the efficiency factor approach of Seth and Page [40] to constant humidity tensile creep results. Efficiency factors were calculated based on the ultrasonic elastic moduli of sheets prior to tensile creep testing. The efficiency factors were applied in the same manner as was done by Seth and Page [40] and resulted in the isochronous tensile creep curves being superimposed upon one another. It was concluded the efficiency factors relate how well the existing bonding allows the structure to effectively distribute load throughout the sheet. Bonding can only influence deformation when a less then a fully efficient condition exists. Coffin [13] also came to the same conclusions with regard to constant humidity tensile creep and concluded that there is no reason to suspect that accelerated creep should be any different; if paper is fully efficient, changes in bonding should not affect accelerated creep.

8.3 Experimental

8.3.1 Pulp and Preparation

NIST standard reference material 8495 Northern Softwood Bleached Kraft Pulp was used in this study. The pulp arrived in dry lap sheets in a hermitically sealed package. The pulp had remained sealed for approximately 15 years. The pulp was refined in a valley beater at a charge of 300 O.D. grams per batch for 30 minutes. The final pulp Canadian Standard Freeness was targeted at 400 ml. The pulp was prepared in such a manner to create straight, conformable fibers that would easily bond. Prior to making handsheets, the pulp slurry was treated with either a debonder or a bonder or received no treatment. The debonder used was a cationic surfactant (Incrosoft AS-55), from Croda, while the bonder used was locust bean gum, from Sigma-Aldrich. Bonder and debonder were added to the pulp slurry and mixed for 1 minute at dosages of 0.45% and 0.11% by weight, respectively.

8.3.2 Handsheets

Handsheets were made using a 210 mm x 210 mm Williams handsheet mold. A 100 mesh screen was used as the forming wire. The handsheets made from the treated pulp slurries were targeted to have an oven dry basis weight of 90 g/m^2. Sheets were wet pressed at either 1.03 MPa or 0.17 MPa, depending on sample set. Sheets were pressed for five minutes, followed by a blotter change, and pressed again at the same level for two minutes. Gloss plates were not used. Handsheets were dried on a drum dryer under full restraint at 0.14 MPa steam pressure for 5 minutes. All sheets were immediately bagged and placed in a 23°C and 50% RH room for conditioning prior to testing. The

process used insured that for each press load (1.03 MPa and 0.17 MPa), sheets were produced with similar calipers and densities and most importantly similar relative bonded areas. Wet pressing acts to consolidate the sheet, thereby altering the caliper, density, and relative bonded area of the sheet. The sheets pressed at low loads had a lower relative bonded area than those pressed at high load. The addition of bonder and debonder does not alter the relative bonded area, but instead increases or decreases the specific bond strength. Given equal relative bonded area and different specific bond strengths, the overall amount of bonding is altered. Therefore, with each group of sheets, low and high load pressed, there were sheets with enhanced, degraded, and unchanged levels of specific bond strength.

8.3.3 Physical and Creep Testing

Extensive physical testing was conducted, including handsheet grammage, hard caliper, ultrasonic velocities, formation, light scatter, zero-span tensile strength, z-directional tensile strength, and in-plane tensile strength. In-plane tensile measurements were made using an Instron tester with jaw spacing of 140 mm to be consistent with creep testing spans. Stress-strain curves were recorded for each of the in-plane tensile tests. Although no direct measurement of specific bond strength is made in this study, differences in z-directional tensile strength will indicate a change in specific bond strength when relative bonded area remains constant. Within each set of handsheets, density was held constant and thereby relative bonded area, by careful control of refining, pressing, and drying.

Creep testing was conducted using the IPST tensile creep tester under constant and cyclic relative humidity conditions. In all cases a 6.94 kg tensile dead load (2.68 N/mm initial applied stress) was used. Displacements were recorded using linear variable displacement transducers (LVDT sensors) with the output signals sent to a computer based data acquisition system. Constant humidity creep testing was conducted at 23 °C and 25% RH as well as 23 °C and 75% RH. Samples were cut into 170 mm x 25 mm wide strips, mounted and conditioned for 24 hours at 23 °C and the desired constant humidity level (either 25% RH or 75% RH) prior to application of load. The free length of the samples after mounting was 140 mm. Cyclic humidity testing was conducted by applying the tensile dead load to test samples for three hours at 23 °C and 50% RH, followed by cycling the relative humidity 10 times between 25% RH and 75% RH. One cycle consisted of a 1 minute ramp to 25% RH, maintaining the relative humidity at 25% for one hour, followed by a 5 minute ramp from 25% RH to 75% RH, and maintaining the relative humidity at 75% for 1 hour. Light scatter of creep test strips were measured prior to and after creep testing to measure relative bonded area change. The basis for using light scatter as a means to measure changes in relative bonded area in paper has been previously demonstrated [53, 54].

8.4 Results

8.4.1 High Load Wet Pressed Sheets

The first of two sets of results presented here are for sheets treated with debonder, nothing (control), or bonder that were wet pressed at high load (1.03 MPa) resulting in high density, high relative bonded area and specific bond strength (i.e. highly bonded)

sheets. The high press load results in the creation of sheets that are fully efficient loaded structures. Table 14 shows the physical testing results for these sheets.

Table 14 Physical Testing Results from the High Load Wet Pressed Sheets

Sheet Treatment	Grammage (g/m^2)	Hard Caliper (mm)	Apparent Density (g/cm^3)	Formation Number	Ultrasonic Modulus (km^2/s^2)
Debonder	101.1	0.145	0.697	33.8	10.9
Control	100.5	0.144	0.698	33.3	10.9
Bonder	101.4	0.145	0.699	32.8	11.2
Variation	0.9%	0.7%	0.1%	3.0%	2.8%

Sheet Treatment	Light Scatter (m^2/g)	Z-Tensile (N/mm^2)	Tensile (N/mm)	Failure Strain (%)	Zero-Span (N/mm)
Debonder	23.4	0.637	9.54	2.87	15.4
Control	22.8	0.656	10.7	3.31	15.8
Bonder	22.3	0.802	12.2	3.88	15.3
Variation	4.9%	25.9%	27.9%	35.2%	3.3%

The data from physical testing presented in Table 14 shows that sheets treated with debonder and bonder did not show significant differences from the control with regard to grammage, hard caliper, apparent density, formation, and zero-span tensile strength. Deformation behavior, as indicated by the ultrasonic elastic modulus data in Table 14 and stress-strain curves shown in Figure 97 were similar for all three sets. The differences in the sheets were in z-directional tensile strength, tensile strength, and strain to failure, caused predominantly by differences in specific bond strength. Figure 97 shows that sheets treated with debonder had the lowest specific bond strength, while the sheets treated with bonder had the highest specific bond strength and illustrates how deformation between the three sets of sheets remain similar.

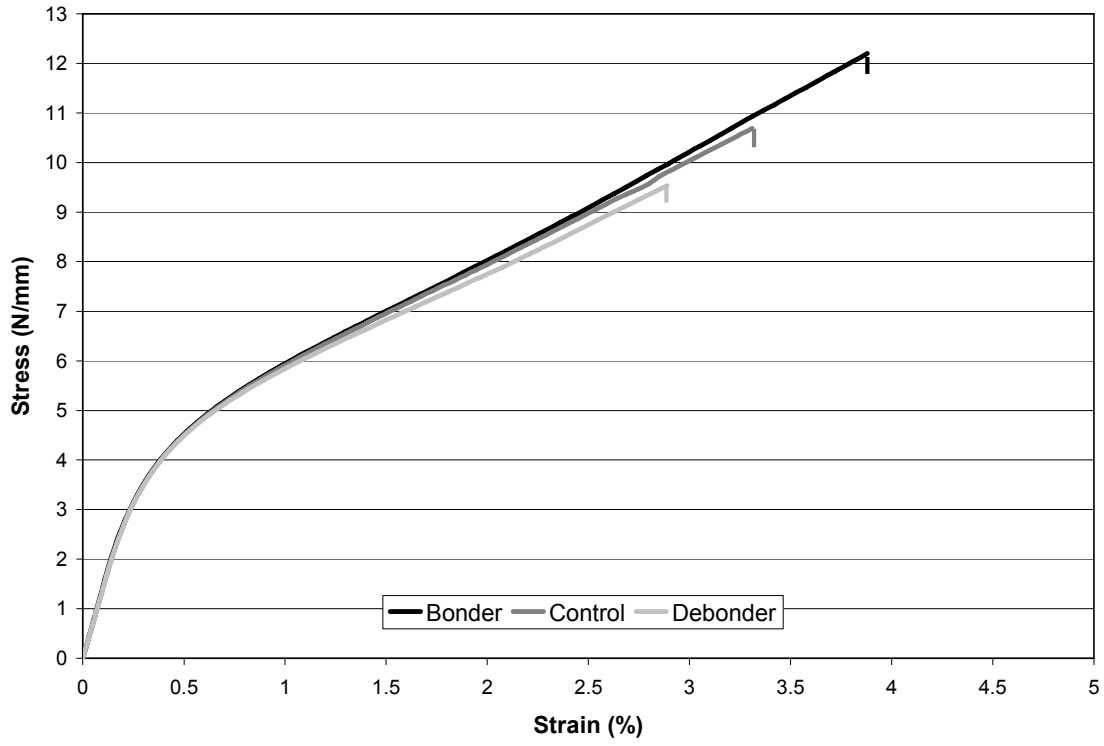

Figure 97 Stress-Strain Curves from Instron Tensile Testing of High Load Wet Pressed Sheets

These results demonstrate that it is possible to create three sets of handsheets with similar deformation behavior, similar relative bonded area, and different specific bond strengths. These results were expected as the work of Seth and Page [40], Chapter 5, and Chapter 7 have shown that at high levels of bonding, a fully efficient loaded paper structure can be created where elastic modulus plateaus and differences in specific bond strength do not affect deformation behavior, but do influence failure behavior. Overall, the physical testing results confirm that the three cases represent fully efficient loaded structures.

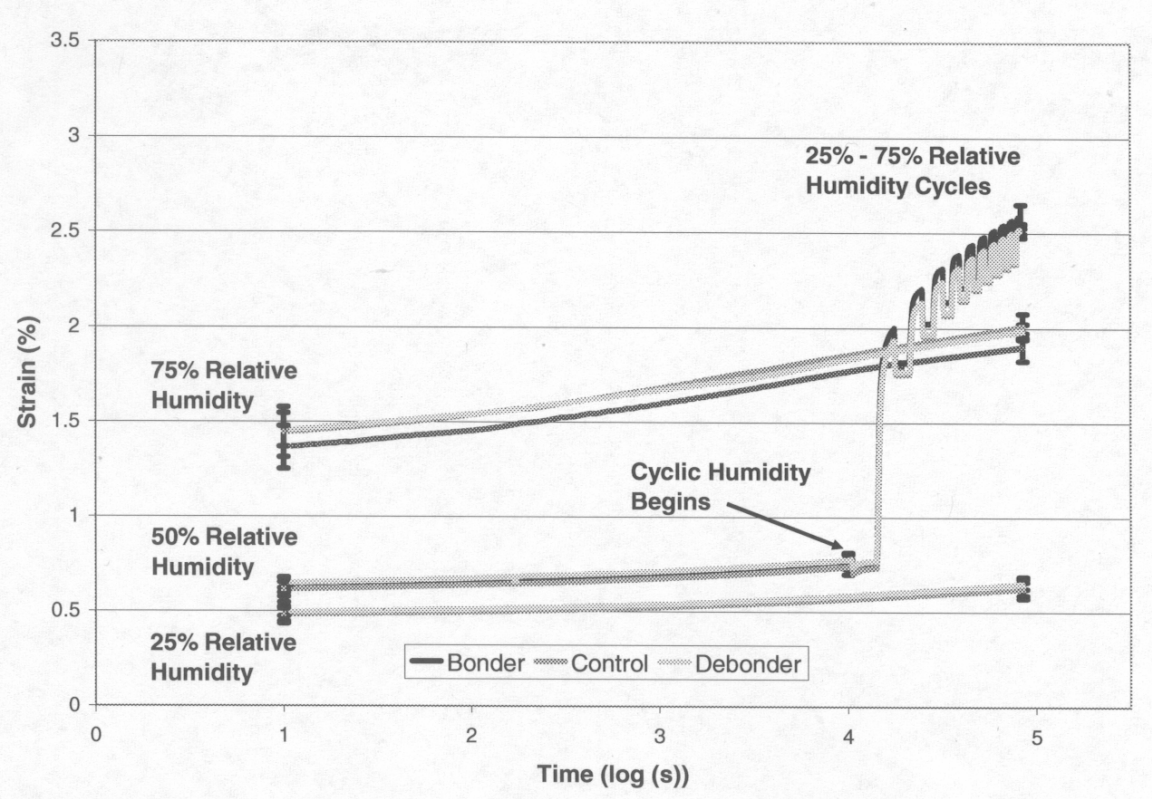

Figure 98 Creep Curves from High Load Wet Pressed Sheets

The creep behavior results shown in Figure 98 follow the same trend as the physical testing data. Overall, as illustrated in Figure 98, creep curves generated at a constant 25% RH and 75% RH show good overlap and fall within standard error bars (standard deviation divided by the square root of the sample size), indicating they have creep behaviors that cannot be differentiated from each other. These curves were generated to show the constant humidity behaviors of the different sheet types at the high and low humidity conditions which were later used in the accelerated creep testing. It also confirms that the difference in relative humidity between 25% RH and 75% RH is not changing the relationship between the debonder, control, and bonder sheets; the relationship being that their creep behaviors cannot be differentiated from each other. The

moisture contents of the sheets are about 5% at 25% RH, 6% at 50% RH, and 10% at 75% RH for all the cases.

Figure 98 also shows the complete accelerated creep tests for all three sheet types (bonder, control, and debonder). The accelerated creep results are shown by the curves which began at 50% RH and were held at that level until humidity cycling began at log(s) = 4. The accelerated creep curves are similar to those for constant humidity creep as they show good overlap and fall within standard error bars in the constant 50% RH portion and the cyclic humidity portion of the curves. This indicates they also have creep behaviors that cannot be differentiated from each other. This is further indicated in Figure 99, where the cyclic humidity portions of the curves are enlarged. The figure shows clearly that the accelerated creep curves have a higher creep rate than the constant humidity creep curves at 75% RH. This result was expected as an increased creep rate is a characteristic of accelerated creep. The results from this set of sheets show that creep behavior, whether measured under constant humidity or cyclic humidity, remains unchanged by differences in specific bond strength if a fully efficient structure exists.

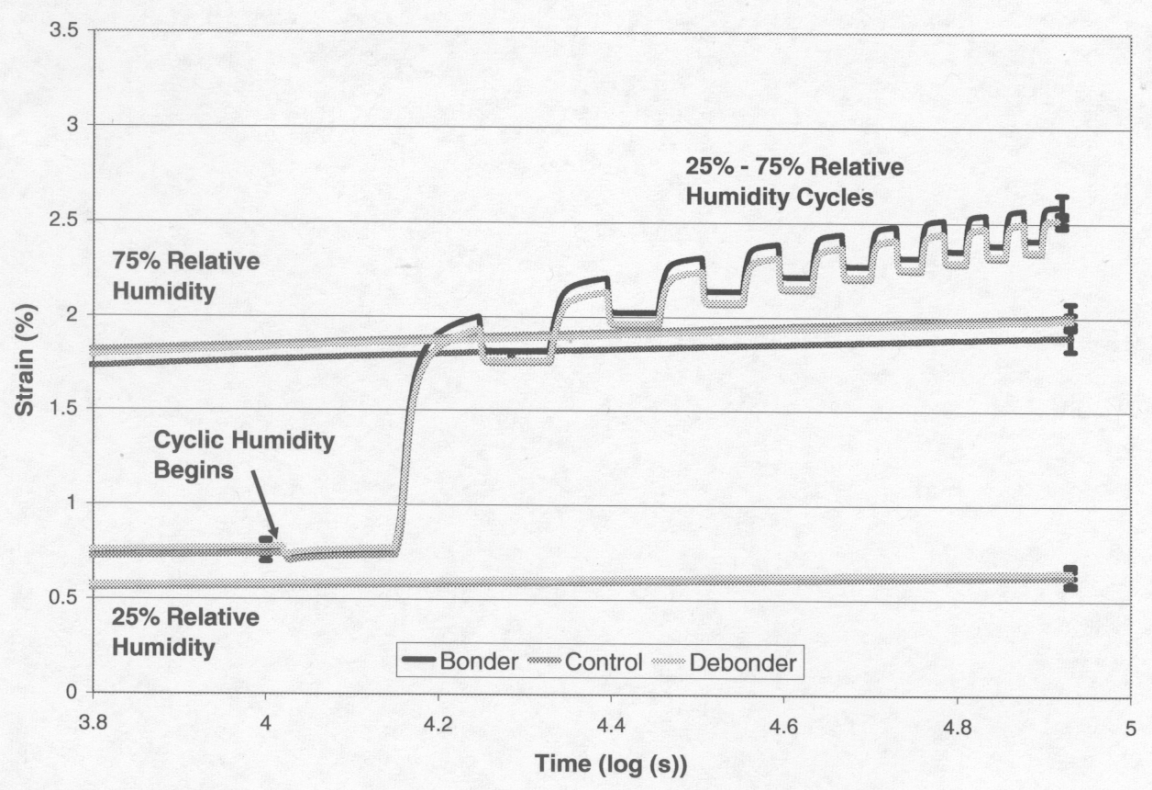

Figure 99 Enlarged View of Accelerated Creep from High Load Wet Pressed Sheets

8.4.2 Low Load Wet Pressed Sheets

The second set of results presented are for sheets treated with debonder, nothing (control), or bonder and wet pressed at low load (0.17 MPa), resulting in lower density, lower relative bonded area, and lower specific bond strength than the highly pressed case. The lower press load resulted in sheets that had inefficiently loaded structures. Table 15 shows the physical testing results for these low load wet pressed sheets.

Table 15 Physical Results from Low Load Wet Pressed Sheets

Sheet Treatment	Grammage (g/m^2)	Hard Caliper (mm)	Apparent Density (g/cm^3)	Formation Number	Ultrasonic Modulus (km^2/s^2)
Debonder	98.2	0.162	0.606	32.8	9.79
Control	97.4	0.160	0.609	32.8	10.3
Bonder	98.5	0.160	0.616	31.6	10.8
Variation	1.1%	1.3%	1.7%	3.8%	10.3%

Sheet Treatment	Light Scatter (m^2/g)	Z-Tensile (N/mm^2)	Tensile (N/mm)	Failure Strain (%)	Zero-Span (N/mm)
Debonder	29.8	0.405	8.78	3.27	15.7
Control	29.2	0.539	9.71	3.36	16.1
Bonder	27.7	0.611	11.2	3.58	15.5
Variation	7.6%	50.9%	27.6%	9.5%	3.9%

As with the high load wet pressed case, the data from physical testing presented in Table 15 showed that sheets treated with debonder and bonder did not show significant differences from the control with regard to grammage, hard caliper, formation, and zero-span tensile strength. The low load wet pressed sheets behaved in the same manner as the high load wet pressed sheets with regards to z-directional tensile strength, tensile strength, and strain to failure. Sheets treated with debonder had the lowest specific bond strength, while the sheets treated with bonder had the highest specific bond strength.

The major noticeable differences between the low load wet pressed sheets and the high load wet pressed sheets are that the low load wet pressed sheets have lower apparent density and greater light scatter indicating a lower relative bonded area than the high load wet pressed sheets. The deformation behavior of the low load wet pressed sheets was also different than that of the high load wet pressed sheets. This behavior, which can be correlated with bonding, is shown in the ultrasonic elastic modulus results of Table 15

and the stress-strain curves shown in Figure 100. The low load wet pressed sheets have lower moduli, more compliant stress-strain curves, and are weaker than the high load wet pressed sheets.

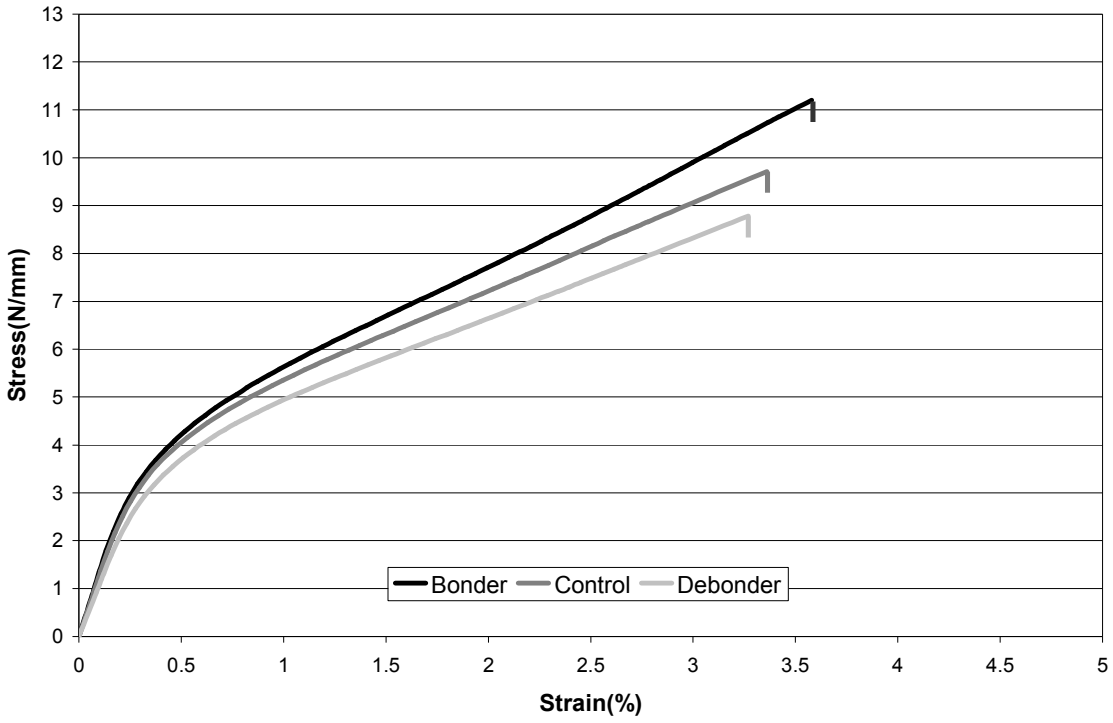

Figure 100 Stress-Strain Curves from Instron Tensile Testing of Low Load Wet Pressed Sheets

These results were expected as the work of Seth and Page [40] and Chapter 5 show at lower levels of bonding, an inefficient loaded paper structure is created where elastic modulus has not reached a plateau, and differences in specific bond strength and relative bonded area do affect deformation behavior and failure behavior. Overall, the physical testing results confirm that the three cases represent inefficient loaded structures.

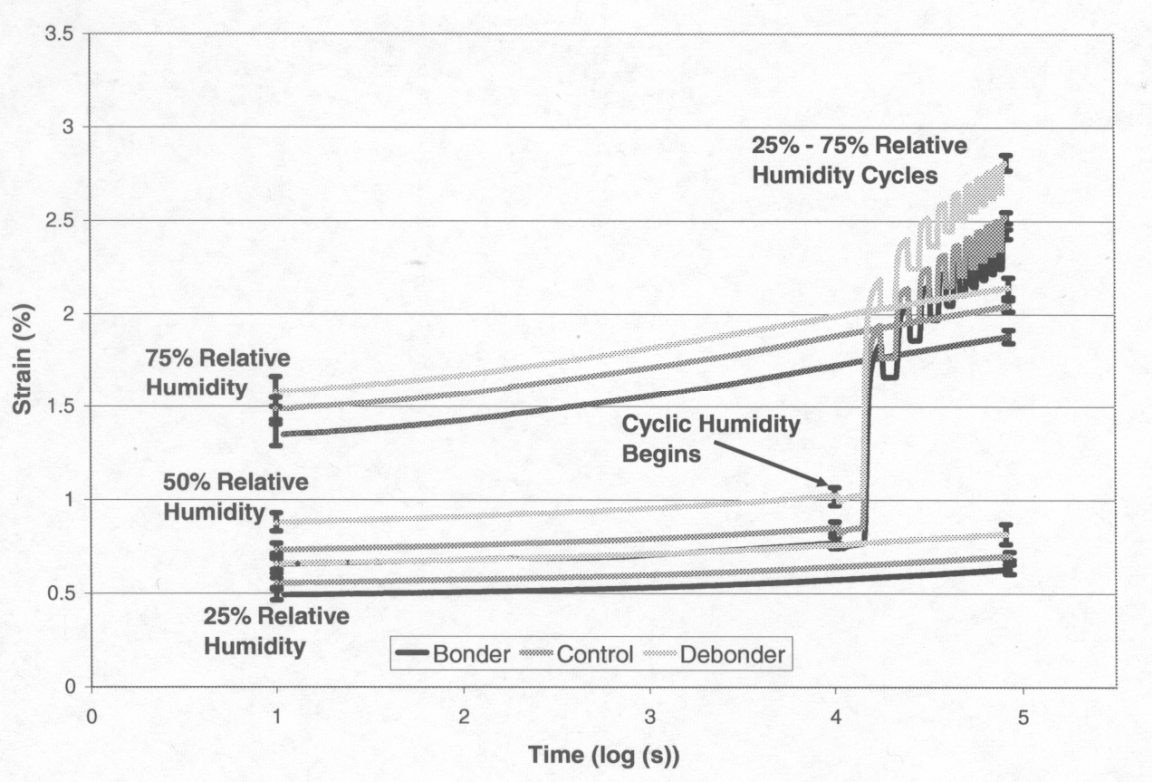

Figure 101 Creep Curves from Low Load Wet Pressed Sheets

The creep behavior results follow the same trend as the physical testing data. As illustrated in Figure 101, creep curves generated at a constant 25% RH and 75% RH do not show good overlap and do not fall within standard error bars, indicating they have creep behaviors that are different from each other. In fact, the debonder sheets tested at 25% RH overlap with the bonder treated sheets on the 50% RH portion of the accelerated creep curve. The accelerated creep curves are similar to those for the constant humidity creep curves as they show poor overlap and do not fall within standard error bars in the constant 50% RH portion or the cyclic humidity portion of the curves. This similarity between constant humidity creep and accelerated creep behavior was also observed in the high press load curves. The accelerated creep behavior is more clearly indicated in Figure

102 where the cyclic humidity portions of the curves are enlarged. Again, it is seen clearly that the accelerated creep curves show a higher creep rate than the constant humidity creep curves at 75% RH. As in the previous tests, the moisture contents of the sheets are about 5% at 25% RH, 6% at 50% RH, and 10% at 75% RH for all the cases.

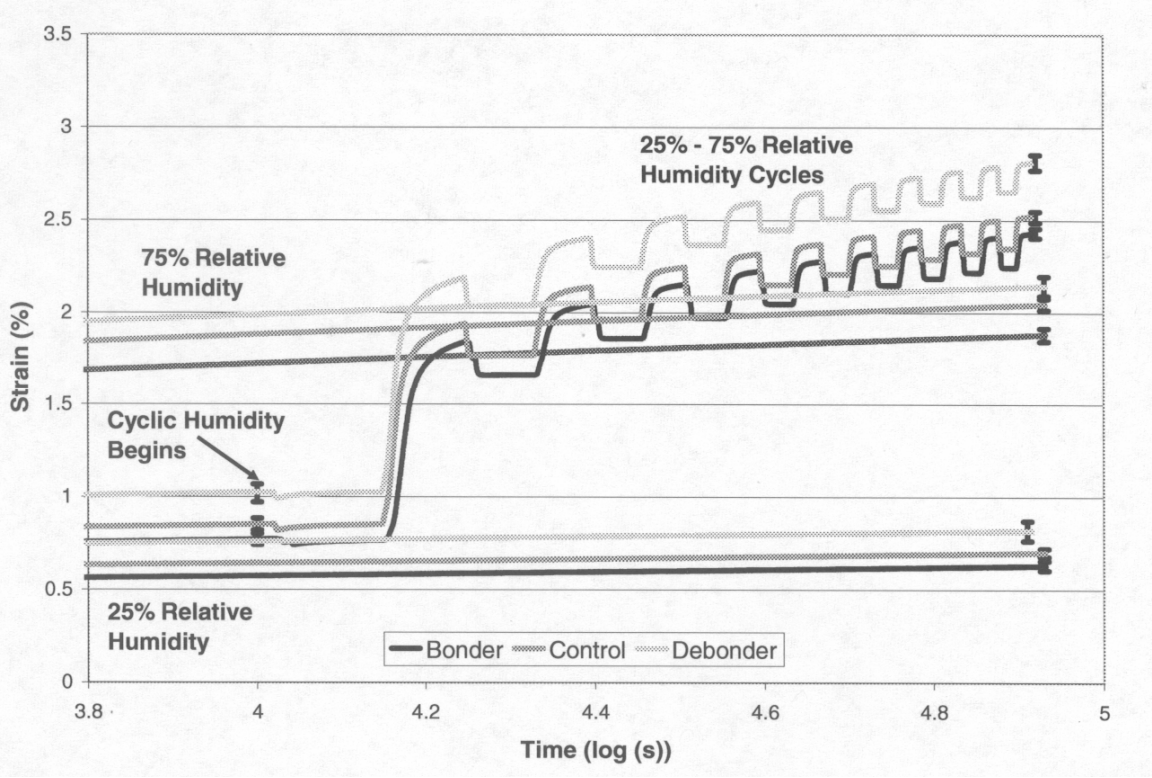

Figure 102 Enlarged View of Accelerated Creep from Low Load Wet Pressed Sheets

8.4.3 Light Scatter Results

Table 16 compares, for the high load wet pressed sheets, the total strain from accelerated creep testing versus the change in light scatter. Recalling that changes in light scatter are directly related to changes in bonded area, it is clear that bonded area loss did not have an influence on the deformation of the high load wet pressed sheets. The amount

of strain is similar for the three sheet types, yet the bonded area decreased to differing degrees. The data shows that light scatter change was over 100% higher with the debonder treated sheets than the bonder treated sheets while the deformations were the same.

Table 16 Accelerated Creep Test Results for High Load Wet Pressed Sheets

Sheet Treatment	Light Scatter Change (m^2/g)	Total Strain (%)
Debonder	1.37	2.52
Control	0.67	2.51
Bonder	0.27	2.59
Variation	>100%	3.2%

The data in Table 17 show the same trend with light scatter for the low load wet pressing case, as the strain increased the bonded area decreased. The data shows the light scatter change was over 100% higher for the debonder treated sheets than the bonder treated sheets; however, the deformations were over 15% different. Overall, these light scatter results for accelerated creep are consistent with what was observed with constant humidity creep behavior in Chapter 5.

Table 17 Accelerated Creep Test Results for Low Load Wet Pressed Sheets

Sheet Treatment	Light Scatter Change (m^2/g)	Total Strain (%)
Debonder	1.42	2.81
Control	1.11	2.52
Bonder	0.60	2.43
Variation	>100%	15.6%

8.5 Discussion

8.5.1 Analysis of Behavior

As paper reaches higher levels of bonding, relative bonded area and specific bond strength will reach or surpass a point beyond which only fiber deformation controls paper deformation behavior. This occurs because a sufficient amount of bonding exists within the paper structure to effectively and evenly distribute load throughout the fiber network. This can be considered to be a fully efficient structure. If a bonder is added to paper where bonding has already reached or surpassed this point, the increase in specific bond strength will not result in a change in creep behavior. If a debonder is added to paper and it does not reduce specific bond strength to a point where bonding is below this point, creep behavior will also remain unchanged. This is analogous to the work of Seth and Page [40] where they showed that the elastic modulus and stress-strain curve in paper remained unchanged at differing levels of specific bond strength as long as the paper's structure remained fully efficiently loaded.

It was shown in Chapter 5 and Chapter 7 that debonder, control, and bonder treated sheets subjected to high load wet pressing had the same constant humidity creep behavior when testing was conducted at 50% RH. In this study, constant humidity creep curves of debonder, control, and bonder treated sheets at the high load wet pressed

condition coincided when tested at 25% RH (moisture content is 5%) and when tested at 75% RH (moisture content is 10%). This shows that such deformation is controlled by the fibers, not the bonds and that the paper can remain a fully efficient loaded structure at a range of moisture contents. This demonstrates that the differences seen in creep behaviors when comparing curves measured at 25% RH and 75% RH are due to moisture induced changes in the fibers. In a fully efficient structure, moisture induced changes in the bonds, if any, do not influence the deformation behavior.

In contrast, if paper has a low level of bonding as was the case with the low load wet pressed sheets in this study, the combination of relative bonded area and specific bond strength will be at a point where bonding will influence the paper deformation. This occurs because bonding within the paper structure is insufficient to effectively distribute load through the fiber network; it is not a fully efficient loaded structure. If a debonder is added to paper, specific bond strength will decrease, acting to further deteriorate the paper's ability to effectively distribute load through the fiber network during deformation. This will lead to increased creep. If a bonder is added, it acts to increase the paper's ability to distribute load effectively, decreasing creep. Eventually, enough bonder could be added to increase specific bond strength enough to produce a fully efficient structure.

It was shown in Chapter 5 that debonder, control, and bonder treated sheets subjected to low load wet pressing had different constant humidity creep behavior when testing was done at 50% RH. In this study, similar results were obtained when testing was performed at 25% RH and 75% RH. The creep curves for the three sheet types did not coincide at either of these humidity levels, thus demonstrating that with inefficiently

loaded structures, bonding does influence deformation and must be taken into account in the deformation across a wide range of moisture levels.

An objective of this study was to determine if accelerated creep would respond to changes in bonding in the same manner as occurs with constant humidity creep. As the results in Figure 98, Figure 99, Figure 101, and Figure 102 show that was the case. When the high load wet pressed, fully efficient loaded sheets were tested, the constant humidity creep behaviors were the same and the accelerated creep behaviors were the same regardless of sheet specific bond strength. When the low load wet pressed, inefficiently loaded sheets were tested, the constant humidity creep behaviors were different and the accelerated creep behaviors were different; the differences corresponded to differences in specific bond strength. From these results, it is concluded that bonding has no additional effect on accelerated creep behavior beyond that which is already imparted by the constant humidity creep. If paper is a fully efficient loaded structure, only fiber deformation dictates constant humidity creep behavior and therefore it is also only fiber deformation which dictates accelerated creep behavior. Changing bonding will not alter either constant humidity or accelerated creep behavior. As illustrated in Table 16, bonded area loss was greater with the debonder treated sheets versus the bonder treated sheets, yet that did not have an impact of deformation. If paper is an inefficient loaded structure, both fiber deformation and bonding dictate constant humidity creep behavior and therefore both factors also dictate accelerated creep behavior. Hence, changing bonding will alter constant humidity creep behavior, thus resulting in differences in accelerated creep behavior as well.

8.5.2 Insights into the Accelerated Creep Mechanism

There are many differing opinions with regard to the accelerated creep mechanism. The purpose of this work was to investigate what role bonding plays in accelerated creep in order to assess the validity of such mechanisms. Based on the results from this study, in a sheet with a fully efficient loaded structure, the bonding can be changed significantly, via the addition of bonder or debonder, with no impact on the accelerated creep behavior. Therefore, in this case, the mechanism responsible for the increased amount of creep seen beyond what is observed under constant humidity conditions cannot be one which involves bonding. Sheets with an inefficient loaded structure did demonstrate accelerated creep behavior which was influenced by bonding, however, it would not be reasonable to expect that two different mechanisms, one for efficiently loaded structures and one more inefficiently loaded structures were in operation. As a result, the most probable mechanism is that proposed by Habeger and Coffin [78, 81, 82]. As humidity is changed, moisture diffuses into the sheet causing a moisture gradient to form. Given enough time the gradient will disappear, but once humidity is changed again, a new moisture gradient will be created. As moisture greatly influences the properties and behavior of fibers (elastic modulus and hygroexpansion), a moisture gradient will lead to an uneven stress distribution. Furthermore, if humidity is cycled, the moisture gradient and uneven stress distribution will cycle as well. Combined with the non-linear deformation behavior of paper, this uneven stress distribution leads to increased creep behavior under cyclic humidity conditions.

Material heterogeneity can act to amplify this effect as differences in elastic modulus and hygroexpansivity already exist. This was shown by Coffin and Habeger [83]

as multi-ply sheets made with different furnishes resulted in increased accelerated creep. Alfthan [84-87] pointed out that material heterogeneity also exists within a fiber network as anisotropic fiber swelling (hygroexpansivity) over bonded segments can lead to stress concentrations and more creep during moisture sorption. This is the basis for his modeling work with respect to accelerated creep in paper. Coffin [13] stated:

> ***Accelerated creep can occur in materials where (1) the creep behavior is nonlinear such that cycling load gives more creep than the average load and (2) stress distributions are created due to material heterogeneity and/or moisture gradients.***

This mechanism explains accelerated creep phenomena using the inherent creep behavior of the material as it responds to stress and does not introduce any additional mechanisms or phenomena. The work in this study offers further support for the Habeger and Coffin mechanism [78] as it demonstrated that the influence of bonding on accelerated creep is no greater than the influence of bonding on the constant humidity creep; the interaction between bonding and constant humidity creep determines the accelerated creep response. When sheets are fully efficient, constant humidity creep and accelerated creep are the same (as shown in Figure 98 and Figure 99). This is despite differences in bonded area loss as indicated in Table 16. When sheets are inefficient, constant humidity creep and accelerated creep are different (as shown in Figure 101 and Figure 102). This can be further analyzed using the results presented in Table 18.

Table 18 Amount of Creep Strain during Humidity Cycles in Accelerated Creep Testing

Sheet Treatment	Cycle 1 Strain (%)	Cycle 2 Strain (%)	Cycles 3-4 Strain (%)	Cycles 5-6 Strain (%)	Cycles 7-10 Strain (%)
Debonder Low 0.17 MPa	1.12	0.21	0.19	0.12	0.10
Control Low 0.17 MPa	1.09	0.20	0.18	0.09	0.11
Bonder Low 0.17 MPa	1.07	0.21	0.18	0.09	0.11
Debonder High 1.03 MPa	1.16	0.20	0.17	0.10	0.11
Control High 1.03 MPa	1.19	0.20	0.18	0.09	0.11
Bonder High 1.03 MPa	1.23	0.21	0.18	0.09	0.11

Table 18 shows the amount of creep deformation measured during each of the humidity cycles of accelerated creep testing for both the low load wet pressed sheets (labeled as 0.17 MPa) and the high load wet pressed sheets (labeled as 1.03 MPa). Cycle strains are calculated by taking the difference in strains at the end of each cycle, which is just before the humidity ramps from 75% RH to 25% RH. With the exception of the first humidity cycle, the deformations of the low load wet pressed sheets during humidity cycling are consistent with the deformations seen with the high load wet pressed sheets. Table 18 shows that a slightly lower amount of deformation is seen with the low load wet pressed sheets in the first humidity cycle compared to that of the high load wet pressed sheets. The work of Nilsson [113] showed that the diffusion of moisture through paper was strongly dependent on the density. Therefore, in this study, the lower density, low load wet pressed sheets should diffuse moisture faster than the higher density, high load wet pressed sheets. This will result in the low load wet pressed sheets having a lesser moisture gradient and as a result, a lesser uneven stress distribution. Figure 101 and

Figure 102 show that low load wet pressed sheets were shown to have different accelerated creep curves. Based on the data in Table 18, it is clear the reason why the accelerated creep curves were different was not due to humidity cycling, but rather the deformation that occurred during constant humidity creep. While the bonding was different, there was no further influence on the cyclic humidity portion of the curves (the accelerated creep portion). This offers more support for the moisture sorption mechanism as the cause for accelerated creep.

Further justification for the moisture sorption mechanism for accelerated creep can be found in its similarity to the mechanism by which bonding influences deformation. In the case of accelerated creep, moisture sorption will cause an uneven stress distribution due to material heterogeneity and/or moisture gradients. Similarly, insufficient bonding results in an inefficiently loaded structure, which is characterized by an uneven load distribution, and as a result an uneven stress distribution. An uneven stress distribution can produce greater deformations than an even distribution, as portions of the material exceed the elastic limit, reducing the total area of material supporting the load. This effect is accentuated when the load is applied to a non-linear material because areas of the sheet under higher stress will creep un-proportionally more than areas of the sheet under lower stress.

Alfthan [84-87] focused primarily on material heterogeneity as the mechanism for accelerated creep. However, through his modeling work, he showed that moisture sorption will cause anisotropic swelling at fiber crossings and lead to the formation of stress concentrations at and around bonded segments. This provided insight into possible details of the moisture sorption mechanism. The data from this study cannot be used to

draw conclusions with regards to where within the fibers extra strain associated with accelerated creep originates. The data only definitively show that in a fully efficient structure, bonding does not influence accelerated creep strain. Alfthan [84-87] assumed a no slip condition at the bonds and proposes the extra strain associated with accelerated creep occurs or originates preferentially within the fibers at and around bonded segments, which does not conflict with the results presented here. A no slip condition at the bonds implies that stress is only being transferred through the fiber network bonds (efficiently or inefficiently). Accepting the no slip condition, any actual bonded area loss can not be a contributor to accelerated creep. Any bonded area loss must be seen as a consequence of strain, not a cause of strain. Page [66, 68] points out in his work with stress-strain behavior, that bonded area loss is a strain-induced phenomenon and is a result produced by straining, not a cause. This conclusion was also reached with regard to constant humidity creep behavior based on the results of Chapter 7. It appears accelerated creep is no different. While it could be argued from the work of Alfthan [84-87] that the mere presence of bonding in a fiber network contributes towards accelerated creep, the results of this study support the assertion that the primary mechanism is heterogeneity (the anisotropic nature of the fibers), not bonding.

A differing viewpoint on the accelerated creep mechanism is proposed by Haslach [88-90]. He contends that bonding, more specifically bonded area loss, plays an important role in accelerated creep. Evidence to support this is given by Sedlachek [73]. He showed that individual fibers do not exhibit an accelerated creep behavior. It would seem logical to conclude that if fibers do not show accelerated creep, the mechanism behind accelerated creep must involve bonds. A counter argument is that proposed by

Habeger and Coffin [91]. They explain the results of Sedlachek [73] using their own accelerated creep mechanism. Individual fibers do not show accelerated creep because sorption occurs so quickly, moisture gradients and therefore stress gradients do not have a chance to form or persist. They contend, if sorption time could be increased or ramp time and cycle time could be sufficiently reduced, individual fibers would exhibit accelerated creep. Furthermore, they point out the work of Sedlachek [73] does show it is "on the verge" of accelerated creep as it shows more creep than the average between the constant humidity curves at the moisture extremes. This explanation combined with the work from this study, leads to the conclusion that a bonding mechanism does not explain the difference between constant humidity creep and accelerated creep behavior.

8.6 Conclusions

The accelerated creep results from this study further support the argument presented by Habeger and Coffin [78] that the mechanisms behind constant humidity creep and accelerated creep are the same. The increased amount of strain associated with accelerated creep occurs because uneven stress distributions result from moisture sorption. These uneven stress distributions cause more creep than a uniform stress distribution of the same average stress due to material non-linearity. Changes in bonding and bond structure are not contributors to accelerated creep. If that were the case, bonding would influence accelerated creep differently than constant humidity creep. The results from this study demonstrate this was not the case as accelerated creep behavior shows the same behavior as constant humidity creep behavior with regard to bonding.

CHAPTER 9: OVERALL CONCLUSIONS

Overall, the role of bonding in the tensile creep behavior was explored within this thesis. Within each results chapter, conclusions were drawn with regard to this. In Chapter 5 it was shown that creep behavior in paper will reach a minimum as higher levels of bonding are achieved. This is because improving bonding will only have an effect on creep behavior until an efficiently loaded structure is created, a structure which can effectively distribute load. Once the point is passed where the paper structure becomes fully efficient, only creep failure time can be increased with increased levels of bonding. This substantiates the premise that a fully efficient structure is not influenced by bonding with regard to deformation behavior, only failure behavior. This in effect shows that differences or similarities in deformation behavior do not necessarily correspond to differences or similarities in failure behavior with regard to creep or other physical properties.

In addition, it is possible to apply efficiency factors to the creep data of inefficiently loaded structures and create a data set that superimposes with creep data from an efficiently loaded structure. This efficiency factor can be calculated by relating elastic modulus data and still applies to the time dependent viscoelastic deformation seen with stress-strain behavior and creep behavior. The efficiency factor, in effect relates how well the existing bonding allows the structure to effectively distribute load throughout the sheet, a structure where deformation originates within the fiber and bonding can only influence deformation at a less then fully efficient loaded condition. This relation will

hold true as long as efficiency factor does not decrease with strain due to excessive relative bonded area loss (sheet damage).

Based on the results presented in Chapter 5, two models are presented in Chapter 6, one empirical and one rheological. These models are derived drawing upon the characteristics of the fibers, with bonding influence being accounted for using an efficiency factor. This is especially true for the rheological model, which draws upon the knowledge of the deformation behavior of cellulose, hemicelluloses, lignin (if present), and the molecular network associated with each of these fiber components. The rheological model also separates creep behavior into its initial elastic, primary creep, and secondary creep components. Inter-fiber bonds (relative bonded area and specific bond strength) are taken into account through use of efficiency factors which represent how effectively bonding is distributing load throughout the fibers within the paper. As a result, these models make it possible to predict the creep behavior at a range of bonding levels; all that is needed is the creep data from paper at one level of bonding. Then, using efficiency factors, the creep behavior of paper at any other level of bonding can be found. This will hold true as long as fibers (either type or amount of defects), formation, and orientation (both fiber and drying orientation) are not changed. The results from Chapter 6 confirm that bonding influence in paper can be accounted for with an easily derived efficiency factor.

In Chapter 5, it was found that creep behavior in a fully efficient loaded structure is not influenced by the initial level of bonding and subsequent loss of bonded area. Chapter 7 showed the reason for this, as the average level of bonded area loss is small and skewed towards many bonds failing partially and few failing significantly. As a

result, the stress distribution in paper during creep should not be significantly disrupted and behavior will remain unaffected. It was concluded that bonded area loss is a strain-induced phenomenon; bonded area loss is not a cause of strain, rather an effect. As such, deformation behavior in paper during creep is dictated solely by the fibers and its loading efficiency. Although creep behavior can be shown to be affected by the level of bonding in an inefficient loaded structure, the results in Chapter 5 show subsequent bonded area loss during straining does not further influence (degrade) behavior. This will hold true until an extreme case is achieved, where the initial level of bonding is so small any loss in bonded area would significantly disrupt the stress distribution within the sheet.

With the knowledge gained from the results of Chapter 5 and 7, the accelerated creep behavior of paper in tension was also studied. The results from this study further support the argument that the mechanisms behind constant humidity creep and accelerated creep are the same. The increased amount of strain associated with accelerated creep occurs because uneven stress distributions result from moisture sorption. These uneven stress distributions cause more creep than a uniform stress distribution of the same average stress due to material non-linearity. Changes in bonding and bond structure are not contributors to accelerated creep. If that were the case, bonding would influence accelerated creep differently than constant humidity creep. The results from Chapter 8 demonstrate this is not the case, as accelerated creep behavior shows the same behavior as constant humidity creep behavior with regard to bonding.

Overall, all the results incorporated into this thesis lead to the conclusion that tensile creep behavior in paper is no different than stress-strain behavior with regards to the influence of bonding. This has not been shown before. Specifically, this means

bonding influence in tensile creep behavior is related to sheet efficiency and how effectively stress is distributed within the structure, and that bonded area loss is a strain-induced phenomenon. This indicates that the time duration of the deformation test is of no consequence with regard to the influence of bonding. This means that the influence of bonding on elastic modulus, stress-strain behavior, and creep behavior will be the same. Furthermore, the cycling of moisture as with accelerated creep tests shows that bonding influence is still the same as constant humidity testing conditions. That is, bonding is not the cause of accelerated creep behavior. The implications of these results are that once bonding influence on deformation is known, it can easily be accounted for with an efficiency factor. This will allow more complex analyses of other variables that influence tensile creep (and other deformations) in paper without having to consider bonding influence.

CHAPTER 10: RECOMMENDATIONS FOR FUTURE WORK

Within this thesis, the main objective was to determine the role of bonding on creep behavior of paper under the most fundamental of circumstances and controlled conditions. This was done because fundamental knowledge of creep behavior in paper was lacking, making it difficult to effectively conduct experiments under more complex and practical conditions. As a result, creep behavior was analyzed under tension using laboratory sheets produced from the same fibers, under the same drying conditions and orientations. If work were to continue in this area, there are many different avenues of research that can be conducted.

The same set of experiments outlined in Chapters 5, 7, and 8 could be conducted under compressive loading conditions. While the role of bonding may now be defined under tension, it does not necessarily mean it will be the same under compression. Under compressive conditions, additional deformation mechanisms such as buckling and slip planes can come into play. These extra variables could be influenced by bonding to an extent where a fully efficient sheet under tension is not efficient under compression. Conversely, if it is found that the role of bonding is the same in compression and tension, tension experiments could be conducted in future studies with more confidence to their relevance towards compressive creep behavior. This is because the results would be comparable to compressive creep results and therefore be used in place of them. This would eliminate the need to apply complicated and unstandardized compressive creep testing techniques.

In addition, experimentation could be conducted under differing drying conditions and orientations. It would be interesting to determine how changing drying conditions and fiber orientation would influence the efficiency of the bonds. On that same line, additives other than the bonder and debonder used for this study could be analyzed.

It is also necessary to look at different types of fibers and different fiber properties. It should be explored to whether it is possible to create a fully efficient loaded structure if fibers are recycled, possess a significant amount of defects, or if they are not as conformable. Other than using pressing and refining to influence bonding, changes in drying conditions, use of additives, and changes in fiber orientation can be used as variables. These all can be used to determine the possibility of creating a fully efficient loaded structure with fibers that are less than ideal.

Finally, the concept of paper efficiency needs to be explored further. In the case of this thesis and other researchers work, efficiency is found through measurement and comparison of elastic modulus data. There would be merit in exploring whether it is possible to effectively predict paper efficiency by analyzing bonding itself. By either changing relative bonded area or specific bond strength, it may be possible to find a relationship between efficiency and bonding that is predictable.

APPENDIX A: ERROR ANALYSIS

In any scientific analysis, it is important to address the issue of error with regard to experimental data. According to Bevington and Robinson [114], experimental data will have a degree of random error associated with them. This random error can arise from two sources of uncertainty. The first is systematic error which is introduced by the amount of precision associated with experimental instrumentation and technique (or method). The second is additional uncertainty associated with variations (or fluctuations within the data); variation that cannot be explained by instrumentation or technique.

Within this thesis, a significant amount of data is presented, all with random error (variation) associated with them. When necessary, the random error of the data was treated statistically to determine if conclusions could or could not be drawn. To aid in this, multiple sheet test cases (made using different wet pressing levels, additive treatments, and refining levels) were made so comparisons between more than two sets of results could be made, allowing trends to be observed. Table 19 shows how many sheet test cases were used and analyzed in the results chapters. These include the Chapter 5 analysis of bonding influence and creep behavior, the Chapter 7 microscopic analysis of bonded area loss and creep behavior and the Chapter 8 analysis of bonding influence and accelerated creep behavior. The data from Chapter 5 were also used to validate the creep modeling presented in Chapter 6.

Table 19 Sheet Test Cases Analyzed per Results Chapter

Results Chapter	Sheet Test Cases Analyzed
Chapter 5	9
Chapter 7	3
Chapter 8	6

Within each of these sheet test cases, a certain number of measurement repetitions were made for all the physical testing, creep testing, and microscopy analysis conducted. Table 20 shows the test repetitions made for the physical tests presented in the results chapters. Table 21, Table 22, and Table 23 show the test repetitions made for the creep tests and microscopy analysis presented in the results chapters.

Table 20 Physical Testing Repetitions per Sheet Test Case

Physical Test	Repetitions for Chapter 5	Repetitions for Chapter 7	Repetitions for Chapter 8
Grammage (g/m^2)	8-18	5	8
Caliper (mm)	40-90	25	40
Ultrasonic Modulus (km^2/s^2)	5-9	5	5
Formation	8-13	0	8
Light Scatter (m^2/g)	18-36	0	24
Zero-Span (N/mm)	10-18	10	12
Z-Tensile (N/mm2)	8-16	10	12
Tensile Stress (N/mm)	20-36	10	16
Tensile Strain (%)	10-22	10	8

Table 21 Creep Testing Repetitions per Sheet Test Case in Chapter 5

Test	Initial Applied Stresses (N/mm) Tested	Repetitions per Initial Applied Stress (N/mm)	Total Number of Creep Tests
50% RH Creep Test	4-10	4-12	19-67

Table 22 Creep Testing and Microscopy Testing Repetitions per Sheet Test Case in Chapter 7

Test	Initial Applied Stresses (N/mm) Tested	Repetitions per Initial Applied Stress (N/mm)	Total Number of Tests
50% RH Creep Test	2	4-5	9-10
Microscopy Images (Bonds Analyzed)	2	35-48	62-94

Table 23 Accelerated Creep Testing Repetitions per Sheet Test Case in Chapter 8

Tests	Initial Applied Stresses (N/mm) Tested	Repetitions per Initial Applied Stress (N/mm)	Total Number of Tests
25% RH Creep Test	1	5-7	5-7
75% RH Creep Test	1	5-7	5-7
Accelerated Creep Test (25-75% RH Range)	1	8-11	8-11

Statistically, all data will have variation associated with them that can be analyzed using standard deviation and knowledge of the parent distribution. Within this thesis, tests known to possess higher variation and importance were subjected to an increased number of measurements (when possible) to improve certainty of results. Often, this certainty was visualized in many figures with the use of standard error bars. This is considered to be a valid technique in showing where the actual mean value of the data lies with high confidence [114, 115]. Standard error is easily calculated using Equation 45, where e is standard error, s is standard deviation and n is sample size (or repetition in measurement).

$$e = \frac{s}{\sqrt{n}}$$

Equation 45 Standard Error Calculation [114, 115]

In addition, systematic error was taken into account. Ideally, systematic error should be the same or smaller then the amount of observed random error. In some cases, the systematic error can be higher then the random error. This is an important concern as statistical analysis may under predict variation, leading to false conclusions, if systematic error is not considered. Therefore, the focus of the remainder of this appendix is on systematic errors or inherent measurement and procedural error associated with testing. When systematic error was found to be too high, even when it was shown to be sound statistically, data were eliminated from consideration.

In many cases, finding the systematic error of a measurement is straightforward. It can be easily found by determining the measurement tolerances associated with the experimental instrumentation and technique (or method). For example, when measuring caliper, the micrometer measures to a tolerance of 0.001 mm. Therefore, the systematic error is ±0.001 mm. On the other hand, when two or more measurements with error associated with them are used to calculate another value, the error propagates. For example, if the density measurement is needed, grammage is divided by caliper. Both grammage and caliper have error associated with their measurements and will propagate that error to the density measurement. To calculate this error, the error propagation calculation derived from Bevington and Robinson [114] and shown in Equation 46 is used.

$$e_y = \sqrt{\sum_{i=1}^{n} \left(\frac{\partial y}{\partial x_i} \right)^2 (e_{xi})^2}$$

Equation 46 Error Propagation Calculation [114]

In Equation 46, e_y represents the error associated with the calculated value, y. The measurements used to calculate e_y are x_i, and the associated errors e_{xi}, where i is the number measurements used to calculate y. For example, if a density measurement is made, the error of the density measurement (e_y) would be calculated from the square root of the sum of:

- density (y) partially differentiated with respect to grammage (x_1) all squared, multiplied by the error associated with grammage (e_{x1}) squared.
- and density (y) partially differentiated with respect to caliper (x_2) all squared, multiplied by the error associated with caliper (e_{x2}) squared.

The following tables show the error associated with all relevant measurements made within this thesis. In each table, the minimum and maximum values for each measurement are presented with their associated error and percent error (relative error). As a result, a range of error is presented between which all measurements will fall. Measurements, in which propagated errors were calculated using Equation 46, are marked with an asterisk. Table 24 shows error measurements for grammage, caliper and apparent density.

Table 24 Error Measurements for Grammage, Caliper and Apparent Density

Measurement	Min Value	Max Value	Min Value Error	Max Value Error	Min Value % Error	Max Value % Error
mass (g)	3.01	3.21	0.01	0.01	0.33	0.31
*area (m^2)	0.0317	0.0317	0.0002	0.0002	0.63	0.63
***Grammage (g/m^2)**	**94.9**	**101.4**	**0.7**	**0.7**	**0.74**	**0.69**
Caliper (mm)	**0.115**	**0.230**	**0.001**	**0.001**	**0.87**	**0.43**
***Apparent Density (g/cm^3)**	**0.433**	**0.832**	**0.004**	**0.010**	**0.92**	**1.20**

Based on the errors shown in Table 24, it is clear that the systematic errors associated with grammage, caliper, and apparent density are small and not a significant issue with regards to evaluation of data. Therefore, it is safe to deal with the variation of this data statistically without worry of systematic error leading to false conclusions.

Table 25 shows error measurements for non-destructive physical testing.

Table 25 Error Measurements for Non-Destructive Physical Testing

Measurement	Min Value	Max Value	Min Value Error	Max Value Error	Min Value % Error	Max Value % Error
Ultrasonic Modulus (km^2/s^2)	**7.18**	**11.2**	**0.01**	**0.1**	**0.14**	**0.89**
***Efficiency Factor**	**0.64**	**1.00**	**0.01**	**0.02**	**1.56**	**2.00**
Formation	**31.3**	**35.4**	**0.1**	**0.1**	**0.32**	**0.28**
R_0	65.1	77.3	0.1	0.1	0.15	0.13
R_∞	91.1	92.1	0.1	0.1	0.11	0.11
***Light Scatter (m^2/g)**	**19.8**	**35.5**	**0.2**	**0.3**	**1.01**	**0.85**
***1.03 MPa Pressed Sheets- Light Scatter Δ (m^2/g)**	**0.27**	**5.16**	**0.22**	**0.22**	**81.5**	**4.26**
***0.17 MPa Pressed Sheets- Light Scatter Δ (m^2/g)**	**0.60**	**3.18**	**0.28**	**0.29**	**46.7**	**9.12**

Based on the errors shown in Table 25, it is clear the systematic errors associated with ultrasonic modulus data, efficiency factors, formation, and light scatter are small and not a significant issue with regards to evaluation of data. Therefore, it is safe to deal with the variation of this data statistically without worry of systematic error leading to false conclusions. With regards to light scatter change, both high load and low load wet pressed sheets showed high levels of systematic error. As a result, this error was taken into account, to make sure it did not exceed the random error. In addition, increased sample sizes were used, repetition of experimentation, and additional independent testing meant to corroborate light scatter change data was conducted. This was done prior to any conclusions being drawn.

Table 26 shows error measurements for destructive physical testing.

Table 26 Error Measurements for Destructive Physical Testing

Measurement	Min Value	Max Value	Min Value Error	Max Value Error	Min Value % Error	Max Value % Error
Zero-Span (N/mm)	**14.4**	**16.7**	**0.1**	**0.1**	**0.69**	**0.60**
Z-Tensile (N/mm2)	**0.207**	**0.927**	**0.001**	**0.001**	**0.48**	**0.11**
Load (N)	25.0	305.0	0.5	0.5	2.00	0.16
Width (mm)	25.0	25.0	0.5	0.5	2.00	2.00
***Tensile Stress (N/mm)**	**1.00**	**12.2**	**0.03**	**0.3**	**3.00**	**2.46**
Displacement (mm)	0.35	5.91	0.03	0.03	8.57	0.51
Length (mm)	140	140	3	3	2.14	2.14
***Tensile Strain (%)**	**0.25**	**4.22**	**0.03**	**0.09**	**12.0**	**2.13**

Based on the errors shown in Table 26, it is clear that the systematic errors associated with zero-span testing, z-directional tensile testing, and tensile stress are small and not a significant issue with regards to evaluation of data. Therefore, it is safe to deal with the variation of this data statistically without worry of systematic error leading to false conclusions. The same can be said for tensile strain, in most cases. Where tensile strain error becomes high (only on a relative basis), is at the initial portion of stress-strain curve data within this thesis. Since modulus data is measured ultrasonically, not from stress-strain data, this error at this low strain is not a significant factor in data analysis.

Table 27 shows error measurements for creep testing.

Table 27 Error Measurements for Creep Testing

Measurement	Min Value	Max Value	Min Value Error	Max Value Error	Min Value % Error	Max Value % Error
Load (N)	29.75	179.25	0.01	0.01	0.034	0.0056
Width (mm)	25.0	25.0	0.5	0.5	2.00	2.00
***Creep Stress (N/mm)**	**1.19**	**7.17**	**0.03**	**0.15**	**2.52**	**2.09**
Displacement (mm)	0.126	5.516	0.001	0.001	0.79	0.018
Length (mm)	140	140	3	3	2.14	2.14
***Creep Strain (%)**	**0.09**	**3.94**	**0.01**	**0.09**	**11.1**	**2.28**
Creep Time (s)	**10**	**86400**	**1**	**1**	**10.0**	**0.0012**

Based on the errors shown in Table 27, it is clear that the systematic error associated creep stress is small and not a significant issue with regards to evaluation of data. Therefore, it is safe to deal with the variation of this data statistically without worry of systematic error leading to false conclusions. The same can be said for creep strain in most cases. Like tensile strain, creep strain error becomes high (only on a relative basis), at low strains. Again, this is not a significant issue, as the absolute error is small. With regards to creep time, the error is high at short times. As a result, all data under ten seconds were eliminated because they were too variable. This showed up dramatically in the statistical analysis as well, especially when attempting to draw any conclusions from strain data at time equal to one second.

Table 28 shows error measurements for microscopy measurements.

Table 28 Error Measurements for Microscopy Measurements

Measurement	Min Value	Max Value	Min Value Error	Max Value Error	Min Value % Error	Max Value % Error
Bonded Area (μm^2)	**807.9**	**1038.1**	**0.1**	**0.1**	**0.012**	**0.010**
***Bonded Area Δ (μm^2)**	**17.1**	**134.9**	**0.2**	**0.2**	**1.17**	**0.15**
***Bonded Area Δ (%)**	**1.65**	**16.7**	**0.02**	**0.1**	**1.21**	**0.60**

Based on the errors shown in Table 28, it is clear that the systematic errors associated with all the microscopy data is not a significant issue with regards to evaluation of data. Therefore, it is safe to deal with the variation of this data statistically without worry of systematic error leading to false conclusions. Furthermore, this data acts to independently confirm light scatter change findings, which do have large errors associated with them.

APPENDIX B: DETAILED DERIVATION OF EQUATION 38

Within Chapter 6, Equation 38 is the basis for the primary creep component of the rheological model. Equation 38 is the particular solution of the differential equation shown in Equation 37. The mathematics involved to gain this solution is rigorous and presented within this appendix. This appendix begins with Equation 47, which is identical to Equation 37 and solves for Equation 57, which is identical to Equation 38.

$$\frac{d\varepsilon_1}{dt} = B_1 \sinh\left(\frac{\sigma_o - E_1\varepsilon_1}{A_1}\right)$$

Equation 47 Differential Equation of the Linear Spring Element Connected in Parallel to a Non-Linear Eyring Dashpot Element for the Primary Creep Strain Component of the Rheological Model

$$\frac{d\varepsilon_1}{\sinh(a+b\varepsilon)} = B_1 dt$$

$$a = \frac{\sigma_o}{A_1} \qquad b = -\frac{E_1}{A_1}$$

Equation 48 Reorganization and Simplification of Equation 47

$$\frac{dx}{b\sinh(x)} = B_1 dt$$

$$x = a + b\varepsilon \qquad dx = bd\varepsilon$$

Equation 49 Integral Substitution on Left Half of Equation 48

$$\frac{1}{b}\ln\left(\tanh\frac{x}{2}\right)=B_1t+C_i$$

Equation 50 Integration of Equation 49 Using the Indefinite Integral Tables from Rade and Westergren [116]

$$-\frac{A_1}{E_1}\ln\left(\tanh\frac{\sigma_o-E_1\varepsilon}{2A_1}\right)=B_1t+C_i$$

Equation 51 Indefinite Solution from Equation 50 Replacing b and x with Their Actual Values

$$C_i=-\frac{A_1}{E_1}\ln\left(\tanh\frac{\sigma_o}{2A_1}\right)$$

Equation 52 Value of the Constant (C_i) in Equation 51 if $\varepsilon = 0$ at $t = 0$

$$-\frac{A_1}{E_1}\ln\left(\tanh\frac{\sigma_o-E_1\varepsilon}{2A_1}\right)=B_1t+-\frac{A_1}{E_1}\ln\left(\tanh\frac{\sigma_o}{2A_1}\right)$$

Equation 53 Solution of Equation 51 by Replacing the Constant (C) with Equation 52

$$\ln\left(\frac{\tanh\frac{\sigma_o-E_1\varepsilon}{2A_1}}{\tanh\frac{\sigma_o}{2A_1}}\right)=\frac{-E_1B_1t}{A_1}$$

Equation 54 Algebraic Manipulation of Equation 53

$$\tanh\left(\frac{\sigma_o - E_1\varepsilon}{2A_1}\right) = \tanh\left(\frac{\sigma_o}{2A_1}\right)\exp\left(\frac{-E_1B_1t}{A_1}\right)$$

Equation 55 Algebraic Manipulation of Equation 54

$$\sigma_o - E_1\varepsilon = 2A_1\tanh^{-1}\left[\tanh\left(\frac{\sigma_o}{2A_1}\right)\exp\left(\frac{-E_1B_1t}{A_1}\right)\right]$$

Equation 56 Algebraic Manipulation of Equation 55

$$\varepsilon_1 = \frac{1}{E_1}\left(\sigma_o - 2A_1\tanh^{-1}\left[\tanh\left(\frac{\sigma_o}{2A_1}\right)\exp\left(-\frac{E_1B_1t}{A_1}\right)\right]\right)$$

Equation 57 Solution of the Differential Equation for the Linear Spring Element Connected in Parallel to a Non-Linear Eyring Dashpot Element for the Primary Creep Strain Component of the Rheological Model

REFERENCES

[1] M. Kortschot, "The Role of the Fibre in the Structural Hierarchy of Paper," in *Fundamentals of Papermaking, Transactions of the 9th Fundamental Research Symposium*, C. Baker, Ed. Cambridge, UK: FRC, 1997, pp. 351-399.

[2] A. Panshin and C. De Zeeuw, *Textbook of Wood Technology*. New York, NY, USA: McGraw-Hill, 1980.

[3] C. Biermann, *Handbook of Pulping and Papermaking*. San Diego, CA, USA: Academic Press, 1996.

[4] E. Retulainen, K. Niskanen, and N. Nilsen, "Fibers and Bonds, Chapter 2," in *Paper Physics, Book 16*, K. Niskanen, Ed. Jyvaskyla, Finland: Fapet Oy, 1998, pp. 54-87.

[5] R. Atalla, "The Structures of Cellulose," in *Materials Interactions Relevant to the Pulp, Paper, and Wood Industries, Volume 197*, D. Caufield, J. Passaretti, and S. Sobczynski, Eds. Pittsburgh, PA, USA: Materials Research Society, 1990, pp. 89-98.

[6] W. Findley, J. Lai, and K. Onaran, *Creep and Relaxation of Nonlinear Viscoelastic Materials*. New York, USA: Dover Publications, Inc., 1989.

[7] J. Gere, *Mechanics of Materials*. Pacific Grove, CA, USA: Brooks/Cole, Thomson Learning, 2001.

[8] L. Malvern, *Introduction to the Mechanics of a Continuous Medium*. Englewood Cliffs, NJ, USA: Prentice-Hall, Inc., 1969.

[9] R. Panton, *Incompressible Flow*. New York, NY, USA: John Wiley & Sons, Inc., 1996.

[10] J. Waterhouse, "The Mechanical Properties of Paper, Chapter 4," in *Pulp and Paper Manufacture, Volume 9*, M. Kouris, Ed. Atlanta, GA, USA: Joint Textbook Committee of the Paper Industry, 1992.

[11] R. Young and P. Lovell, *Introduction to Polymers*. Cheltenham, UK: Stanley Thornes (Publishers) Ltd., 1991.

[12] A. Drozdov, *Viscoelastic Structures*. San Diego, CA, USA: Academic Press, 1998.

[13] D. Coffin, "The Creep Response of Paper," in *Advances in Paper Science and Technology, Transactions of the 13th Fundamental Research Symposium*, S. Anson, Ed. Cambridge, UK: FRC, 2005, pp. 651-747.

[14] J. Panek, C. Fellers, and T. Haraldsson, "Principles of Evaluation for the Creep of Paperboard in Constant and Cyclic Humidity Environments," *Nordic Pulp and Paper Research Journal*, vol. 19(2), pp. 155-163, 2004.

[15] P. Kolseth and A. De Ruvo, "The Measurement of Viscoelastic Behavior for the Characterization of Time, Temperature, and Humidity Dependent Properties, Chapter 2," in *Handbook of Physical Testing of Paper*, R. Mark, Ed. New York, NY, USA: Marcel Dekker, Inc., 1983, pp. 255-322.

[16] K. Niskanen, "Rheology and Moisture Effects, Chapter 8," in *Paper Physics, Book 16*, K. Niskanen, Ed. Jyvaskyla, Finland: Fapet Oy, 1998, pp. 260-283.

[17] L. Salmén and R. Hagen, "Viscoelastic Properties, Chapter 2," in *Handbook of Physical Testing of Paper*, R. Mark, C. Habeger, J. Borch, and M. Lyne, Eds. New York, NY, USA: Marcel Dekker, Inc., 2002, pp. 77-113.

[18] C. Soremark, C. Fellers, and L. Henriksson, "Mechano-Sorptive Creep of Paper," in *Products of Papermaking, Transactions of the 10th Fundamental Research Symposium*, C. Baker, Ed. Oxford, UK: FRC, 1993, pp. 547-574.

[19] R. Meredith, *The Mechanical Properties of Textile Fibres*. New York, NY, USA: Interscience Publishers, Inc., 1956.

[20] W. Findley, "Mechanism and Mechanics of Creep of Plastics," *SPE Journal*, vol. 16(1), pp. 57-65, 1960.

[21] G. Halsey, H. White, and H. Eyring, "Mechanical Properties of Textiles, I," *Textile Research Journal*, vol. 15(9), pp. 295-311, 1945.

[22] H. Holland, G. Halsey, and H. Eyring, "Mechanical Propeties of Textiles, VI. A Study of Creep of Fibers," *Textile Research Journal*, vol. 16(5), pp. 201-210, 1946.

[23] A. Tobolsky and H. Eyring, "Mechanical Properties of Polymeric Materials," *Journal of Chemical Physics*, vol. 11(3), pp. 125-134, 1943.

[24] H. Eyring, "Viscosity, Plasticity and Diffusion as Examples of Absolute Reaction Rates," *Journal of Chemical Physics*, vol. 4(4), pp. 283-295, 1936.

[25] T. Alfrey, *Mechanical Behavior of High Polymers*. New York, NY, USA: Interscience Publishers, Inc., 1948.

[26] A. Olsson and L. Salmén, "Molecular Mechanisms Involved in Creep Phenomena of Paper," *Journal of Applied Polymer Science*, vol. 79, pp. 1590-1595, 2001.

[27] J. Ferry, *Viscoelastic Properties of Polymers*. New York, NY, USA: Wiley & Sons, Inc., 1961.

[28] L. Salmén and E. Back, "The Effect of Temperature and Humidity on the Elastic Modulus of Paper," presented at 1979 TAPPI International Paper Physics Conference, pp. 47-52, 1979.

[29] L. Salmén and E. Back, "Effect of Temperature on Stress-Strain Properties of Dry Papers," *Svensk Papperstidning*, vol. 81(10), pp. 341-346, 1978.

[30] R. Benson, "Effects of Relative Humidity and Temperature on Tensile Stress-Strain Properties of Kraft Linerboard," *Tappi Journal*, vol. 54(5), pp. 699-703, 1971.

[31] A. Vorakunpinij. *The Effect of Paper Structure on the Deviation Between Tensile and Compressive Creep Responses*. Doctoral Thesis. Institute of Paper Science and Technology, Atlanta, GA, USA, 2003.

[32] J. Van den Akker, "Structure and Tensile Characteristics of Paper," *Tappi Journal*, vol. 53(3), pp. 388-400, 1970.

[33] H. Rance, "Some New Studies in the Strength Properties of Paper," in *Technical Section of the Paper Maker's Association of Great Britain and Ireland*. London, UK: The Paper Maker's Association of Great Britain and Ireland, 1948, pp. 449-475.

[34] B. Steenberg, "Paper as a Viscoelastic Body," *Svensk Papperstidning*, vol. 50(6), pp. 127-140, 1947.

[35] S. Mason, "The Rheology of Paper," *Pulp and Paper Magazine of Canada*, vol. 49, pp. 207-221, 1948.

[36] J. Brezinski, "The Creep Properties of Paper," *Tappi Journal*, vol. 39(2), pp. 116-128, 1956.

[37] J. Brezinski. *A Study of the Viscoelasticity of Paper by Means of Tensile Creep Tests*. Doctoral Thesis. Institute of Paper Chemistry, Appleton, Wisconsin, USA, 1955.

[38] R. Hill, "The Creep Behavior of Individual Pulp Fibers Under Tensile Stress," *Tappi Journal*, vol. 50(8), pp. 432-440, 1967.

[39] R. Hill. *The Creep Behavior of Individual Pulp Fibers Under Tensile Stress*. Doctoral Thesis. Institute of Paper Chemistry, Appleton, Wisconsin, USA, 1967.

[40] R. Seth and D. Page, "The Stress Strain Curve of Paper," in *The Role of Fundamental Research in Papermaking, Transactions of the 7th Fundamental Research Symposium*, J. Brander, Ed. Cambridge, UK: FRC, 1981, pp. 421-452.

[41] D. Page, "A Theory for the Tensile Strength of Paper," *Tappi Journal*, vol. 52(4), pp. 674-681, 1969.

[42] J. Clark, "Bonding of Cellulose Surfaces, Chapter 7," in *Pulp Technology and Treatment for Paper*: Miller Freeman Publishing, 1978, pp. 145-159.

[43] W. Campbell, "The Mechanism of Bonding," *Tappi Journal*, vol. 42(12), pp. 999-1001, 1959.

[44] A. Nissan, "General Principles of Adhesion," in *The Formation and Structure of Paper, Transactions of the 2nd Fundamental Research Symposium*, F. Bolam, Ed. Oxford, UK: FRC, 1961, pp. 119-130.

[45] A. Nissan and S. Sternstein, "Cellulose-Fiber Bonding," *Tappi Journal*, vol. 47(1), pp. 1-6, 1964.

[46] A. McKenzie, "Diffusion Theory of Adhesion Applied to Interfiber Bonding," *Appita*, vol. 37(7), pp. 580-583, 1984.

[47] D. Goring, "Thermal Sofetening, Adhesive Properties and Glass Transitions in Lignin, Hemicellulose and Cellulose," in *Consolidation of the Paper Web, Transactions of the 3rd Fundamental Research Symposium*, F. Bolam, Ed. Cambridge, UK: FRC, 1965, pp. 555-568.

[48] V. Byrd, "Flow and Adhesion of Hemicellulose and Lignin During Press Drying," presented at The 1979 Tappi Annual Meeting, pp. 15-21, 1979.

[49] V. Byrd, "How Bonds Develop During Web Consolidation," *PTI*, pp. 240-243, 1986.

[50] N. Takamura, "Studies on Hot Pressing and Drying Process in the Production of Fibreboard III, Softening of Fibre Components in Hot Pressing of Fibre Mat," *Journal of the Japan Wood Research Society*, vol. 14(2), pp. 75-79, 1968.

[51] K. Niskanen, I. Kajanto, and P. Pakarien, "Paper Structure, Chapter 1," in *Paper Physics, Book 16*, K. Niskanen, Ed. Jyvaskyla, Finland: Fapet Oy, 1998, pp. 14-53.

[52] D. Page, P. Tydeman, and M. Hunt, "A Study of Fibre-Fibre Bonding by Direct Observation," in *The Formation and Structure of Paper, Transactions of the 2nd Fundamental Research Symposium*, F. Bolam, Ed. Oxford, UK: FRC, 1961, pp. 171-203.

[53] S. Parsons, "Optical Characteristics of Paper as a Function of Fiber Classification," *Technical Association Papers*, vol. 25, pp. 360-368, 1942.

[54] W. Haselton. *An Investigation of the Adsorption of Gas by Wood and Its Components and Gas Adsorption Techniques as a Means of Studying the Area and Structure of Pulp and Paper*. Doctoral Thesis. Institute of Paper Chemistry, Appleton, Wisconsin, USA, 1953.

[55] W. Ingmanson and E. Thode, "Factors Contributing to the Strength of a Sheet of Paper," *Tappi Journal*, vol. 42(1), pp. 83-93, 1959.

[56] E. Retulainen and K. Ebeling, "Fibre-Fibre Bonding and Ways of Characterizing Bond Strength," *Appita*, vol. 46(4), pp. 282-288, 1993.

[57] U. Mohlin, "Cellulose Fibre Bonding," *Svensk Papperstidning*, vol. 77(4), pp. 131-135, 1974.

[58] R. Stratton, "Characterization of Fibre-Fibre Bond Strength from Out-of-Plane Paper Mechanical Properties," *Journal of Pulp and Paper Science*, vol. 19(1), pp. J6-J11, 1993.

[59] J. Parker, "The Effects of Ethylamine Decrystallization of Cellulose Fibers on the Viscoelastic Properties of Paper," *Tappi Journal*, vol. 45(12), pp. 936-943, 1962.

[60] J. Schulz. *The Effect of Strain Applied During Drying on the Mechanical Behavior of Paper*. Doctoral Thesis. Institute of Paper Chemistry, Appleton, WI, USA, 1961.

[61] J. Schulz, "Effect of Straining During Drying on the Mechanical and Viscoelastic Behavior of Paper," *Tappi Journal*, vol. 44(10), pp. 736-744, 1961.

[62] I. Sanborn, "A Study of Irreversible, Stress-Induced Changes in the Macrostructure of Paper," *Tappi Journal*, vol. 45(6), pp. 465-474, 1962.

[63] I. Sanborn. *A Study of Irreversible, Stress-Induced Changes in the Macrostructure of Paper*. Doctoral Thesis. Institute of Paper Chemistry, Appleton, WI, USA, 1961.

[64] V. Byrd. *An Investigation of Handsheet Structural and Property Changes During and After Creep Under Constant and Cyclic Relative Humidity Environments*. Doctoral Thesis. North Carolina State University, Raleigh, North Carolina, USA, 1971.

[65] J. Van den Akker, "The Elastic and Rheological Properties of Papermaking Fibers," *Tappi Journal*, vol. 33(8), pp. 398-402, 1950.

[66] D. Page, "The Meaning of Nordman Bond Strength," *Nordic Pulp and Paper Research Journal*, vol. 17(1), pp. 39-44, 2002.

[67] D. Page, P. Tydeman, and M. Hunt, "The Behavior of Fibre-to-Fibre Bonds In Sheets Under Dynamic Conditions," in *The Formation and Structure of Paper, Transactions of the 2nd Fundamental Research Symposium*, F. Bolam, Ed. Oxford, UK: FRC, 1961, pp. 249-276.

[68] D. Page, "The Meaning of Nordman Bond Strength," presented at The 2002 Progress in Paper Physics Seminar, Finger Lakes/ Syracuse, USA, pp. 2, 2002.

[69] M. Pecht, M. Johnson, and R. Rowlands, "Constituative Equations for the Creep of Paper," *Tappi Journal*, vol. 67(5), pp. 106-108, 1984.

[70] M. Pecht and M. Johnson, "The Strain Response of Paper Under Various Constant Regain States," *Tappi Journal*, vol. 68(1), pp. 90-93, 1985.

[71] J. Pommier, J. Poustis, and C. Castets, "A Proposed Mechanism as a New Model for the Packaging Papers Behaviour," presented at The 1992 Progress in Paper Physics Seminar, Otaniemi, Finland, pp. 59-61, 1992.

[72] L. Agbezuge, "Numerical Determination of Internal Stress and Viscoelastic Parameters for Xerographic Papers," *Polymer Engineering and Science*, vol. 21(9), pp. 538-541, 1981.

[73] K. Sedlachek. *The Effect of Hemicelluloses and Cyclic Humidity on the Creep of Single Fibers* Doctoral Thesis. Institute of Paper Science and Technology, Atlanta, Georgia, USA, 1995.

[74] V. Byrd, "Effect of Relative Humidity Changes During Creep on Handsheet Paper Properties," *Tappi Journal*, vol. 55(2), pp. 247-252, 1972.

[75] V. Byrd, "Effect of Relative Humidty Changes on Compressive Creep Response of Paper," *Tappi Journal*, vol. 55(11), pp. 1612-1613, 1972.

[76] L. Armstrong and G. Christensen, "Effects of Moisture Changes on Creep in Wood," *Nature*, vol. 185(4716), pp. 862-863, 1960.

[77] L. Armstrong and G. Christensen, "Influences of Moisture Changes on Deformation of Wood Under Stress," *Nature*, vol. 191(4791), pp. 869-870, 1961.

[78] C. Habeger and D. Coffin, "The Role of Stress Concentrations in Accelerated Creep and Sorption-Induced Physical Aging," *Journal of Pulp and Paper Science*, vol. 26(4), pp. 145-157, 2000.

[79] J. Wang, D. Dillard, and F. Kamke, "Transient Moisture Effects in Materials," *Journal of Material Science*, vol. 26, pp. 5113-5126, 1991.

[80] J. Wang, D. Dillard, M. Wolcott, F. Kamke, and G. Wilkes, "Transient Moisture Effects in Fibers and Composite Materials," *Journal of Composite Materials*, vol. 24, pp. 994-1009, 1990.

[81] D. Coffin and C. Habeger, "Accelerated Creep Mechanics: Part I," presented at The 4th International Symposium on Moisture and Creep Effects of Paper, Board, and Containers, Grenoble, France, pp. 106-120, 1999.

[82] C. Habeger and D. Coffin, "Accelerated Creep Mechanics: Part II," presented at The 4th International Symposium on Moisture and Creep Effects of Paper, Board and Containers, Grenoble, France, pp. 121-133, 1999.

[83] D. Coffin and C. Habeger, "The Practical Influence of Heterogeneity on the Tensile Accelerated Creep in Paper," *Tappi Journal*, vol. 84, pp. 174-182, 2001.

[84] J. Alfthan, "The Effect of Humidity Cycle Amplitude on Accelerated Tensile Creep of Paper," *Mechanics of Time-Dependent Materials*, vol. 8, pp. 289-302, 2004.

[85] J. Alfthan, "Linear Constituative Model for Mechano-Sorptive Creep in Paper," *International Journal of Solids and Structures*, vol. 42, pp. 6261-6276, 2005.

[86] J. Alfthan, "A Simplified Network Model for Mechano-Sorptive Creep in Paper," *Journal of Pulp and Paper Science*, vol. 29(7), pp. 228-234, 2003.

[87] J. Alfthan, P. Gudmundson, and S. Ostlund, "A Micromechanical Model of Mechanosorptive Creep in Paper," *Journal of Pulp and Paper Science*, vol. 28(3), pp. 98-104, 2002.

[88] H. Haslach, "The Mechanics of Moisture Accelerated Tensile Creep in Paper," *Tappi Journal*, vol. 77(10), pp. 179-186, 1994.

[89] H. Haslach, "Mechanisms of Moisture Accelerated Tensile Creep in Paper," presented at 1992 ASME Mechanics of Cellulosic Materials Winter Annual Meeting, Anaheim, CA, USA, pp. 39-47, 1992.

[90] H. Haslach, "The Moisture and Rate-Dependent Mechanical Properties of Paper," *Mechanics of Time-Dependent Materials*, vol. 4, pp. 169-210, 2000.

[91] C. Habeger, D. Coffin, and B. Hojjatie, "Influence of Humidity Cycling Parameters on the Moisture Accelerated Creep of Polymeric Fibers," *Journal of Polymer Science: Part B: Polymer Physics*, vol. 39, pp. 2048-2062, 2001.

[92] A. DeMaio and T. Patterson, "Influence of Fiber-Fiber Bonding on the Tensile Creep Compliance of Paper," in *Advances in Paper Science and Technology, Transactions of the 13th Fundamental Research Symposium*, S. Anson, Ed. Cambridge, UK: FRC, 2005, pp. 749-775.

[93] A. DeMaio, R. Lowe, T. Patterson, and A. Ragauskas, "Direct Observations of Bonding Influence on the Tensile Creep Behavior of Paper," *Nordic Pulp and Paper Research Journal*, vol. 21(3), 2006.

[94] A. DeMaio and T. Patterson, "Influence of Bonding on the Tensile Creep Behavior of Paper in a Cyclic Humidity Environment," *Mechanics of Time-Dependent Materials*, (accepted- publication date pending).

[95] R. Ampulski, "Report of Investigation, Reference Materials 8495- Northern Softwood Bleached Kraft Pulp and 8496- Eucalyptus Hardwood Bleached Kraft Pulp," National Insititute of Standards and Technology, 2001.

[96] *Tappi Test Methods 2004-2005*. Atlanta, USA: Tappi Press, 2004.

[97] D. Page, "The Beating of Chemical Pulps-The Action and the Effects," in *Fundamentals of Papermaking, Transactions of the 9th Fundamental Research Symposium*, C. Baker, Ed. Cambridge, UK: FRC, 1989, pp. 1-37.

[98] D. Page and R. Seth, "The Elastic Modulus of Paper, II. The Importance of Foiber Modulus, Bonding and Fiber :Length," *Tappi Journal*, vol. 63(6), pp. 113-116, 1980.

[99] D. Page and R. Seth, "The Elastic Modulus of Paper, III. The Effects of Dislocations, Microcompressions, Curl, Crimp and Kinks," *Tappi Journal*, vol. 63(10), pp. 99-102, 1980.

[100] D. Page, R. Seth, and J. De Grace, "The Elastic Modulus of Paper, I. The Controlling Mechanisms," *Tappi Journal*, vol. 62(9), pp. 99-102, 1979.

[101] H. Leech, "An Investigation of the Reasons for Increase in Paper Strength When Locust Bean Gum is Used as a Beater Adhesive," *Tappi Journal*, vol. 37(8), pp. 343-349, 1954.

[102] T. Lindstrom, L. Walberg, and T. Larsson, "On the Nature of Joint Strength in Paper-A Review of Dry and Wet Strength Resins Used in Paper Manufacturing," in *Advances in Paper Science and Technology, Transactions of the 13th Fundamental Research Symposium*, S. Anson, Ed. Cambridge, UK: FRC, 2005, pp. 457-562.

[103] D. Page, "Fibre-to-Fibre Bonds," *Paper Technology*, vol. 1(4), pp. 407-411, 1960.

[104] R. Lowe, A. Ragauskas, and D. Page, "Imaging Fibre Deformations," in *Advances in Paper Science and Technology, Transactions of the 13th Fundamental Reseach Symposium*, S. Anson, Ed. Cambridge, UK: FRC, 2005, pp. 921-941.

[105] R. Mann, G. Baum, and C. Habeger, "Determination of All Nine Orthotropic Elastic Constants for Machine-Made Paper," *Tappi Journal*, vol. 63(2), pp. 163-166, 1980.

[106] G. Baum, D. Brennan, and C. Habeger, "Orthotropic Elastic Constants of Paper," *Tappi Journal*, vol. 64(8), pp. 97-101, 1981.

[107] F. Johanson and J. Kubat, "Measurements of Stress Relaxation in Paper," *Svensk Papperstidning*, vol. 67(20), pp. 822-832, 1964.

[108] J. Skowronski and E. Szwarcsztajn, "Studies on Visco-Elastic and Plastic Properties of Paper, Part II. The Nature of Elasticity and Viscoelasticity of Paper," *Przeglad Papierniczy*, vol. 36(9), pp. 321-326, 1980.

[109] J. Waterhouse, "Residual Stresses in Paper and Board, Chapter 10," in *Handbook of Physical Testing of Paper, Volume 1*, R. Mark, C. Habeger, J. Borch, and M. Lyne, Eds. New York, NY, USA: Marcel Dekker, Inc., 2002, pp. 527-562.

[110] M. Htun and A. De Ruvo, "Correlation Between the Drying Stress and the Internal Stress in Paper," *Tappi Journal*, vol. 61(6), pp. 75-77, 1978.

[111] M. Htun and A. de Ruvo, "Relationship Between Drying Stresses and Internal Stresses and the Mechanical Properties of Paper," in *Fibre-Water Interactions in Papermaking, Transactions of the 6th Fundamental Research Symposium*, F. Bolam, Ed. Oxford, UK: FRC, 1977, pp. 477-487.

[112] M. Htun, "Internal Stress in Paper, Chapter 11," in *Paper, Structure and Properties*, J. Bristow and P. Kolseth, Eds. New York, NY, USA: Marcel Dekker, Inc., 1986, pp. 227-239.

[113] L. Nilsson, "The Diffusion of Water Vapour Through Pulp and Paper," *Drying Technology*, vol. 11, pp. 1205-1225, 1993.

[114] P. Bevington and D. Robinson, *Data Reduction and Error Analysis*. New York, USA: McGraw-Hill, 2003.

[115] L. Lapin, *Modern Engineering Statistics*. Belmont, CA, USA: Wadsworth Publishing Company, 1997.

[116] L. Rade and B. Westergren, *Mathematics Handbook*. New York, NY, USA: Springer, 1999.

VITA

Andrew DeMaio, born 1976 in Syracuse, New York, graduated in the fall of 1999 from the SUNY College of Environmental Science and Forestry at Syracuse University. There, he received a Bachelor of Sciences Degree in Paper Science and Engineering with high honors. Following undergraduate school, Andrew went to work as a process engineer for Hollingsworth and Vose Company in Greenwich, New York. In the fall of 2001, Andrew left industry and moved to Atlanta, Georgia to pursue a PhD at the Institute of Paper Science and Technology at Georgia Tech. As part of the Woodruff School of Mechanical Engineering, he focused his research efforts in the paper physics area. Specifically, this involved how paper's structural characteristics influenced creep behavior. Paramount to this was discerning what role bonding played in the creep behavior of paper. Andrew has presented research in this area at several conferences and has published as well. Believing that a balance in lifestyle is important, Andrew has found that reading, golfing, hiking, traveling, and spending time with friends, family and colleagues has effectively complemented his research while at Georgia Tech.